# ENVIRONMENTALLY FRIENDLY PULTRUSION


MUHAMMAD SHAFIQ IRFAN

A thesis submitted to the University of Birmingham for the degree of

DOCTOR OF PHILOSOPHY

School of Metallurgy and Materials
College of Engineering and Physical Sciences
University of Birmingham, U.K.

May 2013

# ABSTRACT

The primary aim of this research programme was to develop an environmentally-friendly pultrusion technique for the production of fibre-reinforced composites. This technique is referred to as "clean pultrusion". In this new manufacturing technique, the resin bath used in the conventional pultrusion process was replaced with a custom-built resin impregnator. The resin impregnator was designed and built to impregnate the rovings using a combination of pin, injection and capillary-based impregnation. An integral aspect of the clean pultrusion process was the spreading of the filaments in the rovings, via mechanical means, prior to impregnation. A new method was developed and modelled to spread the filaments in the rovings via a "tension-release" process. The observations made during the initial fibre spreading experiments were used to design and construct an automated fibre spreading rig. The Taguchi method was used to design the experimental matrix to optimise the parameters that were considered to affect the spreading of the filaments in the rovings via the custom-made fibre spreading rig.

The conventional and clean pultrusion techniques were used in conjunction with E-glass fibres and three classes of resins: epoxy, vinyl ester and polyurethane. The clean pultrusion technique was demonstrated successfully in the laboratory and at the premises of Pultrex Ltd, UK. With reference to the polyurethane resin system, a custom-built resin dispenser was provided by CTM Equipment & CTM UK Ltd. Here, the isocyanate and polyol were contained in separate reservoirs and delivered, on demand, via precision gear pumps to a Kenics® static mixer. The static mixer was connected to the resin impregnator where the spread fibres were impregnated. In the case of the epoxy and vinyl ester resin systems, pre-mixed resins were dispensed to the resin impregnator via a pressure-pot.

The physical, mechanical and thermo-mechanical properties of the composites pultruded using the clean and conventional techniques were analysed and compared. It was found that the composites manufactured using the clean pultrusion had lower void content when compared to those manufactured using the conventional resin bath-based technique. It was also found that the composites manufactured via the clean pultrusion technique exhibited better mechanical properties.

It is common practice for an internal mould release to be blended in with the resin formulation. This study found that in instances where the internal mould release was applied externally, the mechanical properties were superior.

The thermo-mechanical properties of the pultruded composites were similar for each class of resin system when using the conventional and clean pultrusion techniques. Visual inspection and optical microscopy of polished sections demonstrated that the degree of impregnation was consistently higher for the composites manufactured via the clean pultrusion method.

A life cycle assessment (LCA) was performed to compare the environmental impact of the clean and conventional pultrusion processes. The LCA demonstrated conclusively that the clean pultrusion technique offers several significant advantages with regard to: (i) reduction in the volume of solvent required to clean the equipment at the end of each production schedule; (ii) reduction in the volume of waste resin; (iii) reduction in the time taken to clean the equipment; and (iv) situations where the resin dispenser is used in conjunction with the clean pultrusion technique, the need for manual mixing of the components of the resin is avoided.

The new pultrusion technique consisting of an integrated fibre spreading rig, a resin dispensing unit and an impregnation unit was demonstrated as being a viable method to pultrude composites without using a resin bath.

*This thesis is dedicated to*

***my late wife and daughter***

*(their sudden departure taught me that there are certain things in life which are uncontrollable)*

***&***

***my parents and siblings***

*(for their unconditional love and support during the time I spent away from home for my studies).*

# ACKNOWLEDGEMENTS

I would like to thank my supervisor Professor Gerard Fernando for giving me the opportunity to work on this project. His deep sense of knowledge, guidance, thoughtfulness and dedication to his work always inspired me to a great extent. I am also hugely indebted to Prof. Fernando's immense support during the write-up of my thesis.

Appreciation is due to my colleagues in the Sensors and Composites Group for their help and support. Especially to Dr Raj Machavaram, a great friend, who not only helped me in my research work but with whom I explored a lot of cinemas and restaurants in Birmingham. I would also like to thank Dr Liwei Wang, Dr Surya Pandita, Mark Paget, Frank Biddlestone, Fran Nieves, Claire Wait, Mick Cunningham, Mrs. Tracy Parkes, Mrs. Anne Cabezas, Mrs. Kay Jones, Mrs. Jenny Henderson, Dr Nick Shotton-Gale, Dr Ramani Mahendran, Dr Dee Harris, Sebastian Ballard, Richard Murray, Samuel Ojo and Abilash Kumar for helping me during my work in one way or another.

I am very grateful for the funding and support given by the Engineering and Physical Sciences Research Council (EPSRC) and Technology Strategy Board (TSB). Appreciation is due to the industrial partners involved in the project including Colin Leek (Pultrex Ltd.), Shane and Ruth Wootton (CTM Equipment & CTM UK Ltd), Mark Hudson (PPG Industries), Merv Laycock and Stefan Helsemans (Huntsman Polyurethanes). Also I wish to extend my thanks to the University of Engineering and Technology, Lahore, Pakistan for granting me leave to continue my higher education.

I am also grateful to my friends Sarmad Ali Khan and Debajyoti Bhaduri with whom I spent some great time during my stay in the UK.

Finally, I am indebted to my parents and siblings for their support and unconditional love. I can never re-pay their dedication and the sacrifices they have made for me.

# TABLE OF CONTENTS

# LIST OF FIGURES

# LIST OF TABLES

# 1 INTRODUCTION

## 1.1 BACKGROUND

Pultrusion is one of the fastest growing composite production technique for manufacturing profiles of constant cross-section (Vázquez and Escobar, 2012). Common pultrusion profiles include solid rods, hollow tubes, flat sheets, and beams of a variety of cross-sections, including angles, channels and wide-flanged sections. These components are used in a wide range of industrial sectors such as construction, electrical, marine and transportation (Peters, 1998, Starr, 2000, Mallick, 2008, Pultrex, 2012).

The pultrusion processes can be divided into two types based on the methodology used to impregnate the reinforcements. These are resin bath and resin injection-based pultrusion (Sumerak, 2000, Shaw-Stewart and Sumerak, 2000, Strong, 2008). In the resin bath-based approach, an open resin bath is used to impregnate the rovings. A number of researchers have reported on the environmental problems associated with the emission of undesirable chemicals from the resin bath-based manufacturing process. For example, the emission of styrene in case of unsaturated polyester resin systems (Lackey et al., 1997, Raday, 2006, Cambell, 2010). The need to reduce the emission of volatile organics to the environment has been highlighted in several European directives such as the solvent emission directive (SED) 1999/13/EC (European Commision, 1999) and the products directive (PD) 2004/42/EC (European Commission, 2004).

In order to overcome the emission related problems associated with open-bath-based impregnation, an injection-type impregnation has been developed previously for pultrusion. Here a resin-injection die is employed where the resin is forced into the rovings at high

pressure (400 to 2700 kPa). Up to 90% reduction in the emission of styrene has been reported for resin-injection pultrusion (Shaw-Stewart and Sumerak, 2000). However, the dies used in resin-injection pultrusion are generally longer and the design is more intricate. The associated cost is higher when compared to conventional dies (Shaw-Stewart and Sumerak, 2000, Cambell, 2010). It has also been reported that the rovings in the chamber of the resin-injection die are compressed (packed) thus making the impregnation less efficient (Strong, 2008).

The following section presents a brief discussion on the perceived problems with the deployment of the conventional pultrusion methods:

(i) Impregnation efficiency: Since a large number of rovings are used in the pultrusion process, it is more convenient and cheaper to draw the roving from the inner bore of the creel. This method of drawing the rovings does not require the creels to be mounted on shafts with bearings and tension-controllers. However, it does mean that the rovings will be twisted as they are drawn from the centre of the creel. In addition to the intrinsic twists in the filaments contained in the roving these twists can have an effect on the mechanical properties of the composite (Shah et al., 2013). Furthermore, twists can influence the rate of impregnation (Pandita et al., 2012).

The distribution of the binder in the rovings can be variable and this too can affect the impregnation efficiency. In situations where the binder is present in high concentrations, spreading the filaments can break up any clumps. This is likely to improve the impregnation process.

(ii) Impregnation method: Resin-injection pultrusion has been reported widely in the literature. However, as stated previously, the rovings are compacted into the impregnation chamber and this is not ideal for rapid impregnation. Moreover, the potential for the resin to

cure in the vicinity of the impregnation chamber needs to be considered especially if it is located in close proximity to the die. The cost associated with the high-pressure pumps, pipes, and complex impregnation chambers can be prohibitive. A potential solution to this problem is to spread the rovings prior to impregnation where the impregnation unit is enclosed with easily demountable covers to control any unwanted emissions to the atmosphere. This strategy will also enable flexibility in the design of the resin impregnator where different modes of impregnation, such as capillary, pin and pressure-based impregnation can be integrated.

(iii) Weighing and mixing the resin: The mixing of the various components of the resin is generally carried out manually. If electrical or pneumatic mixing devices are used, they have to be cleaned at the end of each shift or prior to the resin curing. There is potential for unintentional errors in weighing the required quantities of the resin, hardener, catalyst, filler and pigment. A potential solution to mitigate these concerns is to store the various components in separate containers and to dispense them on demand to a static mixer using conventional resin delivery systems. Examples of resin delivery systems include piston, gear and peristaltic pumps where the stoichiometry of the resin and hardener can be controlled as required.

(iv) Feedback control: With reference to conventional resin bath-based pultrusion, the mode of impregnation can be affected adversely if the pultrusion speed is increased above a certain value. In other words, it is generally not possible to influence the impregnation process if one or more of the processing variables (pultrusion speed, tension, temperature, etc) are altered. However, if an electronic resin delivery system is employed, it will be possible to control the resin delivery rate. Furthermore, it will also be possible to control the temperature of the resin

by using electrical heating at specified locations as required. It will also be possible to link the fibre haul-off rate to the resin delivery system via an encoder. This will enable synchronisation between the pultrusion speed and the resin dispensing rate.

(v) Waste resin and solvent utilisation: With reference to resin bath-based impregnation, the liquid level of the mixed resin system has to be maintained at a specified level to ensure that the rovings are immersed fully as they are drawn through. This volume of the mixed resin has to be disposed of at the end of each production cycle. Failing to do so will result in curing of the resin in the resin bath. Since thermosetting resins are exothermic, it is inadvisable to cure large volumes of waste resin in one operation. Hence, the waste has to be split into smaller volumes for curing to minimise the probability of the resin exotherming. The overall volume of the device that is used for impregnating the rovings can be minimised if the impregnation process can be made more efficient. One way to achieve this is to spread the filaments in the roving. This in turn will enable the impregnation "container" to be miniaturised thus, offering a route to minimise the volume of solvent required for cleaning purposes. The container or impregnation unit can also be made from "non-stick" materials such as polytetrafluoroethylene (PTFE) or ultra-high-molecular-weight polyethylene (UHMWPE).

The above-mentioned issues were considered in detail in this research project and techniques were developed to overcome the various concerns. The overall strategy consisted of five distinct aspects. The first was a detailed investigation to develop techniques to spread the filaments in a roving without inducing damage. The second element was the modelling, design, construction and evaluation of impregnation units to negate the need for a resin bath. The third strategy was to initiate the design and construction of a resin delivery system where the components of the resin were stored separately and pumped on-demand to a static mixer.

The option of enabling the delivery of pre-mixed resin was undertaken where a pressure-pot was deployed. The fourth aspect of the strategy was to enable feedback control between the resin delivery unit and the fibre haul-off rate via an encoder. Finally, a detailed life cycle assessment (LCA) was undertaken to assess the "green credentials" of the clean pultrusion technique when compared with the conventional manufacturing process.

## 1.2 AIMS OF THE STUDY

The primary aim of this research was to develop an environmentally-friendly pultrusion process (termed as clean pultrusion). The specific aims of the research were as follows.

(i) To design and evaluate a rig for the lateral spreading of the rovings.

(ii) To design and evaluate resin impregnators to develop the clean pultrusion technique.

(iii) To demonstrate the clean pultrusion technology in the laboratory and under industrial conditions.

(iv) To compare the properties of the composites obtained using the clean and conventional pultrusion processes.

(v) To undertake an LCA on the clean and conventional pultrusion processes.

## 1.3 STRUCTURE OF THE THESIS

This thesis consists of the following chapters.

Chapter 2 presents the literature review and it covers the major aspects of the project including pultrusion, fibre spreading, resin impregnation and the LCA of polymer composites.

Chapter 3 covers the design of the fibre spreading rig, resin impregnators and resin dispenser. The experimental aspects to fulfil the objectives of the project are also discussed including a

description of the materials and instruments used, and the techniques that were used to characterise the resins and the pultruded composites.

Chapter 4 presents the results obtained using the experimental procedures outlined in Chapter 3 and a discussion of the results.

Chapter 5 summarises the conclusions drawn from this study and recommendations for the future research.

Appendix-A provides a list of the papers published by the author and those under review (submitted) and in preparation.

Appendix-B presents copies of papers published by the author as the first-author.

Appendix-C presents a summary of the properties of pultruded composites manufactured in this project using the resin bath, resin impregnator designs PUL-I and PUL-II.

Appendix-D gives a summary of the experimental protocol for pultrusion with polyurethane resin system including the safety requirements and procedures that were used when working with isocyanates.

Appendix-E provides the detail of the environmental impact categories used for the LCA studies.

# 2 LITERATURE REVIEW

This section presents a review of the literature on topics associated with pultrusion, fibre, spreading, models for predicting the impregnation of rovings and use of LCA in the field of polymer composites.

## 2.1 PULTRUSION

### *2.1.1 Description of the process*

A schematic illustration of an idealised conventional dip-type resin bath-based pultrusion line is shown in Figure 1. With reference to Figure 1, the bulk of the reinforcements consist of continuous rovings which are usually supplied from the centre-pull creels (item i). In addition to the rovings, layers of chopped strand mats (item ii) are used to improve the transverse strength of the pultruded composite. The creels are placed on a creel stand (item iii). The rovings from the creel stand are threaded through the guide plates (item v and vi) via eyelets (item iv). The materials used for the eyelets are generally ceramics, steel, PTFE or UHMWPE. The guide plates (items v and vi) are made from polypropylene (PP), PTFE or high-molecular-weight polyethylene (HMWPE). It is essential for the rovings to pass through the eyelets and guide plates without crossing-over each other. In some instances, the rovings are threaded through polymeric tubes to guide them from the creel stand to the pultrusion assembly line.

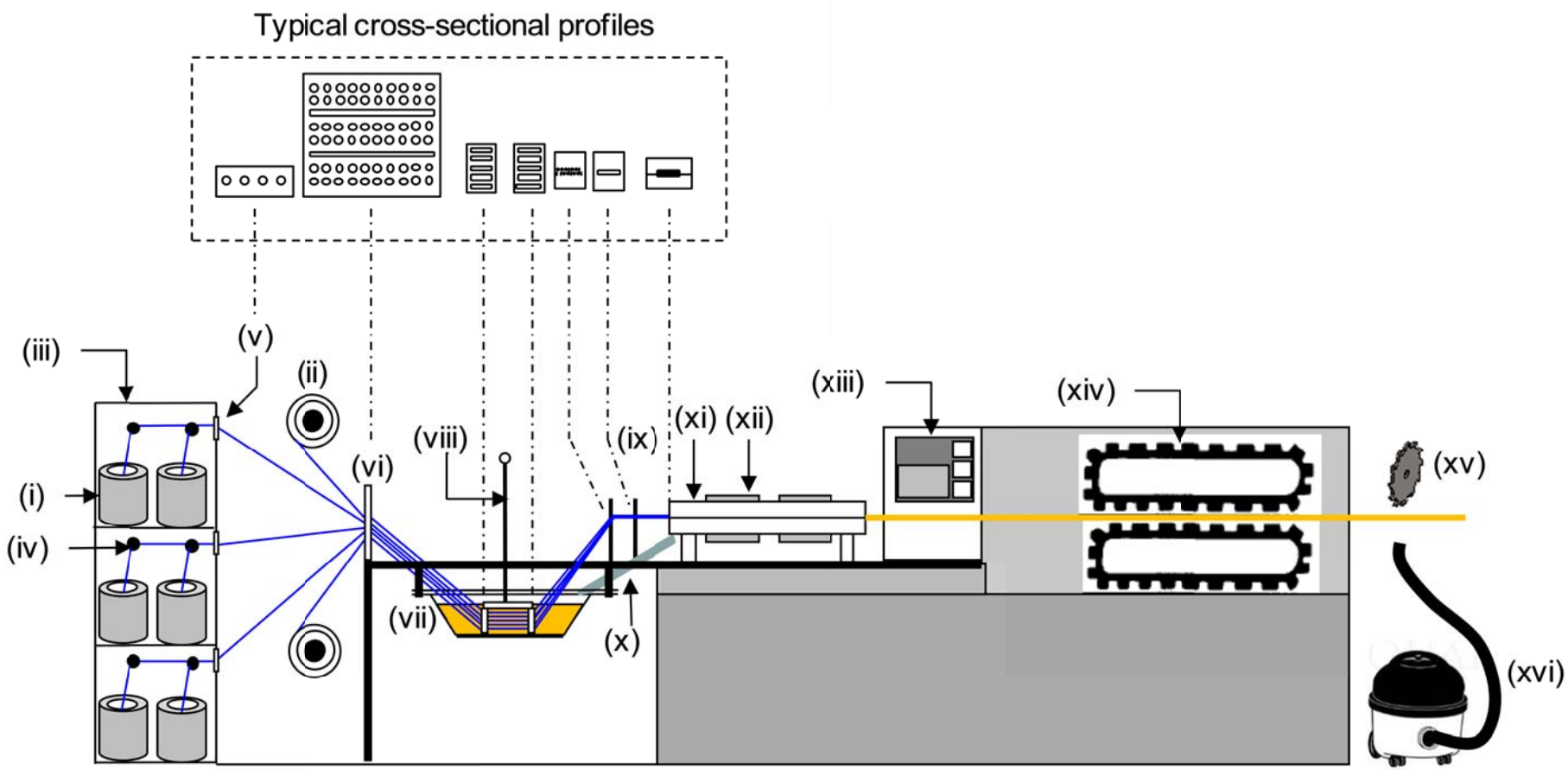


**Figure 1 Schematic illustration of an experimental setup for a conventional dip-type resin bath pultrusion process. The key components are coded as follows: (i) creels; (ii) chopped strand mats; (iii) creel stand; (iv) eyelets; (v) guide plate-I; (vi) guide plate-II; (vii) dip-type resin bath; (viii) plunger; (ix) pre-forming guides; (x) drip tray; (xi) die; (xii) heating elements; (xiii) control system; (xiv) cleat-type tractor puller; (xv) cutter; and (xvi) debris collection device. The cross-sectional profiles are illustrated on the top of the schematic illustration.**

The rovings are then threaded through the plunger (item viii). This enables the rovings to be lowered into the resin bath (item vii). The impregnated rovings exit the resin bath and the excess resin is removed by passing them through pre-forming guides (item ix). The pre-forming guides are made from HMWPE, PP or steel and the profile resembles the shape of the die. The pre-forming guides not only remove the excess resin from the rovings but also consolidate them prior to entering the die. The number and the arrangement of the pre-forming guides depend on the complexity of the profile. A resin drip tray (item x) is used to channel the resin that drips from the pre-forming guides and die. It is common to use channel-profiles made of pultruded polyester/E-glass profiles as the drip trays.

The chrome-plated matched metal dies (item xi) are used to consolidate and cure the impregnated rovings. The heat required for curing the impregnated rovings is provided via strip heaters (item xii). The cured pultruded profile from the die is pulled via a continuous cleat-type tractor puller (item xiv), continuous belt-type tractor puller or reciprocating-pullers. Finally, the pultruded composite is cut to the required length by a cut-off saw (item xv). A debris collection device (item xvi) is used to collect the debris from the cutting operation.

### *2.1.2 Fibre reinforcements*

Examples of typical reinforcements used in pultrusion include glass, carbon and aramid fibres. The hybrids of carbon and aramid with glass have also been reported (Starr, 2000). A comparison of the properties of common fibres used in pultrusion is given in Table 1. Glass fibres are used in over 95% of the pultruded products (Gauchel et al., 2000, Starr, 2000, Thomason, 2012). There are various types of glass fibres available depending on the chemical composition; the most popular form is E-glass. The coding system and chemical composition of the most common types of glass fibres is presented in Table 2.

**Table 1 Comparison of selected reinforcements used in pultrusion (Mazumdar, 2000).**

| Fibre type | Diameter (μm) | Density ($kg/m^3$) | Tensile modulus (GPa) | Tensile strength (GPa) | Elongation at break (%) |
|---|---|---|---|---|---|
| E-glass | 7-25 | 2540 | 70 | 3.45 | 4.8 |
| S-glass | 15 | 2500 | 86 | 4.5 | 5.7 |
| Carbon (HM*) | 7.5 | 1900 | 400 | 1.8 | 1.5 |
| Carbon (HS†) | 7.5 | 1700 | 240 | 2.6 | 0.8 |
| Aramid | 12 | 1405 | 130 | 2.8 | 2.5 |
| * HM: high-modulus<br>† HS: high-strength | | | | | |

**Table 2 Summary of selected characteristic compositions of E, S and C-glass fibres. The composition stated is provided in weight % (Sumerak, 2000, Hull and Clyne, 1996, ASTM Standards, 2011).**

| Coding | Characteristics | Composition | | | | | |
|---|---|---|---|---|---|---|---|
| | | $SiO_2$ | $Al_2O_3$ | CaO | MgO | $Ba_2O_3$ | $Na_2O$ |
| E, electrical | Low electrical conductivity | 52.4 | 14.5 | 17.2 | 4.6 | 10.6 | 0.8 |
| S, strength | High strength | 64.4 | 25 | ---- | 10.3 | ---- | 0.3 |
| C, chemical | High chemical durability | 64.4 | 4.1 | 13.4 | 3.3 | 4.7 | 9.6 |

A discussion on the manufacturing technique for the production of the glass fibres is presented in Appendix-B. Since E-glass fibres were used in the current study, the following section gives a brief discussion on the key terminology.

The general term used to express the linear density of rovings is *tex* (mass of the roving in grams per 1000 metres). The number of filaments in a roving ($N_F$) can be calculated from a

knowledge of the roving tex, radius of filaments ($r_F$) and density ($\rho$) of the glass using the following relationship (Fibremax Composites, 1999):

$$N_F = \frac{1000 \times tex}{\pi r_F^2 \rho} \qquad \textbf{Equation 1}$$

The roving packages or creels can be classified into two types depending on the mode of drawing the rovings: outside-pull and centre-pull creels. The outside-pull roving packages have a core cardboard tube which is placed on a support assembly as shown in Figure 2(a). The centre-pull creels are stacked on shelves and the roving is drawn from the centre.

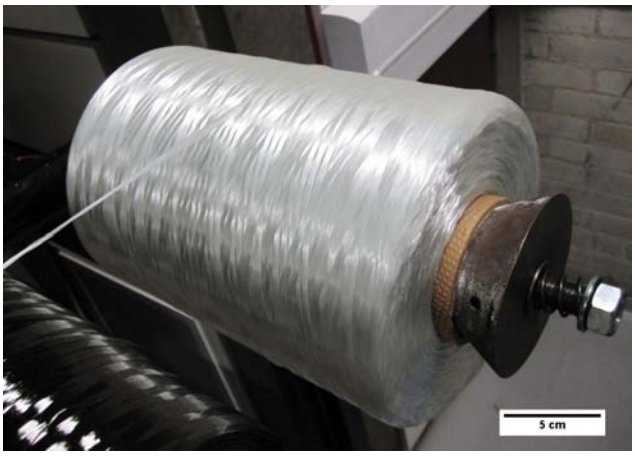


(a)


(b)

**Figure 2 Glass fibre packages: (a) outside-pull; and (b) centre-pull.**

An important feature of the centre-pull creels is the presence of twist in the roving due to drawing the roving from the inner bore; see Figure 2(b). This twist can be detrimental in operations where lateral spreading of the rovings is desired (Irfan et al., 2011). A comparison of the basic features of the centre-pull and outside-pull creels is provided in Table 3.

**Table 3 Features of centre-pull and outside-pull fibre packages.**

| Centre-pull | Outside-pull |
|---|---|
| Ability to easily transfer from one roving pack to another for continuous processing and higher operating efficiency. | More process downtime; due to difficulty in transferring from package to package. |
| Minimal packaging waste because no core is required. | Need to dispose of inside cardboard tubes. |
| Simple design of the creel stand. | Need rotating spindles or mandrels. |
| Twist in the roving. | Minimum twist. |
| Simple tensioning mechanism to keep the rovings taut. | Need more complex tensioning methods and devices. |

### *2.1.3 Thermosetting resins*

Unsaturated polyesters are one of the most widely used resin systems in pultrusion. Styrene monomer is generally used as a diluent and a reactive cross-linking agent to form the cross-linked structure (Hoa, 2009). Polyester resins are said to provide good corrosion and electrical

resistance. Properties such as the brittleness or toughness of polyester resins differ based on their backbone chemical structure (Strong, 2008).

Vinyl esters are used as an alternative to polyesters when improved corrosion resistance, toughness and better chemical resistance is required (Bogner et al., 2000). The high shrinkage of polyesters (5-12 %) and vinyl esters (5.4-10.3 %) provide a processing advantage in that it helps the composite to shrink away from the die, thus reducing the friction and pulling forces required. Both polyesters and vinyl esters show good processing characteristics such as pultrusion at faster speeds and easier separation from the walls of the die (Cambell, 2010, Shaw-Stewart and Sumerak, 2000).

Epoxy resins are used where higher mechanical properties and property-retention at higher temperatures are desired. They also have good corrosion and electrical resistance. Epoxies provide better dimensional control due to relatively low cure shrinkage (1-4 %). However, they are three to six times more expensive than unsaturated polyester resins (Hoa, 2009).

Polyurethane resin systems are comparatively new in the field of pultrusion. One of the unique features of polyurethanes is that the final properties can be manipulated by changing the isocyanate/polyol ratio (Joshi et al., 1999). However, commercially available polyurethane resin systems have short gel-times, hence resin injection-based pultrusion is preferred with these systems (Joshi et al., 1999, Connolly, 2005a, Connolly, 2006, Connolly, 2008).

Additives such as fillers and colorants are frequently added to the resin formulations to reduce the cost or to obtain the desired properties. A comparison of the properties of selected resins used for pultrusion is summarised in Table 4.

**Table 4 Typical properties of common thermoset resins that are used to manufacture composites via pultrusion (Mallick, 2008, Connolly, 2005b, Joshi, 2000).**

| Materials | Density ($kg/m^3 \times 10^3$) | Tensile Modulus (GPa) | Tensile Strength (MPa) | Cure shrinkage (%) |
|---|---|---|---|---|
| Polyester | 1.1-1.4 | 1.6-4.1 | 36-95 | 5.0-12.0 |
| Vinyl ester | 1.1-1.3 | 3.0-3.5 | 73-81 | 5.4-10.3 |
| Polyurethane | 1.1-1.2 | 2.2-3.3 | 49-75 | 2.0-2.5 |
| Epoxy | 1.2-1.4 | 2.5-5.0 | 50-130 | 1.0-4.0 |

### *2.1.4 Important features associated with pultrusion*

The key aspects of the pultrusion process are considered in this section.

(i) *Selection of the resin and reinforcement*. The choice of the resin system and the fibre type is dictated by the required properties and the intended end-use application. A key requirement is that the fibres should be compatible with the resin system. Commercial fibre manufacturers supply the fibres with a resin-specific sizing or binder. For example Hybon® 2026 E-glass rovings from PPG are designed to be compatible with unsaturated polyester, vinyl ester and epoxy resin systems (PPG Fibre Glass, 2012).

(ii) *Resin impregnation*. A prerequisite in the production of advanced fibre reinforced composites is that the rovings have to be impregnated thoroughly by the matrix. Poor impregnation can cause voids and a poor interface between the fibres and the resin; and this will have a detrimental effect on the mechanical properties (Shaw-Stewart and Sumerak, 2000). The methods of impregnation commonly used in pultrusion are discussed in Section 2.1.5.

(iii) *Forming guides*. The forming guides remove the excess resin and entrapped air from the impregnated rovings; however, they also increase the tension in the rovings. A careful selection of the profile of the guides is essential to avoid fibrous build up due to fibre damage and snagging of the rovings.

(iv) *Selection of the process parameters*. The temperature profile in the die is a critical process parameter in pultrusion (Sumerak, 2000). A schematic illustration of the thermal environment and the cure profile in the pultrusion die is depicted in Figure 3. The die provides the thermal energy required for curing but the exothermic heat generated from the curing reaction also contributes towards the curing process (Campbell, 2004).

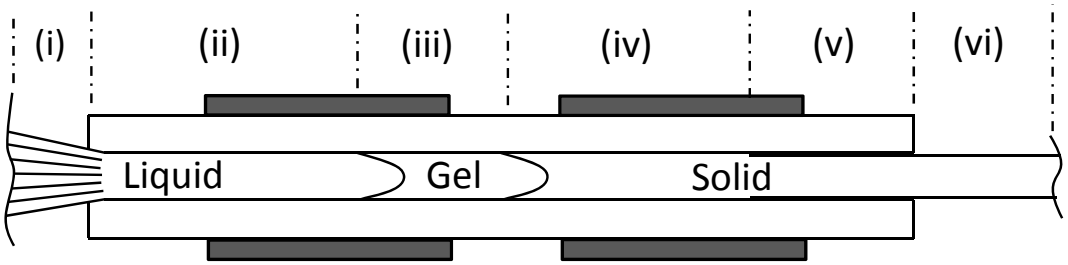


**Figure 3 A schematic illustration of the thermal and cure environments in the pultrusion die. Details of zones indicated are as follows: (i) resin impregnated reinforcements enter the die; (ii) compaction of the impregnated rovings and heat transfer from the die to the impregnated rovings; (iii) commencement of gelation; (iv) the exotherm generated by the cross-linking resin elevates the temperature within the die; (v) shrinkage of the resin causing separation of the profile from the die; and (vi) convective heat dissipation from the cured composite. Adapted from Sumerak (2001).**

A number of researchers have focused on the thermal and curing behaviour occurring inside the die to optimise the pultrusion process. In essence, models have been developed taking into account heat transfer in to the die and the cure kinetics of the resin to predict the optimal thermal characteristics (Han et al., 1986, Batch and Macosko, 1993, Pitchumani and Yao, 1993, Gorthala et al., 1994).

Kim et al. (1997) published a model for the pultrusion of thermosetting resin composites. Their model consisted of two sub-models namely, thermo-chemical and pulling force. The results from the model were compared with experimental data and a good cross-correlation was seen. Sumerak (2001) related the design features of the die to the temperature distribution and cure kinetics within the die using finite element analysis (FEA). It was shown that the presence of an air gap between the die and the heat source can cause a temperature drop, thus leading to different thermal conditions than the uniform temperature distribution assumed in the model.

Li et al. (2003a, 2003b, 2009) performed pultrusion experiments with a vinyl ester resin and demonstrated that by increasing the length of the die and an efficient control of the heating zones, the quality of the pultruded composites could be improved. They also found that a longer length of the die did not increase the pulling-force. This is because after the gel zone, the composite separates from the die walls and thus the friction between the composite and the die walls is lower (See Figure 3). This observation may be true for resin systems with higher shrinkage, for example polyester and vinyl ester; however for resins with lower shrinkage, such as epoxy, the pulling-force is likely to increase in proportion to the length of the die.

Yen et al. (2006) used the data obtained from differential scanning calorimetry experiments conducted on a neat resin system to estimate the required set-temperature for the die. A conversion-temperature curve was generated from a dynamic heating experiment of the resin in the DSC and a suitable die temperature was selected; this corresponded to the temperature where the resin system had reached over 70% conversion.

### *2.1.5 Impregnation methods*

In this section, the impregnation methods employed for the pultrusion of composites are described.

(i) *Dip-type open resin bath*: A description of the dip-type open bath was described in Section 2.1.1. A schematic illustration of this method is shown in Figure 4. This technique is used frequently in the production of pultruded composites. An issue with this impregnation method is the emission of styrene when using polyester resin. Hence, efficient local exhaust ventilation (LEV) has to be used (Campbell, 2004).

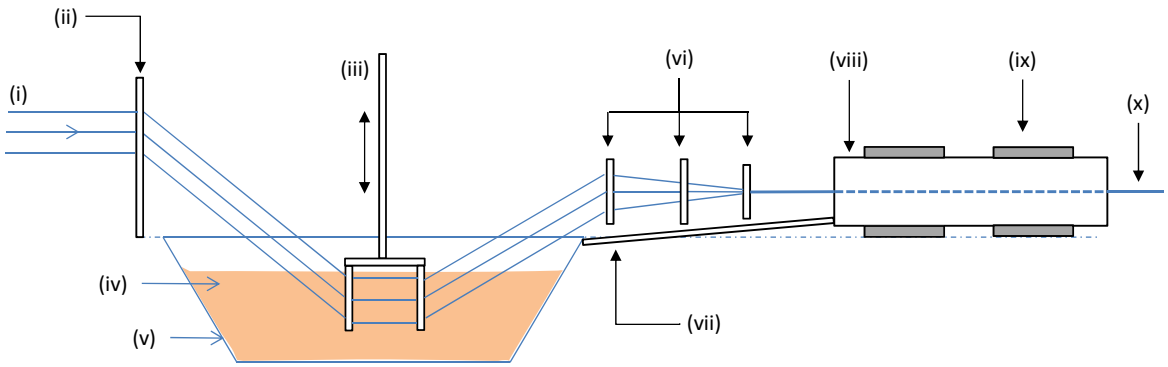


**Figure 4 Schematic illustration of the conventional dip-bath resin impregnation system. The key components are coded as follows: (i) rovings; (ii) guide plate; (iii) plunger; (iv) resin; (v) resin bath; (vi) pre-forming guides; (vii) drip tray; (viii) die; (ix) heating elements; and (x) cured composite profile.**

(ii) *Straight-through resin bath*: A schematic illustration of the straight-through resin bath is shown in Figure 5. With this type of impregnation, the rovings pass horizontally through a covered resin bath via slots cut in the guide plates at the entry and exit regions of the bath. The resin-drips at the slots of the guide plates are collected in a container and a recirculation pump is used to feed the resin back to the bath. The straight-through designs are also used for reinforcements that are susceptible to fracture if they are fed through a dip-type resin bath (Shaw-Stewart and Sumerak, 2000, Sumerak, 2000).

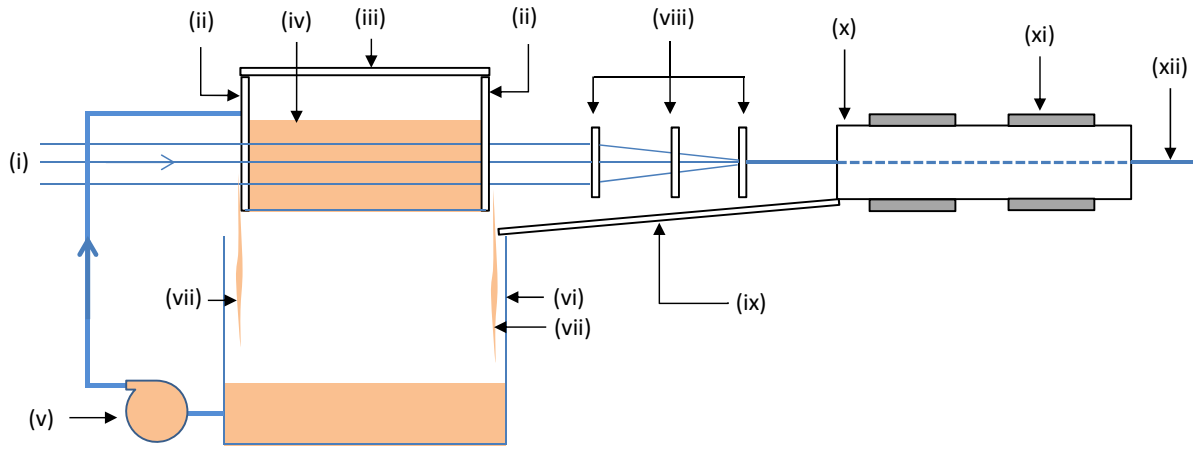


**Figure 5 Schematic illustration of the straight-through resin bath impregnation process. The key components are coded as follows: (i) rovings; (ii) guide plate; (iii) top-lid; (iv) resin; (v) recirculation pump; (vi) container to collect the resin drips; (vii) resin drips; (viii) pre-forming guides; (ix) drip tray; (x) die; (xi) heating elements; and (xii) cured composite profile.**

(iii) *Resin-injection pultrusion*: A schematic illustration of the resin-injection pultrusion is shown in Figure 6. In this method, the rovings are fed into a cavity where the resin is injected under pressure (400 to 2700 kPa). This enclosed injection system is said to reduce the emission of styrene by up to 90% (Shaw-Stewart and Sumerak, 2000).

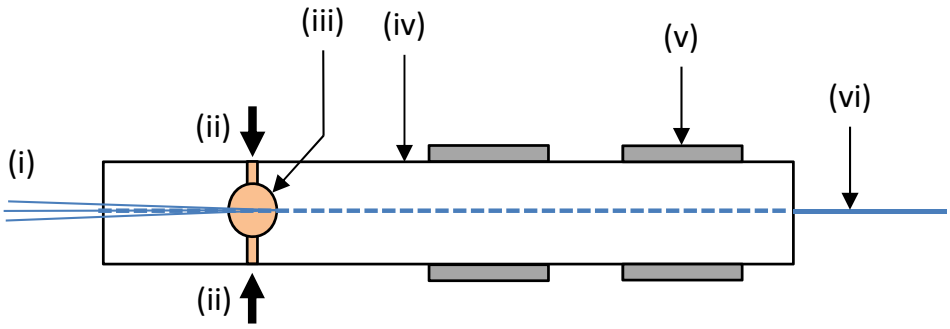


**Figure 6 Schematic illustration of the resin-injection pultrusion process. The key components are coded as follows: (i) rovings; (ii) resin-injection under pressure; (iii) cavity; (iv) die; (v) heating elements; and (vi) cured composite profile.**

Lackey et al. (1997) described the experimental evaluation of a resin-injection pultrusion system in some detail. The factors affecting the resin-injection process such as the design of the injection chamber, resin injection pressure and the type of roving used were addressed. It was shown that the resin-injection pultrusion process provides environmental benefits over

the conventional open-bath pultrusion technique. The resin injection pressure required to impregnate an E-glass roving pack consisting of 4400 tex rovings with a die cross-section of 25.4 mm × 3.18 mm was in the range 1378-2067 kPa. The viscosity of the resin used in that study was 0.5 Pa·s. The quality of the impregnated rovings was determined by visual inspection. They also evaluated the flexural properties of pultruded composites. It was reported that it was difficult to impregnate all the rovings when reinforcing mats were used. They recommended that the packing of the rovings inside the injection chamber, and the geometry of the chamber, should be selected such that it promotes flow of the resin through the rovings.

A number of researchers have modelled the resin-injection pultrusion process (Kommu et al., 1998, Voorakaranam and Joseph, 1998, Voorakaranam et al., 1999, Srinivasagupta et al., 2003a, Srinivasagupta et al., 2003b, Srinivasagupta and Kardos, 2004). Rahatekar and Roux (2003) simulated the effects of the pultrusion speed, fibre volume fraction, viscosity of the resin and the compression ratio (taper) of the injection chamber on the impregnation process for a polyester/glass roving system. The compression ratio was defined as the ratio of the depth of the injection chamber entrance to the thickness of cured composite. It was shown that when the pultrusion speed, viscosity of the resin and the fibre volume fraction were increased, a higher injection pressure was required to impregnate the rovings completely. However, the injection pressure required for complete impregnation was found to decrease when the compression ratio was increased.

Jeswani et al. (2007, 2008, 2009) simulated the effects of multiple resin-injection ports and geometry of the injection chamber on the resin impregnation process. It was shown that lower injection pressures were required for injection of the resin via slot-injection when compared to

discrete port-injection. Jeswani and Roux (2010) also investigated the situation where the resin-injection chamber was detached from the die. A schematic illustration of the detached die resin-injection pultrusion design is shown in Figure 7. It was shown that lower injection pressures were required for the detached die designs.

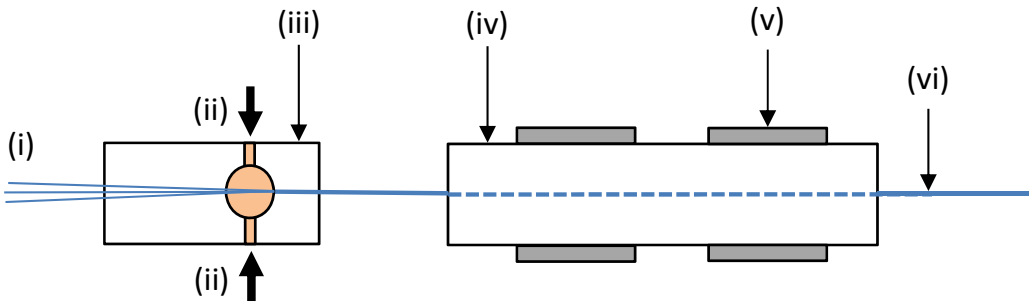


**Figure 7 Schematic illustration of the design of the detached die resin-injection pultrusion system. The key components are coded as follows: (i) rovings; (ii) resin injection under pressure; (iii) resin-injection chamber; (iv) die; (v) heating elements; and (vi) cured composite.**

Palikhel et al. (2012) also investigated the pultrusion of composites using a detached die resin-injection system. They concluded that using compression ratios of 3 and 4, a resin injection pressure of 0.002 MPa was suffice to impregnate the rovings as compared to 1.72 MPa when the compression ratio was 1. The reason for this decrease in the injection pressure was that at higher compression ratios (3 to 4), the filaments in the rovings were not packed as tightly as in the case with lower compression ratios (1 to 2); thus it was said to be easier for the resin to impregnate the rovings.

Recently, Bansal et al. (2012) conducted a comparative study on the effect of the dimensions and shape of the resin-injection chamber on the impregnation of the rovings for the detached die resin-injection pultrusion process. Three geometries of the resin-injection chamber were considered as shown in Figure 8(a-c). Subsequent to evaluation of composites produced using

these chambers, it was concluded that the conical resin-injection chamber as shown in Figure 8(c) impregnated the rovings more efficiently than the other two designs.

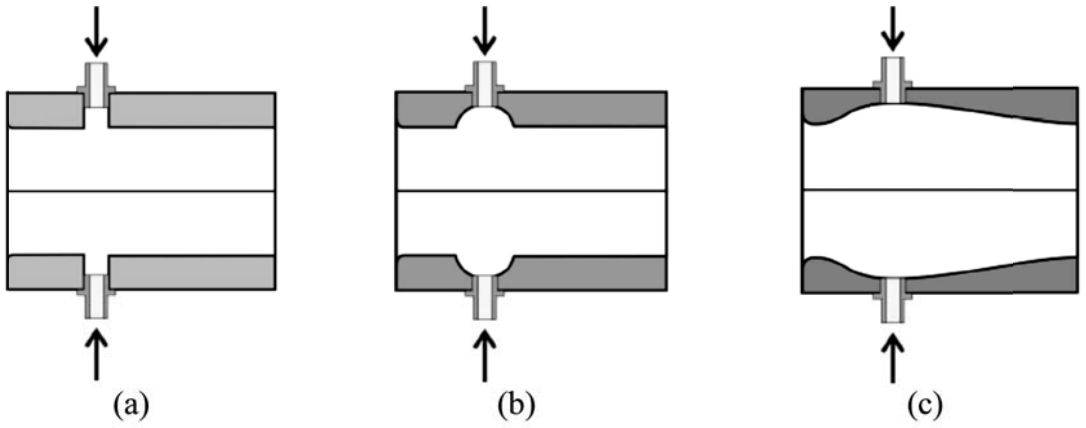


**Figure 8 Schematic illustrations of the resin-injection chambers used by Bansal et al. (2012): (a) straight-through resin-injection chamber; (b) semi-spherical resin-injection chamber; and (c) conical resin-injection chamber.**

## 2.2 FIBRE SPREADING

### *2.2.1 Rationale for fibre spreading*

The process of "fibre spreading" can be defined as lateral separation of the individual filaments within a roving in such a way that the thickness of the roving is decreased with a corresponding increase in the width. The motivation behind spreading the rovings is to aid the impregnation process. With reference to Equation 2, it can be seen from Darcy's equation that reducing the transverse dimension of the roving reduces the time required for through-thickness impregnation (Irfan et al., 2011, Pandita et al., 2012):

$$t = \frac{\eta}{2K}\frac{Z^2}{\Delta P} \qquad \textbf{Equation 2}$$

where $t$ is the time required for the resin to penetrate the roving, $Z$ is the thickness of the roving, $\eta$ is the viscosity of the liquid, $K$ is the coefficient of permeability and $\Delta P$ is the pressure differential across the thickness. A simulation of Equation 2 is presented in Figure 3 where it can be seen that a reduction in the thickness of the roving leads to a corresponding decrease in the time taken for through-thickness impregnation.

The relationship between the thickness and the width of the roving can be obtained from Equation 3:

$$Z = \frac{W}{A} \qquad \textbf{Equation 3}$$

where $W$ and $A$ are the width and cross-sectional area of the roving respectively. It is assumed that the profile of the spread roving was rectangular. A graphical representation of Equation 3 is presented in Figure 9.

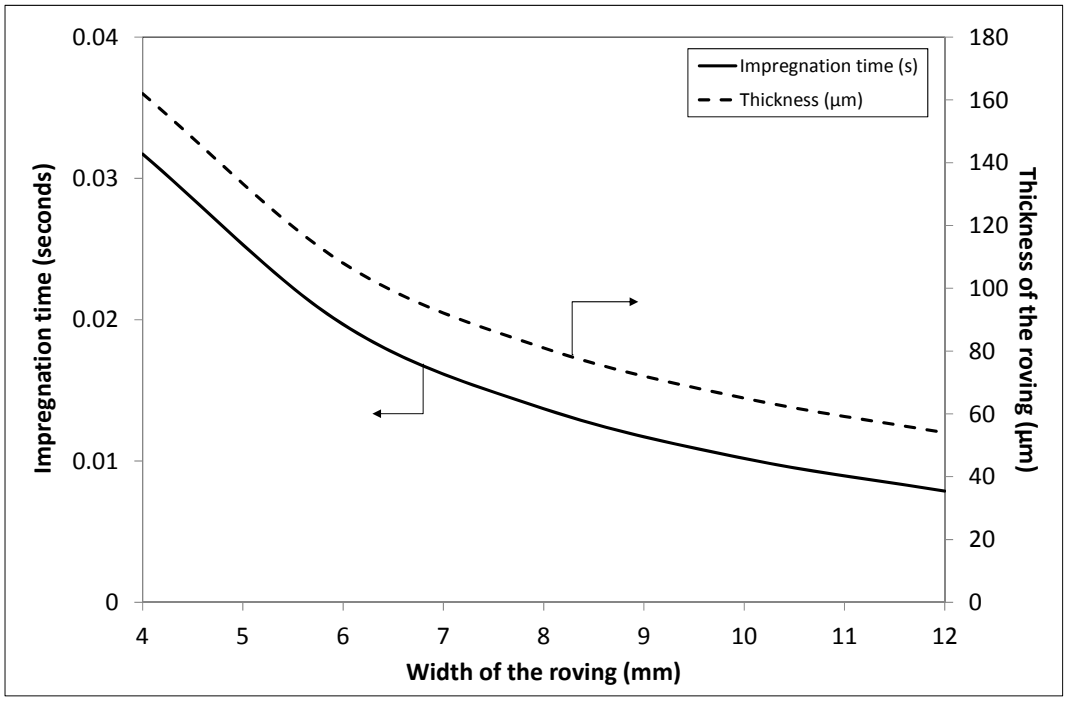


**Figure 9 Simulation of the effect of fibre spreading on the impregnation time and roving thickness (Pandita et al., 2012).**

A number of fibre spreading techniques have been reported in the literature and these can be broadly classified as: (a) mechanical; (b) vibration; (c) pneumatic; (d) acoustic; and (f) electrostatic. Regardless of the technique that is used to induce fibre spreading, following requirements need to be considered:

(i) *Minimal damage to the fibres*: The forces involved in the lateral spreading of rovings may cause the damage to the fibres. Excessive fibre damage can be detrimental to the mechanical properties of the composite. During the production of glass fibres, the individual filaments are coated with a binder solution which serves as a lubricant to minimise abrasion damage. The binder also serves to "bond" the individual filament together. In order to enable the efficient lateral spreading of the individual filaments within a roving, the mechanical integrity of the binder has to be broken without inducing secondary damage to the reinforcement (Fernando et al., 2009).

(ii) *Health and Safety*: The generation of air-borne silica particles is an issue during the separation of glass fibres. Any respirable fibre particles can be a potential health risk to the respiratory system (Christensson et al., 1999).

(iii) *Extent of fibre spreading*: This will depend predominantly on the fibre type and the intended production method for the composite. With thermosetting resin systems and manufacturing techniques such as pultrusion and filament winding, a reduction in the apparent "thickness" of the roving will aid transverse impregnation (Pandita et al., 2012). In situations where "centre-pull" creels are used, the roving is unwound from the inner bore; this induces a twist in the roving. The degree of fibre spreading will be influenced adversely by the degree of twists (Irfan et al., 2011).

### *2.2.2 Techniques for fibre spreading*

A review of the techniques (Fernando et al., 2009) used to spread the filaments in a roving is presented in this section where the majority of the reports are patents.

#### 2.2.2.1 Mechanical

Van den Hoven (1981) described a cylindrical guide with an array of grooves for changing the width of continuous textile filaments, see Figure 10. With this arrangement of grooves, it was stated that it was possible to control the width of the roving by rotating the cylindrical guide roller to the required angle until the desired width was reached. This technique can cause snagging and damage to the glass rovings if they are twisted.

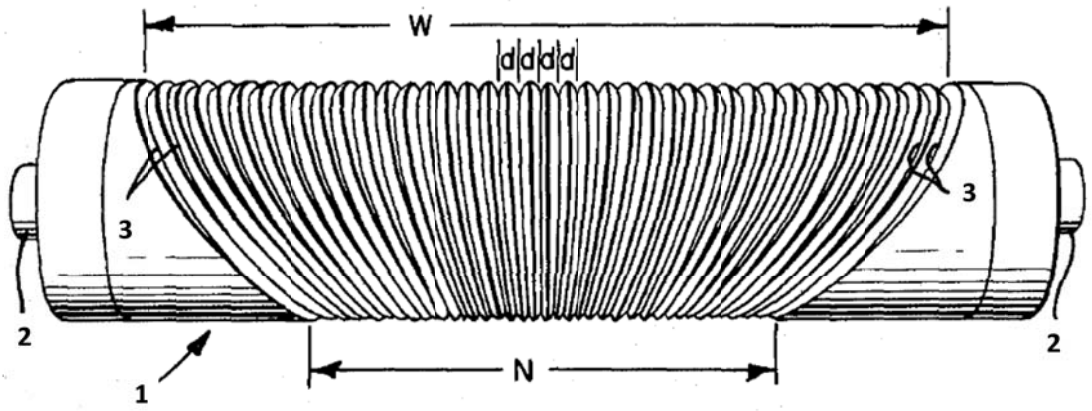


**Figure 10 Schematic illustration of the grooved roller with non-parallel grooves. Adapted from Van den Hoven (1981). The numbered items are as follows: (1) grooved guide; (2) shaft; (3) grooves; (N) minimum dimension; (W) maximum dimension; and (d) distance between consecutive grooves.**

Nakagawa and Ohsora (1992) discussed the use of bevelled rollers to induce the spreading of rovings. Convex rollers which had their respective axis mounted on a circular platform were used to induce fibre spreading.

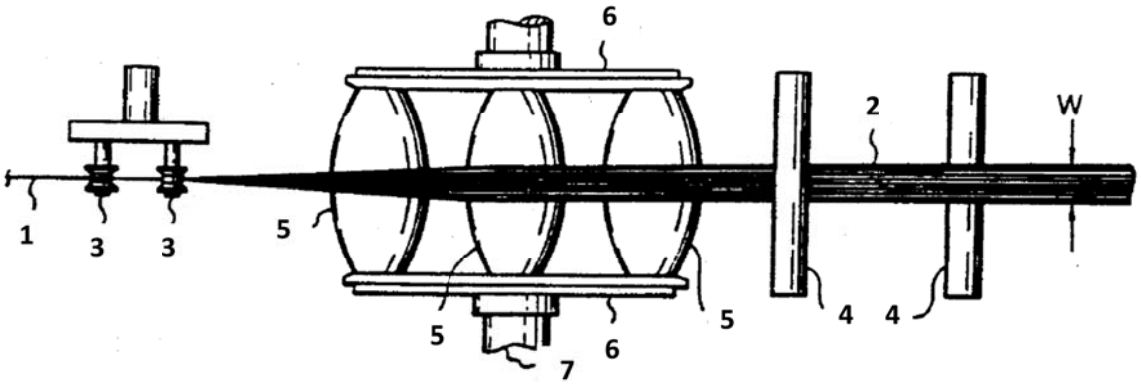


**Figure 11 Schematic illustration of the bevelled rollers. Adapted from Nakagawa and Ohsora (1992). The numbered items are as follow: (1) un-spread fibre roving; (2) spread fibre roving; (3) guide rollers; (4) fixer rollers; (5) four roller elements; (6) disk plates; (7) rotating shaft; and (W) width of the spread roving.**

The bevelled roller elements had a radius of curvature in the range 30 mm to 100 mm. It was mentioned that the smaller the radius of curvature, the larger the width of the fibre separation. However, it was stated that for bevelled rollers with a smaller radius of curvature, the probability of the fibres falling to the sides was greater. Similar conclusions were also

reported by Bates (1988). The rationale for mounting the bevelled pins on a rotating carousel is reasonable as it would reduce wear and the friction between the contact surface and the fibres. However, the efficiency of the spreading will be dependent on the rotation rate of the carousel and the haul-off rate of the rovings. Furthermore, the spacing between the bevelled rollers will also have a significant effect on the degree of spreading. Marissen et al. (2000) also illustrated the use of powered rotating bevelled pins for pultrusion of thermoplastic resins. Regrettably, little information was provided on the geometry of the rollers and its effects on fibre spreading.

Lifke et al. (2000) proposed the system illustrated in Figure 12 for spreading rovings. The proposed design consisted of expandable tubes between two angled support discs, as shown in Figure 12.

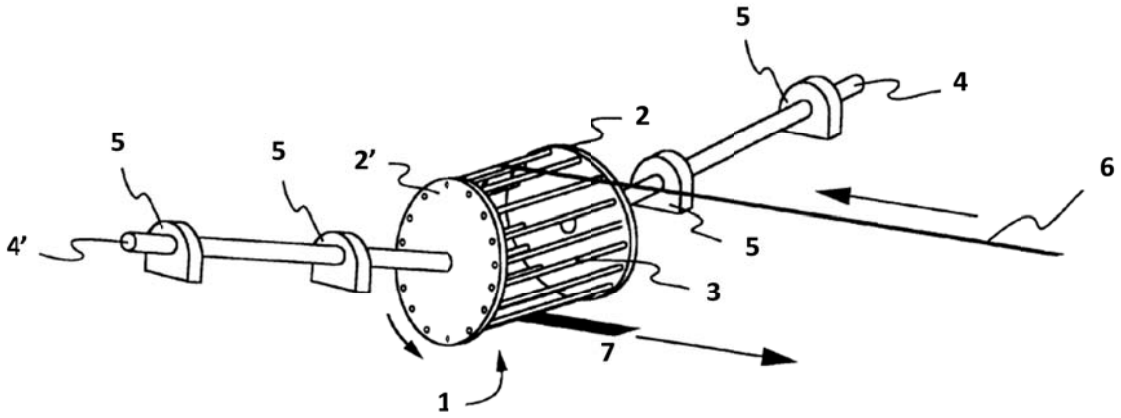


**Figure 12 Isometric view of the expandable fibre spreaders described by Lifke et al. (2000). Numbered items are as follow: (1) fibre spreader; (2, 2') support discs; (3) expandable bands; (4, 4') shafts; (5) supporting bearings; (6) inlet roving; and (7) spread roving.**

The proposed invention was claimed to be satisfactory for a variety of fibres including glass and carbon. The inventors claimed that their proposed setup could provide improved fibre spreading when compared to pneumatic, electrostatic, vacuum or vibration-based techniques. It was further claimed that the proposed process was flexible in that: (a) the support disk

angles could be varied; (b) a number of spreaders could be used to obtain the desired degree of fibre spreading; and (c) different operating speeds could be used, ranging between 3 m/min to 90 m/min. This is an ingenious design that is aimed at overcoming some of the problems associated with fixed-pin fibre-spreaders. For example, it overcomes the issue of the tension associated with the use of multiple static pins. The plates holding the pins can flex and one of them is angled in relation to the opposite face; this, in effect will serve as a bevelled roller. A perceived drawback with this design is that at high fibre tensions, there could be a tendency for the side-plates to bend inwards thus serving as a convex roller.

Krueger (2001) proposed a spreading system consisting of rollers with a group of pins attached to its outer surface for improved and controlled spreading of rovings. This design was said to give uniform fibre spreading. However, the fine pins on the surface of the roller could cause damage to the twisted rovings. Kiss et al. (2002) described the combined use of smooth grooved rollers and crown splitter-bar for spreading and subsequently splitting a carbon fibre tow. This technique may work for fibres without any twists. It is envisaged that the proposed device will induce significant damage to twisted reinforcing rovings**.**

Guirman et al. (2005) used a process where curved rollers termed as “banana bars” were used to spread the rovings. Unfortunately, details were not provided about the geometry of the curve rollers. In effect, the geometry presented in Figure 13 (component 3c) is similar in function to the bevelled pin as the fibres are in contact with the convex portion of the bent bar.

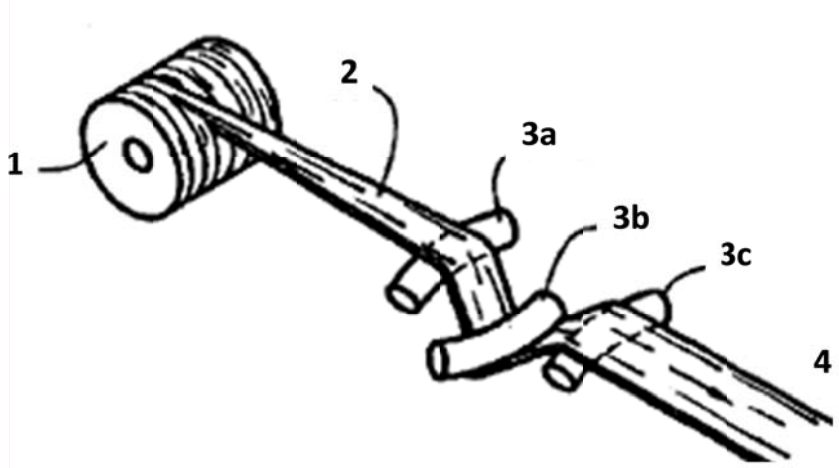


**Figure 13 Schematic of the curved "banana" rollers proposed by Guirman et al. (2005). Numbered items are as follow: (1) fibre spools; (2) un-spread roving; (3a, 3b and 3c) curved bars; and (4) spread roving.**

#### 2.2.2.2 Vibration

Yamamoto et al. (1988) presented a method for manufacturing prepregs where fibre spreading was achieved using freely-rotating vibrating rollers. The reinforcements mentioned were organic or inorganic fibres with and without sizing. In the case of sized fibres, a furnace was used prior to spreading means to burn-off the sizing and thus improving spreading.

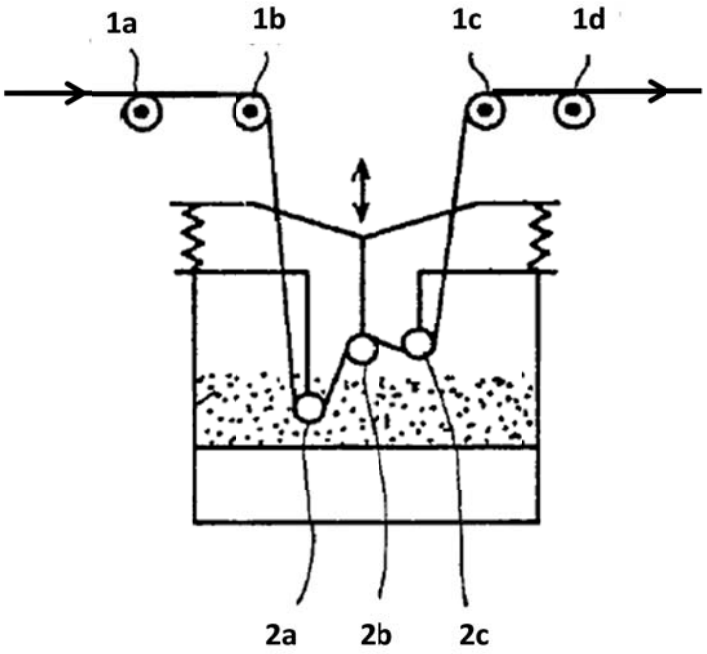


**Figure 14 Schematic illustration of the fibre spreading setup proposed by Yamamoto et al. (1988). The numbered items are as follow: (1a, 1b, 1c, and 1d) guide rollers; (2a, 2b and 2c) freely rotatable rollers; and horizontal arrows show the fibre direction.**

It was recommended that tension should be applied during the spreading process but it should not be very high as a higher tension could cause fibre damage. Rollers were vibrated at 20 - 40 Hz; the amplitude of the vibration was 0.3 - 2 mm. The spread rovings were directed to an impregnation chamber for further processing.

Sager (1990) proposed a method using vibrating rollers (or rods) for spreading the rovings. The vibration was achieved by magnetic means or by an electrical frequency generator. It was claimed that use of vibration for achieving fibre spreading reduced the extent of fibre breakage and increased the operating speed of the manufacturing process. A schematic illustration of the proposed device is presented in Figure 15. It was stated that the fibres could be glass or carbon having about 2000 filaments in a single roving. It is proposed that this technique will not be efficient in situations where the filaments are held by a binder as the energy required to ensure de-cohesion of the binder may not be sufficient with a single pin and vibration.

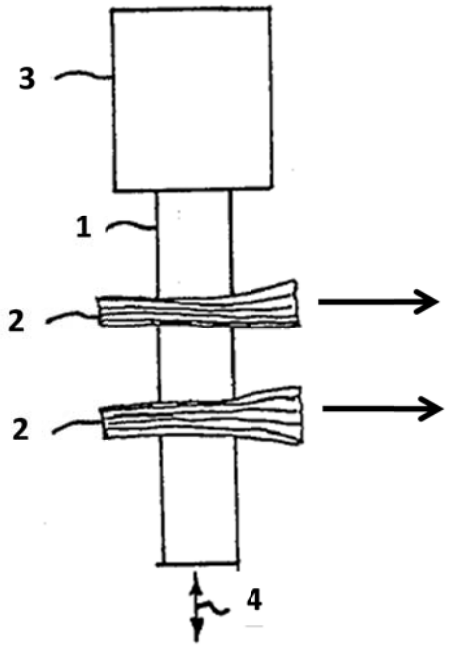


**Figure 15 Schematic illustration of an axially vibrating rod for spreading rovings proposed by Sagar (1990). The coded items are as follow: (1) round metal rod; (2) rovings; (3) vibrating device; and (4) vibration direction.**

Akase et al. (2000) proposed a fibre spreading setup, as shown in Figure 16, where they used rollers with different diameters, across which rovings were passed at sharp angles, to induce lateral spreading. Some of the rollers were vibrated in axial direction to enhance the spreading; this method was used for the production of prepregs.

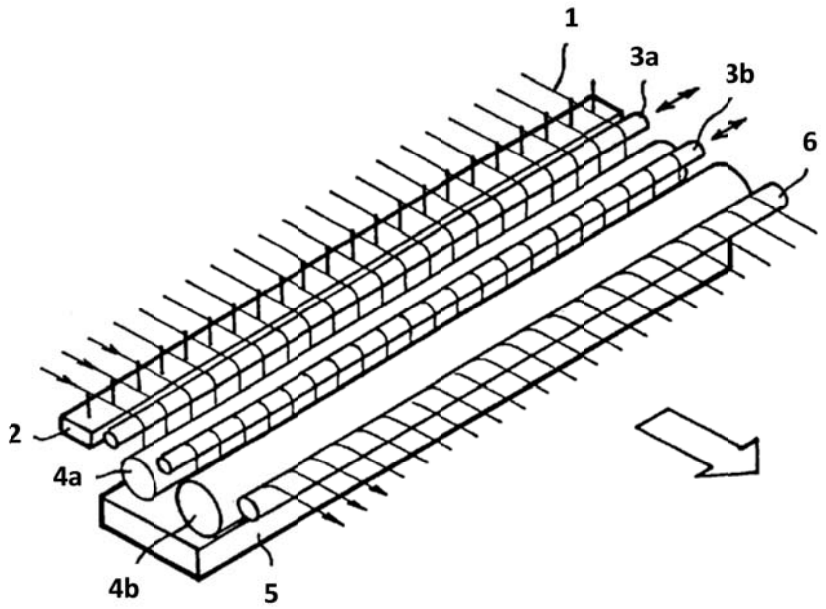


**Figure 16 Schematic illustration of the fibre spreading rollers proposed by Akase et al. (2000). The numbered items are as follow: (1) fibres; (2) comb; (3a and 3b) vibrating rollers; (4a and 4b) non-vibrating rollers; (5) roller heating means; and (6) free revolving rollers.**

With reference to Figure 16, the key features of this patent are as follows: (a) vibrating rollers (20 to 50 mm diameter) in the axial direction with a frequency within the range of 3 to 60 Hz; (b) pressing the reinforcing roving onto the surface of a roller (50 to 120 mm diameter) located immediately downstream of the vibrating roller; (c) 2 to10 pairs of rollers could be involved in the spreading operation; (d) the distance between the vibrating and non-vibrating rollers was in the range 10 to 100 mm; and (e) fibres throughput rates were 4.8 to 30 m/min. The fire spreading device was said to be applicable for glass, carbon or polyaramid fibres. In a proposed modification of the roller system, it was mentioned that either vibrating or non-

vibrating rollers could be heated (70 to 140 °C) to reduce the effect of fibre sizing or binder system.

Tanaka et al. (2004) proposed a fibre spreading method using mechanical and vibration means using a series of rollers. In addition to rollers which were in contact with the rovings continuously, a separate reciprocating member e.g. vibrating roller, which contacts fibres periodically was proposed to achieve enhanced fibre spreading. The reciprocating member was vibrated between 1 and 100 Hz.

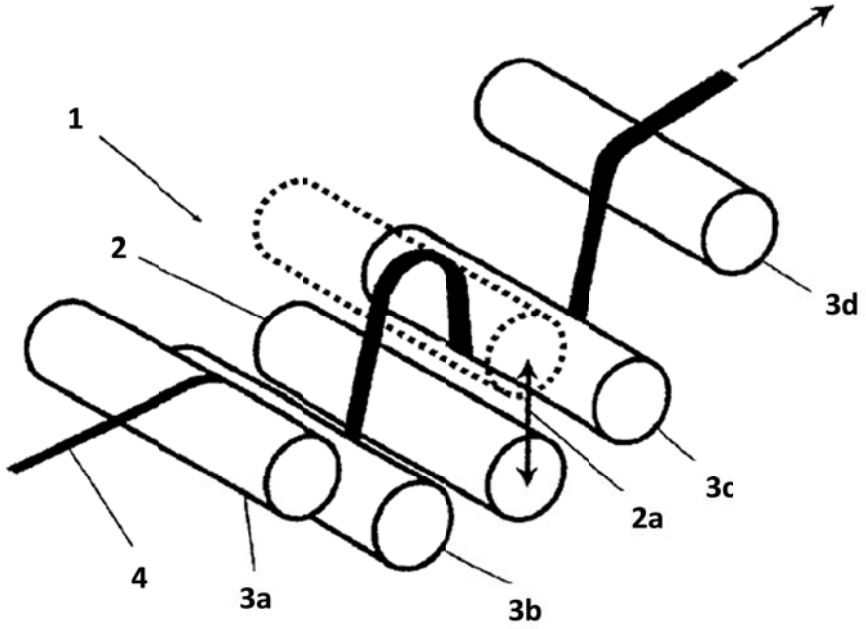


**Figure 17 Schematic illustration of the fibre spreading rollers proposed by Tanaka et al. (2004). The numbered items are as follow: (1) fibre spreading device; (2) reciprocating rollers; (2a) movement of reciprocating rollers; (3a, 3b, 3c and 3d) fixed rollers; and (4) roving.**

In a proposed modification to the roller system, it was mentioned that either vibrating or non-vibrating rollers could be heated in the range 70 to 250 °C to reduce the effect of the fibre sizing. In another proposed modification, the use of gas to further enhance fibre spreading was proposed. This patent essentially follows the same approach as discussed by Akase et al. (2000); both these patents originated from Toray Industries, Inc., Japan.

#### 2.2.2.3 Pneumatic/Vacuum

Daniels (1971) described a process for pneumatically-assisted spreading of carbon tows. In this process, the carbon tow was introduced through a Venturi-based spreader where the air was blown in opposite direction. Pryor (1985) discussed a manufacturing process for cigarette filters, in which, high velocity gaseous jets were used to spread the fibres in one of the steps. There is no doubt that this technique will be efficient in "volumising" the tow but its impact on impregnation and the resultant void content would be negative. It is also envisaged that this mode of separating the filaments could potentially be more damaging to their mechanical properties.

Chung et al. (1986) proposed a device for manufacturing prepregs from thermoplastic resin and carbon fibres as shown in Figure 18. They used gas jets at pressures in the range 275 – 415 kPa to spread carbon tows. A similar technique was later reported by Ames et al. (2001). The air-jet fibre separating device consisted of a box into which compressed air was fed through an adjustable gas metering device. One or more gas injection ports were positioned at right-angles to the moving fibre to enable the air-jet to impinge on the fibres in a perpendicular direction thus inducing fibre separation. McMohan et al. (1989) suggested a modification of the gas jet system in which two thermoplastic fibres were intermixed with carbon fibres after spreading them separately. Thermoplastic fibres were spread using a yarn separating comb whilst gas-jets were used for carbon fibre as discussed by Chung et al. (1986).

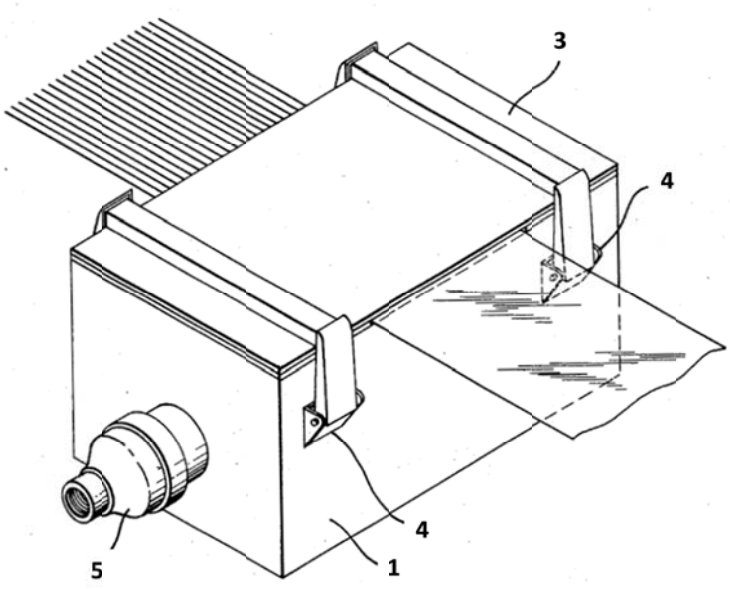


(a)

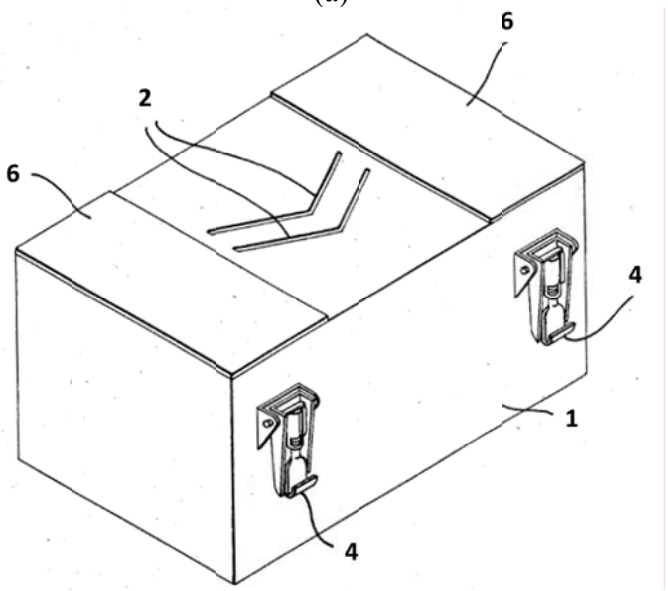


(b)

**Figure 18 Schematic illustration of the gas jet system used for fibre spreading by Chung et al. (1986) (a) closed apparatus in operation and (b) top opened. The numbered items are as follows: (1) gas box; (2) gas exit ports; (3) air box cover; (4) attachment clamps; (5) adjustable gas metering means; and (6) shims.**

Baucom et al. (1991) reported on a technique that employed "side air suction" where the rovings are 'pulled' apart to achieve fibre spreading. The efficiency of this technique in inducing fibre separation is debatable as the tension on the fibres within the chamber will

have to be reduced to enable lateral movement. Furthermore, it is not clear as to how a twisted roving will perform as far as lateral separation of the filaments is concerned.

Newell and Puzianowski (1999) developed a pneumatic fibre spreading system for spreading Kevlar and carbon fibres; this was based on the Venturi effect.

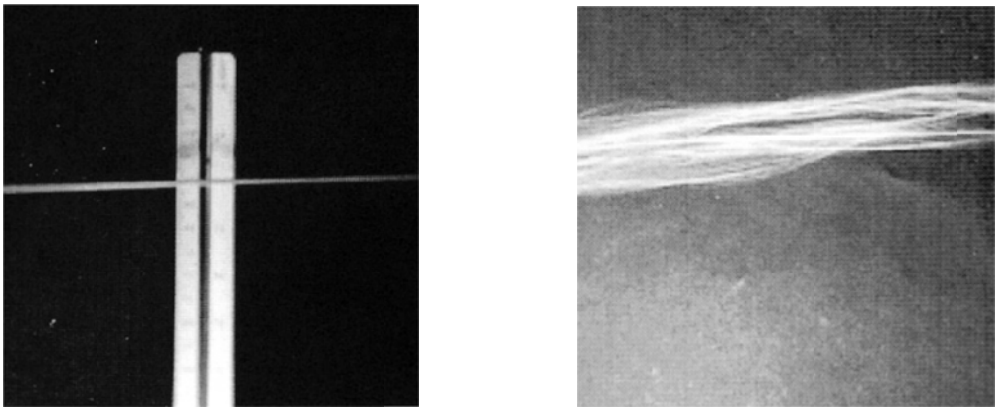

(a) (b)

**Figure 19 Photograph of a Kevlar tow used in the spreading experiments by Newell and Puzianowski (1999): (a) as-received; and (b) after spreading.**

The extent of fibre spreading was evaluated using high-speed photography. It was noted in previous studies that high-tension in the rovings would reduce the extent of spreading and this issue was resolved by incorporating pinch rollers to guide the rovings to spreading setup. Two axial Venturi fibre spreaders were used in series to accomplish fibre spreading. It was concluded that a combination of pinch rollers and Venturi chambers could provide a means for achieving efficient fibre spreading.

With reference to Figure 19b, the net outcome is best described as "volumised" tow as opposed to a spread tow. This distinction needs to be made as most fibre spreading techniques based on pneumatics will tend to increase the apparent "volume" of the tow (or roving). In the case of an idealised mechanical-based spreading system, the thickness of the roving is reduced along with a corresponding increase in the width.

Kawabe et al. (2006, 2008) proposed a process of fibre spreading in which downward air flow was applied to a roving whereby the force normal to the roving was said to cause spreading of the roving.

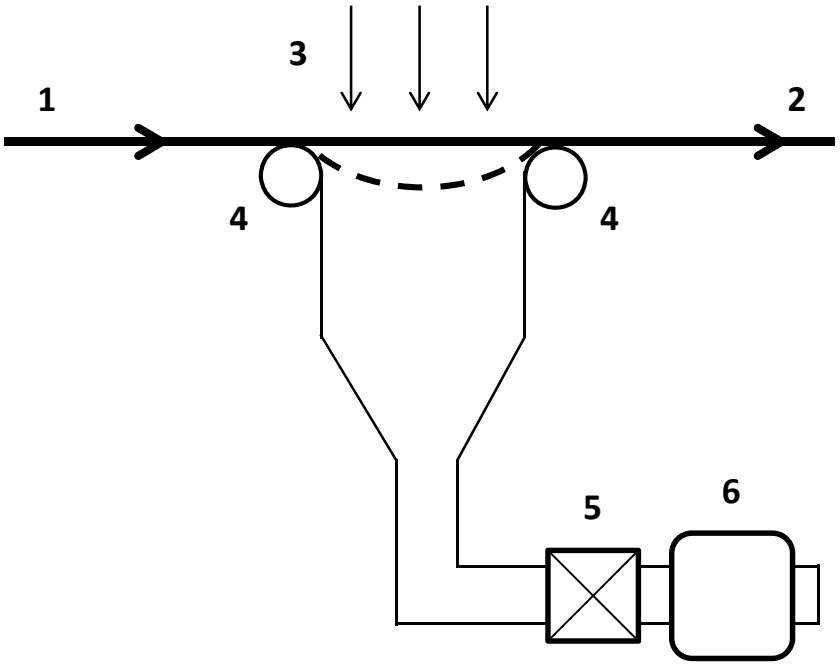


**Figure 20 Schematic illustration of pneumatic fibre spreading proposed by Kawabe and Tomoda (2006). The numbered items are as follows: (1) input roving; (2) spread roving; (3) air; (4) guide pins; (5) flow-rate adjustment valve; and (6) suction air pump. The dotted line is drawn to show the trajectory of the roving when air was applied.**

Air velocities up to 20 m/sec where used and the rovings were spread between a pair of 10 mm diameter steel cylindrical pins (see Figure 20). It was stated that heat could be applied to promote fibre spreading. In the case of an epoxy-based sizing agent, it was suggested that temperatures in the range 80-150 $^{\circ}$C could be used to heat the rovings. As with most air-based separation of fibres, containment of fibre fragments and debris is an important consideration.

#### 2.2.2.4 Acoustic

Hall (1972) described a method and apparatus for spreading a roving using a loud-speaker-based arrangement as shown in Figure 21.

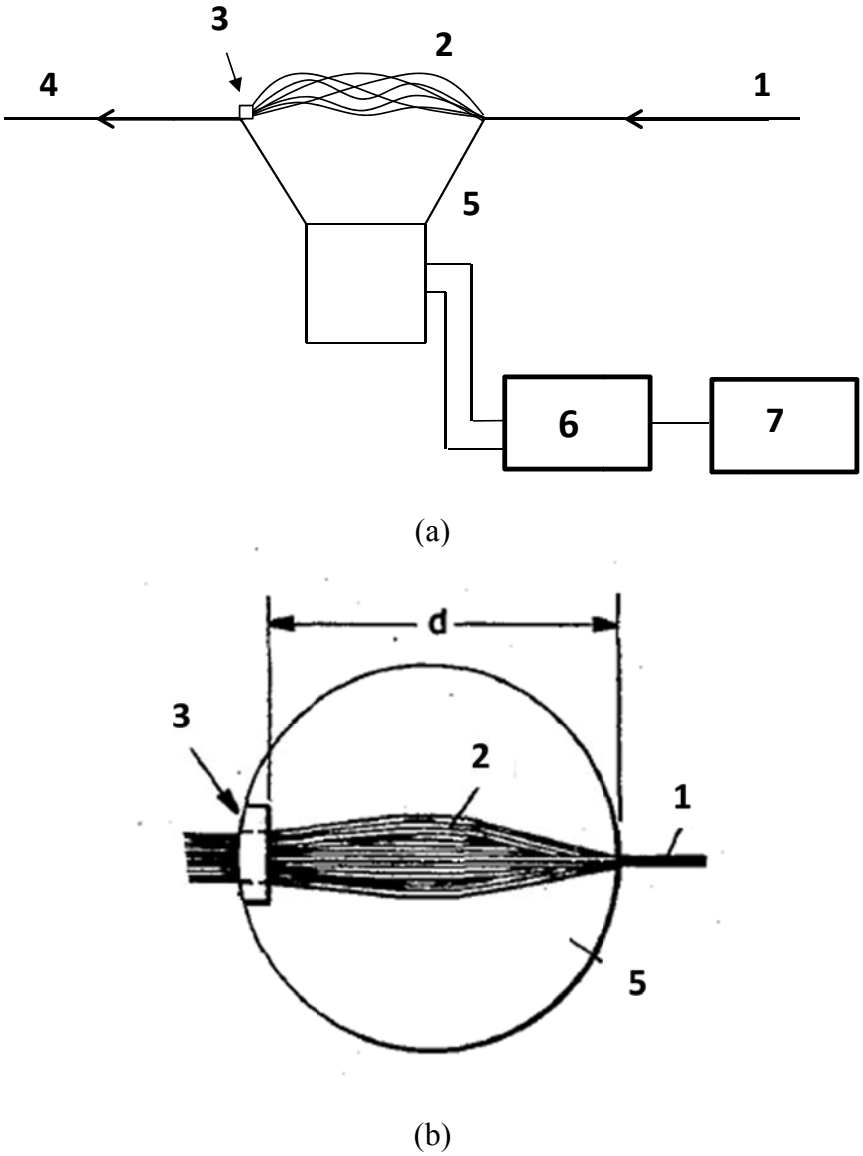


**Figure 21 Schematic illustration of the fibre spreading system proposed by Hall (1972). (a) side view and (b) top view. The coded items are as follow: (1) roving; (2) spread filaments; (3) guide; (4) spread roving; (5) loud-speaker; (6) amplifier; and (7) audio signal generator.**

The fibre spreading was achieved using a pulsating air-flow. With this method, the roving is unrestrained and can be damaged and controlling the fibre spacing within the spread roving

would be difficult. Iyer and Drzal (1991a, 1991b) tried to solve the issue of fibre damage by introducing strain in the rovings. They proposed a method for fibre spreading using acoustic energy from a speaker or alternative devices for vibrating the gaseous medium over which rovings were traversed in a zigzag manner, as shown in Figure 22. It was claimed that a pulsating flow of energy in a gaseous medium can spread the rovings and that the width of the spread roving was a function of: (a) the tension on the roving; and (b) the amplitude of the acoustic wave. They elaborated that the acoustic speakers could be operated with air or any other selected gas, for example, oxygen or nitrogen. With reference to Figure 22, the recommended audio-level in the speaker system was in the range 80 - 130 dB. The "preferred" frequency was said to be between 32 - 39 Hz, but they went on to state that it could be audio or ultrasonic, ranging from 1 - 20,000 Hz. It was also specified that the rods could be fixed or rotating.

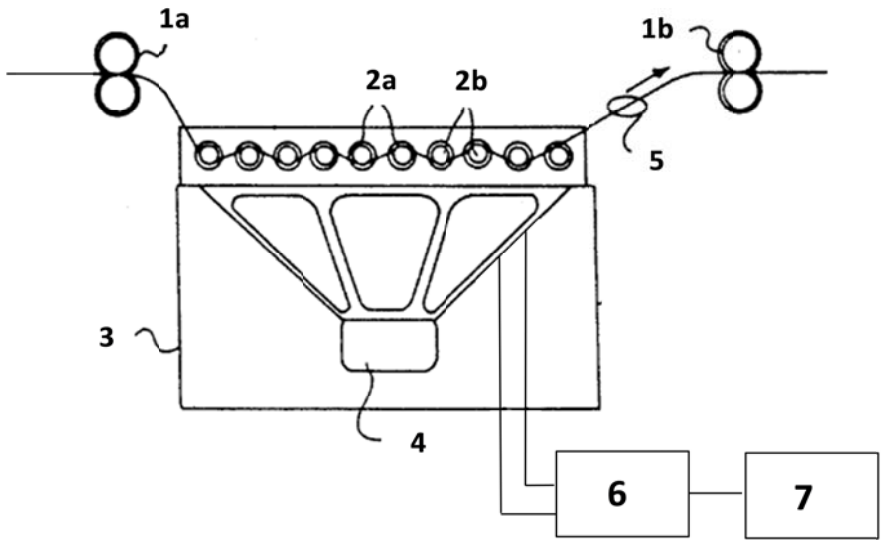


**Figure 22 Schematic illustration of the cabinet and speaker as proposed by Iyer and Drzal (1991a). The coded items are as follow: (1a, 1b) nip rollers; (2a, 2b) spreading rods; (3) speaker housing; (4) speaker; (5) fibre guide; (6) amplifier; and (7) audio signal generator.**

It is not clear if this technique could be used with rovings that possess a twist with a binder system. There is no doubt that a multiple roller based fibre spreading device will induce

significant fibre spreading but the associated tension will also be significantly high. It is also necessary to establish the relative contributions to spreading by the pins and the acoustic/ultrasonic excitation. The practicality of this device is questionable, as pins are mounted on the same pair of side-supports. In other words, rethreading any broken rovings will be difficult.

#### 2.2.2.5 Electrostatic

Many researchers have proposed electrostatic means to spread the rovings. Primarily, in all these studies, the rovings are either conductive by nature or are made conductive by some external means (Niina et al., 1964). A charge is applied on the rovings by contact-charging. Finally, the charged rovings are passed through a neutral field or a field with opposite-charge where the force of attraction between the opposite charges is utilised to spread the rovings. Various configuration have been proposed to attain the spreading by this principle (Niina et al., 1964, Uchiyama et al., 1972, Uchiyama et al., 1973, Sternberg, 1976, Peritt et al., 1993, Nestler et al., 2007).

Yamamoto et al. (1988) has discussed that electrostatic-based fibre separation may not provide uniform spreading and that it could cause fibre damage or 'fuzzing'. Most of the reported work on the deployment of electrostatics for fibre spreading is concerned primarily with carbon fibres.

### *2.2.3 Hypothesis on mechanically-induced fibre spreading*

In the current study, a mechanical means for spreading the rovings was developed. Mechanically induced fibre spreading is generally achieved by passing the rovings over fixed pins or rollers. A schematic illustration of an as-received and a spread roving, over a pin, is shown in Figure 23.

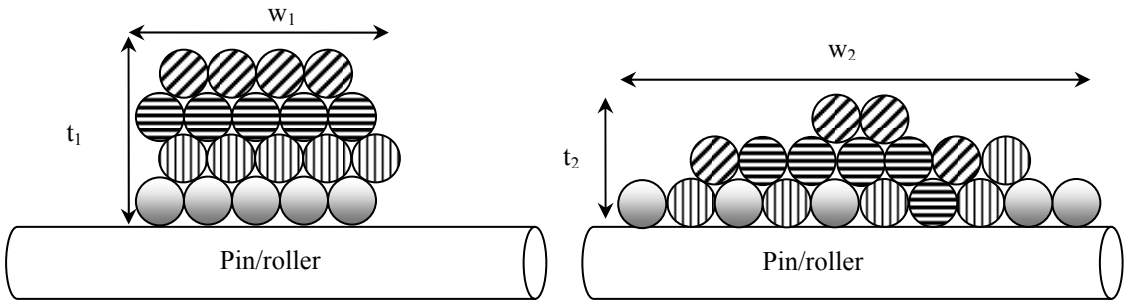


(a) (b)

**Figure 23 Schematic illustration of a roving on a pin or roller: (a) as-received roving; and (b) spread roving. Here $t_1 > t_2$ and $w_1 < w_2$. (Irfan et al., 2011)**

With reference to Figure 23(a), the idealised spatial location of each layer of the reinforcing fibres in a roving is indicated. The nominal thickness and width of the as-received roving is represented by '$t_1$' and '$w_1$' respectively. In reality, the meandering of the individual filaments cannot be controlled accurately. However, in an idealised case, when the roving is traversed over a pin, the tension on the fibres will try and force them into the interstitial spaces. In other words, the fibre layer that is in intimate contact with the pin will be forced sideways to accommodate the fibres above it. This is illustrated in Figure 23(b) where the fibres from the second layer are forced down. The same scenario can be envisaged with the fibre layers that are above the second layer of fibres. The sideways movement of the fibres will be influenced significantly by the tension on the fibres and the friction between the fibres and the pin. If the tension is too high, lateral movement will be impeded and hence the degree of spreading will be lower. The degree of adhesion between the binder and the fibres and the inter-fibre friction will also dictate the ease with which fibre spreading can be achieved.

The question of whether a pin or roller is better for inducing fibre spreading is not straightforward. Intuitively, the roller will afford a lower degree of friction between the fibres and the surface of the roller. However it is speculated that the forces that the fibres into the interstitial spaces as described previously will be lower. Hence, the degree of fibre spreading

for a given set of conditions is likely to be higher for a pin when compared to an equivalent diameter roller (Fernando et al., 2009).

### *2.2.4 Wilson's model*

Wilson (1997) proposed a mathematical model to estimate the lateral spreading of fibres in a roving under tension as it was made to pass over a bar. The proposed model used the cross-sectional area of the roving and the lateral displacement of the bar to estimate the fibre spreading. In order to correlate various parameters influencing the geometry of the roving, frames of reference corresponding to the initial and final positions of the roving were defined. The location of the bar with respect to the initial position of the roving, the roving geometry and the resultant of the tension components acting on the fibres in the roving across the width of the bar were considered in this model. The model does not account for the frictional forces between the fibres or between the fibres and the bar. The roving was assumed to have no twisting or entanglement of fibres and no relative motion between the fibres in the longitudinal direction.

Following equation was derived to estimate the width of the roving:

$$W = (12\,AH)^{1/3} \qquad \textbf{Equation 4}$$

where $W$ is the estimated width of the spread roving, $A$ is the cross-sectional area of the roving and $H$ is the lateral displacement between two cylindrical spreading bars defined as $L\cos\alpha$.

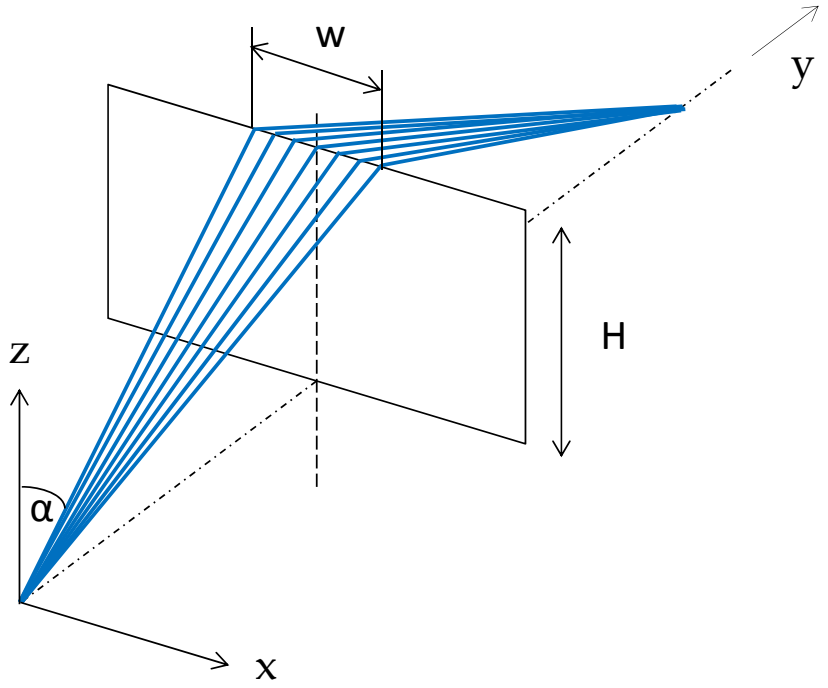


**Figure 24 Schematic illustration of the experimental setup used by Wilson (1997). Here *H* is the lateral displacement and *W* is width of the spread roving.**

Wilson (1997) investigated the spreading of a polyamide rovings consisting of $10^5$ filaments with an average diameter of 23 μm. A tow of cotton yarns consisting of about 600-700 threads was also used in a separate experiment. The degree of fibre spreading was found to be independent of the tension in the roving and the mode of gripping of the roving. The model estimates were compared against the experimental measurements and were found to differ with in 10-15%.

The model proposed by Wilson (1997) was extended by Irfan et al. (2011) for estimating the spreading over second bar in a symmetric configuration. Experiments were also conducted to study the effect of changing the lateral displacement (*H*) by changing *L* and *α* independently. Further details are presented in the Appendix-B of this thesis (Irfan et al., 2011).

## 2.3 RESIN IMPREGNATION

The impregnation of the reinforcements with the resin is one of the process factors, in any composite manufacturing process, which must be controlled carefully in order to obtain composites of good quality. The mechanical properties of composites such as the inter-laminar shear strength (ILSS), compressive strength, impact resistance and fatigue life, are reduced as a results of voids (Peltonen and Järvelä, 1992, Lackey et al., 1997, Binetruy et al., 1998, Shaw-Stewart and Sumerak, 2000).

In a bed of uniformly distributed spheres, as shown in Figure 25(a), the resin impregnation is generally assumed to be independent of direction of flow. However in an ideal roving, as shown in Figure 25(b), the ability of the resin to infiltrate the filaments is different with respect to the axial (x-direction), transverse (y-direction) and through-thickness (z-directions) directions.

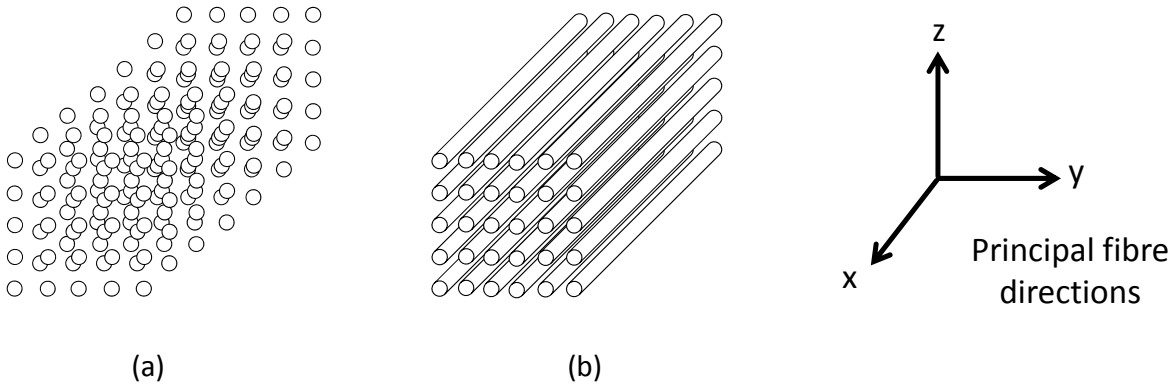


**Figure 25 Schematic illustration of: (a) an idealised porous structure consisting of uniformly distributed spheres; and (b) an idealised array of unidirectional filaments in a roving.**

### *2.3.1 Basic equations relating to impregnation*

Generally, Darcy's law is used to describe the flow of a resin through fibrous reinforcements. It can be written in a generalised form as (Gebart, 1992):

$$q = \frac{K}{\mu}\frac{\Delta P}{Z}$$ **Equation 5**

where $q$ is the flow rate of the fluid per unit area, $K$ is described as the coefficient of permeability, $\Delta P$ is the liquid pressure drop over a filament bed of thickness $Z$ and $\mu$ is the Newtonian fluid viscosity. By integrating Darcy's equation, the following expression is obtained for the time required for the impregnation of a roving with thickness ($Z$):

$$t = \frac{\mu}{2K}\frac{Z^2}{\Delta P}$$ **Equation 6**

where $t$ is time required to impregnate the roving with thickness ($Z$). An inspection of the above equation reveals that in order to accelerate the impregnation, a number of conditions must be fulfilled. These include: (i) higher values for the driving pressure ($\Delta P$) and permeability coefficient ($K$), and (ii) lower values for the resin viscosity ($\mu$) and the roving thickness ($Z$).

Foley and Gillespie (2005) expressed the integrated form of Darcy's law in terms of a cylindrical co-ordinate system:

$$t_{imp} = \mu(1 - v_f)r_o^{\,2}\left[\frac{c_1^{\,2}(\ln(1/c_1)^2 + 1) - c_2^{\,2}(\ln(1/c_2)^2 + 1)}{4K_p(P_c + P_{app})}\right]$$ **Equation 7**

where $K_p$ is the coefficient of permeability in the radial direction, $P_c$ is the capillary pressure, $P_{app}$ is the applied (mechanical) pressure, $\mu$ is the viscosity of the resin, $v_f$ is the fibre volume fraction of the roving, $c_1$ and $c_2$ are the parameters relating the radius of the roving to the flow-front. With reference to Figure 26, $r_i$ is the infiltrated roving radius and $r_o$ is the radius of the roving. The parameters $c_1$ and $c_2$ vary from 1 (un-impregnated roving) to $r_f/r_o$ (fully impregnated roving), and here $r_f$ is the radius of a single filament. The above-mentioned

relationship was based on the principle of progressive motion of the resin between the fibres inside a circular roving as discussed by Lee and Springer (1987).

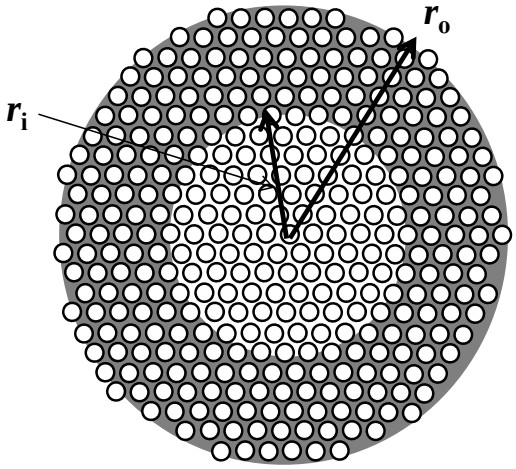


**Figure 26 Schematic illustration of the fibre impregnation in a circular roving (Foley and Gillespie, 2005). The grey region represents resin impregnated area.**

Equation 7 was modified for a rectangular roving by Pandita et al. (2012):

$$t_{imp} = \eta(1-v_f)Z^2\left[\frac{s_1^{\,2}(\ln(1/s_1)^2+1)-s_2^{\,2}(\ln(1/s_2)^2+1)}{4K_T(P_c+P_{app})}\right] \qquad \textbf{Equation 8}$$

where $K_T$ is the coefficient of transverse permeability and $Z$ is the thickness of the roving. $s_1$ and $s_2$ are the parameters for a rectangular array of rovings corresponding to $c_1$ and $c_2$. A schematic illustration of the rectangular roving considered by Pandita et al. (2012) is shown in Figure 27.

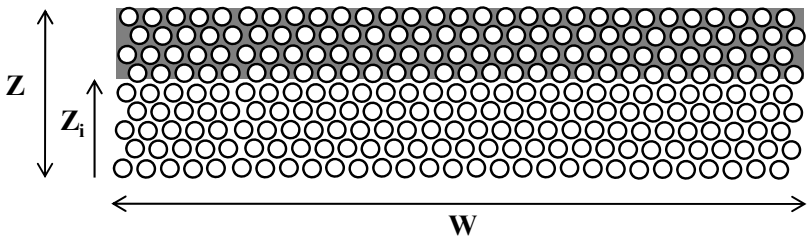


**Figure 27 Schematic illustration of fibre impregnation in an array of a rectangular rovings (Pandita et al., 2012). The grey region represents the impregnated area. Here $Z_i$ is the thickness of the roving that is not impregnated.**

It can be seen from Equations 6 and 8 that decreasing the thickness of the roving will aid transverse resin impregnation. The effect of fibre spreading (width) on the time required for impregnation is shown in Figure 28.

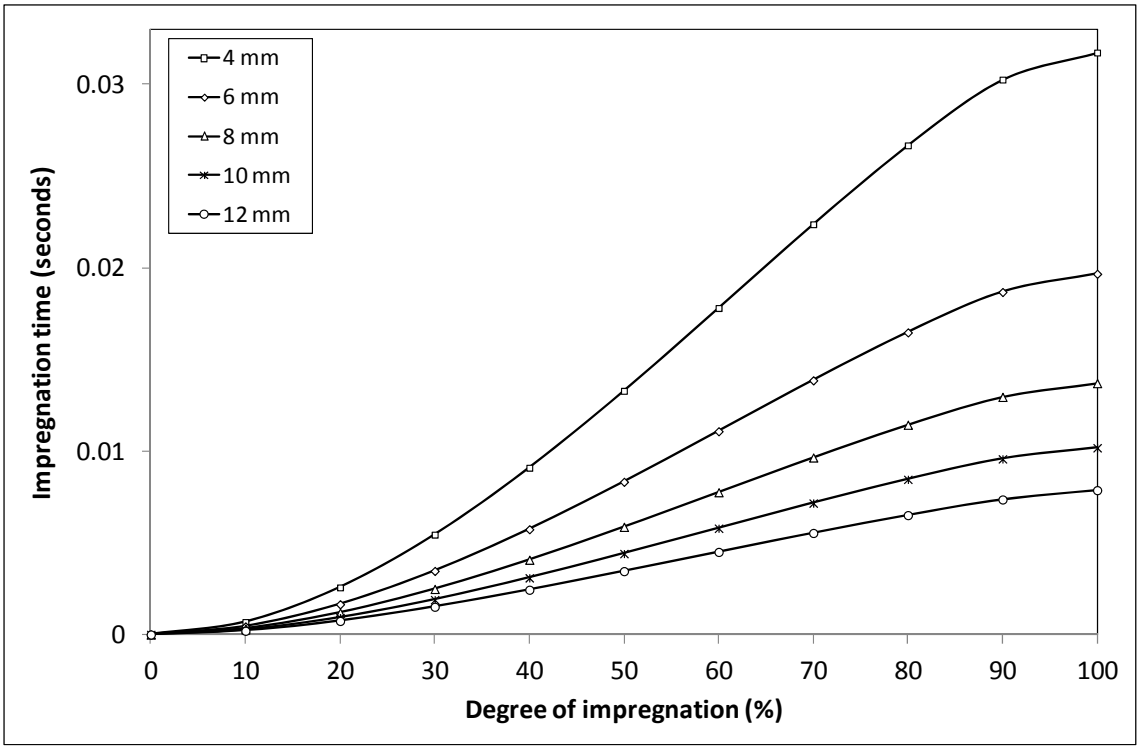


**Figure 28 Simulation of Equation 8 showing the relationships between the degree of impregnation and the impregnation time for rovings of specified widths (Pandita et al., 2012).**

The impregnation curves shown in Figure 28 are applicable where the roving is stationary and the primary impregnation is in the transverse direction. However, the impregnation for continuous composite manufacturing processes such as pultrusion, where the roving is being hauled-off, is more complicated. Here, due consideration needs to be given to parameters such as the linear haul-off rate of the roving ($V$), the tension in the roving ($T$), the mechanism of resin pick-up and the interactions between the moving roving with the static components of the resin impregnation unit. These aspects are discussed in Section 2.3.4.

### *2.3.2 The coefficient of permeability (K)*

The coefficient of permeability ($K$) defines the rate of resin flow per unit area for an impregnation system; this has to be determined experimentally or estimated theoretically. A number of researchers have proposed relationships to estimate the coefficient of permeability. With reference to a Cartesian coordinate system, the three principal components of permeability in x, y and z directions are denoted as $K_x$, $K_y$ and $K_z$ (See Figure 25). The relationships describing the flow of liquids through a porous bed, as shown in Figure 25(a), assume that the principle permeability coefficients are similar in the three principle directions:

$$K_x = K_y = K_z \qquad \textbf{Equation 9}$$

On the other hand, in the case of a roving structure shown in Figure 25(b), the flow paths and the resistance to flow are direction-dependent as discussed previously. In order to simplify matters, the assumption is made that the flows in y and z-directions are equal (transverse isotropic assumption). Hence:

$$K_y = K_z = K_T \qquad \textbf{Equation 10}$$

where $K_T$ represents the coefficient of permeability in transverse and through-thickness directions. Also, for the ideal roving shown in Figure 25:

$$K_T \neq K_x \qquad \textbf{Equation 11}$$

Here Equations 10 and 11 are only applicable for the unidirectional roving structure as shown in Figure 25(b).

A number of models have been proposed to estimate the permeability coefficients. Gebart (1992) investigated the axial and transverse permeability of unidirectional reinforcements. A relationship for the coefficient of axial permeability ($K_x$) was proposed:

$$K_x = \frac{8r_f^2}{c}\frac{(1-v_f)^3}{v_f^2}$$ **Equation 12**

where $r_f$ is radius of the filament in the roving, $v_f$ is the fibre volume fraction of the roving, c is a dimensionless shape factor which is equal to 57 for a quadratic array of fibres and 53 for an hexagonal array.

Gebart (1992) also derived following relationships for predicting the transverse permeability for two fibre architectures :

$$K_{y,\ quadratic} = \frac{16r_f^2}{9\pi\sqrt{2}}\left(\sqrt{\frac{v_A}{v_f}}-1\right)^{5/2}$$ **Equation 13**

$$K_{y,\ hexagonal} = \frac{16r_f^2}{9\pi\sqrt{6}}\left(\sqrt{\frac{v_A}{v_f}}-1\right)^{5/2}$$ **Equation 14**

where $v_A$ is the maximum packing capacity of a roving which were assigned 0.906 and 0.785 for hexagonal and square filament architectures respectively.

The coefficients of axial and transverse permeability as a function of the fibre volume fraction are shown in Figure 29. Here the curves were generated using Equations 12 and 14. It is clear that both coefficients decrease with an increase in the fibre volume fraction. This decrease is related to the compaction of the filaments at higher volume fraction which restricts the flow of the liquid. The theoretical maximum fibre volume fractions assuming a hexagonal or square packing of filaments within the rovings are 90.7 % and 78.5 % respectively. However, the actual composites have non-regular packing and as a consequence the practical limit for commercial unidirectional composites is 70 % (Hull and Clyne, 1996).

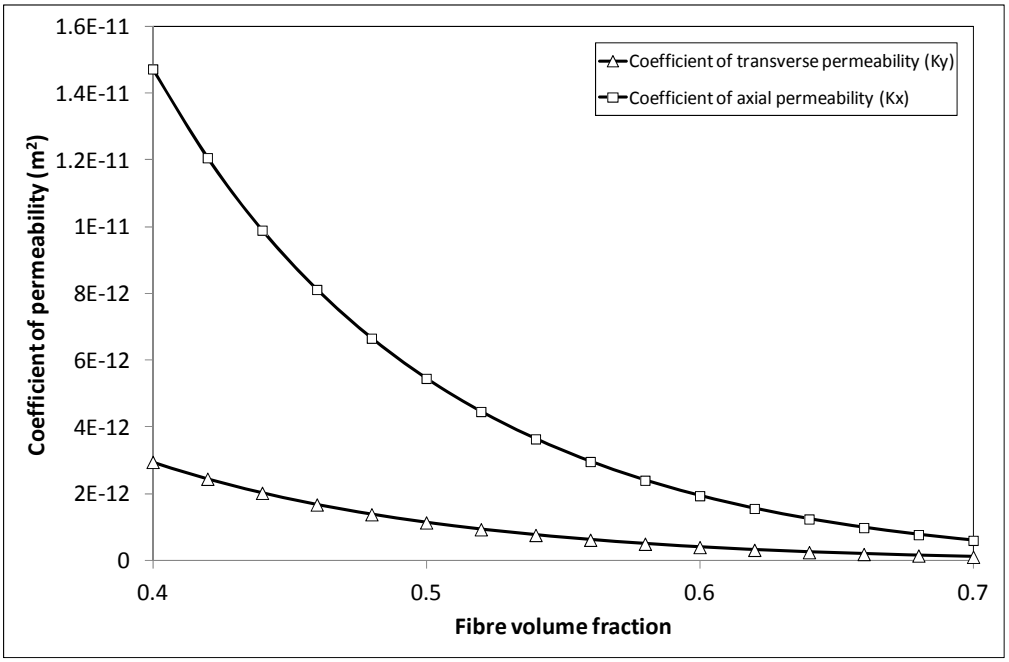


**Figure 29 Simulation of the coefficients of axial and transverse permeability as a function of the fibre volume fraction. These graphs were simulated using Equations 12 and 14.**

Selected models for the estimation of axial and transverse permeability coefficients reported by other researchers are summarised in Table 5.

**Table 5 Selected permeability models reported by Carman (1937), Cai and Berdichevsky (1993) and Berdichevsky and Cai (1993).**

| Researcher | Axial Permeability |
|---|---|
| Carman (1937) | $K = \frac{D_f^2}{16k}\frac{(1-V_f)^3}{V_f^2}$ |
| Cai and Berdichevsky (1993) | $K = \frac{r_f^2}{8V_f}\left[\ln\left(\frac{1}{V_f{}^2}\right) - (3-V_f)(1-V_f)\right]$ |
| Berdichevsky and Cai (1993) | $K_x = 0.111\frac{r_f^2}{V_f}\ln\left(\frac{1}{V_f}\right)\exp\left[-1.54V_f - 2.82V_f^2\right]$ |
| | **Transverse Permeability** |
| Carman (1937) | $K = \frac{D_f^2}{16k}\frac{(1-V_f)^3}{V_f^2}$ |
| Cai and Berdichevsky (1993) | $K = \frac{r_f^2}{8V_f}\left[\ln\left(\frac{1}{V_f}\right) - \frac{1-V_f^2}{1+V_f^2}\right]$ |
| Berdichevsky and Cai (1993) | $K = 0.229r_f^2\left[\frac{1.814}{V_A} - 1\right]\left[\frac{1-\sqrt{V_f/V_A}}{V_f/V_A}\right]^{2.5}$ |

### *2.3.3 Factors affecting resin impregnation*

A number of factors can affect the impregnation process and a brief discussion on this is presented in the following section.

#### 2.3.3.1 Fibre-resin interactions

The impregnation is influenced strongly by the interaction between the resin and the fibres. The extent of wetting of the fibres by the resin can be defined by the contact angle ($\theta$) which is measured from the tangent to the fibre at the fibre/resin contact, as shown in Figure 30.

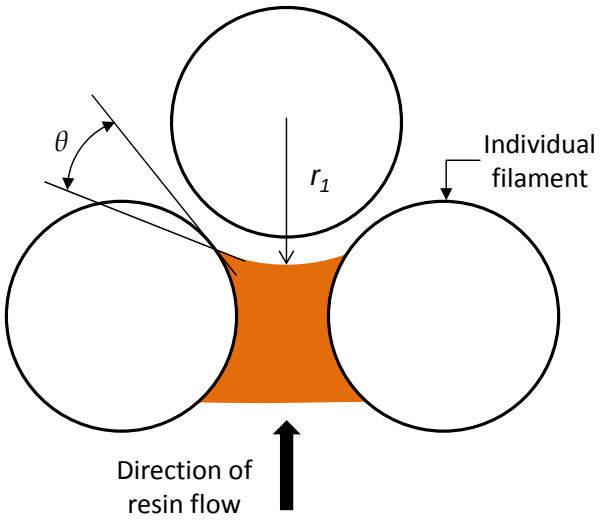


**Figure 30 Schematic illustration of the resin meniscus between three filaments. Here $r_1$ is defined as the principal radius of the meniscus (Foley and Gillespie, 2005).**

The relationship for the contact angle can be expressed as:

$$\cos\theta = \frac{\sigma_{SV} - \sigma_{SL}}{\sigma_{LV}} \qquad \textbf{Equation 15}$$

where $\sigma_{SV}$ is the solid–vapour surface tension, $\sigma_{SL}$ is the solid–liquid surface tension and $\sigma_{LV}$ is the liquid–vapour surface tension (Foley and Gillespie, 2005). The concentration and the type of the binder on the fibres can also influence the impregnation process. Morii et al. (1999) showed that for phenolic/E-glass composites, the impregnation improved when a phenolic

compatible sizing was used on the fibres. The improvement in the impregnation resulted in enhanced mechanical properties of the composites.

### 2.3.3.2 Roving tex and the radius of the filaments

Lackey et al. (1997) found using a resin-injection pultrusion process, it was more difficult to impregnate carbon tows with a filament radius of 3.5 μm when compared to glass rovings with a filament radius of 12 μm. This was said to be related to the packing of the filaments in the roving; as the radius of the filaments decreases, the packing of the filaments increases and hence, the localised fibre volume fraction increases. The effect of fibre volume fraction on the coefficient of permeability was shown in Figure 29. The impregnation times versus the degree of impregnation for three E-glass rovings with different tex are shown in Figure 31.Here it can be seen that the impregnation time is increased with an increase in the roving tex (Pandita et al., 2012). These observation are applicable for both resin-bath and resin-injection pultrusion.

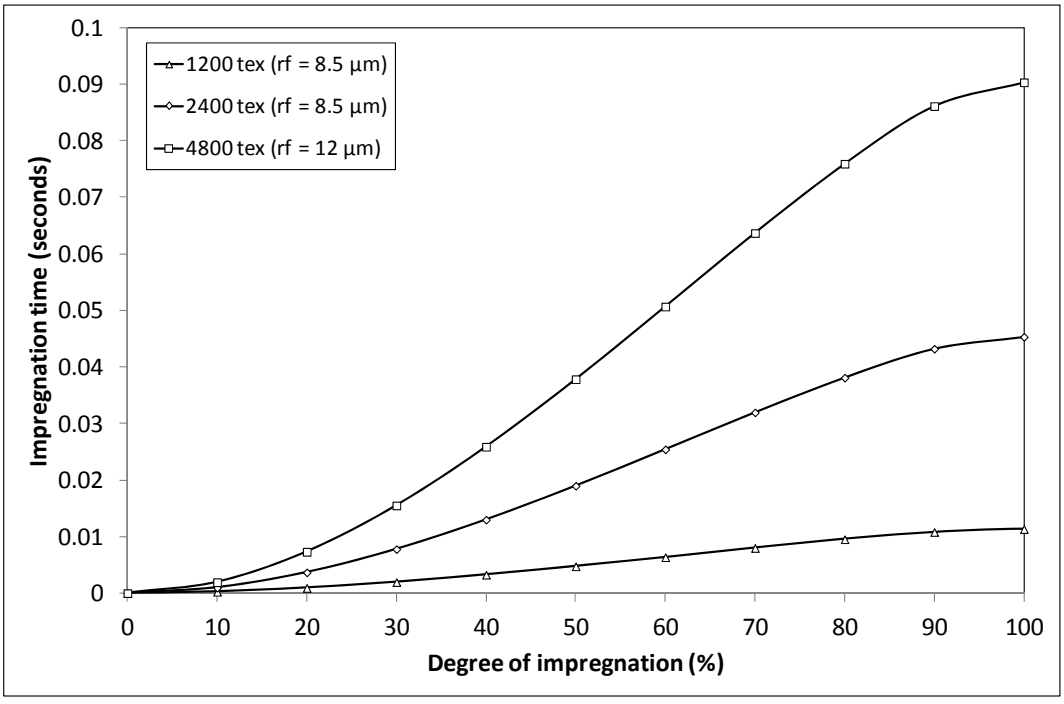


**Figure 31 Effect of roving tex on the impregnation time and degree of impregnation. Equation 8 was used to generate these curves (Pandita et al., 2012).**

### 2.3.3.3 Pressure

Generally, when the term "pressure" is used in the context of composite processing, it refers to the applied pressure that is used to force the liquid resin into the rovings. However, there are other forces involved in the impregnation process including vacuum, gravitational and capillary pressure. The total pressure involved during processing ($P_t$) can be expressed as (Ahn et al., 1991):

$$P_t = P_m + P_g + P_v + P_c \qquad \textbf{Equation 16}$$

where $P_m$ is the applied pressure, $P_g$ is the gravitational pressure, $P_v$ is the vacuum pressure and $P_c$ is the capillary pressure. Generally, the gravitational pressure is much lower than applied pressure and it can be ignored (Ahn et al., 1991). The vacuum pressure becomes important in the processes such as autoclave processing and vacuum-assisted resin transfer moulding (VA-RTM). However, in some processes, the capillary pressure may be comparable to the mechanical pressure as well as the vacuum pressure. The effect of injection pressure on the impregnation of an E-glass roving is shown in Figure 32.

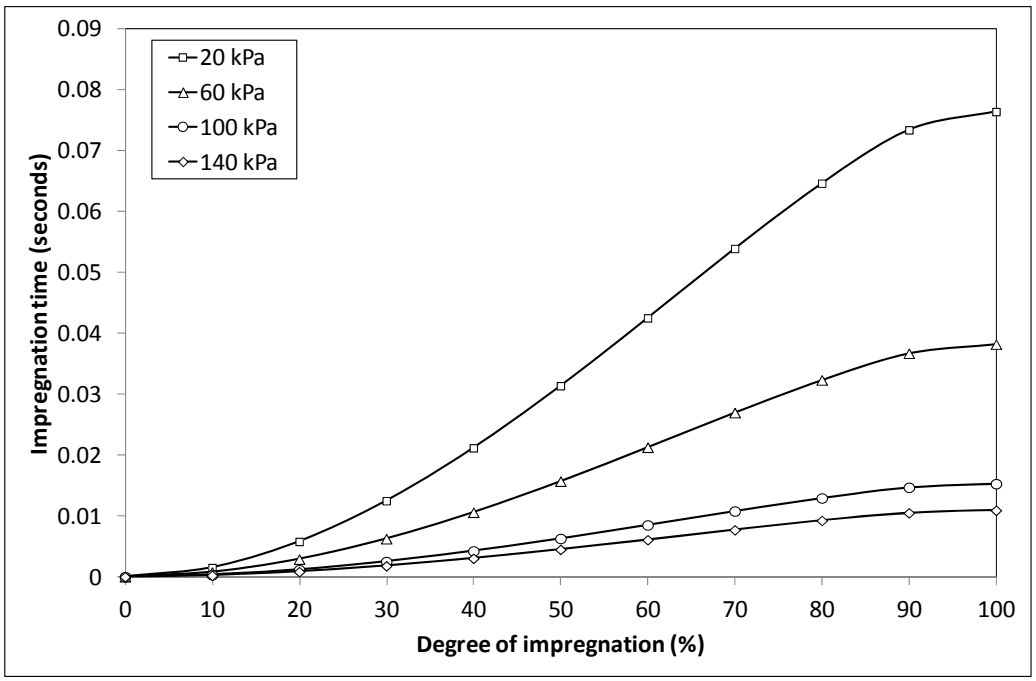


**Figure 32 Effect of injection pressure on the impregnation time (Pandita et al., 2012). The simulations were generated for the impregnation of an epoxy resin into an E-glass roving using Equation 8.**

Micro-flow models assume that the capillary pressure enhances resin impregnation whilst entrapped gas in the rovings hinders it. The importance of capillary flow has been highlighted by other researchers (Bayramli and Powell, 1992, Young, 1996, Binétruy et al., 1997). The capillary pressure ($P_c$) in a roving can be estimated by using the Young-Laplace equation (Ahn et al., 1991):

$$P_c = \frac{2F}{r_f}\frac{(1-e)}{e}\sigma\cos\theta \qquad \textbf{Equation 17}$$

where, $\sigma$ is the surface tension of the resin; $\theta$ is the contact angle; $r_f$ is radius of a single filament; $e$ is the porosity of the reinforcement and $F$ is the form factor depending on the alignment of the fibres and direction of the resin flow. A simulation of the capillary pressure as a function of fibre volume fraction is shown in Figure 33.

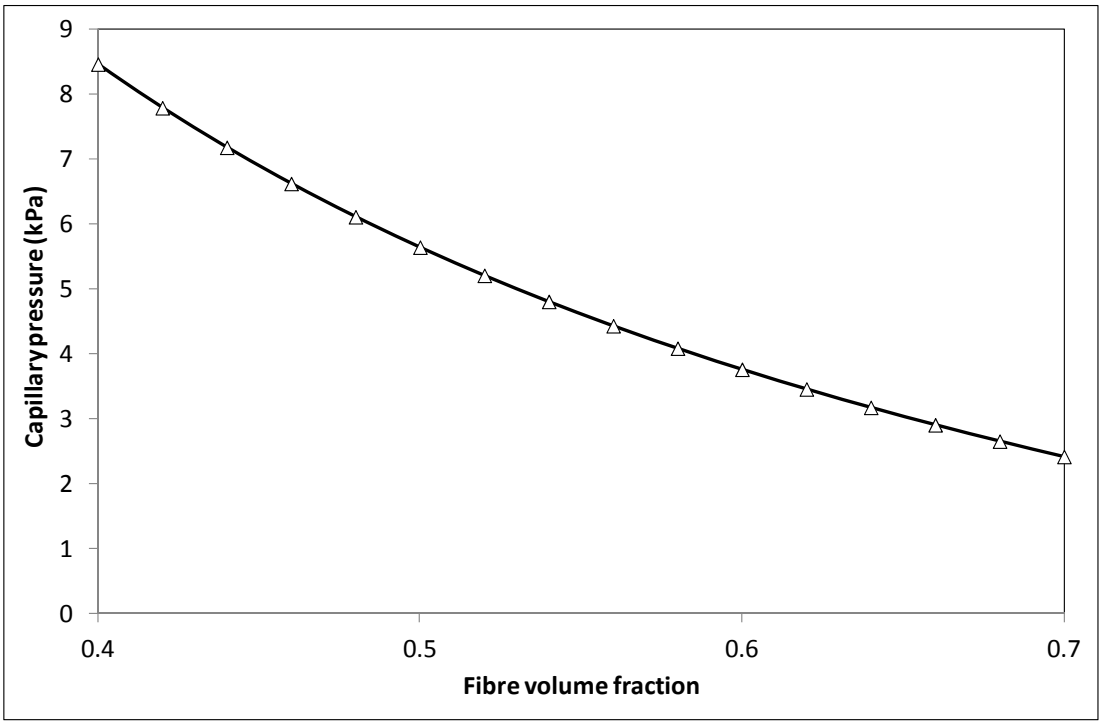


**Figure 33 Simulation of the capillary pressure ($P_c$) in the transverse direction as a function of the fibre volume fraction. The curves were generated for impregnating an epoxy resin into an E-glass roving using Equation 17. Here the filament radius was 8.5 µm.**

#### 2.3.3.4 Tension

Tension in the rovings will compact the filaments within a roving and decrease the coefficient of permeability (Gaymans and Wevers, 1998). Higher tension in the rovings can also cause fibre damage. In case of pin-impregnation, a higher tension in the roving would also increase the pressure in the resin film that is present between the roving and the pin. From a practical point of view, the tension in the roving should be maintained to such a level that the trajectory of the rovings is maintained without inducing any fibre damage.

#### 2.3.3.5 Viscosity of the resin

With reference to Figure 34, it can be seen that for a stationary roving where the resin is assumed to penetrate through-the-thickness, the impregnation time is reduced with a reduction in the viscosity of the resin. This is also clear from Equations 6 and 8.

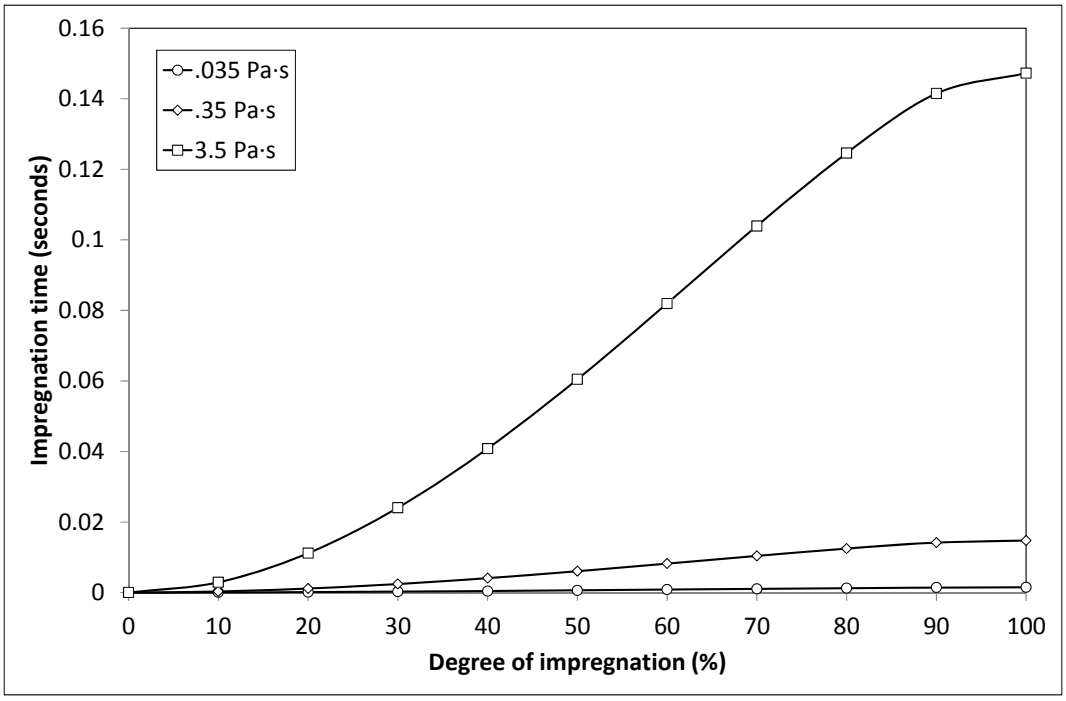


**Figure 34 Simulation of the effect of the resin viscosity on the time and degree of impregnation using Equation 8 (Pandita et al., 2012). The simulations were generated for the impregnation of an epoxy resin into an E-glass roving.**

### *2.3.4 Pin-impregnation*

The following section presents a discussion on pin-based impregnation as it is of relevance to the design of the resin impregnators used in the current study. In the pin-impregnation process, as illustrated in Figure 35, the roving is immersed in the resin and pulled over (or under) a pin. With reference to Figure 35, the resin film that is present between the roving and the pin is squeezed into the roving by the force ($F$) that the roving exerts on the pin. A critical parameter involved in the pin-impregnation process is the pressure that is generated in the wedge section (the resin that is present between the roving and the pin) which forces the resin into the roving as it traverses under the pin.

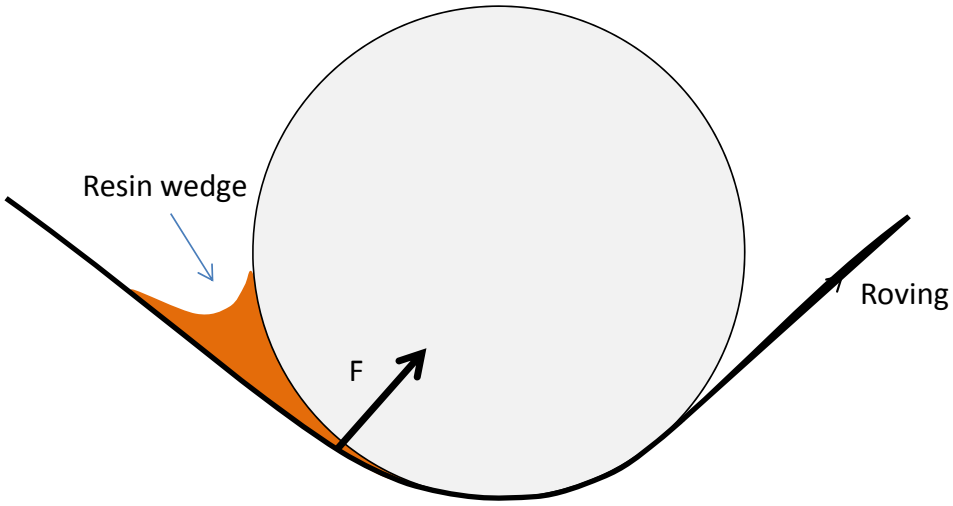


**Figure 35 Schematic illustration of the pin-impregnation process. Here 'F' denotes the force exerted by the roving on the pin. This schematic has been adapted from Chandler et al. (1992) .**

The maximum pressure in the resin wedge can be expressed by the Laplace equation (Bates and Charrier, 1999):

$$P_{\max} = \frac{T}{WR} \qquad \textbf{Equation 18}$$

where $T$ is the tension in the roving, $R$ is the pin radius and $W$ is the width of the roving. However, this equation is applicable for the situations where there is no leakage of the resin from the wedge section. In practical situations involving rovings, there would be some

leakage of liquid from the wedge. Bates et al. (2002) introduced a fitting parameter ($f$) to take into account the leakage-flow:

$$P = f\frac{T}{WR} \qquad \textbf{Equation 19}$$

Here $f$ was assumed to be 0 or 1 for conditions relating to no pressure or maximum pressure in the wedge section respectively.

Chandler et al. (1992) modelled the pin-impregnation process in the resin bath using the lubrication theory. It was proposed that the pin-impregnation process can be divided into four distinct regions as shown in Figure 36.

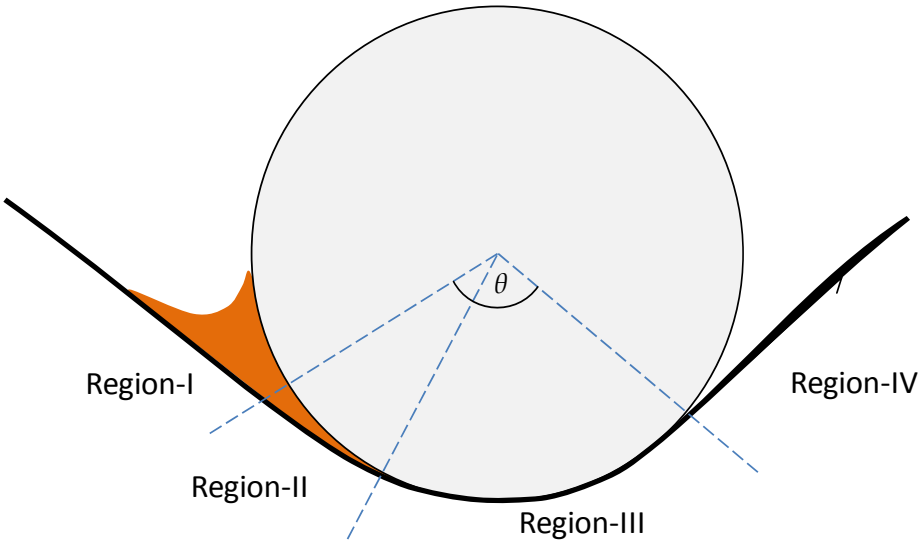


**Figure 36 Schematic illustration of the regions defined by Chandler et al. (1992) for the pin impregnation process.**

With reference to Figure 36, in Region-I, the roving drags resin into the narrow zone between the roving and the pin creating a resin-wedge. The angle at which the roving approaches the pin is determined by the geometry of the system. As the thickness of the resin-wedge decreases, a pressure is generated in the resin film between the roving and pin. In Region-II (*the impregnation zone*), the pressure generated in the resin film causes the resin to be forced

through the thickness of the roving. Chandler et al. (1992) suggested that effective impregnation took place only in this region. The end of the impregnation zone was termed as "dry contact". In Region-III (*the contact zone*) the filaments of the roving are in contact with the surface of the pin; the impregnation in this region was said to be negligible. The combination of Coulomb friction and viscous drag in the resin results in a build-up of tension in the roving in this region. Finally, the roving exits the pin at Region-IV.

It was recommended that in order to improve the efficiency of the pin-impregnation process, the volume of the resin in the wedge-section of the impregnation zone should be increased, and the length of the contact zone should be minimised or eliminated. However, Gaymans and Wevers (1998) suggested that the contact zone (Region-III) can assist in the redistribution of the resin that is present in the rovings. With reference to Figure 36, the profile of the film thickness along the surface of the pin in the different regions is represented in Figure 37.

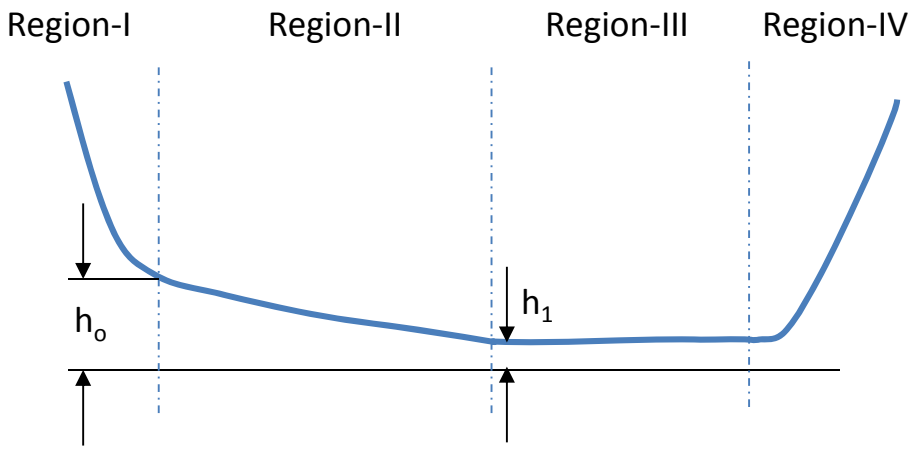


**Figure 37 Schematic illustration of the profile of the resin film thickness in the pin-impregnation regions (Chandler et al., 1992).**

Blok and Rossum (1953) used a flexible impermeable tape in contact with a rotating cylinder, covered with lubricating oil, to derive a relationship for the film thickness ($h_o$) between roving and the pin:

$$h_o = 1.4R\left(\frac{\eta WV}{T}\right)^{2/3} \qquad \textbf{Equation 20}$$

where, $R$ is the radius of the pin, $\eta$ is the viscosity of the liquid; $W$, $V$ and $T$ are the width, velocity and tension in the tape. Bates et al. (2002) termed the dimensionless parameter ($\eta WV/T$) as the 'lubrication number' in their studies. Chandler et al. (1992) suggested that the thickness of resin film at the start of the impregnation zone ($h_o$) could be calculated using:

$$h_o = \left(\frac{\pi^2}{128}\right)^{1/3} R\left(\frac{6W\eta V}{T_o}\right)^{2/3} \qquad \textbf{Equation 21}$$

where, $R$ is the radius of the pin, $\eta$ is the viscosity of the liquid, $W$ is the width of the roving, $V$ is the haul-off speed of the roving and $T_o$ is pre-tension in the roving.

In practice, it is difficult to measure the thickness of the resin film thickness at the end of the impregnation zone ($h_i$). Chandler et al. (1992) reported a value of 50 μm for a 2500 tex glass fibre with Nylon-66 resin. However, Bates et al. (2000) reported a value of 10 μm for a 2400 tex glass fibre using the same resin. In both the cases, the average diameter of the filaments in the roving was 17 μm.

The following relationship was derived by Chandler et al. (1992) to calculate the impregnation zone length ($L_1$):

$$L_1 = \frac{-T_1 + \sqrt{T_1^2 - \frac{\eta^2 V^2 RZ(2h_1 + h_o)}{3Kh_1h_o}(h_1 - h_o)}}{\frac{\eta V(2h_1 + h_o)}{3h_1h_o}} \qquad \textbf{Equation 22}$$

where $h_o$ is the film thickness at the start of the impregnation zone. It was assumed that the resin film thickness varies linearly in the resin impregnation zone. The thickness of the resin film at the exit of the resin impregnation zone is '$h_1$' which remains constant in the contact

zone; $R$ is the pin radius; $\eta$ is the resin viscosity; $V$ is the haul-off rate of the roving; $T_o$ is the initial roving tension; $K$ is the coefficient of permeability and $Z$ is the thickness of the roving.

The tension build-up in a roving in a pin-impregnation process is caused primarily by: (a) inlet tension ($T_o$) on the roving; (b) viscous shear stresses between the roving and the pin surface; and (c) solid–solid friction between the fibres and the pin surfaces (Bates and Charrier, 2000).

The relationships to estimate the tension in each of the regions as described previously in Figure 36 and Figure 38 are summarised in Table 6.

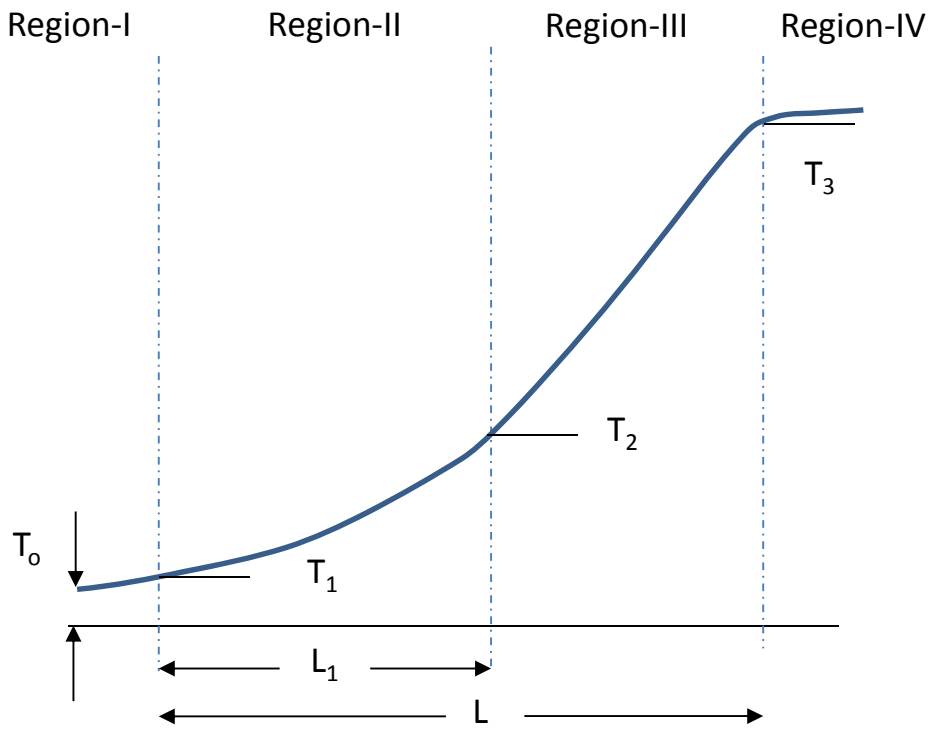


**Figure 38 Development of tension in the roving in the pin-impregnation regions (Chandler et al., 1992). Here $T_o$, $T_1$, $T_2$ and $T_3$ are the roving tension at the start of Region-I, II, III and IV respectively.**

**Table 6 Summary of relevant equation to estimate the tension in the pin-impregnation process (Chandler et al., 1992).**

| | Relationship for tension | |
|---|---|---|
| Region-I | $T_1 = T_o + \frac{5\pi\eta V}{4}\sqrt{\frac{2R}{h_o}}$ | **Equation 23** |
| Region-II | $T_2 = T_1 + \frac{\eta V L_1}{2}\left(\frac{1}{h_o} + \frac{1}{h_1}\right)$ | **Equation 24** |
| Region-III | $T_3 = T_2 + \left(\exp\left(\frac{\mu L_2}{R}\right) - 1\right)\left(T_2 + \frac{\eta V R}{h_1 \mu}\right)$ | **Equation 25** |

The term $\mu$ in Equation 25 denotes the coefficient of friction.

Bates et al. (2000, 2002) also developed a theoretical model to estimate the tension in the roving as a function of the contact angle ($\varphi$) and other process parameters:

$$\frac{dT}{d\varphi} = \eta\left(\frac{V}{h_o}\right)RW + \mu T(1 - f) \qquad \textbf{Equation 26}$$

where, $V$ is the fibre haul-off speed, $R$ is the pin radius, $\mu$ is the coefficient of friction, $W$ is the roving width, $h_o$ is the film thickness at the start of impregnation, $\eta$ is the resin viscosity and $f$ is the fitting parameter shown in Equation 19. It was shown through experimentation that for values of the lubrication number less than 0.0001, $f$ was observed to increase with increasing lubrication number as shown in Figure 39. At higher lubrication values, $f$ approached a value that was independent of the lubrication number.

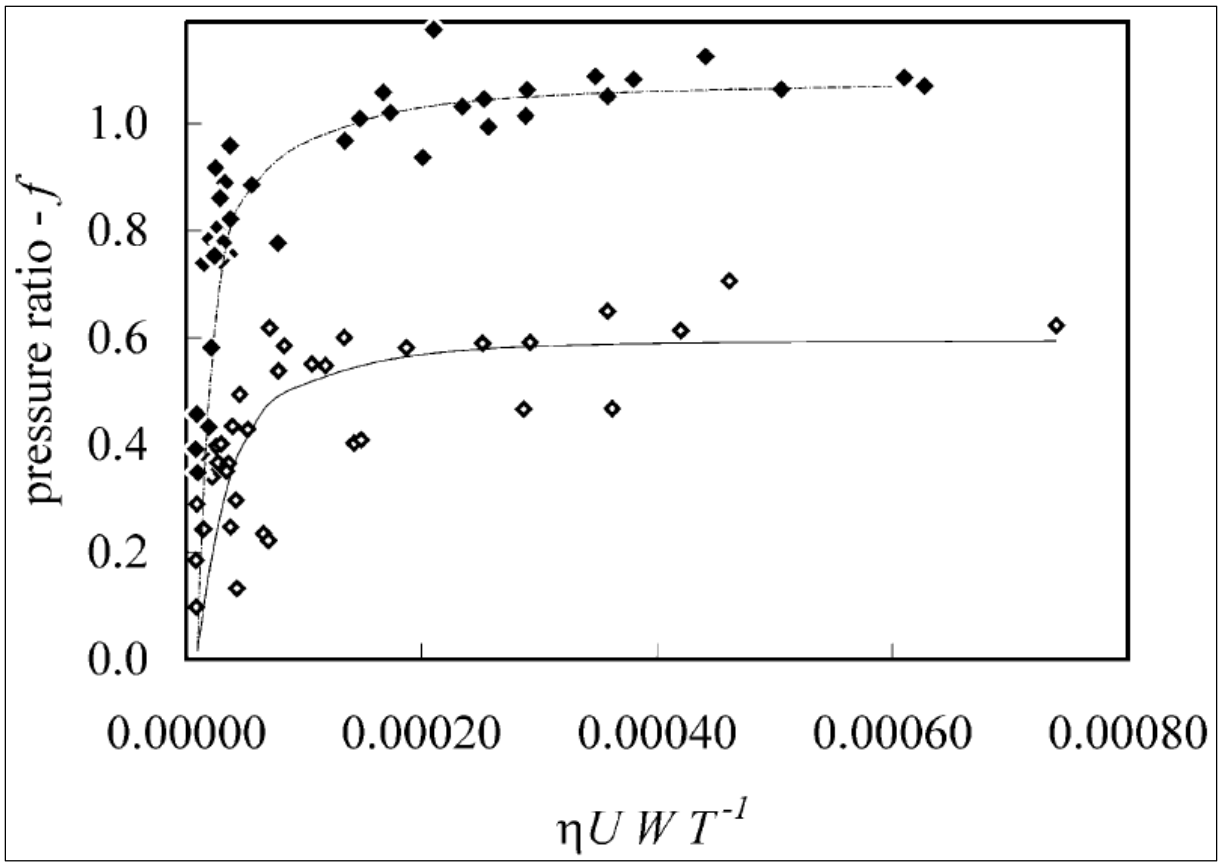


**Figure 39 Plot of pressure ratio (*f* ) versus lubrication number for an impermeable tape (filled diamonds) and glass roving (open diamonds). Reproduced from Bates et al. (2002).**

Weustink (2008) modified the equations proposed by Chandler et al. (1992) for rotating pins (rollers). Here the term $\vartheta_{roller}$ (the component of the roller speed in x-direction) was added to account for the rotation of the roller.

$$L_1 = \frac{-T_1 + \sqrt{T_1^2 - \dfrac{\eta^2 (V + \vartheta_{roller})^2 Rt(2h_1 + h_o)}{3Kh_1 h_o}(h_1 - h_o)}}{\dfrac{\eta (V + \vartheta_{roller})(2h_1 + h_o)}{3h_1 h_o}} \qquad \textbf{Equation 27}$$

$$T_1 = T_o + \frac{5\pi\eta (V + \vartheta_{roller})}{4}\sqrt{\frac{2R}{h_o}} \qquad \textbf{Equation 28}$$

Similarly, the corresponding equations for the tension build-up in Region-II and –III were also developed by changing $V$ to $(V + \vartheta_{roller})$ in Equations 24 and 25 respectively.

Gayman and Wevers (1998) studied the pin-impregnation process using polypropylene resin and E-glass fibres. The rate of impregnation was studied as a function of diameter of the pins, the fibre haul-off speed, melt flow index (MFI) of the resin (hence viscosity), pre-tension in the roving and the number of pins. It was suggested that the impregnation process can be divided into two regions: one where the resin wedge is present between the roving and the pin (*the impregnation zone*) and other where the fibre is in contact with the pin (*the contact zone*). The impregnation rate was faster in the impregnation zone due to presence of the resin film. It was shown that the diameter of the pin and pre-tension in the roving did not affect the overall extent of impregnation.

Xian et al. (2006) reported an analysis of pin-based impregnation for polypropylene where the Taguchi method was used to optimise the impregnation process. The parameters considered were the pre-tension in the roving, temperature of the melt (hence viscosity), the number of pins and the haul-off speed of the roving. It was shown by the analysis of variance (ANOVA) that the roving pre-tension did not affect the impregnation. On the other hand, the fibre haul-off speed, melt temperature, and the number of pins were found to be significant factors as far as the impregnation efficiency was concerned.

Roh and Lee (2012) demonstrated experimentally that the impregnation was improved for thermoplastic resin when the rovings were spread. The impregnation lengths were calculated from the trajectory of the roving and Darcy's equation was used to estimate the theoretical impregnation level. However, they did not elaborate if the concept of the impregnation zone described previously was considered in their analysis. It was not clear as to how the wedge pressure involved in the pin-based impregnation process was calculated.

Wang et al. (2012) optimised the parameters affecting the pin-impregnation process by numerical simulations. An analysis was performed on the resin present in the wedge section between the moving rovings and the pin. A schematic illustration of the resin flow in the resin wedge is shown in Figure 40. A mathematical relationship was proposed to estimate the depth of the roving ($Z_{IMP}$) that had been impregnated via the pin-impregnation process.

$$Z_{IMP} = \frac{\sqrt{144\,W^4K^2 + 12\,KW^2h_o^4} - 12\,W^2K}{h_o^3} \qquad \textbf{Equation 29}$$

where $W$ is the width of the roving, $K$ is the permeability coefficient and $h_o$ is the film thickness at the start of the impregnation zone.

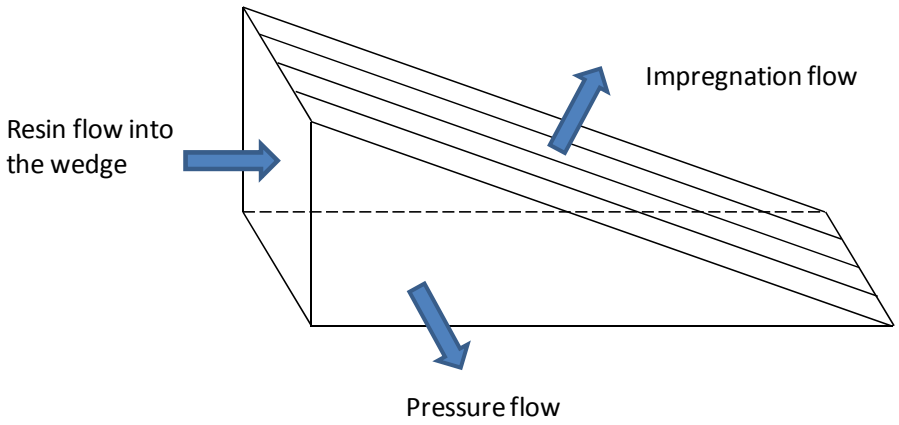


**Figure 40 Schematic illustration of the resin flow in the wedge section during pin-based impregnation (Wang et al., 2012)**

Equation 29 is applicable in the situations where following geometrical condition is satisfied:

$$L_{imp} < L_{\max} = \varphi R \qquad \textbf{Equation 30}$$

where $L_{imp}$ is the estimated length of the wedge section where impregnation takes place and $L_{max}$ is the contact length available for the roving as a result of the pin with a radius ($R$) and contact angle ($\varphi$).

## 2.4 LIFE CYCLE ASSESSMENT

According to ISO 14040, life cycle assessment (LCA) is defined as 'the *compilation and evaluation of the inputs, outputs and the potential environmental impacts of a product system throughout its life cycle*'. It is used to assess the environmental aspects associated with a product or process by identifying the energy consumed, materials used, and emissions over its whole life cycle (Song et al., 2009, Lepech, 2009). International Organization for Standardization (ISO) has issued standards related to LCA including ISO 14040 to ISO 14043 (2006). These standards cover the various aspects of the application of the LCA methodology. An overview of the LCA methodology with some potential applications is shown in Figure 41.

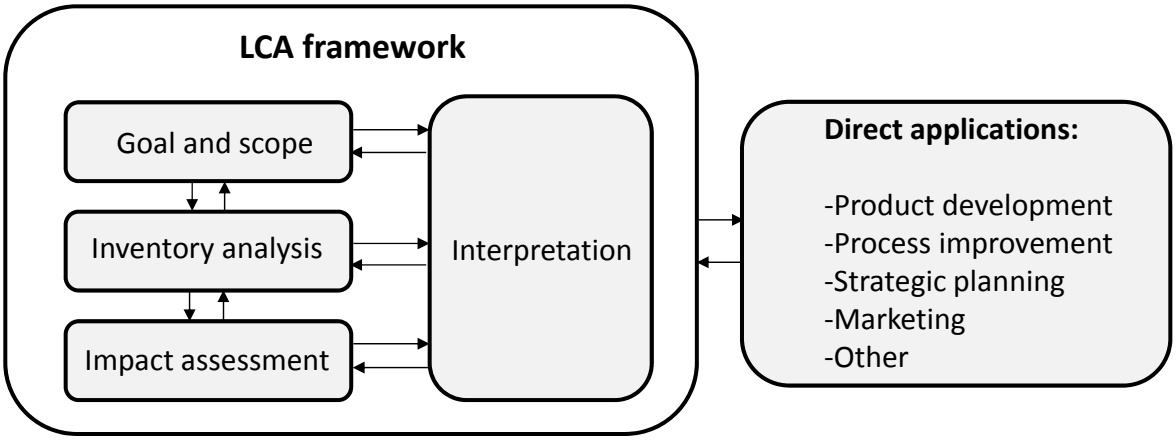


**Figure 41 Life cycle assessment framework according to ISO 14040:2006.**

In the case of a product, a comprehensive LCA would consider all phases during the life cycle of the product, for example, aspects relating to the extraction of the raw materials, design, formulation, processing, manufacturing, packaging, use (reuse) and disposal (generally referred to as '*cradle-to-grave*'). However, a holistic approach to LCA requires the data from all aspects of products' life cycle from extraction of raw materials to disposal. In practice, it can be difficult to obtain relevant and t

raceable data for each step (Murphy, 2004). This is a reason that the goal and scope of LCA must be defined carefully for any application as shown by the LCA framework in Figure 41. Commercial software packages are available to carry out the LCA studies. Examples include GaBi, developed by PE International and SimaPro retailed by PRé Consultants. These software packages offer suitable databases for specified applications.

Some studies have been reported on the application of the LCA for polymer composites. Corbiere-Nicollier et al. (2001) performed an LCA study on the feasibility of using reed fibres as a substitute for glass fibres in the production of polypropylene pallets. Gerkhail (2002) compared plant fibre-based polypropylene composites with glass fibre polypropylene composites for automotive and non-automotive applications. It was shown that in non-automotive applications, the plant fibre-based composites were less environmentally friendly when compared to glass fibre-based composites. It was mentioned that the reason for the plant fibre-based composites for being less environmentally friendly was the use of fungicides, pesticides, herbicides and fertilisers during cultivation of the plants. For automotive applications to achieve the required tensile and impact properties a higher weight of plant fibre-based composites was required when compared to glass/polypropylene composites. This resulted in increased fuel consumption and hence a higher environmental burden.

Pandita et al. (2007) compared the clean filament winding process with a conventional drum-based filament winding. An LCA was performed to compare the impacts of waste resin and solvents. It was shown that the clean filament winding process provided a cleaner working environment with significant reductions in the volumes of waste resin generated and the volume of solvents consumed. Wait (2011) used the clean filament winding process to remanufacture filament wound composites using waste glass fibre fabric strips that were

generated in a weaving process. LCA was used to compare the environmental benefits of the production of filament wound composites using the waste fabric strips.

A limited number of studies have been reported on LCA studies relevant to the pultrusion process. Song et al. (2009) performed an LCA on the pultrusion process by comparing the energies consumed throughout the life time of automotive body panels made from polyethylene terephthalate (PET)/glass fibres with those made from steel and aluminium. A hybrid process model was developed where the economic and environmental constraints were combined. It was shown that the composite products save more energy than when steel was used. However, this was not the case when aluminium was used in the construction.

Ibbotson and Kara (2013) compared I-beams manufactured from glass fibre reinforced composites with those produced from stainless steel. It was shown that the composite I-beam resulted in a 20% reduction in the environmental footprint.

## 2.5 OVERALL SUMMARY OF THE LITERATURE REVIEW

The literature review has covered the important features of the pultrusion method including the techniques that are employed commonly for the impregnation of the rovings. It has been shown that dip-type resin baths are generally used in pultrusion industry. However a number of environmental issues are associated with this type of impregnation, for example, the emission of styrene from the resin bath, disposal of waste resin at the end of the experiment and a need for large volume of cleaning solvent (Lackey et al., 1997, Raday, 2006, Cambell, 2010). An alternative to the resin bath pultrusion technique is the resin-injection pultrusion which can overcome the environmental issues related to the resin bath systems. However, the disadvantages of this method include difficulties in completely impregnating the rovings due to close packing of the filaments and the cost associated with the high-pressure resin

dispensers and specially designed resin-injection dies (Shaw-Stewart and Sumerak, 2000, Cambell, 2010).

Spreading the rovings can improve the impregnation; hence, a review on techniques for fibre spreading is undertaken. The techniques discussed include mechanical, vibration, pneumatic, vacuum, acoustic and electrostatic. With respect to spreading the roving via mechanical means, the width of a roving over a spreading pin can be estimated by Wilson's model (1997). This model was further extended to estimate the spreading at second bar by Irfan et al. (2011).

It is also shown that the key equation in impregnation studies is the Darcy's law. The coefficient of permeability ($K$) in Darcy's equation defines the rate of resin impregnation and can be determined experimentally or estimated theoretically. A number of factors affect the resin impregnation process including fibre-resin interactions, roving tex, filament diameter, resin pressure, roving tension and resin viscosity. The pin-impregnation is a process in which the roving is immersed in the resin and pulled over (or under) a pin. The pressure in the resin wedge that is present between the roving and the pin is the key parameter in determining the extent of impregnation via this method (Chandler et al., 1992, Bates and Ekhator, 2004, Bates et al., 2002, Gaymans and Wevers, 1998, Wang et al., 2012).

Life cycle assessment can be used as a tool to compare the environmental impacts of various composite manufacturing processes. Commercially available softwares, for example GaBi, developed by PE International and SimaPro retailed by PRé Consultants, are generally used to carry out the life cycle assessment.

# 3 DESIGN AND EXPERIMENTS

This chapter provides details of the materials, instruments and experimental approaches used in this study.

## 3.1 MATERIALS

### *3.1.1 Resin systems*

Three resin systems were used in this study. An epoxy resin system was used in the laboratory to evaluate the newly proposed pultrusion method. This was supplied by one of the project partners. A vinyl ester resin system was used in the experiments carried out in the industry because it was the resin of choice for the particular industry (Pultrex Ltd.). Finally a polyurethane resin was also evaluated in industry as part of the project. It was shown that the resin impregnators were capable of handling all three resin systems as the viscosities were within the same range. The detail about the formulations of the resin used is provided below.

(i) *Epoxy resin system*: A commercially available epoxy resin formulation was used for the pultrusion experiments carried out in the laboratory. The details of the formulation are provided in Table 7.

**Table 7 Details of the epoxy resin system used in this study.**

| Commercial name | Chemical family | Supplier | Parts by weight |
|---|---|---|---|
| Araldite® LY556 | Epoxide | Huntsman Advanced Materials | 100 |
| Aradur® 917 | Acid anhydride | Huntsman Advanced Materials | 90 |
| Hardener DY 070 | Heterocyclic amine | Huntsman Advanced Materials | 2 |
| Lumax® OP Wax | Wax | BASF | 4 |

(ii) *Vinyl ester resin system*: Filled and unfilled vinyl ester resin systems were used for the pultrusion experiments carried out at the premises of one of the project partners (Pultrex Ltd). The details of the vinyl ester resin formulation are presented in Table 8.

**Table 8 Details of the filled* and un-filled vinyl ester resin systems used in this study.**

| Commercial name | Chemical family | Parts by weight |
|---|---|---|
| Atlac 430 (Palatal A430) | Vinyl ester resin | 100 |
| Styrene | Reactive solvent | 2 |
| Perkadox 16 | Peroxide | 1 |
| t-butyl peroxybenzoate | Peroxide | 0.5 |
| Tert-Butyl peroxy-2-ethylhexanoate | Peroxide | 0.5 |
| INT-PUL-24 | Mould release | 1 |
| Dolomite Microdol® H Extra | Talc filler | 15 |

*** Dolomote Microdol® H Extra was used as the filler.**

(iii) *Polyurethane resin system*: A newly developed proprietary polyurethane resin system was also used. The resin was developed by one of the project partners. The exact formulation of the resin components have not been disclosed in this thesis because a non-disclosure agreement was signed between the University of Birmingham and the resin supplier.

### *3.1.2 Fibres*

The following section presents the details of the fibre reinforcements that were used for specified experiments:

(i) *E-glass Hybon® 2001*: The 4800 tex E-glass Hybon® 2001 fibres used in this study were supplied by PPG Industries (UK) as part of the project. These were used for the fibre spreading experiments which were carried out manually.

(ii) *E-glass Hybon® 2026*: The 2400 tex E-glass Hybon® 2026 fibres were also supplied by PPG Industries (UK). These were continuous filament, single-end rovings designed specifically to reinforce unsaturated polyester, epoxy, and vinyl ester resin systems. These were used in the pultrusion and fibre spreading experiments using an automated fibre spreading rig.

(iii) *386 Direct Roving*: The 4800 tex E-glass fibres were supplied by Jushi group (China). These fibres were used for the industrial site trials. These rovings were chosen as these were used by the industry where the industrial experiments were carried out.

(iv) *JSK® 689*: The 2400 tex E-glass fibres were supplied by JSK Speciality Glass Fibres Ltd (UK). These fibres were used for some of the polyurethane pultrusion experiments.

**Table 9 Details of the E-glass fibres used in this study.**

| Commercial name | Type | Tex | Nominal fibre diameter | Supplier |
|---|---|---|---|---|
| Hybon® 2001 | E-glass | 4800 | 24 μm | PPG Industries (UK) |
| Hybon® 2026 | E-glass | 2400 | 17 μm | PPG Industries (UK) |
| 386 Direct Roving | E-glass | 4800 | 24 μm | Jushi Group (China) |
| JSK® 689 | E-glass | 2400 | 17 μm | JSK Speciality Glass Fibres Ltd (UK) |

## 3.2 CHARACTERISATION OF THE NEAT RESINS AND PULTRUDED COMPOSITES

This section reports on the experimental procedures that were used to characterise the neat resin and the pultruded composites.

### *3.2.1 Differential scanning calorimetry*

A power-compensation Diamond DSC (Perkin Elmer, UK) was used to study the cure behaviour of the epoxy, unfilled vinyl ester and polyurethane resin systems. This was required to enable the selection of suitable temperatures for the die and to define the pultrusion speeds. For each resin system, the components of the resin system were mixed manually in the required stoichiometric ratio and degassed for ten minutes. In the first set of experiments, the resin was cured using a dynamic mode of heating; here the resin was heated from 30 °C to 200 °C at 5 K minute$^{-1}$. The experiment was repeated three times using the same sample and parameters to determine the magnitude of any residual cure, and the $T_g$.

The conversion curves were generated as a function of temperature using the following relationship (Rabearison et al., 2011):

$$\alpha(T) = \frac{H(T)}{H_U} = \frac{H(T)}{\int_0^{t_f} \left(\frac{dQ}{dt}\right)_f dt} \qquad \textbf{Equation 31}$$

where $\alpha(T)$ is the degree of conversion at temperature $T$, $H(T)$ is the heat generated when the temperature $T$ is reached, $H_U$ is the total enthalpy during a dynamic scan. $H_U$ is calculated by integrating the instantaneous rate of heat generated $(dQ/dt)_f$ from the start of the reaction to time $t_f$. Here, $t_f$ is the time required to complete the reaction during a dynamic DSC scan. The temperature of the die was selected at a point on the conversion curve where greater than 85% of cure had been attained.

In the second set of experiments, the resin systems were cured isothermally at the selected temperatures. The objective of these experiments was to establish the pultrusion speed which would ensure the complete cure of the resin. The samples were maintained at the desired isothermal value for ten minutes and the conversion-time curves were generated using following relationship (Rabearison et al., 2011):

$$\alpha(t) = \frac{H_T}{H_U} \int_0^t \frac{d\beta}{dt} dt \qquad \textbf{Equation 32}$$

where $\alpha(t)$ is the degree of conversion at time $t$, $H_T$ is the total enthalpy from the isothermal scan and $d\beta/dt$ stands for the isothermal reaction rate based on $H_T$.

Finally, dynamic scans were carried out on the cured samples to determine the glass transition temperature ($T_g$).

### *3.2.2 Rheology*

A parallel-plate rheometer (ARES, TA Instruments, UK.) was used to characterise the rheological behaviour of the neat resin systems. The main objective was to obtain information concerning the viscosity of the resin systems at the room temperature. The components of the resin system were mixed and degassed as described previously. Approximately 1 cubic centimetre of the mixed resin system was placed between the parallel plates (25 mm diameter) using a pipette. The tests were performed at room temperature.

### *3.2.3 Dynamic mechanical thermal analysis*

In the case of the neat resin test specimens, plaques were cast between glass plates. A mould release agent (3M™ Spray Mount™ Aerosol by 3M) was used on the glass plates and the plates were secured using G-clamps. The cast samples were cured in a recirculating oven at 140 °C. A water-cooled diamond wheel cutter was used to obtain the samples with

dimensions 50 mm × 6 mm × 2 mm. In the case of the pultruded composites, samples were cut from the pultruded strips using a water-cooled diamond cutter with dimensions 50 mm × 6 mm × 2.2 mm. The edges of the samples were polished using 2500 grit abrasive paper and the samples were stored in a desiccator until required.

A dynamic mechanical analyser (DMA 242 C, NETZSCH) was used to obtain the thermo-mechanical properties of the neat resin system and the pultruded composites. The $T_g$ was obtained from the peak of the loss tangent (*tan δ*). Each sample was clamped in the dual-cantilever fixture and heated from 25 °C to 180 °C at 3 K minute$^{-1}$. The experiments were conducted at 1 Hz. A minimum of three samples were tested for each of the specimen types. A photograph of the experimental setup is shown in Figure 42.

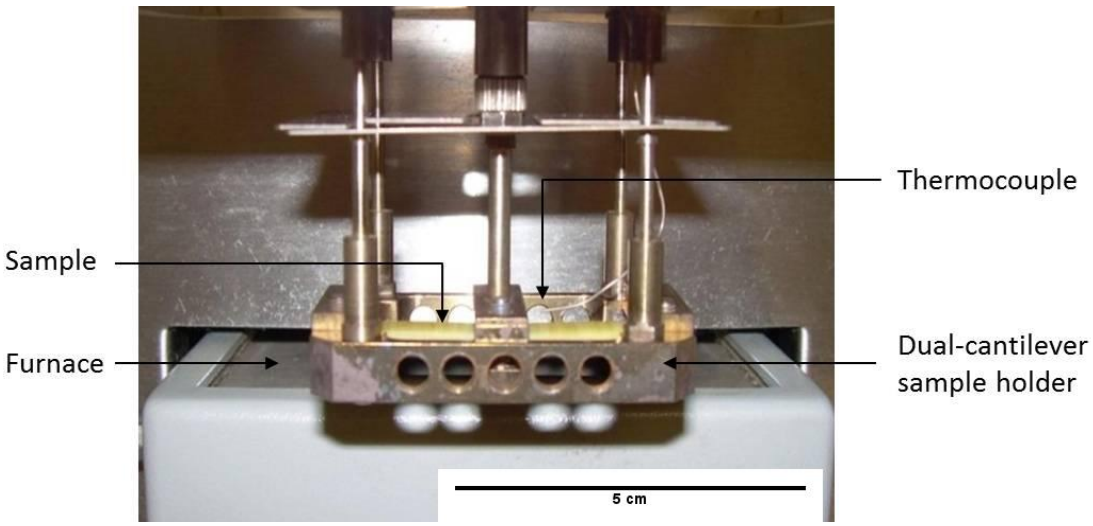


**Figure 42 Experimental configuration for the DMTA set-up.**

### *3.2.4 Density*

The densities of the cured neat resin systems and the pultruded composites were determined by using an OHAUS density measurement kit (Model: AP110S). With reference to the neat resin systems and the pultruded composites, samples with dimensions, 15 mm × 15 mm × 2.2 mm, were cut using a water-cooled diamond wheel cutter. The edges of the samples were

polished using a 2500 grit abrasive paper. The polished samples were dried in an air-recirculating oven at 70 °C for 10 minutes and then stored in desiccators until required.

The density measurements were carried out using the following procedure. The weight of the sample was measured in air and then in water using the experimental setup shown in Figure 43. The following formula was used to calculate the densities ($\rho$) of the neat resin and the pultruded composites:

$$\rho = \frac{W_{air}}{W_{air} - W_{water}} \times \rho_{water} \qquad \textbf{Equation 33}$$

where $W_{air}$ is the weight of the sample in air, $W_{water}$ is the weight of the sample in the water and $\rho_{water}$ is the density of the water at 22 °C. An average of five samples was used for the density measurements.

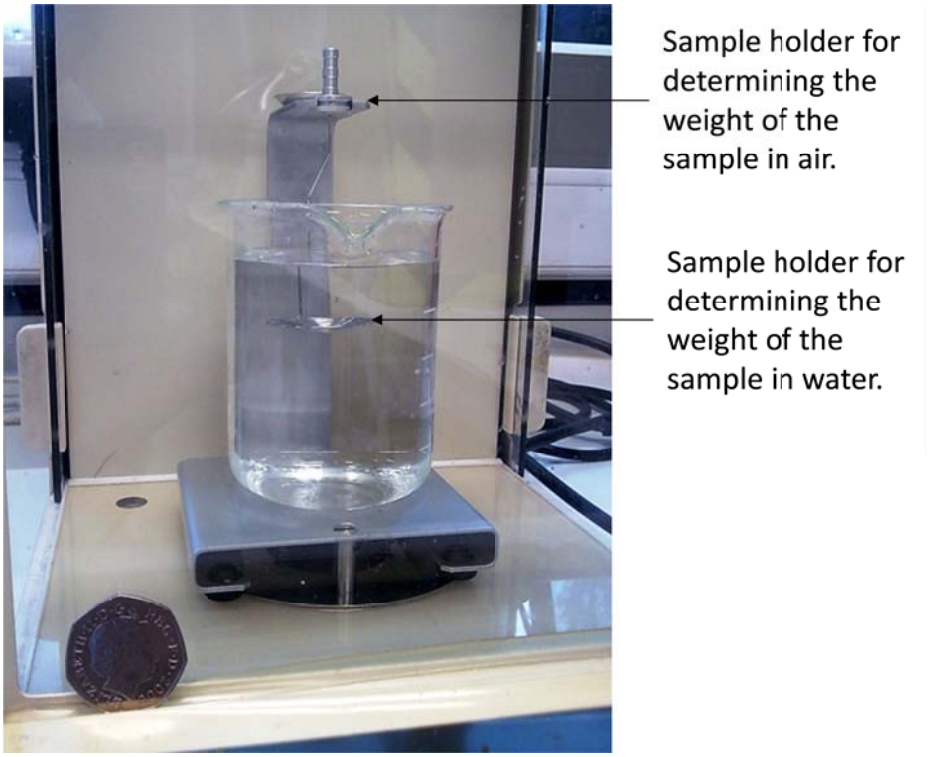


**Figure 43 Photograph showing the experimental set-up for the density measurements fo the neat resins and pultruded composites.**

### *3.2.5 Fibre volume fraction*

With reference to the pultruded composites, the fibre volume fraction was determined by the ignition loss method in accordance with ASTM D 2584-08. The samples that were previously used for the density experiments were used here to determine the fibre volume fraction. Each sample was weighed and then placed in a pre-weighed crucible and transferred to a furnace at 565 °C for 6 hours to burn off the resin. The fibre volume fraction of the composite ($V_f$) was calculated using following relationship:

$$V_f = \frac{\rho_m W_f}{\rho_f W_m - \rho_m W_f} \qquad \textbf{Equation 34}$$

where $W_f$ is the weight of the fibres, $W_m$ is the weight of the matrix, $\rho_f$ and $\rho_m$ are the densities of the fibres and the matrix respectively. The density of the resin was measured from the cast samples (epoxy = 1190 kg/m$^3$ and vinyl ester = 1145 kg/m$^3$) whereas the density of the E-glass fibres (2662 kg/m$^3$) used in this study was obtained from the supplier (PPG Industries, UK. Ltd).

### *3.2.6 Void fractions*

The void fraction ($V_v$) was determined in accordance with ASTM D 2734-03 using the following relationship:

$$V_v = \frac{100(\rho_T - \rho_c)}{\rho_T} \qquad \textbf{Equation 35}$$

where $\rho_T$ and $\rho_c$ are the theoretical and measured densities of the composite respectively. The theoretical density of the composite ($\rho_T$) was calculated using:

$$\rho_T = \frac{100}{\left(\frac{M}{\rho_m} + \frac{R}{\rho_f}\right)} \qquad \textbf{Equation 36}$$

where $M$ and $R$ are the percentage weights of the matrix and the fibres respectively in the composite. In case of the filled composite, the density of the filler was also taken into account when calculating the theoretical density of the composite. The following relationship was used to calculate the theoretical density:

$$\rho_T = \frac{100}{\left(\frac{M}{\rho_m} + \frac{R}{\rho_f} + \frac{F}{\rho_{filler}}\right)} \qquad \textbf{Equation 37}$$

where $F$ is the percentage weight of the filler and $\rho_{filler}$ is the density of the filler.

The void fractions of the composites were also calculated from micrographs using ImageJ image processing software. ImageJ is a public domain, Java-based image processing program developed at the National Institutes of Health (National Institutes of Health, 2013). For calculating the void fraction the JPEG image obtained from the optical microscope was selected. The contrast in the colour of the voids and filled areas was used to calculate the area of the image having voids.

### *3.2.7 Optical microscopy*

Standard metallographic methods for potting and polishing were used for preparing the samples for optical microscopy. Zeiss Axioskop 2 microscope was used to obtain optical micrographs of the polished pultruded samples.

### *3.2.8 Inter-laminar shear strength*

The inter-laminar shear strength (ILSS) of the pultruded composites was measured according to BS EN ISO 14130:1998. The samples with dimensions, 22 mm × 11 mm × 2.2 mm, were cut using a water-cooled diamond wheel cutter. These were polished, dried and stored as described previously. A photograph of the experimental setup for conducting the ILSS test is shown in Figure 44.

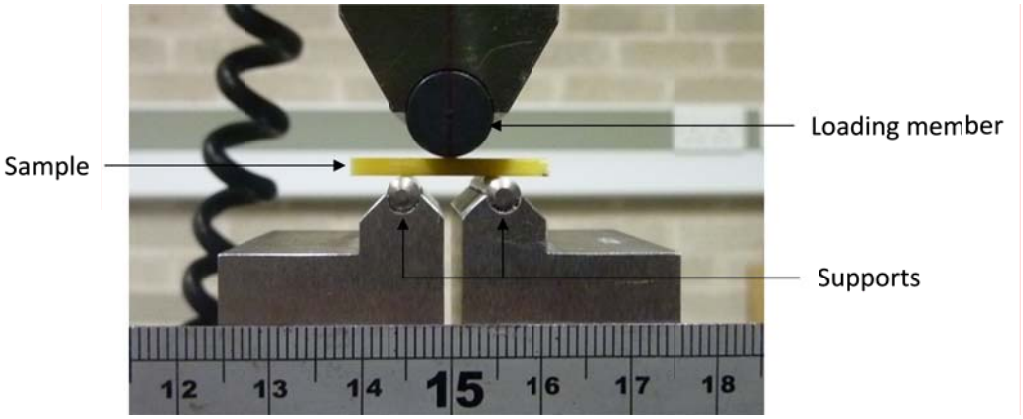


**Figure 44 Photograph showing the experimental set-up for the ILSS test.**

Following equation was used to calculate the ILSS:

$$ILSS = \frac{3}{4} \times \frac{F_M}{bh} \qquad \textbf{Equation 38}$$

where $F_M$ is the maximum (or failure) load, $b$ and $h$ are the width and thickness of the samples respectively.

### *3.2.9 Flexural properties (four-point bending)*

The flexural strength and modulus of the composites were measured according to ASTM D 6272-08. Samples with dimensions, 49 mm × 12.7 mm × 2.2 mm, were prepared and stored as described previously. A photograph of the experimental setup for carrying out the four-point bending experiments is shown in Figure 45.

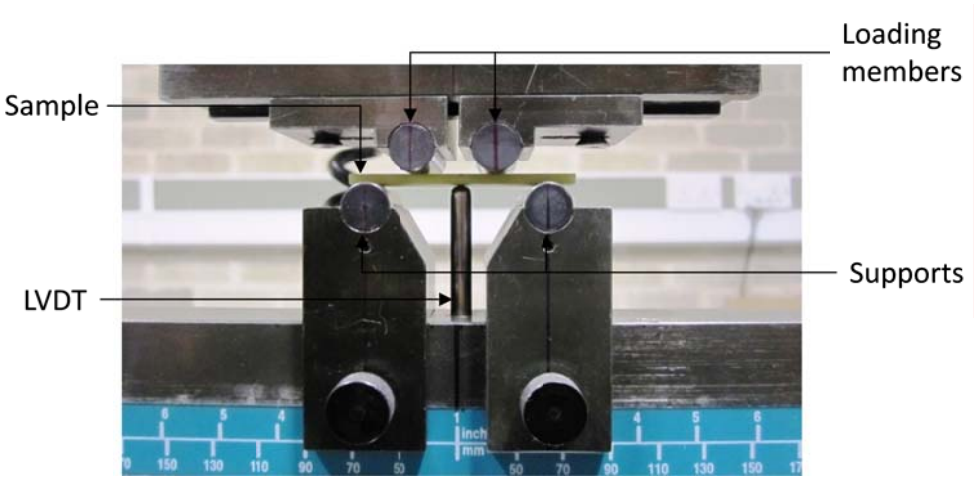


**Figure 45 Photograph showing the experimental set-up for the four-point bend test.**

The following equation was used to calculate the flexural strength (*FS*) of the composites:

$$FS = \frac{3}{4} \times \frac{P_{Max} L}{bh^2} \qquad \textbf{Equation 39}$$

where $P_{Max}$ is the maximum load on the load-deflection curve, $L$ is the length of the support span, $b$ and $h$ are the width and thickness of the sample respectively. The flexural modulus (*FM*) was calculated by using the slope ($m$) of the load-deflection curve and the following relationship:

$$FM = 0.17 \times \frac{L^3 m}{bh^3} \qquad \textbf{Equation 40}$$

## 3.3 COMPONENTS OF THE CLEAN PULTRUSION PROCESS

A schematic illustration of the key components of the clean pultrusion set-up used in this study is shown in Figure 46. A brief discussion on the key items shown in Figure 46 is discussed in this section.

A creel stand (item iii) was built to accommodate up to sixty creels (item i). The fibre-ends from each creel were guided through eyelets (item iv) which were attached to the creel stand. The rovings (item ii) from the creel stand were directed to the first guide plate-I (item v) followed by guide plate-II (item vi). The rovings from the guide plate-II were directed to a custom-made fibre spreading unit (item vii). This is discussed in greater details in Section 3.4.2. The spread rovings from the fibre spreader were directed to the resin impregnation unit (item viii). The design and details of the operation of the resin impregnation unit are discussed in Section 3.5.

After impregnation, the rovings were traversed into a heated die (item xi) where the impregnated rovings are consolidated and cured to a solid. The solid section is hauled off from the die by a cleat-type tractor puller (item xiv). When the desired length has been

pultruded, it is cut using a diamond wheel cutter (item xv). A unique feature of the clean pultrusion process is that the isocyanate and polyol components are stored in separate containers (item a and b) which are part of the resin dispensing unit (item ix). The resin dispensing unit (item ix) consists of four pumps which serves two circuits. The first circuit is a recirculation circuit (item c and d). The recirculation pumps circulate the individual components of the resin system (without mixing). The second set of pumps (item e and f) enables the flow of the individual components (isocyanate and polyol) to a manifold (item g) which in turn directs the individual liquid streams to a static mixer (item x). The technical specifications of the resin dispensing system are discussed in Section 3.6. In case of epoxy and vinyl ester resin systems, a pressure pot with premixed resin was used instead of the resin dispenser.

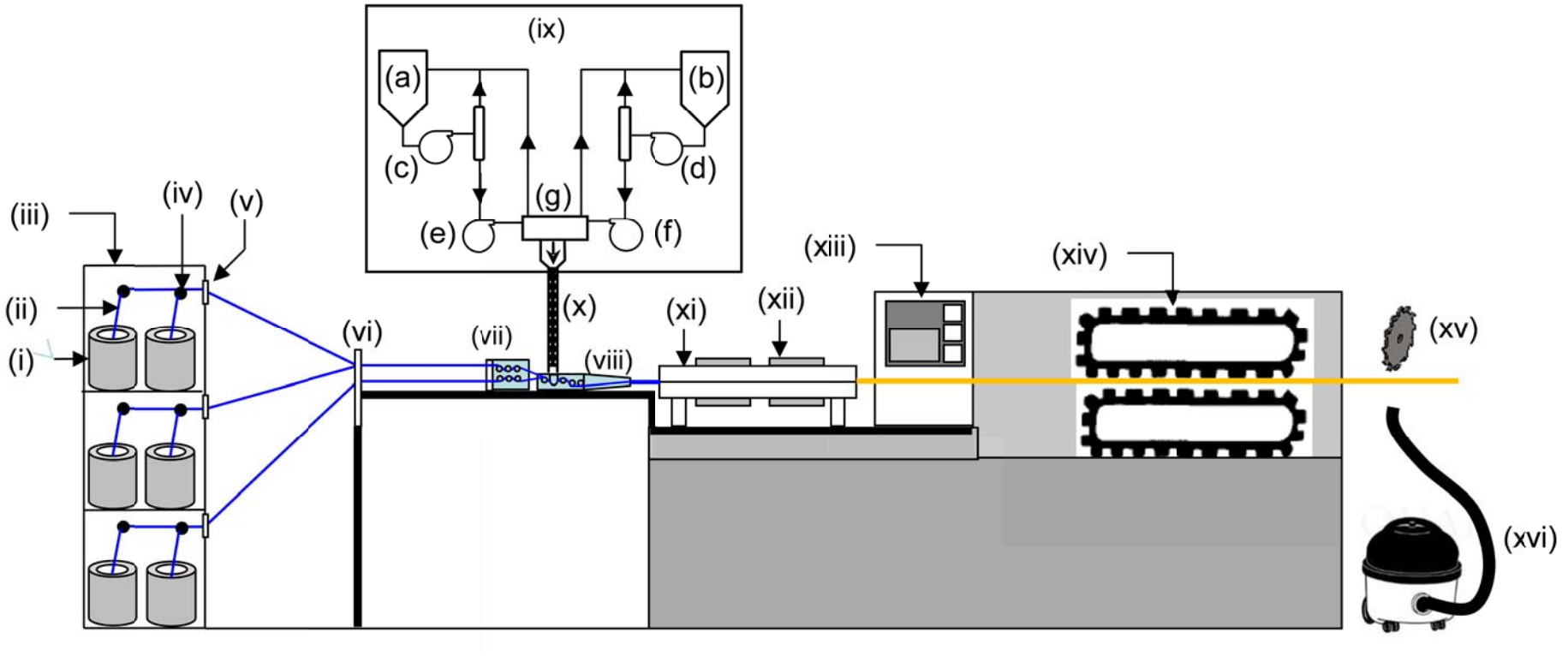


**Figure 46 Schematic illustration of the clean pultrusion concept. The key components are coded as follows: (i) creels; (ii) rovings; (iii) creel stand; (iv) eyelets; (v) guide plate-I; (vi) guide plate-II; (vii) fibre spreading device; (viii) resin impregnator; (ix) resin dispenser; (x) static mixer; (xi) die; (xii) heating elements; (xiii) control system; (xiv) cleat-type tractor puller; (xv) cutter; and (xvi) debris collection device. The coding for resin dispenser (item ix) is as follows: (a) isocyanate reservoir; (b) polyol reservoir; (c and d) recirculation gear pumps; (e and f) metering gear pumps; and (g) manifold.**

The following section presents a discussion on the primary components of the clean pultrusion process namely, the fibre spreading unit, the resin impregnation unit and the resin dispenser.

## 3.4 FIBRE SPREADING

### *3.4.1 Manual fibre spreading experiments via mechanical means*

Wilson (1997) developed a model to describe the spreading of polyamide rovings and cotton yarn as they were traverse backwards and forwards on a pair of pins. The experimental setup used by Wilson is shown in Figure 47 where a roving was fixed at one point (Y) and passed over a pair of rods; a weight was attached at the opposite end of the anchor point (Z) to apply tension to the roving. Rod-2 was included to make the arrangement symmetrical.

With reference to Figure 47, in Wilson's experiments, the spreading of the filaments was achieved by subjecting the roving to a series of back-and-forth motions; this reciprocating motion was carried out a few times until an equilibrium degree of fibre spreading was achieved. The width of the roving was then measured at the top of rod-1. Wilson treated the aggregate of the fibres in the roving as a continuum and derived an expression for the width of the roving, after spreading, at the first rod. The width ($W_1$) of the roving at the centre of the first rod was predicted as:

$$W_1 = (12\,AH)^{1/3} = (12\,AL\cos\alpha)^{1/3} \qquad \textbf{Equation 41}$$

where $A$ is the cross-sectional area of the roving, $\alpha$ is the angle subtended between the vertical and the anchor point (see Figure 47b), $L$ is the length of the roving from the anchor point to the tangential contact point on the first rod and $H$ is defined by the term '$L\cos\alpha$'. The term

'*Lcosα*' was treated as a single parameter representing the combined effect of '*L*' and '*α*'. Wilson named this term as 'lateral displacement'.

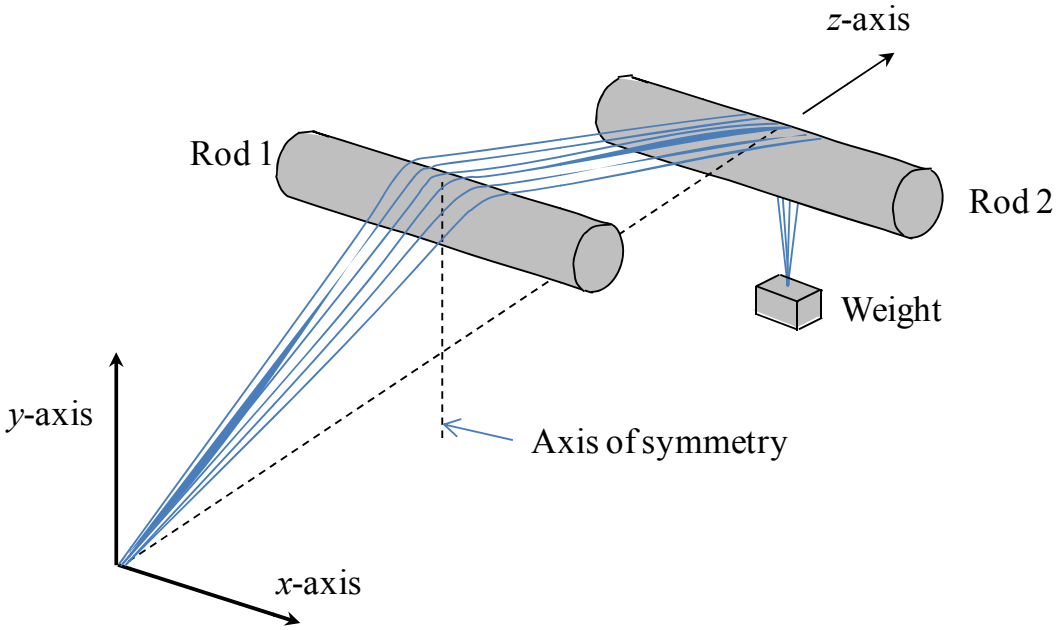


(a)

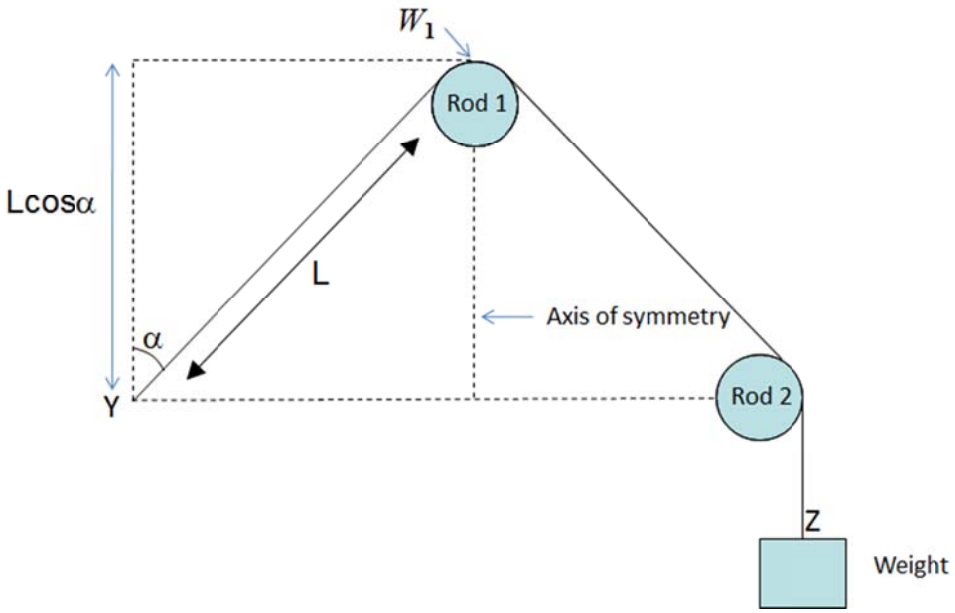


(b)

**Figure 47 Schematic illustration of the experimental setup adopted by Wilson (1997) to study lateral spreading of the individual filaments in a roving: (a) orthotropic view and (b) side view.**

The model proposed by Wilson (1997) was extended to estimate the fibre spreading at the second rod by Irfan et al. (2011). The details of this work are resented in Appendix-B. In the current work, the rig shown in Figure 48 was used to study mechanically-induced fibre spreading of a roving using the procedure previously performed by Wilson.

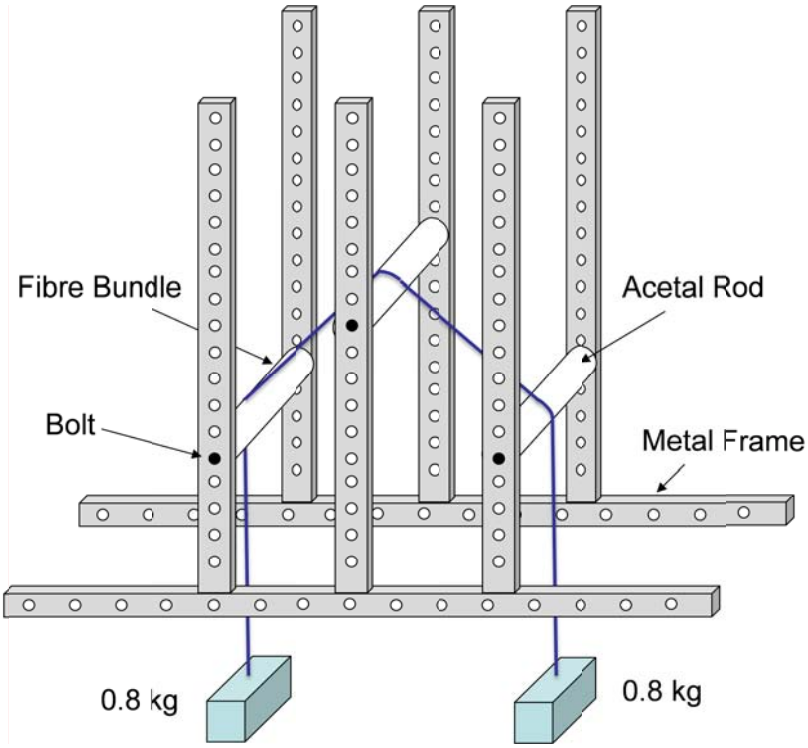


**Figure 48 Schematic illustration of the experimental setup for studying the mechanically induced spreading of a roving (Irfan et al., 2011).**

During the course of this study, it was observed that releasing the tension on the roving enhances the degree of fibre spreading. This observation is presented schematically in Figures 49 and 50. On the basis of this observation, a rig was designed and built to mimic the mechanical forces involved in the reciprocating motion including the observed effect of releasing the tension. With reference to Figure 49, an increase in the width of the E-glass roving as a result of reciprocating cycle is depicted schematically. Further increase in the width via tension-release mechanism is shown in Figure 50.

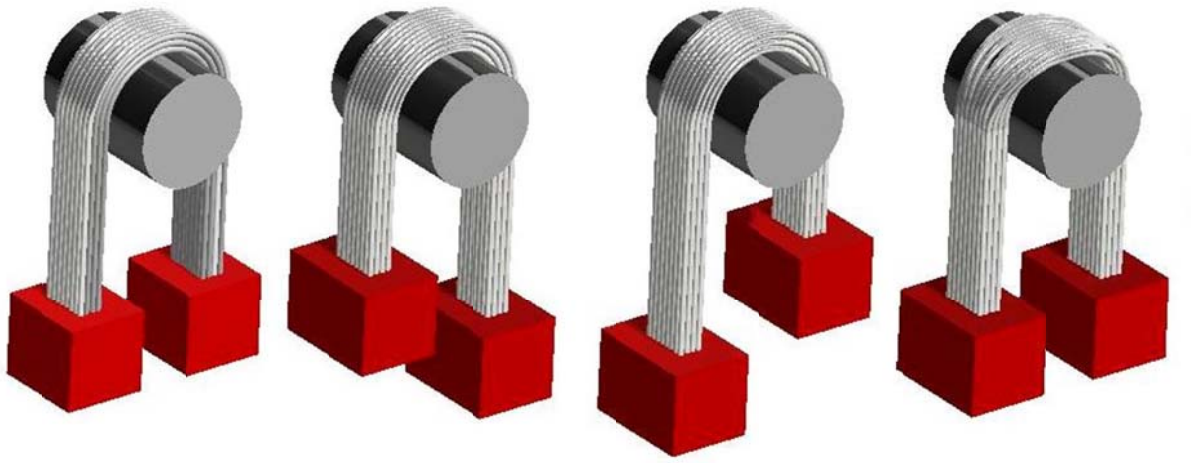

(a) (b) (c) (d)

**Figure 49 Schematic illustration of the reciprocating motion of a roving over a polymer rod. (a) as-received roving; (b) and (c) translation of the roving down and up respectively; (d) spread roving. The rig was designed M. S. Irfan and V. R. Machavaram; and illustrations are provided by F. B. Nieves, University of Birmingham, 2013.**

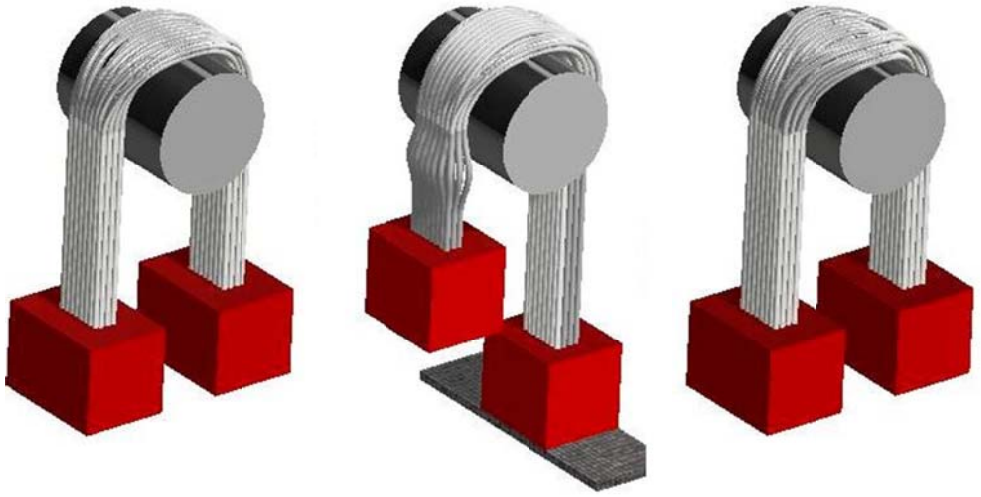

(a) (b) (c)

**Figure 50 Schematic illustration of: (a) spread roving as after applying the "tension-cycle";(b) sideways displacement of the filaments during the "tension-release" process; (c) spread roving after tension-release. The rig was designed M. S. Irfan and V. R. Machavaram; and illustrations are provided by F. B. Nieves, University of Birmingham, 2013.**

### *3.4.2 Automated fibre spreading rig*

With reference to the observations made in Figures 49 and 50, a fibre spreading rig was designed to mimic the mechanical forces involved in the reciprocating motion followed by the tension-releasing process.

#### 3.4.2.1 Design of the fibre spreading rig

A schematic illustration of the fibre spreading rig is presented in Figure 51 and a photograph of the rig is shown in Figure 52. With reference to Figure 51, the fibre spreading rig consists of three motorised roller-disk assemblies which were mounted in a Perspex chassis. Each of the roller-disk assemblies consisted of an acetal central drive shaft, which in turn drives a Perspex bearing housing (disc), positioned at each end of the shaft.

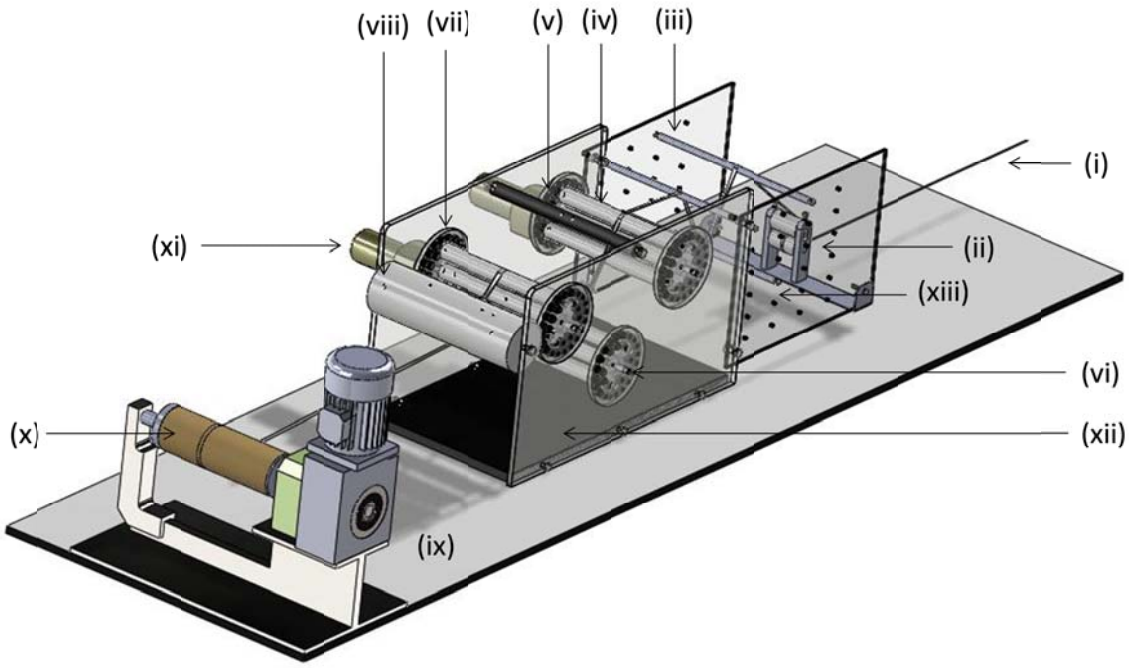


**Figure 51 Schematic illustration of the tension-release rig. The numbered items are as follows: (i) input roving from the creel; (ii) pre-tensioning device; (iii) secondary pre-tensioning bar; (iv) acetal rods; (v) first roller-disk; (vi) second roller-disk; (vii) third roller-disk (measuring point); (viii) exit roller; (ix) haul-off motor; (x) mandrel; (xi) motor for the roller-disk; (xii) perspex frame; and (xiii) perspex frame with a facility to control the secondary tension. Illustration by Francisco Nieves, University of Birmingham, 2013. Rig design by VR Machavaram and construction by Mark Paget, University of Birmingham, 2011.**

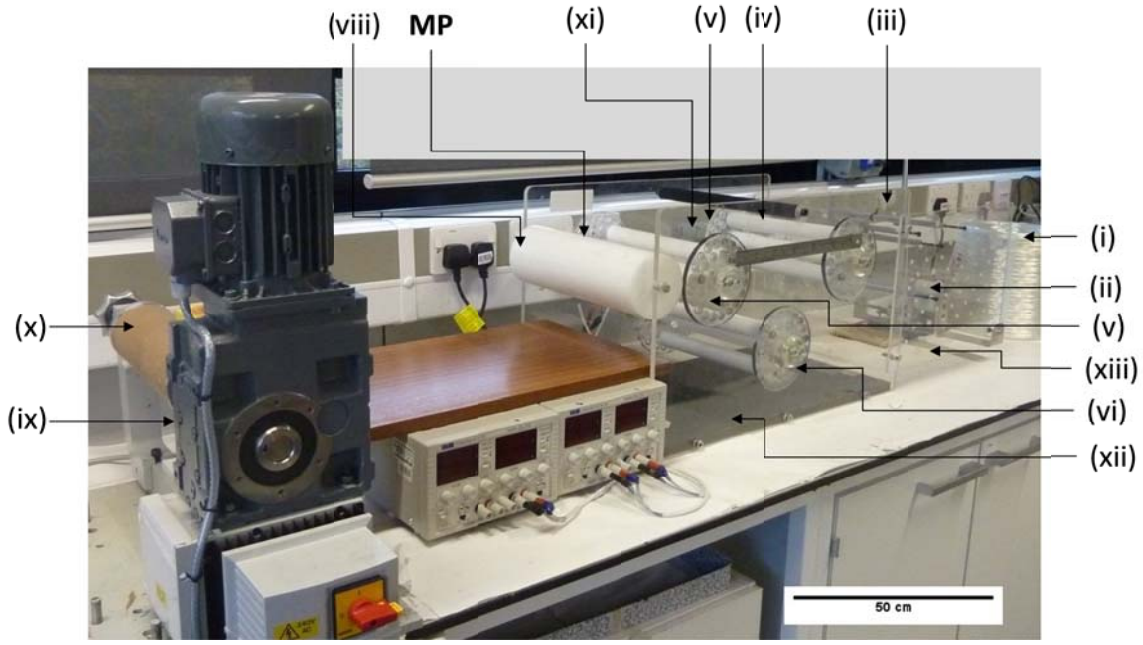


**Figure 52 Photograph of the tension-release fibre spreading rig. The position where the widths of the spread rovings were measured is indicated as MP. For details of the coded items see the caption of Figure 51.**

The bearing housings have multiple recessed positions arranged around their circumference in which ball bearings were fitted to support a series of acetal rollers. The acetal rollers were designed to be "locked" in position if desired to enable them to be used as pins. Each of the rotating roller-disks assembly was driven independently by a 12 volt DC direct-drive motor and gearbox. The rotation rate (clockwise or anti-clockwise) of the roller-disk is controlled by a variable voltage and amperage DC transformer.

The acetal rods (Direct Plastics, UK) used in roller-disk had a diameter of 30 mm and a length of 300 mm. The diameter of the Perspex disk was 150 mm. The revolutions per minute (rpm) of the disks were measured using a digital photo tachometer (Model: RM-1501, RS Calibration). The larger-diameter roller positioned subsequent to the third rotating roller-disk assembly was meant to preserve the spreading achieved as the roving traversed towards the haul-off unit.

### 3.4.2.2 Experimental design for the fibre spreading rig

The following parameters were considered to have an influence on the extent of fibre spreading: (i) the number of rollers or pins on each of the roller-disk; (ii) the diameter of rollers or pins present on each of the roller-disk; (iii) the rotational velocity and the direction of rotation of the roller-disk; (iv) the haul-off speed of the rovings; (v) the magnitude of the friction experienced by the roving; (vi) the tension in the roving; (vii) the degree of twists in the roving; (viii) the binder-content on the roving; and (ix) the tex of the roving.

A mixed level Taguchi experimental design method was used to evaluate the effect of the major parameters that were considered to affect the degree of fibre spreading. The Taguchi method is a fractional factorial design optimisation technique to extract information about an experimental setup by conducting a minimum number of experiments. This is a cost and time-effective method to evaluate the experimental variables associated with a system. The Taguchi method is generally used to study the effect of the main factors on the experimental response. Table 10 enlists the selected factors and their levels. In the context of experimental design, 'factors' are defined as those physical parameters which affect the output response of the experiment, for example, the extent of fibre spreading. The values of the factors chosen for the experiments are termed as their 'levels' (Filippone, 1989). Table 11 show the $L_{18}$ orthogonal array with the eighteen experimental combinations of the chosen factors. Each experiment was repeated ten times. Minitab® software was used to generate the $L_{18}$ array. The response parameters selected for the optimisation were: (a) fibre damage and segmentation (observed visually); and (b) width of the fibre roving after spreading (measured at roller-disk assembly 3, denoted by MP in Figure 52). The widths of the as-received rovings were measured at intervals of 5cm over a length of 5 m using a digital calliper.

**Table 10 Factors and levels selected in the experimental matrix.**

| Factors | Factor description | Level 1 | Level 2 | Level 3 | Level 4 | Level 5 | Level 6 |
|---|---|---|---|---|---|---|---|
| A | Configuration | 1 | 2 | 3 | 4 | 5 | 6 |
| B | Pre-tension (N) | 2 | 6 | 10 | - | - | - |
| C | Pull speed (m/min) | 1 | 3 | 5 | - | - | - |
| D | Disk rotation (rpm) | 25 | 50 | 100 | - | - | - |

* See Figure 53 for the details of each of the rotating roller-disk configurations.

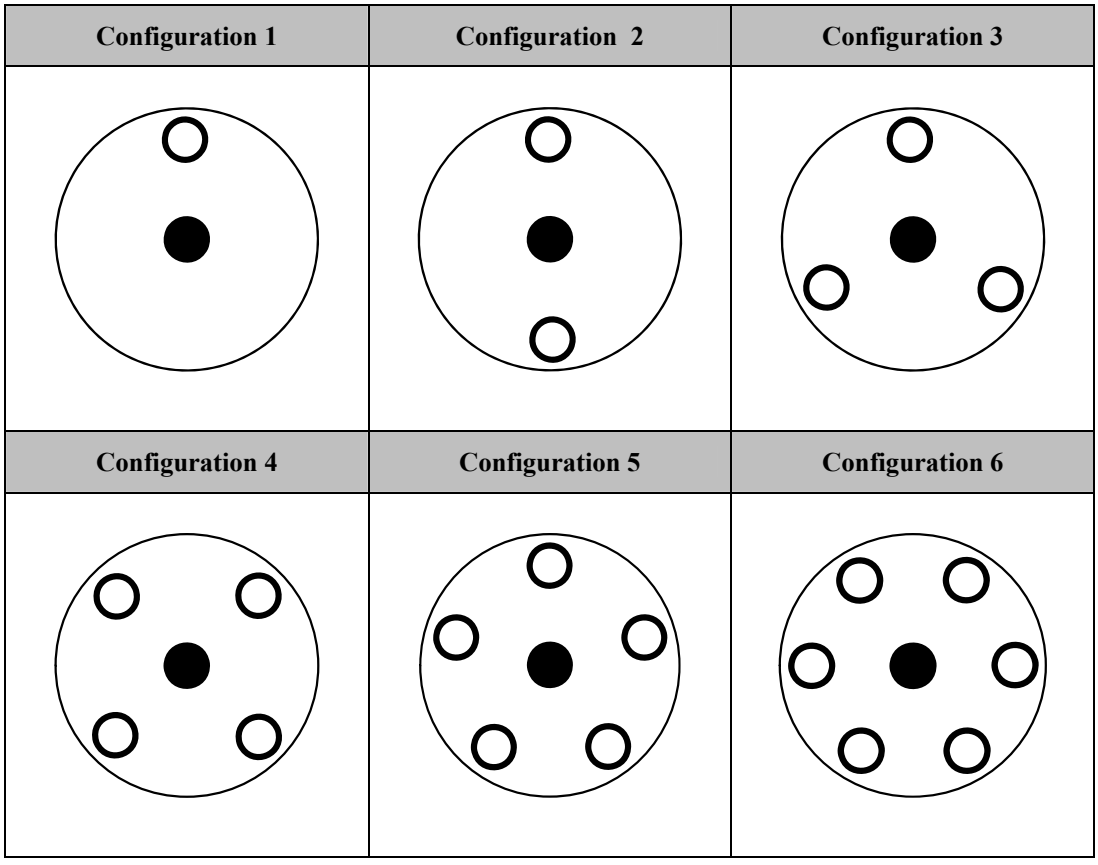


**Figure 53 Details of the roller-disk configurations. Here the solid circle represents the central shaft of the rotating roller-disk assembly and the unfilled circle represents the acetal rollers.**

**Table 11 Taguchi-based experimental matrix for the $L_{18}$ orthogonal array.**

| | Factors and levels | | | |
|---|---|---|---|---|
| **Trial no** | **A** | **B** | **C** | **D** |
| 1 | 1 | 1 | 1 | 1 |
| 2 | 1 | 2 | 2 | 2 |
| 3 | 1 | 3 | 3 | 3 |
| 4 | 2 | 1 | 1 | 2 |
| 5 | 2 | 2 | 2 | 3 |
| 6 | 2 | 3 | 3 | 1 |
| 7 | 3 | 1 | 2 | 1 |
| 8 | 3 | 2 | 3 | 2 |
| 9 | 3 | 3 | 1 | 3 |
| 10 | 4 | 1 | 3 | 3 |
| 11 | 4 | 2 | 1 | 1 |
| 12 | 4 | 3 | 2 | 2 |
| 13 | 5 | 1 | 2 | 3 |
| 14 | 5 | 2 | 3 | 1 |
| 15 | 5 | 3 | 1 | 2 |
| 16 | 6 | 1 | 3 | 2 |
| 17 | 6 | 2 | 1 | 3 |
| 18 | 6 | 3 | 2 | 1 |

### *3.4.3 Compact fibre spreading rig*

The outcome of the fibre spreading experiments that were carried out using the automated fibre spreading rig, as discussed in Section 3.4.2, was used to design a compact version that could be integrated on the pultrusion line. As mentioned previously, primary motivations for spreading the filaments in the rovings are: (i) to break up the binder that hold the filaments together; (ii) to reduce the nominal thickness of the roving (by spreading); and (iii) to enhance the through-thickness impregnation of the resin. Schematic illustrations of this rig are shown in Figure 54. A photograph of the compact fibre spreading unit is shown in Figure 55.

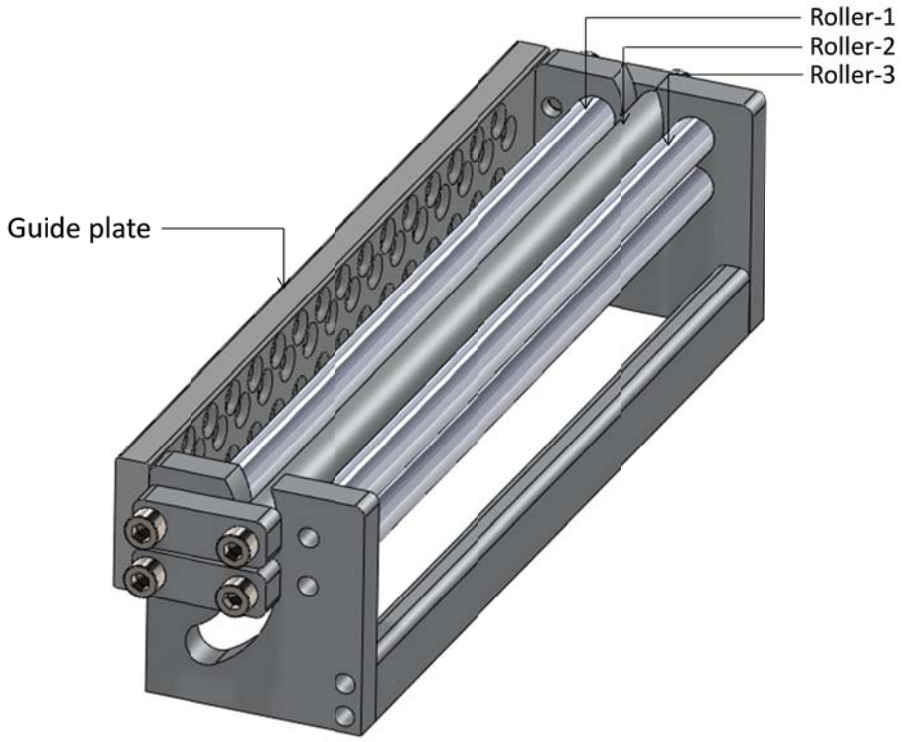


(a)

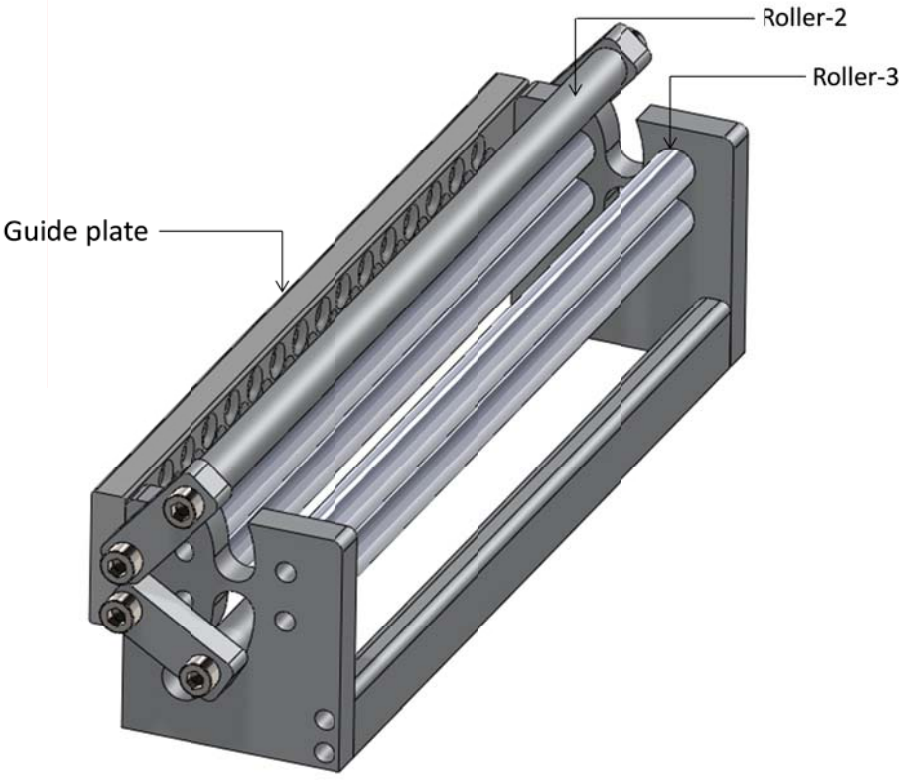


(b)

**Figure 54 Schematic illustration of the compact fibre spreading rig. (a) Closed configuration and (b) Open configuration. Illustration by Francisco Nieves, University of Birmingham, 2013. Rig design and construction by Mark Paget, University of Birmingham, 2011.**

The compact fibre spreading rig which consisted of six aluminium rollers (each having a radius of 5 mm) arranged in two rows. Each row operates independently. The mode of operation of this compact fibre spreading unit is illustrated schematically in Figure 56 where a flexible arm with roller can be positioned as desired to change the trajectory and hence the tension on the rovings. This is illustrated in Figure 56(a-c).

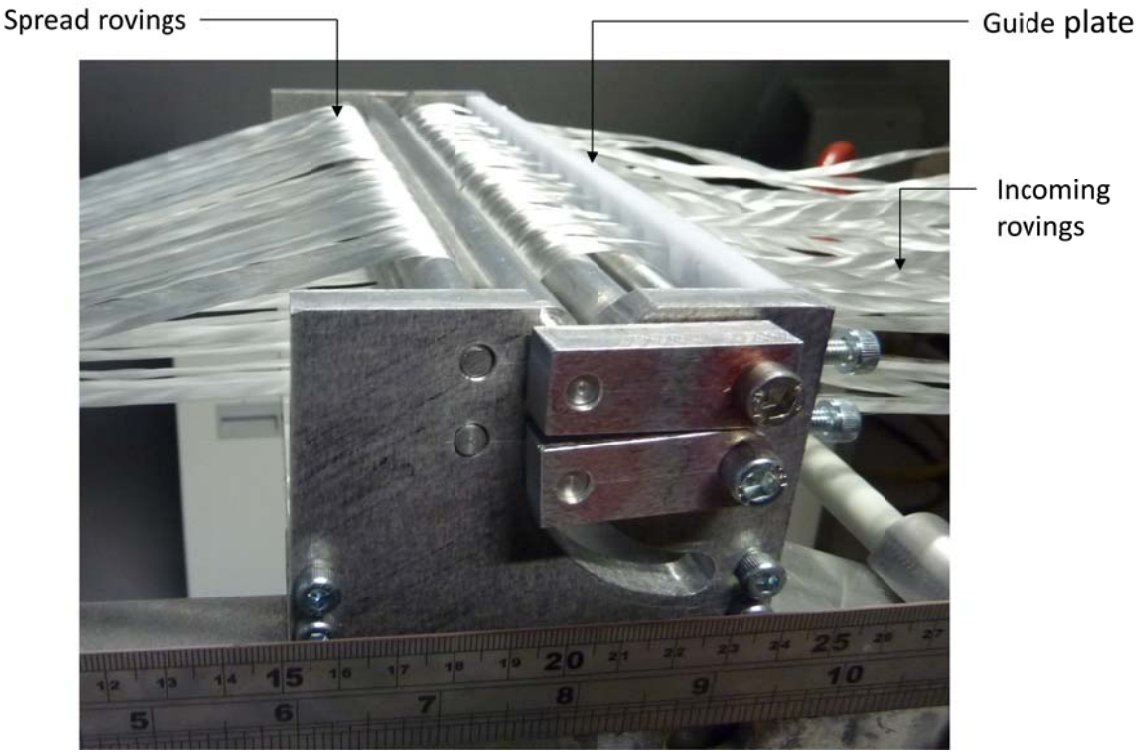


**Figure 55 Photograph of the compact fibre spreading rig.**

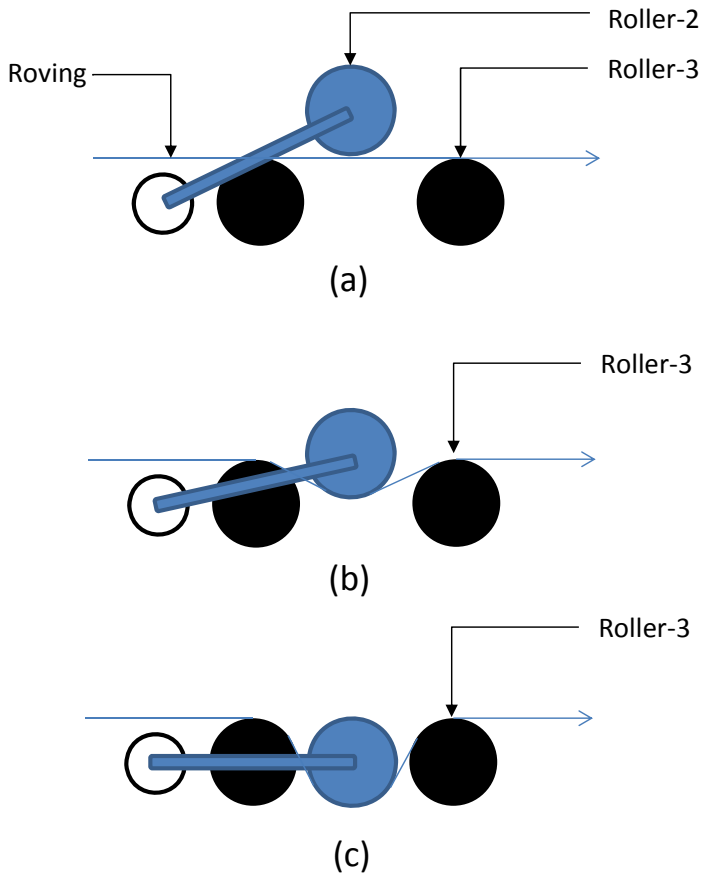


**Figure 56 Schematic illustration of the movement of the centre-roller to control the degree of fibre spreading: (a) setting-I: fully open; (b) setting-II: mid-way; and (c) setting-III: fully closed. The degree of fibre spreading was measured at Roller-3.**

## 3.5 DESIGN OF THE RESIN IMPREGNATORS

### *3.5.1 Design objectives*

The resin impregnators were designed to fulfil the following requirements: (a) to increase the transverse impregnation via spreading the rovings; (b) to control the volume of resin deposited on the rovings; (c) to enable a combination of pin, injection and capillary-impregnation; (d) to facilitate easy threading of the rovings; (e) to enable easy dismantling and cleaning the impregnation unit; (f) to ensure minimal dead-space for the resin to stagnate; and (g) to impose minimal tension on the rovings.

### *3.5.2 Impregnator design*

A schematic illustration of the experimental setup for the compact fibre spreader and the resin impregnation unit is shown in Figure 57. The details of the compact fibre spreading rig were discussed previously in Section 3.4.3. The resin impregnation unit was designed to accommodate sixty (2400 tex) or thirty (4800 tex) E-glass rovings. The number of rovings was selected on the basis of the dimensions of the profile of the die (32 mm × 2.2 mm).

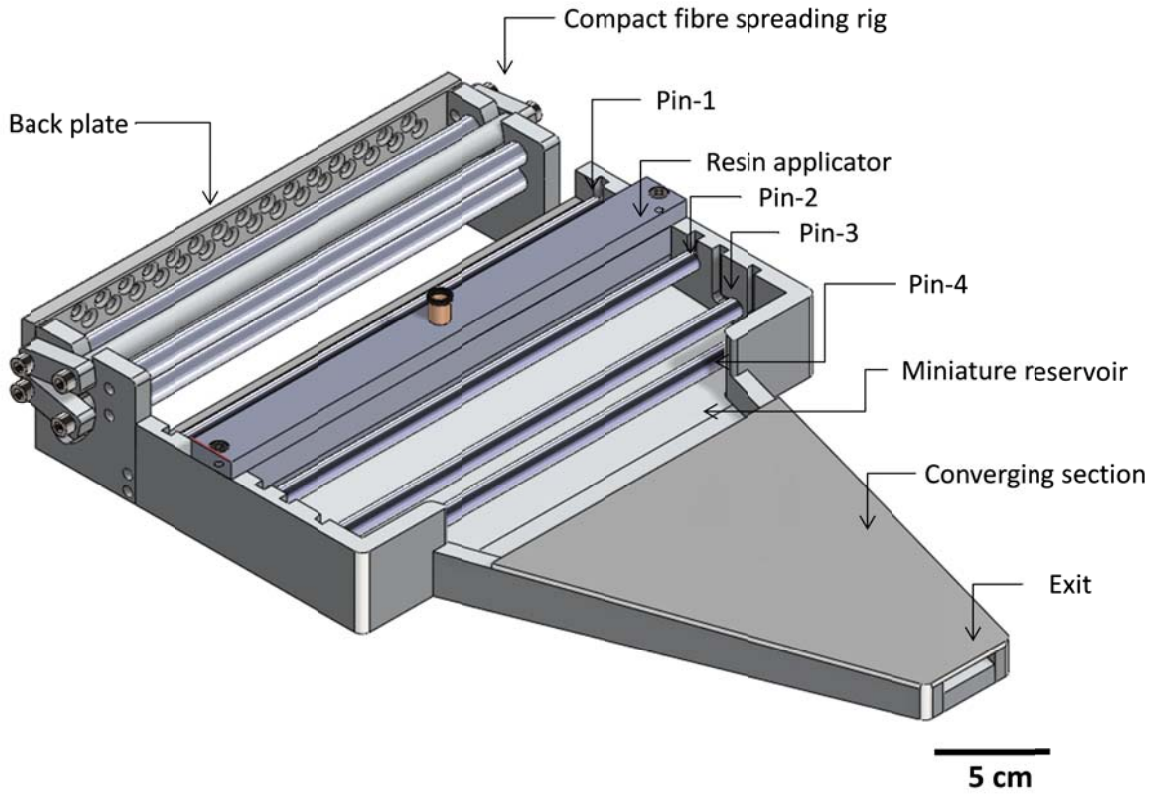


**Figure 57 Schematic illustration of the compact fibre spreading rig and resin impregnation unit. The rig was designed M. S. Irfan, N. Shotton-Gale, M. A. Paget and G. F. Fernando; and illustrations are provided by F. B. Nieves, University of Birmingham, 2013.**

Two resin applicators were designed; one of these was based on pin-impregnation and the other on resin-injection. These were designed such that they could be fitted in the chassis of the resin impregnation unit as shown in Figure 57. A ribbon of the spread rovings from the fibre spreading unit was directed to the resin-applicator where the resin was applied onto the

fibres. With reference to Figure 58(a), resin applicator PUL-I was designed to inject the resin directly into the spread rovings. In the case of resin applicator PUL-II, as shown in Figure 58(b), the resin was fed to the rovings using the curtain-flow concept. Here the resin wedge that is formed between the applicator and in-coming fibre ribbon aids the impregnation process. The side views of the two resin applicators are shown in Figure 59.

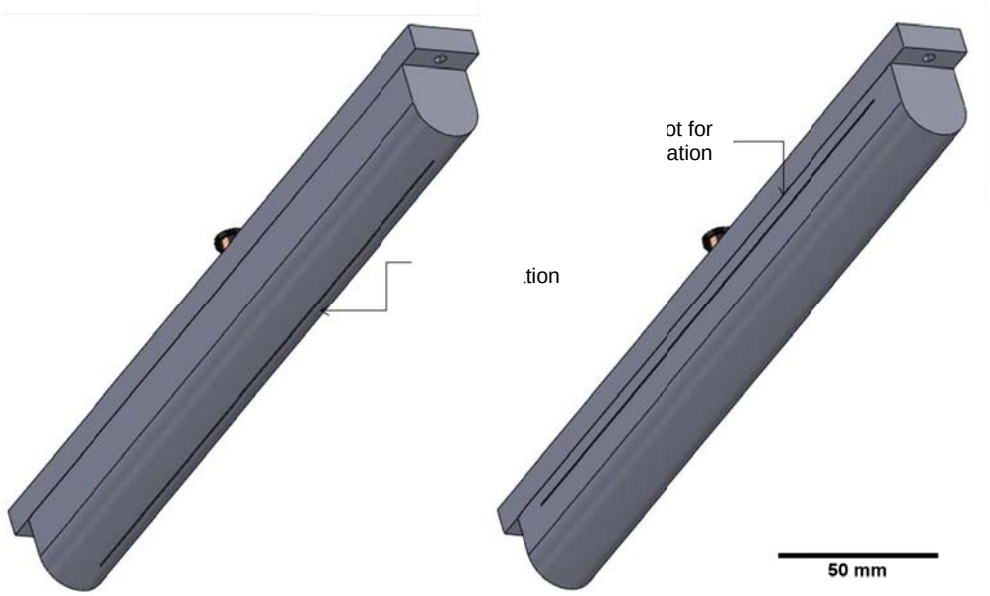


(a) (b)

**Figure 58 Schematic illustrations of the resin applicators: (a) PUL-I; and (b) PUL-II. Illustrations by Francisco Nieves, University of Birmingham, 2013.**

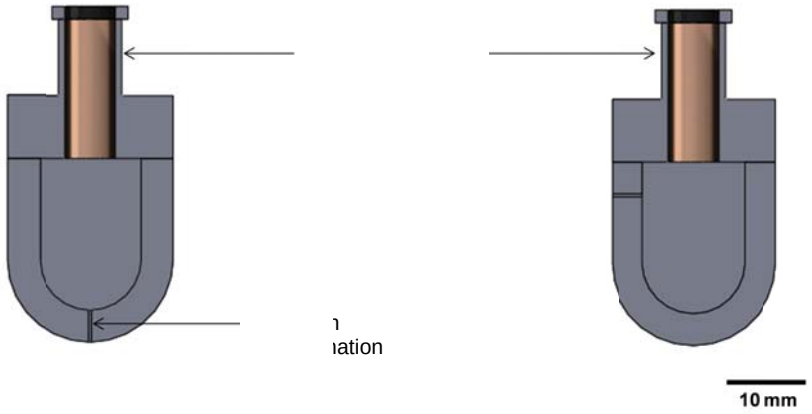


(a) (b)

**Figure 59 Schematic illustrations of the side views of the resin applicators: (a) PUL-I; and (b) PUL-II. Illustrations by Francisco Nieves, University of Birmingham, 2013.**

After the rovings were traversed under the resin applicator, their trajectory is changed as the partially impregnated fibres are passed over a pin and under two further pins as shown in Figures 60(a & b). From here on, the fibres are converged in the "converging section" of the resin impregnation unit. The resin that was squeezed out from the fibres within the converging section of the resin impregnation unit (inclined at an angle of 5°) is guided back to the miniature reservoir. The resin drips from the exit point of the impregnator were negligible.

### *3.5.3 Design calculations*

The efficiency of the resin impregnators was defined by a dimensionless impregnation number ($I_{imp}$). It was assumed that for a particular set of parameters including the pultrusion speed, pre-tension, resin viscosity and fibre type, the value of $I_{imp}$ should be equal to or more than one to obtain complete impregnation. The following section presents a step-wise description of the calculations to obtain the impregnation number ($I_{imp}$) for resin impregnators PUL-I and PUL-II.

#### 3.5.3.1 Step-1: Calculation of the total impregnation length

The overall impregnation length was calculated from geometrical considerations of the impregnators. This was done by dividing the impregnator into seven zones as illustrated in Figures 60 (a and b). A specified mode of impregnation was then assigned to each zone. The impregnation time that is available for the rovings traversing through the resin impregnator is a function of the trajectory of the rovings and pultrusion speed. With reference to Figures 60 (a and b), the contact lengths available in each section of the resin impregnators are summarised in Table 12.

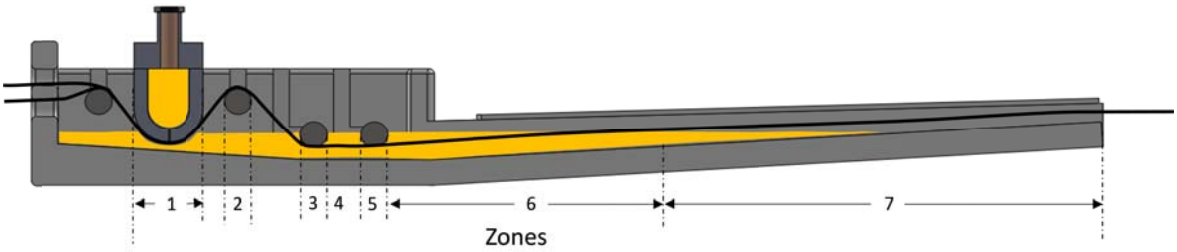


(a)

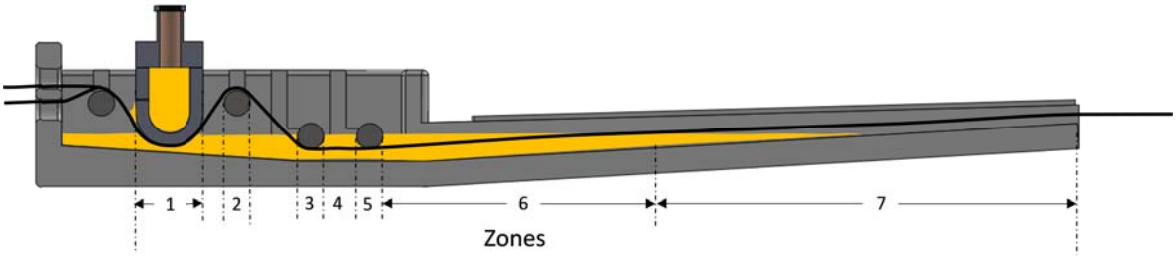


(b)

**Figure 60 Schematic illustration of the resin impregnators showing the trajectory of rovings: (a) resin impregnator PUL-I; and (b) resin impregnator PUL-II. The details of the coding for the different zones are summarised in Table 12. Illustrations by Francisco Nieves, University of Birmingham, 2013.**

**Table 12 Contact length and corresponding mode of impregnation for each zone of the resin impregnators PUL-I and PUL-II. Here contact length is defined as the length for which the roving experiences a particular mode of impregnation in the impregnator.**

| Zone | Contact length (mm) | Impregnation mode (PUL-I) | Impregnation mode (PUL-II) |
|---|---|---|---|
| 1 | 21 | Injection | Pin-impregnation |
| 2 | 10 | Pin-impregnation | Pin-impregnation |
| 3 | 2 | Pin-impregnation | Pin-impregnation |
| 4 | 10 | Capillary | Capillary |
| 5 | 2 | Pin-impregnation | Pin-impregnation |
| 6 | 100 | Capillary | Capillary |
| 7 | 110 | Compaction | Compaction |

The arc lengths along the resin applicator and at zones 2, 3 and 5 were calculated by:

$$L = \frac{\varphi}{180}\pi R \qquad \textbf{Equation 42}$$

where $L$ is the arc length, $\varphi$ is the angle subtended by the roving with the centre of the pin and $R$ is the radius of the pin.

The fixed parameters used for the calculations performed in next sections are given in Table 13.

**Table 13 Summary of the fixed parameters used to calculate the extent of impregnation for impregnators PUL-I and PUL-II.**

| Parameter | Units | Values |
|---|---|---|
| Viscosity of the resin ($\eta$) | Pa·s | 1.03 |
| Fibre volume fraction ($V_f$) | % | 70 |
| Thickness of the roving ($Z$) | μm | 125 |
| Width of the roving ($W$) | mm | 8 |
| Radius of the fibre ($r_f$) | μm | 8.5 |
| Pre-tension in the roving ($T$) | N | 10 |
| Maximum fibre packing ($V_A$) | % | 90.7 |
| Roving architecture | - | Hexagonal |
| Coefficient of transverse permeability ($K$) | $m^2$ | $1.09\times10^{-13}$ [1] |

[1] Calculated using Equation 14.

#### 3.5.3.2 Step-2: Estimation of the extent of injection-based impregnation

The resin was injected directly onto the surface of the fibre ribbon in zone-1 of PUL-I as shown in Figure 60(a). The depth of the impregnation in the roving ($Z_{inj}$) as a result of injection-based impregnation was estimated from following relationship which is derived from Equation 6:

$$Z_{inj} = \sqrt{\frac{2t_{inj}KP_{inj}}{\eta}} \qquad \textbf{Equation 43}$$

where $t_{inj}$ is time available for resin injection and $P_{inj}$ is the resin injection pressure. The time ($t_{inj}$) available for the roving to experience impregnation via resin injection was calculated using:

$$t_{inj} = \frac{L_{inj}}{V} \qquad \textbf{Equation 44}$$

where $L_{inj}$ is the width of the injection-slot (0.4 mm) and $V$ is the pultrusion speed. The extent of injection impregnation ($I_{inj}$) was calculated by:

$$I_{inj} = \frac{Z_{inj}}{Z} \times 100 \qquad \textbf{Equation 45}$$

The estimated percentage impregnation obtained by resin-injection as a function of the three pultrusion speeds used in this study is shown in Figure 61. The simulations were carried out for two types of resin delivery systems; pressure-pot and resin dispenser. This simulation is only applicable for resin impregnator PUL-I.

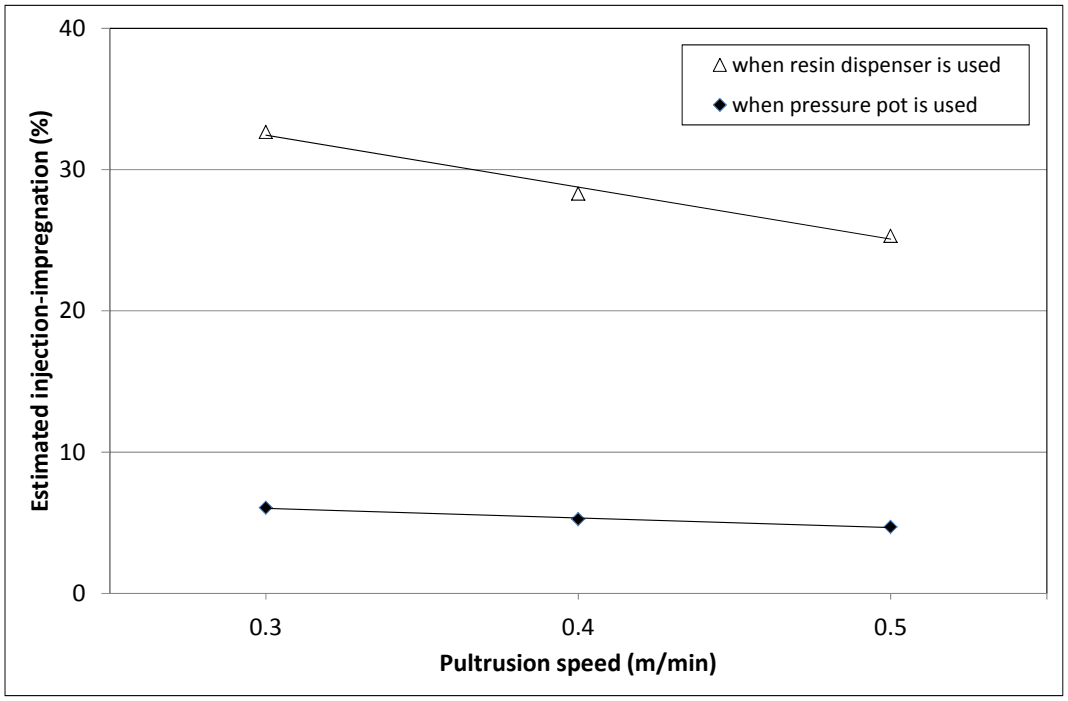


**Figure 61 Simulations for the estimated resin injection-based impregnation for resin impregnator PUL-I as a function of the pultrusion speed.**

### 3.5.3.3 Step-3: Estimation of the extent of pin-impregnation

The thickness of the roving that has been impregnated via pin-impregnation was estimated using Equation 46:

$$Z_{pin} = \sqrt{\frac{2t_{pin}KP_{pin}}{\eta}} \qquad \textbf{Equation 46}$$

$P_{pin}$ was calculated using Equation 18 and $t_{pin}$ was estimated from:

$$t_{pin} = \frac{L_{pin}}{V} \qquad \textbf{Equation 47}$$

where the length available for the roving to experience the pin-impregnation $L_{pin}$ was calculated from Equation 22. The value of $h_1$ that was used to calculate $L_{pin}$ was assumed to be equal to the radius of a single filament (8.5 μm). It has been reported by Chandler et al. (1992) that the $h_1$ can be between the value of the fibre spacing and about half the roving thickness.

The estimated percentage impregnation obtained by pin-impregnation ($I_{pin}$) for each pin was calculated by:

$$I_{pin} = \frac{Z_{pin}}{Z} \times 100 \qquad \textbf{Equation 48}$$

**Table 14 Extent of pin-impregnation in specified zones of the resin impregnator (see Figures 60 (a and b). Here Zone-1 to 4 were acting for PUL-II while only Zone-2 ro 4 were in action for PUL-I.**

| Location | Extent of pin-impregnation (%) | | |
|---|---|---|---|
| | Pultrusion speed | | |
| | 0.3 m/min | 0.4 m/min | 0.5 m/min |
| Zone-1 | 21.19 | 26.42 | 31.01 |
| Zone-2 | 5.22 | 7.02 | 8.63 |
| Zone-3 | 5.22 | 7.02 | 8.63 |
| Zone-5 | 5.22 | 7.02 | 8.63 |
| Total | 36.85 | 47.48 | 56.9 |

The total impregnation due to pin-impregnation as a function of the pultrusion speed is shown in Figure 62.

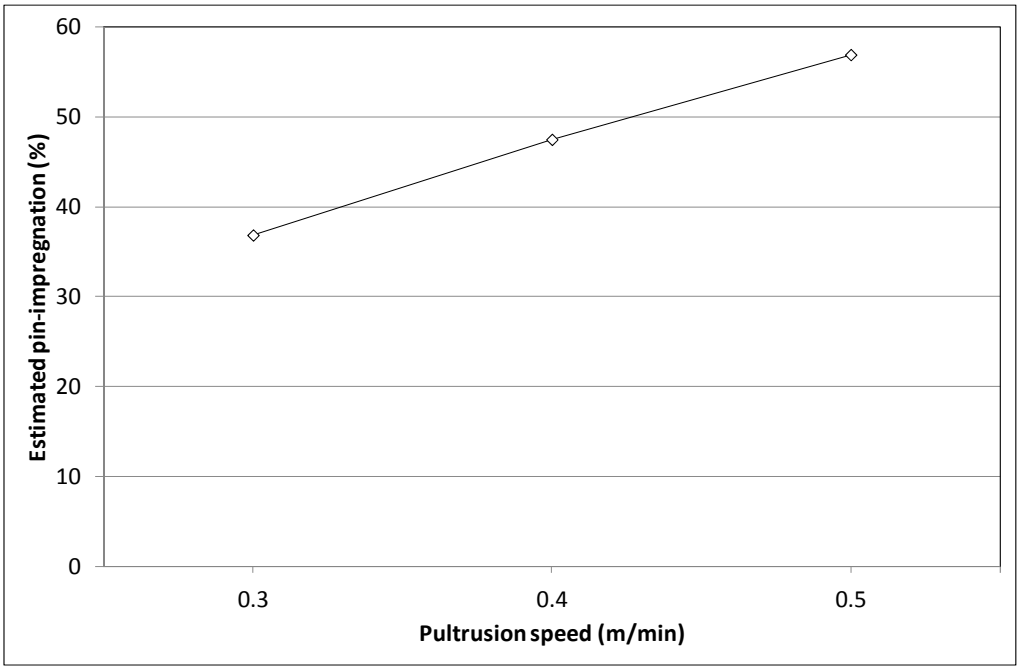


**Figure 62 Estimated degree of pin-impregnation as a function of the pultrusion speed.**

#### 3.5.3.4 Step-4: Estimation of the extent of capillary-impregnation

The zones of the resin impregnators where capillary-impregnation was taking place are depicted in Figure 60 and Table 12. The thickness of the roving that has been impregnated via capillary-impregnation was estimated by:

$$Z_c = \sqrt{\frac{2t_c K P_c}{\eta}} \qquad \textbf{Equation 49}$$

The time for the rovings to experience capillary-impregnation was calculated by:

$$t_c = \frac{L_c}{V} \qquad \textbf{Equation 50}$$

where $t_c$ is the time for capillary-impregnation and $L_c$ is the length available in the impregnator in the zones 4 and 6.

The capillary pressure ($P_c$) was calculated using the following equation (Ahn et al., 1991):

$$P_c = \frac{4\sigma \cos\theta}{D_E} \qquad \textbf{Equation 51}$$

where $P_c$ is the capillary pressure, $\sigma$ is the surface tension of the liquid, $\theta$ is the contact angle between the liquid and the roving, and $D_E$ is the equivalent diameter of the pores in a roving which can be calculated using:

$$D_E = \frac{8r_f}{F}\frac{1-V_f}{V_f} \qquad \textbf{Equation 52}$$

where $r_f$ is the fibre radius, $V_f$ is the fibre volume fraction of the roving and $F$ is the form factor depending on the alignment of the fibres and direction of the resin flow.

The parameters used for the calculations of capillary pressure are summarised in Table 15. The extent of capillary-impregnation ($I_{capillary}$) was calculated using:

$$I_{capillary} = \frac{Z_c}{Z} \times 100 \qquad \textbf{Equation 53}$$

A graphical representation of the total impregnation due to capillary impregnation as a function of the pultrusion speed is presented in Figure 63.

**Table 15 Summary of the parameters used to calculate the impregnation-zone length assuming capillary-impregnation.**

| Parameter | Units | Value |
|---|---|---|
| **Assumed values** | | |
| Surface tension of the epoxy resin ($\zeta$) | N/m | 0.044[1] |
| Contact angle between the fibre and the resin (°) | Degrees | 57[1] |
| Form factor ($F$) | - | 2 |
| Maximum fibre packing ($V_A$) | % | 90.7 |
| Fibre architecture | - | Hexagonal |
| **Calculated values** | | |
| Wetted diameter ($D_E$) | mm | 0.0145 |
| Transverse capillary pressure ($P_c$) | kPa | 6.58 |

[1] from Amico and Lekakou (2002)

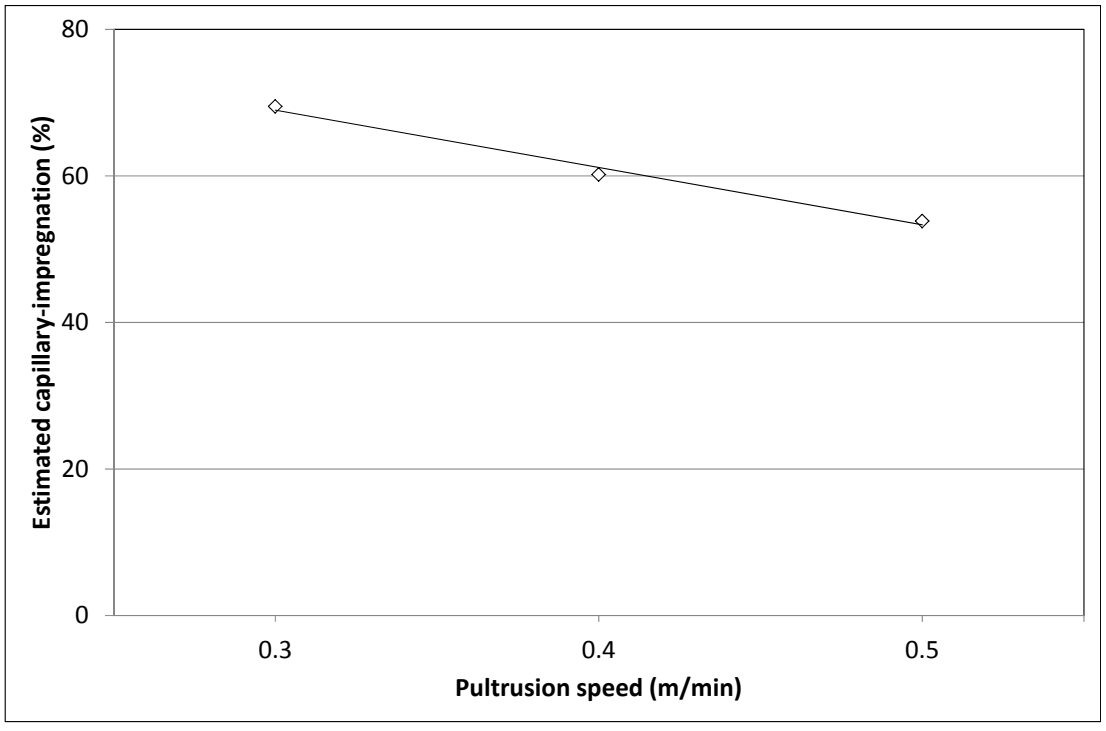


**Figure 63 A simulation of the estimated degree of capillary-impregnation in resin impregnators PUL-I and PUL-II as a function of the pultrusion speed.**

#### 3.5.3.5 Step-5: Estimation of the extent of impregnation in the converging zone

With reference to Figure 57, the "converging" zone represents the case where the impregnated rovings start to converge prior to reaching the exit-point of the resin impregnation unit. In order to estimate the pressure exerted on the impregnated rovings in this "converging" zone (Figure 57), an approach used in the resin-injection pultrusion process was adopted. This converging section gives rise to an increase in the pressure experienced by the impregnated rovings due to compaction (Palikhel et al., 2012). Connolly (2008) used transducers to measure the pressure in the resin-injection chamber. In the current study, the pressure was estimated from the parameters reported by Palikhel et al. (2012).

Palikhel et al. (2012) reported that for a resin-injection chamber with a compression ratio of 4.0 (the resin viscosity was 0.75 Pa.s, with a fibre volume fraction of 68%) the increase in the pressure at the exit of the resin-injection chamber was 378 kPa; the resin injection pressure was 2 kPa. The length of the converging section was 0.15 metres. In the current study, the assumption was made that the pressure-rise in the converging section, for the profile illustrated in Figures 60, the rise in pressure would follow a similar trend as reported by Palikhel et al. (2012). It was also assumed that the pressure at the start of zone-7 was atmospheric. The depth of the impregnation in the roving ($Z_{comp}$) as a result of impregnation due to compaction at the exit of the resin impregnator was estimated from:

$$Z_{comp} = \sqrt{\frac{2t_{comp} KP_{comp}}{\eta}} \qquad \textbf{Equation 54}$$

where $t_{comp}$ is time for impregnation through the compaction zone and $P_{comp}$ is the resin pressure in the compaction zone.

The time for the roving to undergo impregnation via fibre compaction was calculated by:

$$t_{comp} = \frac{L_{comp}}{V} \qquad \textbf{Equation 55}$$

where $t_{comp}$ and $L_{comp}$ are the time and the length respectively for which impregnation through fibre compaction takes place and $V$ is the pultrusion speed. The percentage impregnation due to compaction ($I_{comp}$) in the converging section was calculated by:

$$I_{comp} = \frac{Z_{comp}}{Z} \times 100 \qquad \textbf{Equation 56}$$

The estimated impregnation obtained in the converging section as a function of the three pultrusion speeds used in this study is shown in Figure 64.

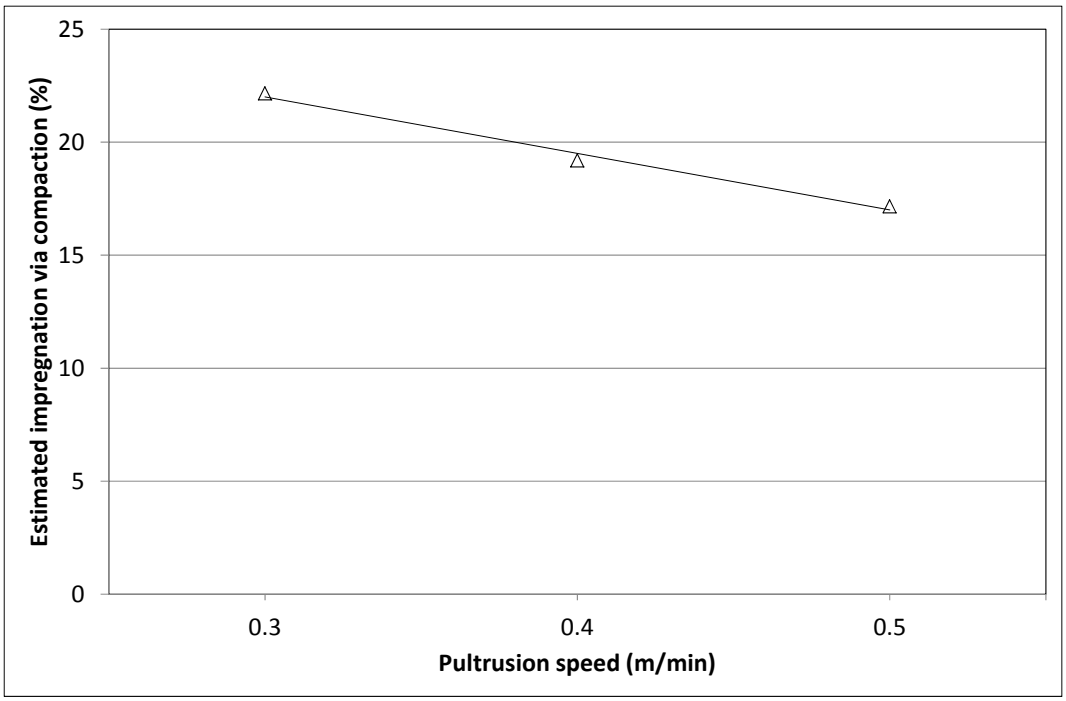


**Figure 64 The estimated degree of impregnation in the converging section (zone-7) of the resin impregnator (see Figure 60 (a and b)) as a function of the pultrusion speed.**

### 3.5.3.6 Step-6: Estimation of the impregnation number

The resin impregnation number ($I_{imp}$) for impregnators PUL-I and PUL-II was determined using the following relationship:

$$I_{imp} = \frac{\left(I_{inj} + I_{pin} + I_{capillary} + I_{comp}\right)}{100} \qquad \textbf{Equation 57}$$

It can be seen from Figure 65 that the impregnation number for both the resin impregnators is greater than unity for the three pultrusion speeds considered in this study. A decreasing trend for the impregnation number with an increase in the pultrusion speed can be seen.

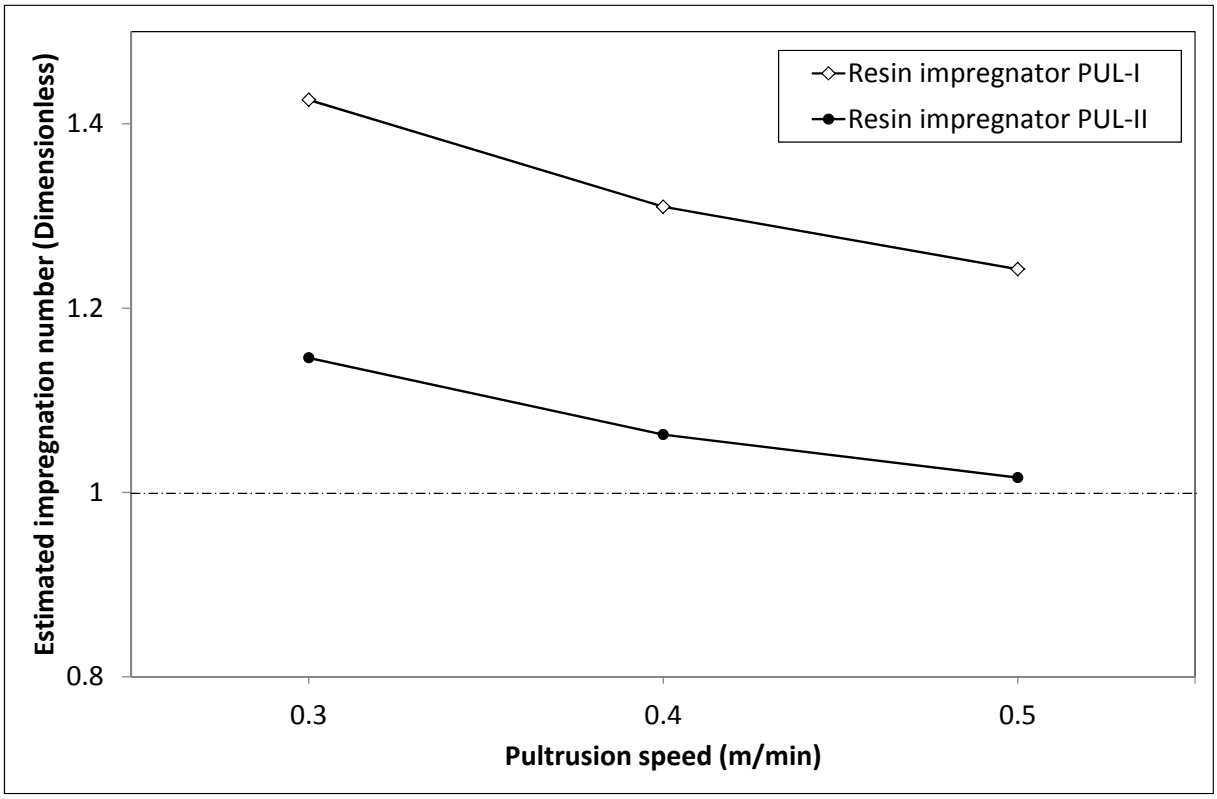


**Figure 65 Simulation of the estimated impregnation number as a function of pultrusion speed.**

The data generated in this section was used to design resin impregnator PUL-I and PUL-II.

## 3.6 RESIN DISPENSER

A resin dispenser was designed in collaboration with CTM Equipment & CTM UK Ltd for the polyurethane resin supplied by one of the project partners. A photograph of the resin dispenser is shown in Figure 66. The details of the requirements for the resin dispenser are set out in the section below.

### *3.6.1 Description of the resin dispenser*

A schematic illustration of the piping and the instrumentation associated with the resin dispenser is shown in Figure 67. In terms of the operation of the equipment, it is divided into two sections: the tank group and the head group.

#### 3.6.1.1 Tank group

The tank group consists of two 5-litre holding tanks which are fitted with electrical-band heaters and temperature measurement probes. These tanks are used for storing the isocyanate (Tank A in Figure 67) and the polyol (Tank B in Figure 67). These chemical holding tanks are coupled to two recirculation gear pumps which circulate the liquids from the tanks of the head group and returns them back to their respective holding tanks via chemical-grade hoses. This recirculation process keeps the liquids in the required state of suspension (they are multi-component liquids) and a uniform temperature is maintained in the system.

#### 3.6.1.2 Head group

The head group comprises of two 0.1 litre accumulators or mini-tanks; one for the isocyanate (item A1) and the other for the polyol (item B1). The mini-tanks are linked to metering pumps which are steel precision gear pumps. These positive-displacement pumps deliver the liquids to the mixing-head and then return them back to their independent recirculation pipe work, via chemical-grade hoses.

The metering pumps are operated through speed-controlled motors via a speed reduction gearbox. This maintains accurate flow of the two liquid streams. Pulsed output flow meters were fitted to the outputs of each metering pumps to monitor the flow rate and to provide feedback for the pump speed-controllers.

The mixing head was designed to recycle the polyol and the isocyanate when the machine is idle; when the command for dispensing is activated, the dispensing head pumps the two liquid streams to the static mixer. Pneumatic controllers are used to enable/disable the conditions between dispensing and recirculating the two liquid streams.


**Figure 66 Photograph of the resin dispenser manufacture by CTM Equipment & CTM UK Ltd.**

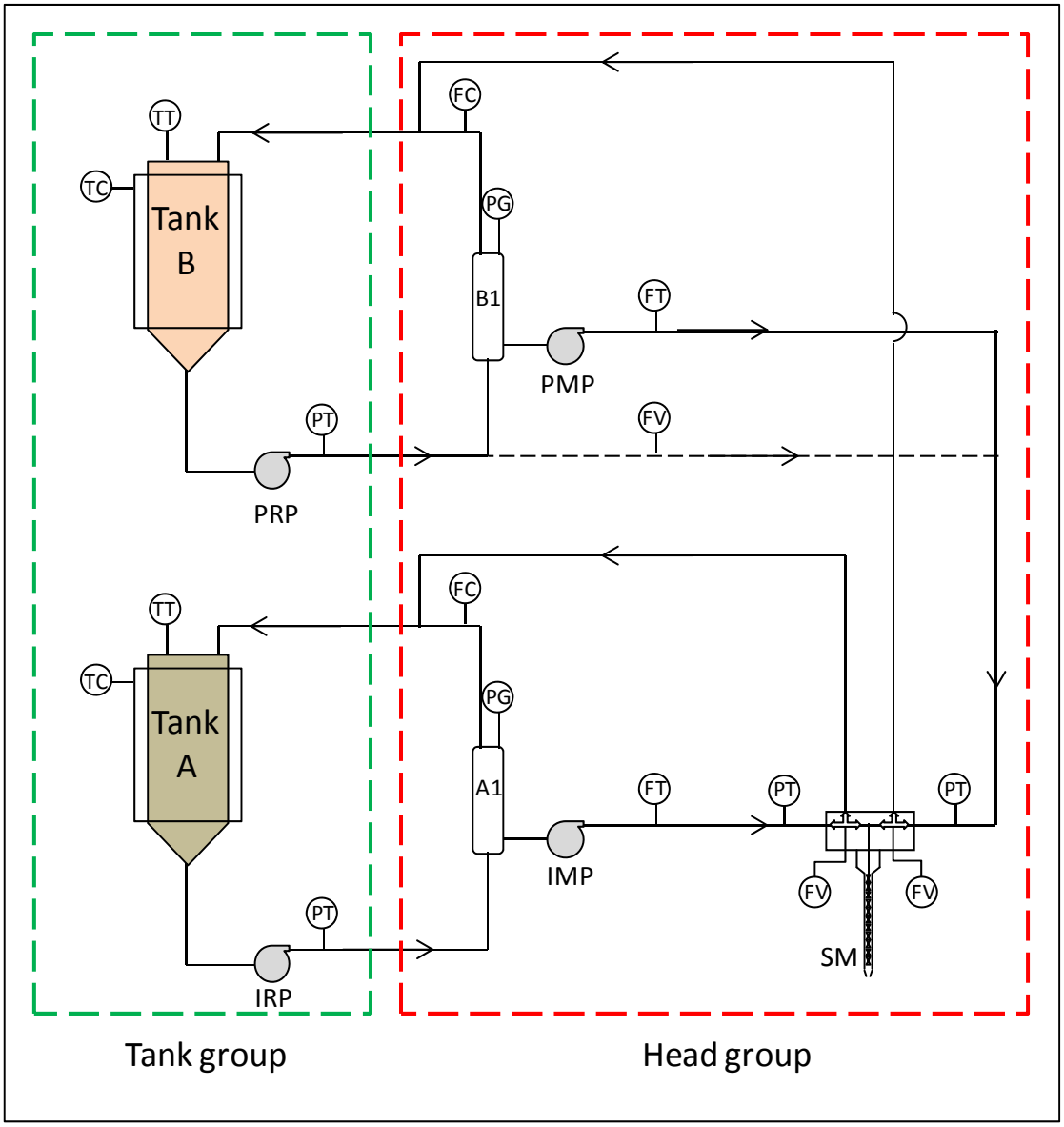


**Figure 67 Schematic illustration of the resin dispenser flow circuit. The coded items are as follows: (Tank A) isocyanate component tank; (Tank B) polyol component tank; (A1) isocyanate mini-tank; (B1) polyol mini-tank; (IRP) isocyanate recirculation pumps; (PRP) polyol recirculation pumps; (IMP) isocyanate metering pumps; (PMP) polyol metering pumps; (SM) static mixer; (TC) temperature controller; (TT) temperature transducer; (PT) pressure transducer; (PG) pressure gauge; (FC) flow control; (FT) flow transducer; and (FV) flow valve.**

### *3.6.2 Calculations to define the resin flow rate required*

The resin dispenser was designed to dispense the polyurethane resin system at the desired flow rates whilst maintaining the isocyanate to polyol ratio. The calculations for the required flow rates for a pultrusion speed of 1 m/min are summarised below:

i. Calculation for the cross-section of the pultruded composite using the dimensions of the die:

   1.2 mm × 27 mm = 32.4 $mm^2$

ii. Calculation for the volume of composite produced per minute:

   1,000 mm × 32.4 $mm^2$ = 32,400 $mm^3$

iii. Estimation of the volume fraction of resin in the composite:

   1 – fibre volume fraction = 1 - 0.60 = 0.40

iv. Calculation for the volume of cured resin in the composite:

   0.40 × 32,400 $mm^3$ = 12,960 $mm^3$

v. The densities of the individual components:

   Density of the isocyanate component = 1.23 $g/cm^3$ (data from the supplier)

   Density of the polyol component = 1.04 $g/cm^3$ (data from the supplier)

   Density of the cured resin = 1.20 $g/cm^3$

vi. Mass of the resin = 12,960 $mm^3$ × 1.2 g $cm^{-3}$ × 0.001 = 15.55 g

   Mass of the isocyanate component = 15.55 × (100/118) = 13.18 g

   Mass of the polyol component = 15.55 × (18/118) = 2.37 g

vii. Volumetric flow rate for the isocyanate component:

   13.18 g / 1.23 g $cm^{-3}$ = 10.71 cc per minute

viii. Volumetric flow rate for the polyol component:

   2.37 g / 1.04 g $cm^{-3}$ = 2.28 cc per minute

Thus, 10.71 cc per minute of the isocyanate component and 2.28 cc per minute of the polyol component are required to pultruded a composite using a die with the dimensions of 1.2 mm × 27 mm; this is for a composite with a 60% fibre volume fraction and a pultrusion speed of 1 metre per minute.

A simulation of the required volumetric flow rates for the isocyanate and polyol components as a function of the pultrusion speed is shown in Figure 68. These calculations were performed for a die with a cross-sectional area of 1.2 mm × 27 mm. The ratio of isocyanate and polyol was 100:18 as recommended by the supplier.

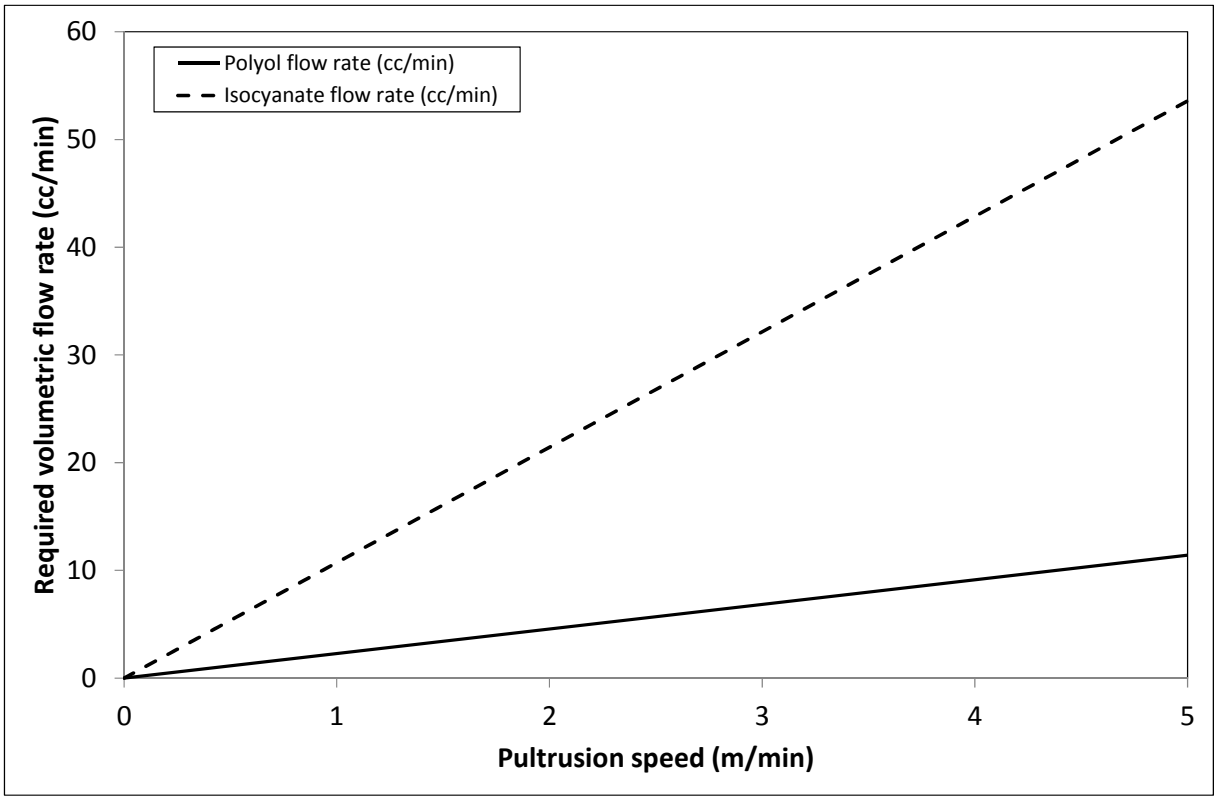


**Figure 68 Simulation showing the required flow rates of isocyanate and polyol components. The calculations were performed according to the required stoichiometric ratios.**

### *3.6.3 Operation of the resin dispensing unit*

The resin dispenser was equipped with the option of creating and storing specific programs for the pultrusion experiments according to the calculations shown in the previous section. The input information required for a typical program is summarised in Table 16. The software routines on the CTM resin dispensing equipment calculate the required flow rate for the given input values.

**Table 16 An example of a typical set of input parameters required for a pultrusion program on the CTM Polyurethanes Ltd resin dispenser.**

| Input parameters | Typical values |
|---|---|
| Pultrusion speed (m/min) | 0.3 |
| Number of rovings | 22 |
| Number of filaments in a roving | 4000 |
| Radius of the filament (cm) | 0.00085 |
| Required fibre volume fraction | 0.65 |
| Stoichiometric ratio of the polyol and isocyanate | 100:18 |
| Density of isocyanate (g/cc) | 1.18 |
| Density of polyol (g/cc) | 1.05 |
| Temperature (°C) | 23 |

### *3.6.4 Calibration*

The resin dispenser was calibrated to verify the output volumes for the isocyanate and polyol. Here individual components were dispensed into a container for a set flow rate and duration. The dispensed liquid was collected in disposable aluminium containers and weighed. The 'calibration factor' on the software routine was adjusted in such a way that the required and measured flow rates coincided.

## 3.7 PULTRUSION EXPERIMENTS

A laboratory-scale pultrusion machine (Model PX100C-3T) was designed and built for this project (TSB Project: AB134K) by Pultrex Ltd. A photograph of the pultrusion machine is shown in Figure 69. This pultrusion machine has a maximum pulling force of 3,000 kg and was equipped with Cleat-type tractor pullers. The maximum profile width that could be pultruded was 100 mm and the maximum haul-off speed of the machine was 4 metres per minute. The pultrusion machine was equipped with the option of operating 12-heating zones independently. In the current study, two and four heaters were attached to the 0.5 metre and 1.0 metre dies respectively. A servo-motor was used to operate the pullers to maintain the required pultrusion speed. The resin dispenser was synchronised with the pultrusion machine so that it could be programmed to dispense the resin system as dictated by the pultrusion speed.

With regard to the pultrusion experiments that were carried out in industry for the site trials, a pultrusion machine designed and built by Pultrex Ltd (Model PX500-6T) with maximum pulling force of 6,000 kg was used. It was equipped with reciprocating pullers and programmable automatic cutting device.


**Figure 69 Photograph of the pultrusion machine (PX100C-3T) used for the pultrusion experiments carried out in the laboratory.**

### *3.7.1 Conventional pultrusion*

Conventional pultrusion experiments with a resin bath were carried out in the laboratory using an epoxy resin system. For the experiments that were performed at an industrial site, vinyl ester and polyurethane resin systems were used. A resin bath with a capacity of five litres was used for all the conventional pultrusion experiments. The details of the resin systems, fibre reinforcements, die temperatures and pultrusion speeds are provided in Table 17. The reason for selecting different resin systems is given in Section 3.1.1.

**Table 17 Detail of the conventional resin bath pultrusion experiments carried out in the laboratory and on site.**

| Resin system | Resin impregnation system | Fibres | Die temperature (°C) | Pultrusion speed (m/min) |
|---|---|---|---|---|
| *Pultrusion trials in the laboratory* | | | | |
| Epoxy | Resin bath | Hybon® 2026 | 160 | 0.3 |
| Epoxy | Resin bath | Hybon® 2026 | 160 | 0.4 |
| Epoxy | Resin bath | Hybon® 2026 | 160 | 0.5 |
| *Pultrusion trials on-site* | | | | |
| Unfilled vinyl ester | Resin bath | 386 Direct Roving | 140 | 0.4 |
| Filled vinyl ester | Resin bath | 386 Direct Roving | 140 | 0.4 |
| Polyurethane | Resin bath | Hybon® 2026 | Zone 1: 120<br>Zone 2: 140 | 0.4 |

The following section provides an overview of the procedures involved with conventional pultrusion: The E-glass fibre creels located on the creel stand (Figure 70A) were threaded

through eyelets to the guide plates attached on the creel stand; these were then passed through a polypropylene guide plate (Figure 70B) and into the resin bath (Figures 72 (C and D)).

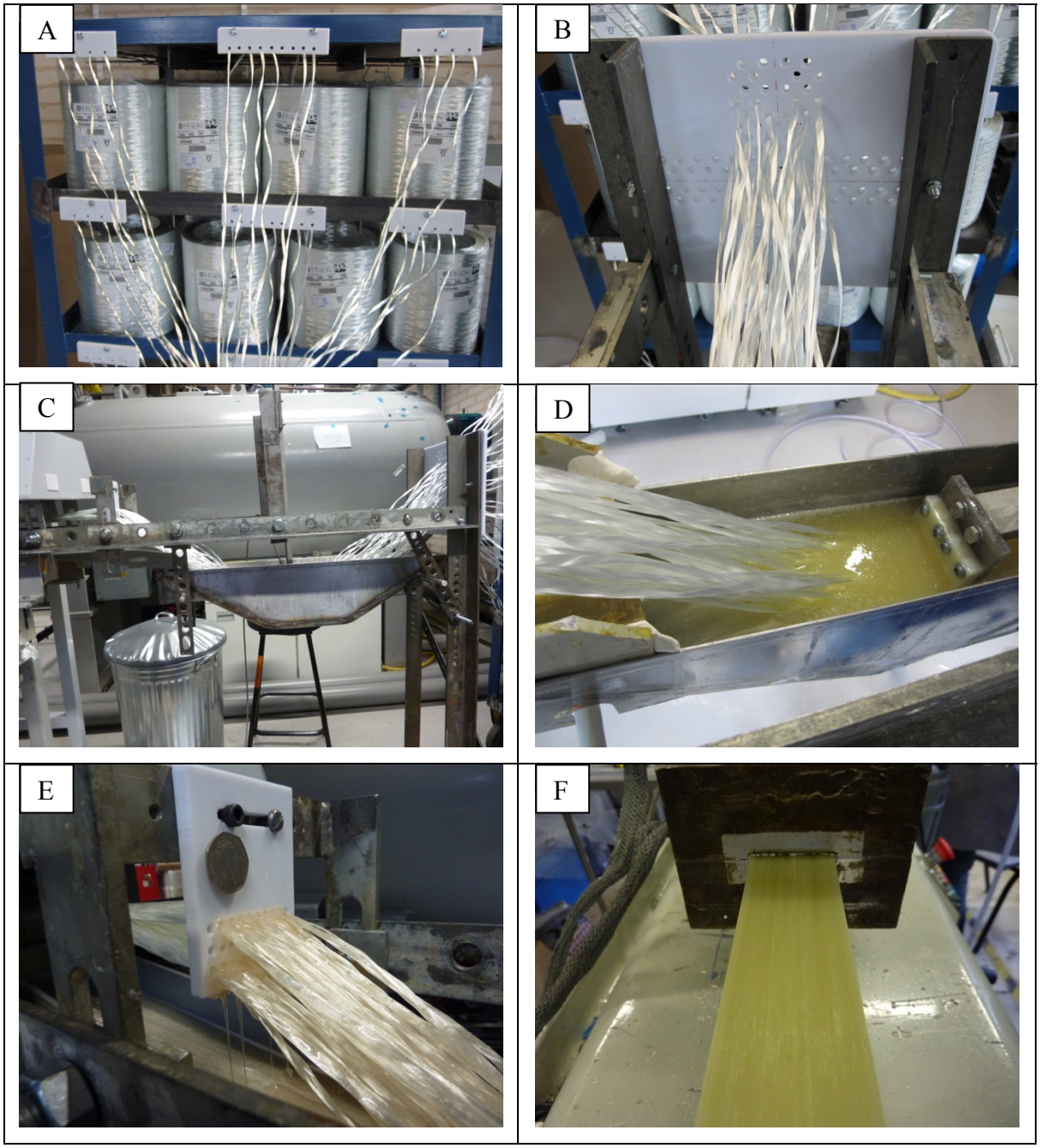


**Figure 70 Photographs showing the key components of conventional pultrusion process: (A) E-glass fibre creels on the creel stand; (B) back guide plate; (C) dip-type resin bath; (D) rovings dipped in the resin bath; (E) pre-forming guides; and (F) pultruded composite exiting the die.**

The resin bath was secured to the frame of the pultrusion machine. After securing the resin bath in position, the fibre rovings were threaded through the plunger, forming plates and the die (Figure 70 C). In order to pass the dry rovings through the die, one roving was threaded with the help of a brass wire. The remaining rovings were threaded through the die by "entangling" each additional roving to one of the threaded rovings at the die entry point, and it was pulled through the die manually. After 20 rovings were threaded in this manner, it was necessary to use the haul-off device (puller). This was achieved by binding the threaded rovings with adhesive tape prior to feeding it to the puller. This method allowed the required number of rovings to be threaded in a continuous manner until the die was packed with the desired number of rovings. Once around forty rovings had been threaded through the die, the roving-pack was coated with a release agent (PAT-672, CRC Ltd) with the introduction of each roving to reduce the friction within the die.

Once the die was threaded, it was heated to the required temperature. The components of the resin were weighed and mixed in the required stoichiometric ratio to give a total volume of five litres. The mixing of the components of the resin was carried out with the aid of a mixing blade attached to a power-drill. The filler and IMR were added in small volumes at a time and mixed. The mixed resin system was poured in to the resin bath (Figure 70D) manually. The "pullers" were started to commence pultrusion.

The pultruded composites were labelled and cut at intervals of 1.5 metres. At the end of the pultrusion experiment, the resin remaining in the bath was transferred into small containers and cured prior to disposal. The components that came into contact with the mixed resin (resin bath, profile guides, plunger and feed-back tray) were removed at the end of each

pultrusion experiment and cleaned using acetone, in a fume cupboard. The volume of the waste resin and solvent used was recorded for the LCA studies.

An experimental protocol was prepared for the pultrusion experiments that were carried out with the polyurethane resin. A summary of this protocol is presented in Appendix-D.

### *3.7.2 Clean pultrusion*

The resin impregnators PUL-I and PUL-II were used for the clean pultrusion trials involving the epoxy resin system that were conducted in the laboratory. Resin impregnator PUL-I was used with the vinyl ester and polyurethane resin systems carried out in industry. In case of epoxy and vinyl ester experiments, the resin system was premixed and transferred to a pressure-pot. The pressure-pot (Figure 71 A) had a 2 litres capacity and was operated using compressed air. The resin dispenser was used for the pultrusion trials where it was necessary to dispense the polyurethane resin system (Figure 71 B). The details of the clean pultrusion experiments are provided in Table 18. The steps involved in the threading the rovings were similar to that described previously for the resin bath-based pultrusion. The compact fibre spreading rig, described in Section 3.4.3, was used to spread the rovings unless stated otherwise. An experiment was also conducted with the epoxy resin where the internal mould release was applied externally to the rovings pack prior to them entering the die (see Figure 71 C). Here the wax was melted in a metal contained and brushed on the exterior of the roving pack prior to its entry into the die.

In a separate experiment, the automated fibre spreading rig, described in Section 3.4.2, was used in conjunction with the pultrusion line. It was placed between the guide plate and resin impregnator. The pultrusion speed and pre-tension was fixed at 0.3 m/min and 10 N respectively. The disk rotation was 100 rpm. Only half of the rovings were spread via the

automated fibre spreading rig as the overall width of the frame of the pultrusion machine was limited. The remaining rovings were spread via the compact fibre spreading unit. The effect of this system on the properties of the composites is provided in Section 4.4.1.

**Table 18 Details of the clean pultrusion experiments carried out in this study.**

| Resin system | Resin impregnation system | Fibres | Die temperature (°C) | Resin delivery method | Pultrusion speed (m/min) |
|---|---|---|---|---|---|
| *Pultrusion trials in the laboratory* | | | | | |
| Epoxy | PUL-I | Hybon® 2026 | 160 | Pressure-pot | 0.3 |
| | | | | | 0.4 |
| | | | | | 0.5 |
| Epoxy | PUL-II | Hybon® 2026 | 160 | Pressure-pot | 0.3 |
| | | | | | 0.4 |
| | | | | | 0.5 |
| Epoxy | PUL-I with spreading rig | Hybon® 2026 | 160 | Pressure-pot | 0.3 |
| Epoxy | PUL-I with external IMR | Hybon® 2026 | 160 | Pressure-pot | 0.3 |
| *Pultrusion trials on-site* | | | | | |
| Unfilled vinyl ester | PUL-I | 386 Direct Roving | 140 | Pressure-pot | 0.4 |
| Filled vinyl ester | PUL-I | 386 Direct Roving | 140 | Pressure-pot | 0.4 |
| Polyurethane | PUL-I | Hybon® 2026 | Zone 1: 120<br>Zone 2: 140 | Resin dispenser | 0.4 |

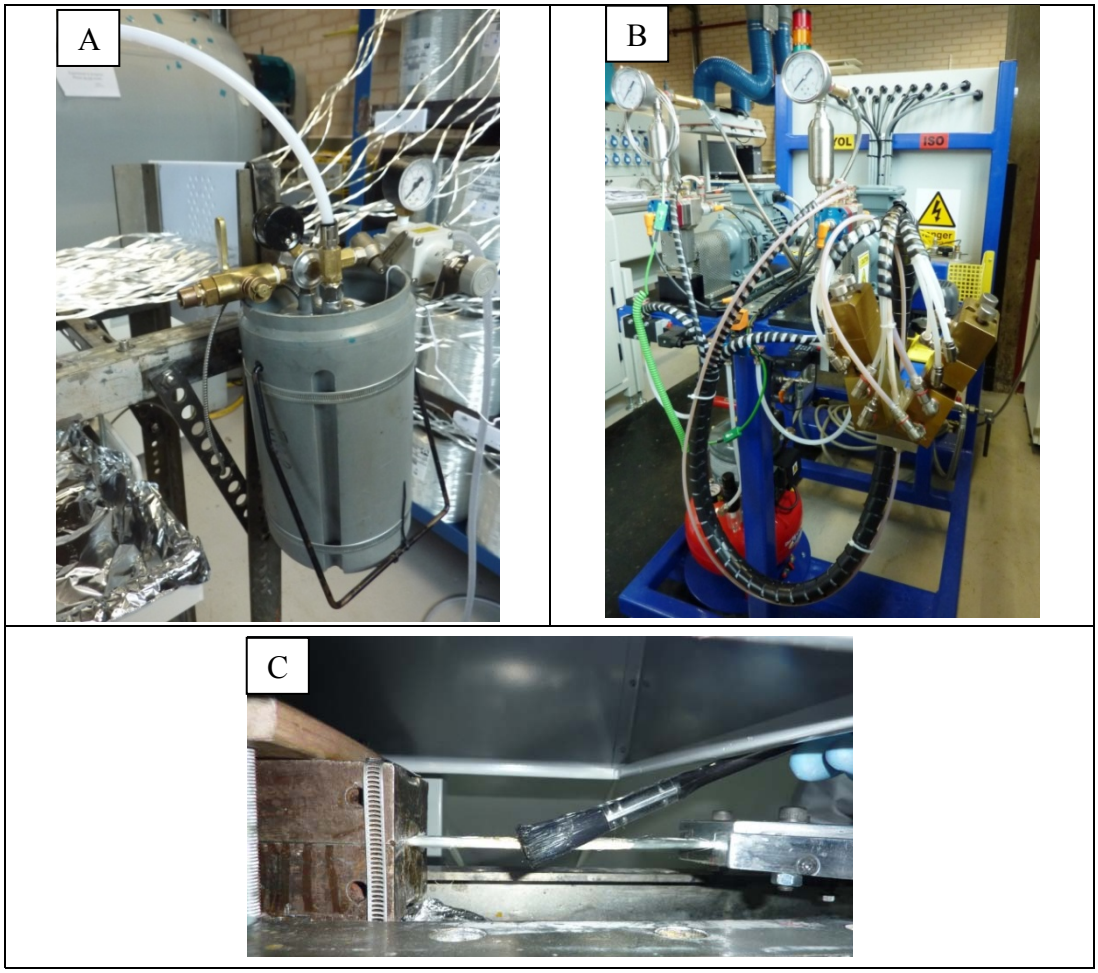


**Figure 71 Resin supply systems for clean pultrusion: (A) pressure-pot for the pultrusion experiments with the epoxy and vinyl ester resin systems; (B) resin dispensing unit for the pultrusion experiments with the polyurethane resin system; and (C) application of IMR on the external surface of the impregnated roving pack.**

## 3.8 LIFE CYCLE ASSESSMENT

### *3.8.1 Development of the LCA templates*

The goal of the life cycle assessment was to compare the environmental impacts of the conventional and clean pultrusion methods. The system boundary that was selected for LCA included the manufacturing phase of the raw materials (resin components, glass fibres and cleaning solvents), the transport of the materials to the laboratory (pultrusion site), power consumption during the pultrusion experiments (resin mixing, die heating, puller, LEV and resin dispenser), volume of solvents needed to clean the contaminated accessories (resin bath, pre-forming guides, plunger, resin impregnators), volume of the waste resin at the end of the experiment and disposal of the cured waste resin. The application and end-of-life phases of the composites were not considered. The LCA templates for the conventional and clean pultrusion are shown in Figures 72 and 73 respectively.

With reference to the LCA template for the conventional pultrusion shown in Figure 72, it was assumed that the materials required for the pultrusion experiment were supplied to the laboratory by a 12-ton cargo truck. The fuel that was used in the transport process has its associated environmental burden which was taken into account during the final environmental assessment. The symbol ‘p’ in the transport blocks in Figure 72 stands for ‘parameterized item’ which means that the amount of fuel that was used during the transport process was normalised to the volume of the materials used. In the next stage, a high-shear mixer was employed to mix the components of the resin system in the conventional pultrusion process. The mixing block was linked to the power that was used during the mixing operation. An LEV system was used to extract the VOCs.

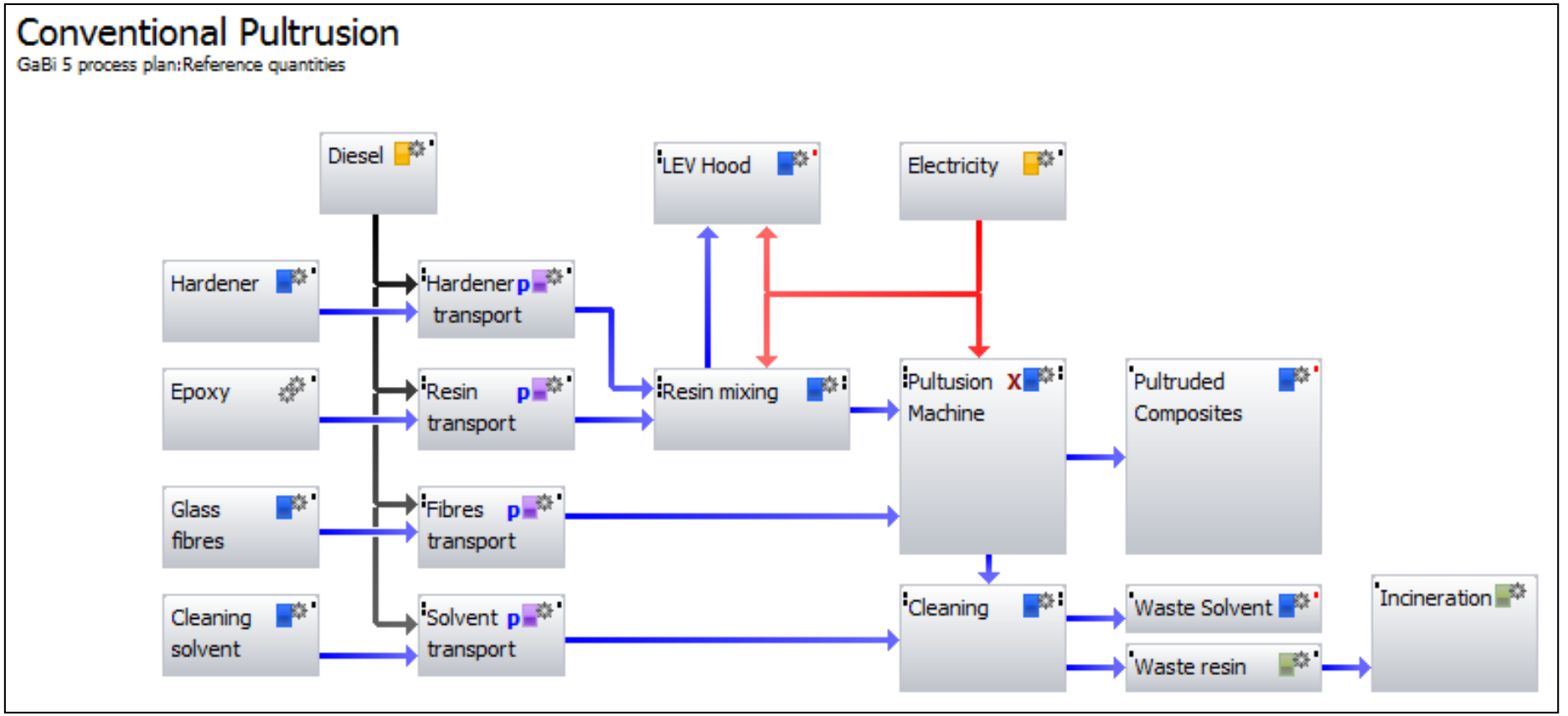


**Figure 72 LCA template for the conventional pultrusion process. The template was generated using GaBi 5.0 software.**

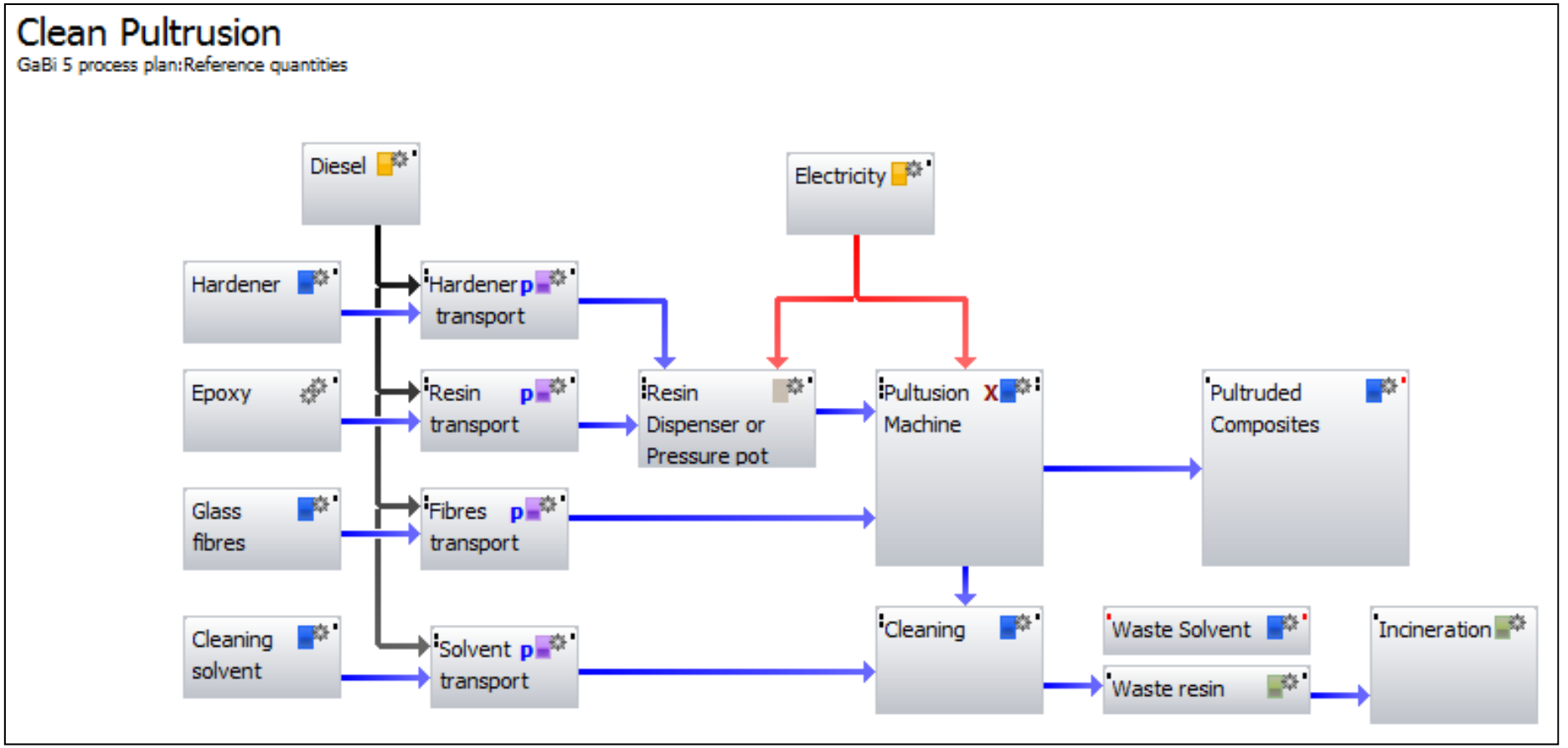


**Figure 73 LCA template for clean pultrusion process. The template was generated using GaBi 5.0 software.**

The mixed resin system was poured in the resin bath (merged in the block 'Pultrusion machine') and the rovings were immersed and traversed though the resin bath. With reference to Figures 72 and 73, an electricity stream was provided to the pultrusion machine to take into account the electrical power consumed during the pultrusion experiment. The electricity-mix that was used in this study was selected for UK industries. As the current study was only limited to the comparison of conventional and clean production processes, the pultruded composites were considered as end-products. At the end of the pultrusion experiment the resin bath and associated accessories were sent to the cleaning operation. Here acetone was used for the cleaning the contaminated items of equipment. The residual resin in the resin bath at the end of the pultrusion trial was collected into small aluminium containers (~50 grams resin per container) and cured at room temperature. It was assumed for this LCA that the waste cured resin is incinerated.

The LCA template for the clean pultrusion is shown in Figure 73. Here the mixing operation was replaced with the option of a pressure pot or the resin dispenser. A compressor was used to operate the pressure pot. An electricity stream was provided to take into account the power consumed by the compressor. In case of resin dispenser, an electricity stream was also provided.

The templates generated are generic and can be used to carry out a LCA for the three resin systems used in this study.

### *3.8.2 Compilation of LCA data*

The first step in collecting the LCA data was to standardise the production time and the quantity of the composite produced. This was required for the normalisation of the LCA data for both processes. For the laboratory-based pultrusion experiments, a typical experiment was

considered to last for two hours. This production time was selected as the basis of the calculations. The data required for the LCA for the epoxy/E-glass composites is presented in Tables 19.

**Table 19 Data generated for the LCA of the conventional and clean pultrusion processes.**

| Item | Conventional pultrusion | Clean pultrusion |
|---|---|---|
| Basis of calculation (hours of production) | 2 | 2 |
| Length of the pultruded composite (m) | 36 | 36 |
| Amount of the rovings used (kg) | 4.65 | 4.65 |
| Amount of the resin used (kg) | 5.00 | 1.04 |
| Amount of the solvent used (kg) | 1.98 | 0.20 |
| Waste resin (kg) | 4.06 | 0.10 |
| Power rating of the compressor for the pressure pot (kW) | N/A | 3 |
| Power rating of the pultrusion machine (kW) | 11 | 11 |
| Power rating of mixer (kW) | 0.38 | N/A |
| Power rating of the LEV system (kW) | 1.5 | 1.5 |

# 4 RESULTS AND DISCUSSION

## 4.1 CHARACTERISATION OF NEAT RESINS

### *4.1.1 Thermal characterisation*

The temperature of the die was selected from the DSC thermograms using the procedure described in Section 3.2.1; this was based on the method proposed by Yen et al. (2006). A dynamic thermogram was used to generate a conversion-temperature curve from which a suitable die temperature was selected. A conversion-time curve was drawn from the isothermal DSC scan, at the chosen temperature, to select the appropriate pultrusion speed.

#### 4.1.1.1 Epoxy

A thermogram obtained from a dynamic DSC heating experiment for the epoxy resin system (Araldite® LY556/Aradur® 917/ Hardener DY 070) is shown in Figure 74 (a). Here a dynamic heating experiment was carried out and the resultant thermogram was used to generate a conversion-temperature curve. The onset of cross-linking, as determined by the thermogram, commences at 55 °C with the peak at 131 °C. The total enthalpy of cure ($H_U$) was - 351 J/g. A conversion curve, as described in Section 3.2.1, was generated from Figure 74 (a) and is shown in Figure 74 (b). With reference to Figure 74 (b) it can be seen that the degree of conversion at 160 °C was 98%. The data provided by the resin manufacturer recommended that this resin system could be cured between 80 °C to 160 °C. Hence, the die temperature for the pultrusion experiment with the epoxy resin system was set at 160 °C.

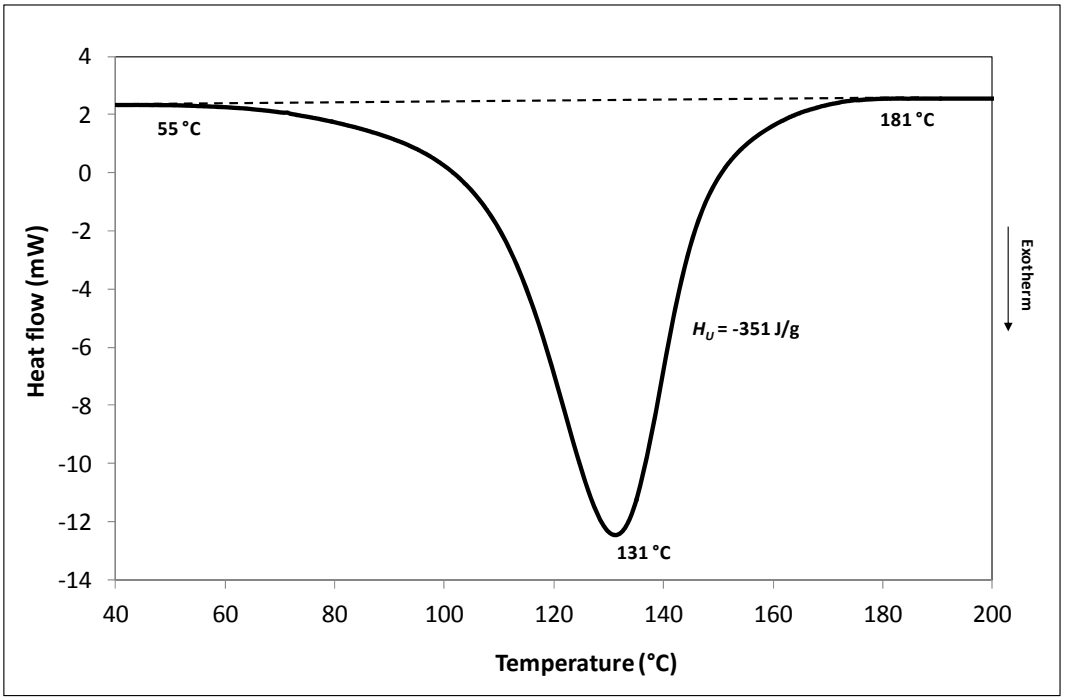


(a)

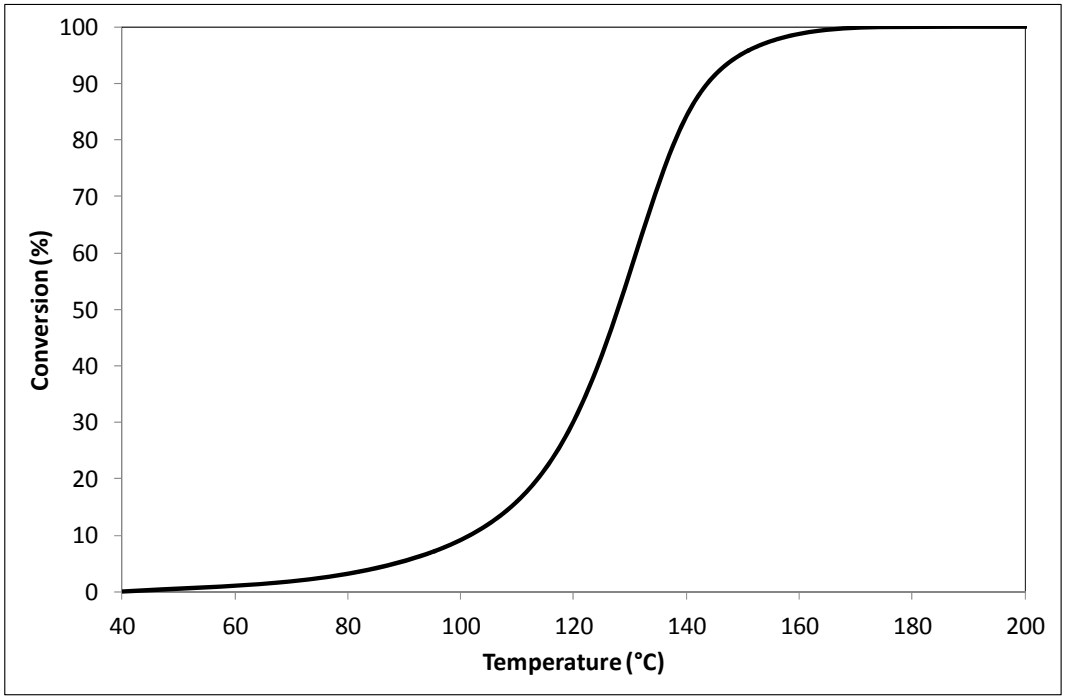


(b)

**Figure 74 (a) DSC thermogram for the epoxy resin obtained by a dynamic scanning experiment at 5 K/min. (b) Conversion versus temperature curve generated from Figure 74 (a).**

The next step was to investigate the effects of pultrusion speed through the die for a specified level of conversion. Here an isothermal DSC experiment was carried out at 160 °C and the

data are presented in Figure 75 (a). A conversion-time curve was generated using the data presented in Figure 75 (a) and it is shown in Figure 75 (b).

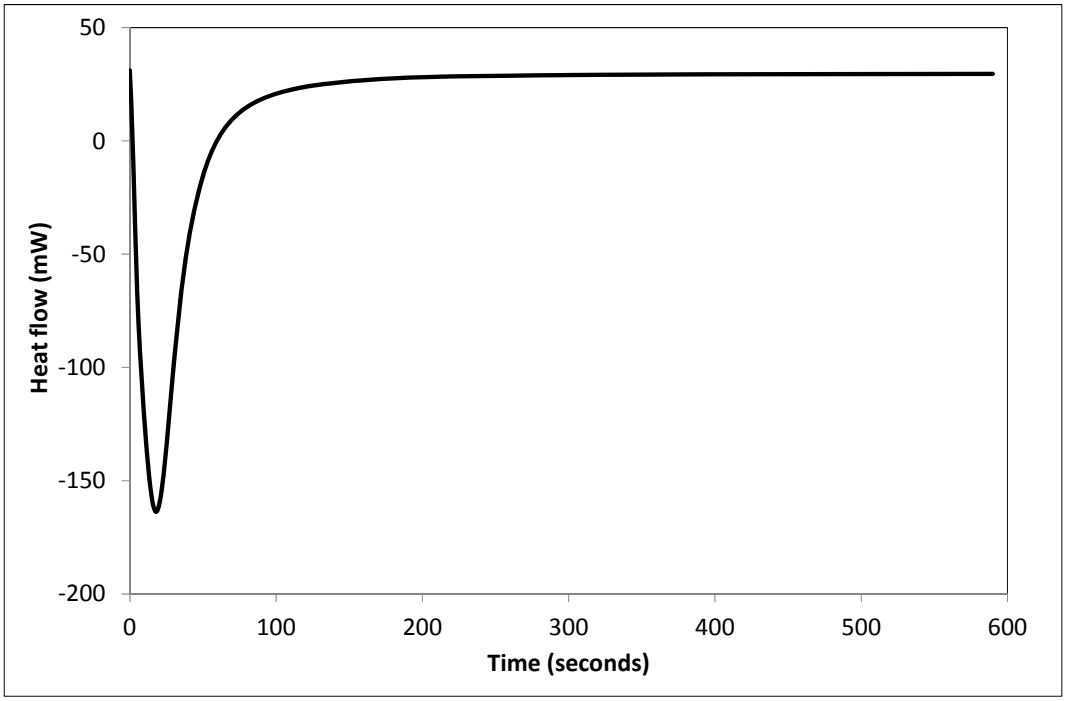


(a)

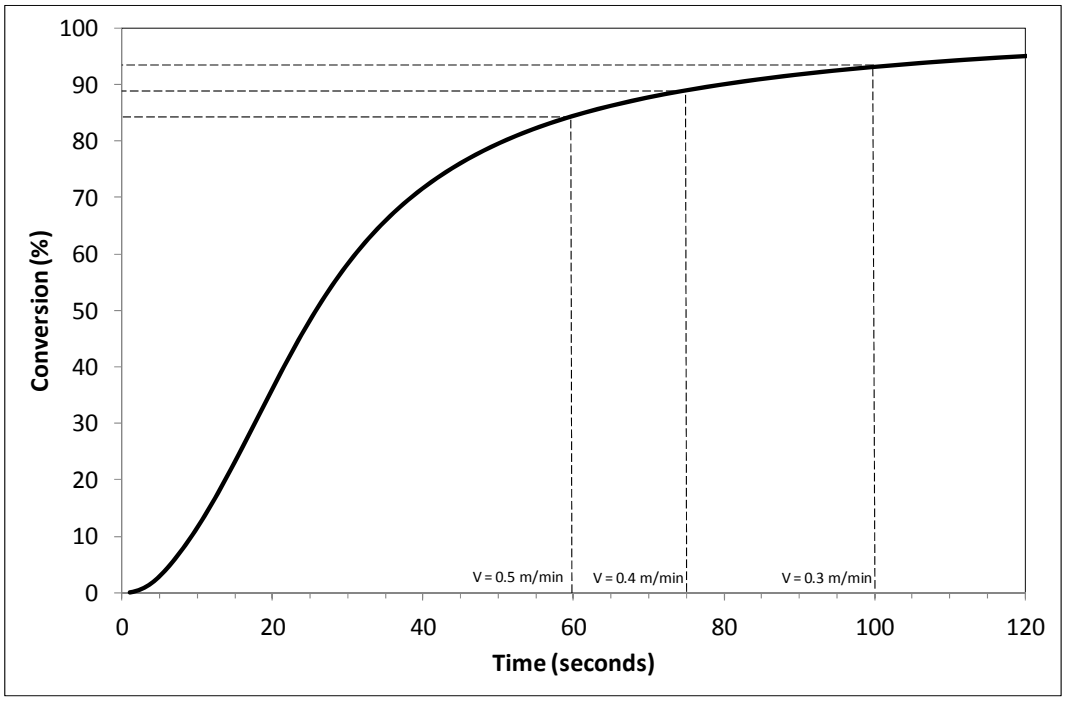


(b)

**Figure 75 Degree of conversion for 160 °C obtained via an isothermal DSC experiment. The corresponding residence time of the rovings in the 0.5 m die for the three pultrusion speed used in this study are also indicated.**

With reference to Figure 75 (b), the vertical lines represent the time that the impregnated rovings reside within the 0.5 m die. It can be seen that as the pultrusion speed is increased, the extent of conversion at 160 °C is reduced. Here, the degree of conversions at the times corresponding to the pultrusion speeds of 0.3, 0.4 and 0.5 m minute$^{-1}$, for a 0.5 m die, were determined. It was shown that for all the pultrusion speed used in this study, the resin conversion was more than 85 %. It must be noted that the thermal behaviour in the die and in the DSC pan is different as the mechanism of heating and sample sizes are different. However, it is assumed that DSC data can be used as a criterion to select suitable pultrusion speeds for the 0.5 metre die.

The samples from the dynamic and the isothermal experiments were re-scanned from room temperature to 180 °C at 20 K/min to determine the glass transition temperatures ($T_g$) of the cured resin. A typical trace from the second dynamic heating of a sample is presented in Figure 76 where the methodology for defining the $T_g$ is also indicated. The average $T_g$ for epoxy LY556 resin was 143.9 ± 2.1 °C. This represents an average of three experiments.

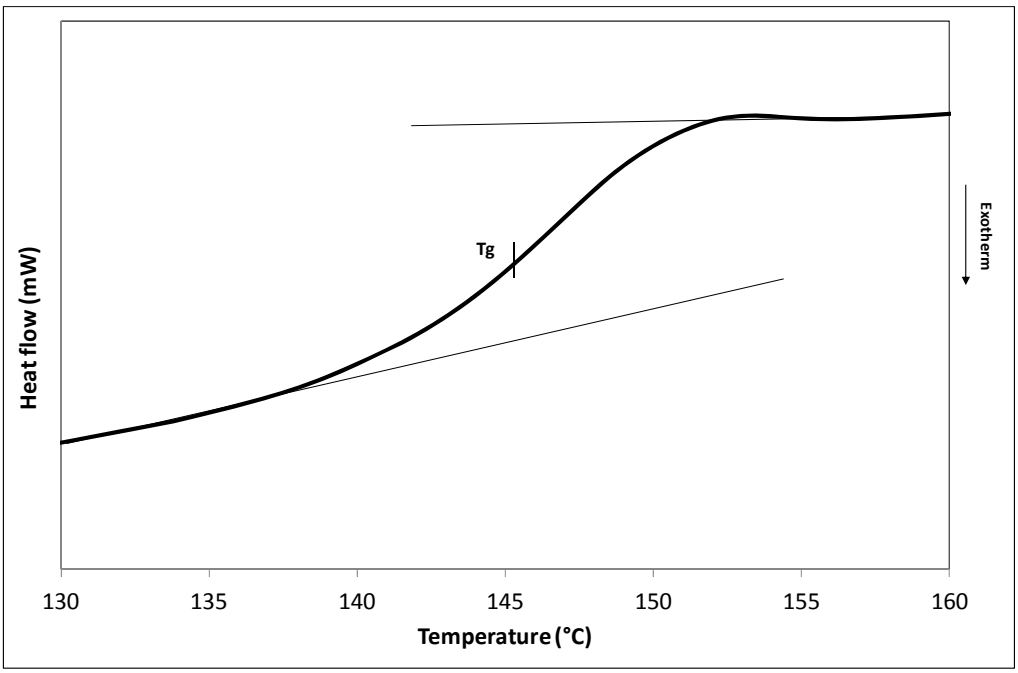


**Figure 76 Definition of the glass transition temperature obtained by a second DSC dynamic scanning experiment for a cured sample of epoxy resin.**

#### 4.1.1.2 Vinyl ester

The experimental procedure as described previously for the epoxy resin system was repeated here to select a suitable die temperature. The conversion-temperature curve for the unfilled vinyl ester resin is shown in Figure 77. It can be seen from Figure 77 that at 140 °C, the conversion of the reaction if nearly 90% complete. This temperature was selected as the die-temperature.

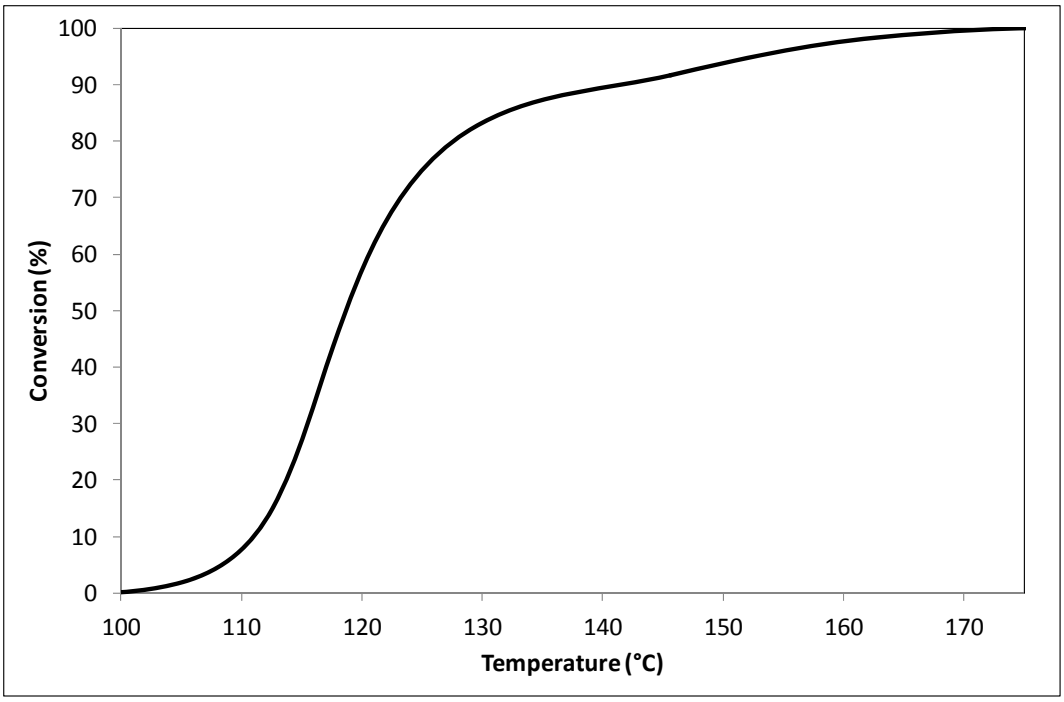


**Figure 77 Conversion versus temperature curve for the unfilled vinyl ester resin. The conversion curve was generated from a dynamic DSC experiment conducted at 5 K/min.**

From an isothermal experiment that was conducted at 140 °C, a conversion curve as a function of time was generated as shown in Figure 78. The pultrusion speed of 0.4 m minute$^{-1}$ was chosen for the experiments with the vinyl ester resin. The degree of conversion at 75-seconds (corresponding to a pultrusion speed of 0.4 m minute$^{-1}$) for a 0.5 m die was nearly 90%.

A typical trace from the second dynamic heating of a sample in the DSC is presented in Figure 79 where the methodology for defining the $T_g$ is also indicated. The average glass

transition temperature ($T_g$) from at least three experiments for the unfilled vinyl ester resin was 117.9±1.8 °C.

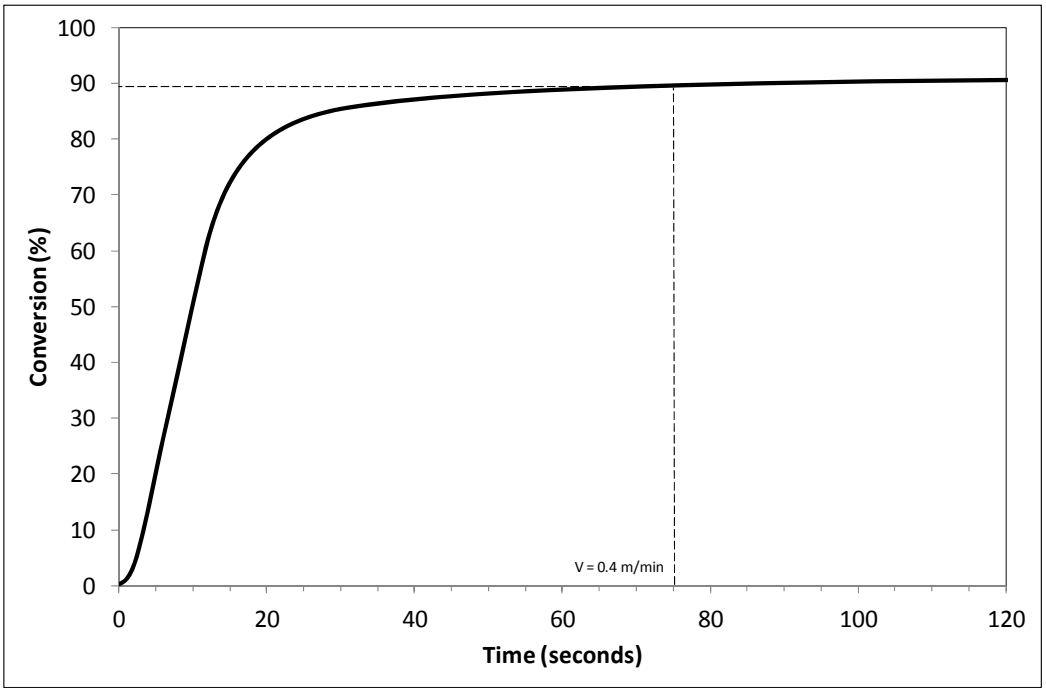


**Figure 78 Degree of conversion at 140 °C for vinyl ester resin obtained via an isothermal DSC experiment. The corresponding residence time of the rovings in the die for a pultrusion speed of 0.4 m/min used in this study is also indicated.**

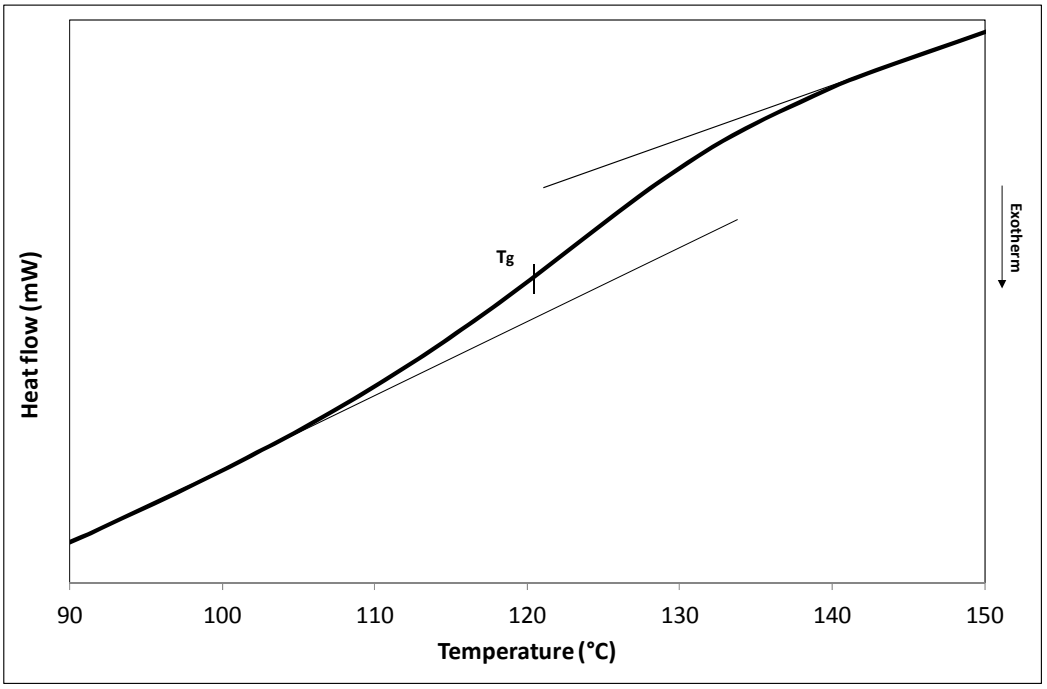


**Figure 79 Glass transition temperature obtained by a second dynamic scanning experiment for a cured vinyl ester sample.**

#### 4.1.1.3 Polyurethane

The supplier of the polyurethane resin recommended that a 1-metre die with two heating zones (120 °C and 160 °C) was required to attain complete cure when pultruding at 0.4 m minute$^{-1}$. As discussed previously, DSC experiments were performed on the neat resin to evaluate the degree of cure at this temperature and pultrusion speed. The conversion-temperature curve for the polyurethane resin is shown in Figure 80 where it is seen that the conversion of the resin at 120 °C is 82%. Furthermore, the resin is cured completely at 160 °C.

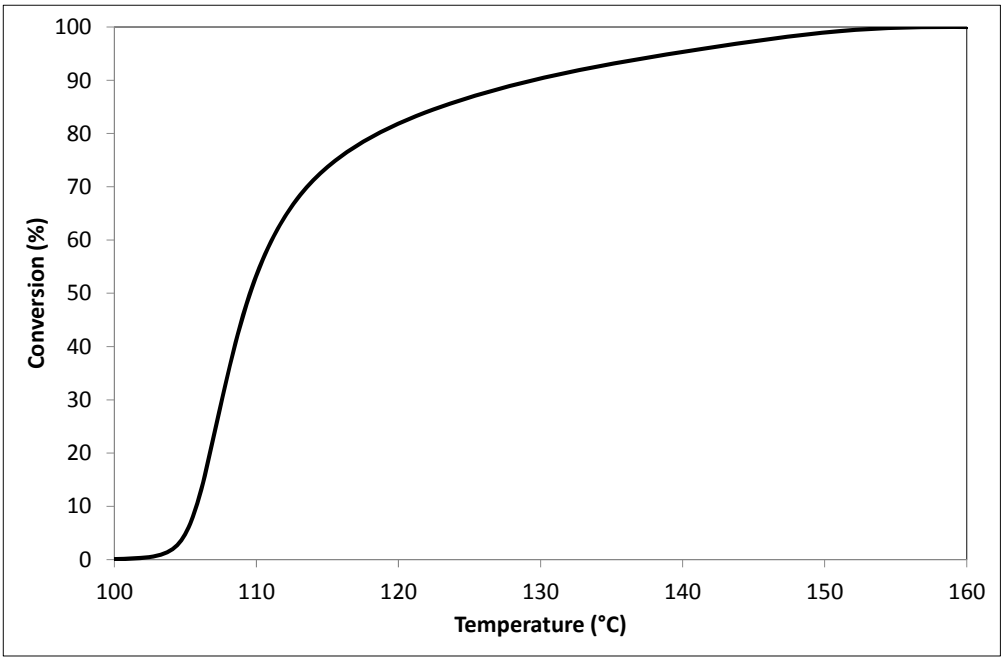


**Figure 80 Conversion versus temperature curve for the polyurethane resin. The conversion curve was generated from a dynamic DSC experiment conducted at 5 K/min.**

From the isothermal experiment conducted at 120 °C, a conversion curve as a function of time was generated and it is presented in Figure 81. The degree of conversion at 75-seconds (corresponding to a pultrusion speed of 0.4 m minute$^{-1}$) for the first half of the 1 m die was nearly 85%. The second half of the die was maintained at 160 °C. Hence, on inspecting Figure 81, it can be assumed that the resin will be fully cross-linked by the time it exits the die.

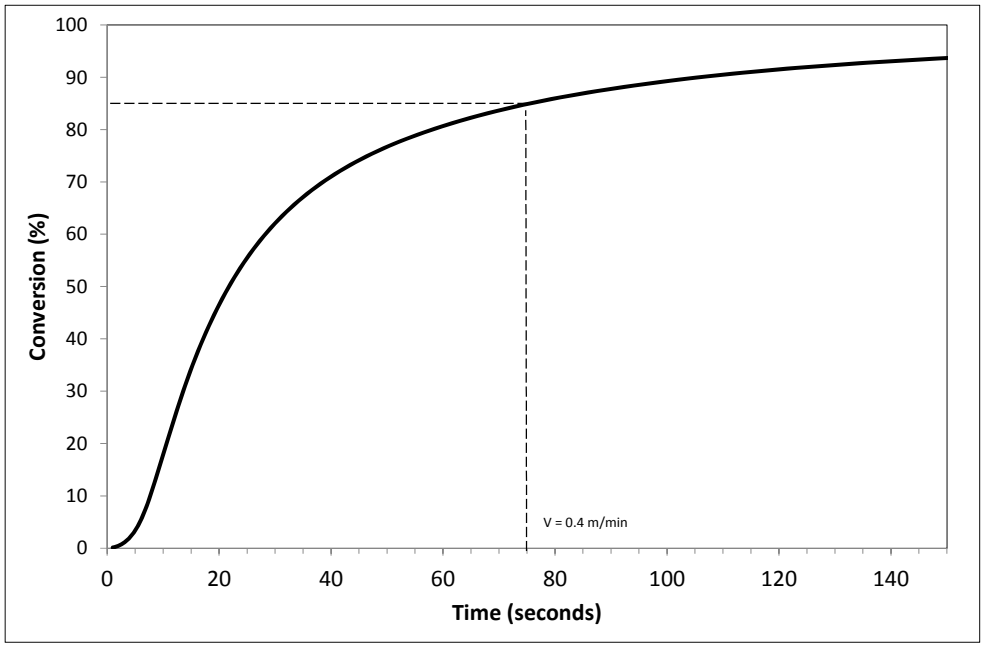


**Figure 81 Degree of conversion for polyurethane resin at 120 °C obtained via an isothermal DSC experiment. The corresponding residence time of the rovings in the first zone of the die for a pultrusion speed of 0.4 m/min used in this study is also indicated.**

A typical trace from the second dynamic heating of a sample using the DSC is presented in Figure 82. The average glass transition temperature ($T_g$) from three experiments for the polyurethane resin was 110.7±3.5 °C.

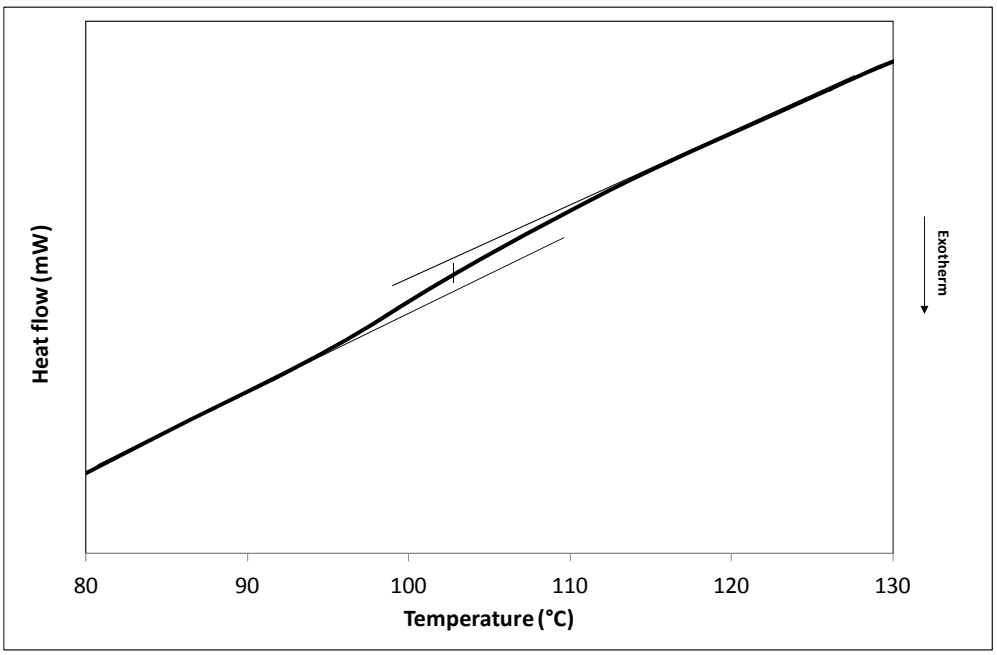


**Figure 82 Glass transition temperatures obtained by a second dynamic DSC scanning experiment for a cured polyurethane sample.**

### *4.1.2 Dynamic mechanical thermal analysis*

The $T_g$ of the neat resin systems was also determined from the peak of the loss tangent (*tan δ*) using the method described in Section 3.2.3. A comparison of the $T_g$ values obtained by DMTA and DSC is summarised in Table 20. It is appreciated that the two techniques operate on different principles and that the $T_g$ values will be different. DMTA data was used to compare the $T_g$ values obtained for composites.

**Table 20 Comparison of the $T_g$ for the neat resin systems obtained from DMTA and DSC experiments.**

| Resin system | $T_g$ from DMTA | $T_g$ from DSC |
|---|---|---|
| Epoxy | 135.9±6.2 °C | 143.9 ± 2.1 °C |
| Vinyl ester (unfilled) | 127.7±2.1 °C | 117.9±1.8 °C |
| Polyurethane | 123.9±0.8 °C | 110.7±3.5 °C |

### *4.1.3 Rheological characterisation*

The viscosities of the neat resin systems were measured at room temperature using a parallel-plate rheometer as described in Section 3.2.2. The average viscosity of a freshly mixed epoxy resin system at room temperature (23 °C) was 1.03 Pa·s. This value was used for the calculations involving the design of the resin impregnators as shown in Section 3.5. The viscosities of the unfilled vinyl ester and polyurethane resin systems at 23 °C were 0.44 Pa·s and 0.60 Pa·s respectively. A comparison of the viscosities of the three resin systems used in this study is presented in Table 21.

**Table 21 Viscosities of the neat resin systems obtained using the parallel-plate rheometer.**

| Resin system | Viscosity |
|---|---|
| Epoxy | 1.03 ± 0.02 Pa·s |
| Vinyl ester (unfilled) | 0.47 ± 0.04 Pa·s |
| Polyurethane | 0.99 ± 0.09 Pa·s |

## 4.2 FIBRE SPREADING

### *4.2.1 Manual fibre spreading experiments via mechanical means*

As described previously, fibre spreading aids through-thickness impregnation. In the first part of the fibre spreading studies reported in this thesis, the rovings were spread manually using the approach described by Wilson (1997) where his model was extended. The details of which were published by Irfan et al. (2011). A copy of this paper is presented in Appendix-B. A summary of the conclusions drawn from that study are presented below.

The aim of this study was to review and further develop the model proposed by Wilson (1997) to predict the mechanically induced spreading of E-glass rovings over rods. The original model for a single-rod system was extended to predict the width, thickness, and profile of the roving at the second rod. An experimental study was undertaken where a rig was constructed to enable plastic rods to be positioned in specified configurations.

The reciprocating motion of the rovings used by Wilson was adopted to induce the lateral separation of the filaments. It was found that six such cycles of the reciprocating motion (termed as "tension-cycles") were necessary to obtain equilibrium in the degree of fibre spreading. Rod diameters of 30, 50, and 100 mm were used. The 30-mm diameter rod was found to be more effective in spreading the rovings. The mechanisms responsible for spreading the filaments in the roving were explained using micromechanics. Releasing the tension in the roving after attaining an equilibrium degree of fibre spreading was found to enhance the degree of lateral spreading. The degree of fibre spreading obtained at rod-1 ($W_1$) via the tension cycling process was 5–10% of the predicted values. However, after tension-release the experimentally derived value exceeded Wilson's estimates by ~30%.

Although the width of the roving was found to increase with additional rods, the increase was not significant. The contour of the cross-sectional profile was determined experimentally and was found to be parabolic. The presence of intrinsic twists in the roving and induced twists caused by drawing the rovings from the centre of the creel was a major cause for the variability in the experimental data. A 350–450% increase in the widths of the rovings was observed when the tension was released (tension-release process). It was concluded that a balance between the number of rods and their relative geometry has to be maintained against the fibre tension generated in the roving. The techniques developed in this work have formed the basis for the development of an automated fibre spreading unit.

### *4.2.2 Automated fibre spreading rig*

Figure 83 shows the individual measurements that were taken at 5 cm intervals over 5 m to quantify the widths of the as-received roving (2400 tex Hybon® 2026). The average width of the as-received E-glass roving was found to be 4.18 ± 0.60 mm. The average binder content determined using the burn-off method was 0.60 ± 0.02 wt%.

The variation in the width of the rovings is also shown in Figure 84. The observed trends in the widths of the as-received rovings, as shown in Figure 84, can be attributed to: (i) the variations in the dimensions of the roving at the top and bottom portions of the creel; (ii) inherent twists in a roving due to the manufacturing process; and (iii) the twists as the rovings are drawn from the centre of the creel.

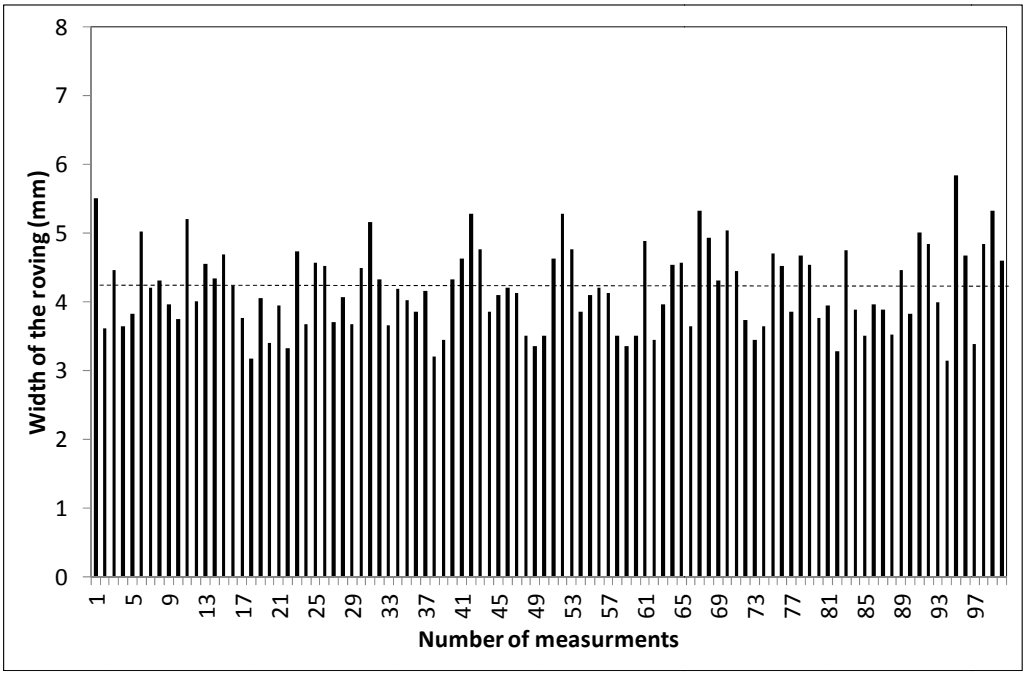


**Figure 83 The variations in the width of as-received roving over 5 m where the measurements were taken every 5 cm. The dotted-line (----) represents the average value.**

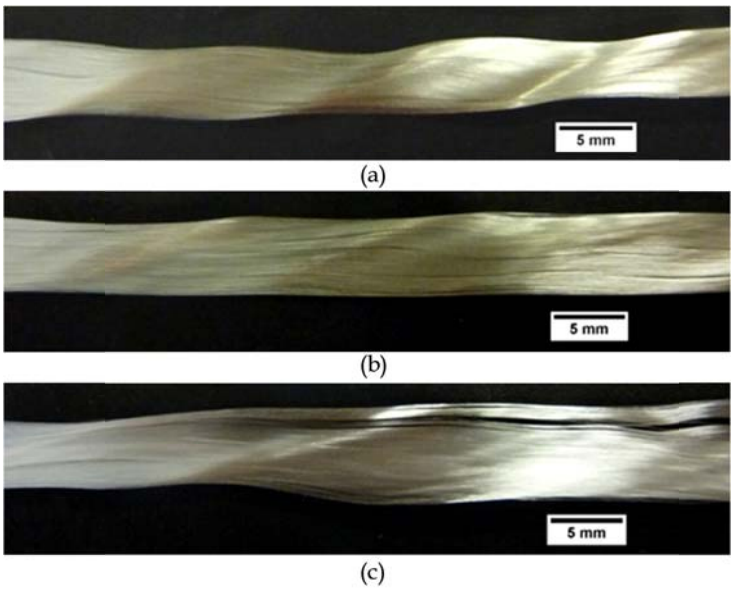


**Figure 84 Photographs illustrating the observed variations in the as-received rovings: (a) striations in the roving caused by the manufacturing process; (b) roving with minor segmentation and (c) wider roving with major segmentation.**

With reference to Figure 84 (a), a high degree of crimp is seen in the roving. This is likely to have resulted from a higher winding tension during the production of the creel. Figure 84 (b) shows a different characteristic where degree of segmentation within the bundle can be

observed. This may have been introduced when the roving is drawn off from the centre under tension where the previously undulated sections are stretched (taut). Figure 84 (c) shows a situation where the segmentation has resulted in "splitting" of roving which is an extreme form of segmentation.

#### 4.2.2.1 Optimal fibre spreading parameters

The automated fibre spreading rig was used to conduct the eighteen experiments summarised in Table 11. Each experiment was repeated ten times and an average value is reported to indicate the extent of fibre spreading that was attained. The width of the post-spread roving was measured as described previously at the top of the third roller-disk as shown in Figure 52. The measured values for the average as-received and spread roving are presented in Figure 85. The error bars in the data shown in Figure 85 can be attributed to the presence of the twist in the rovings and the intrinsic variability in the as-received rovings. No attempt was made to remove the twist.

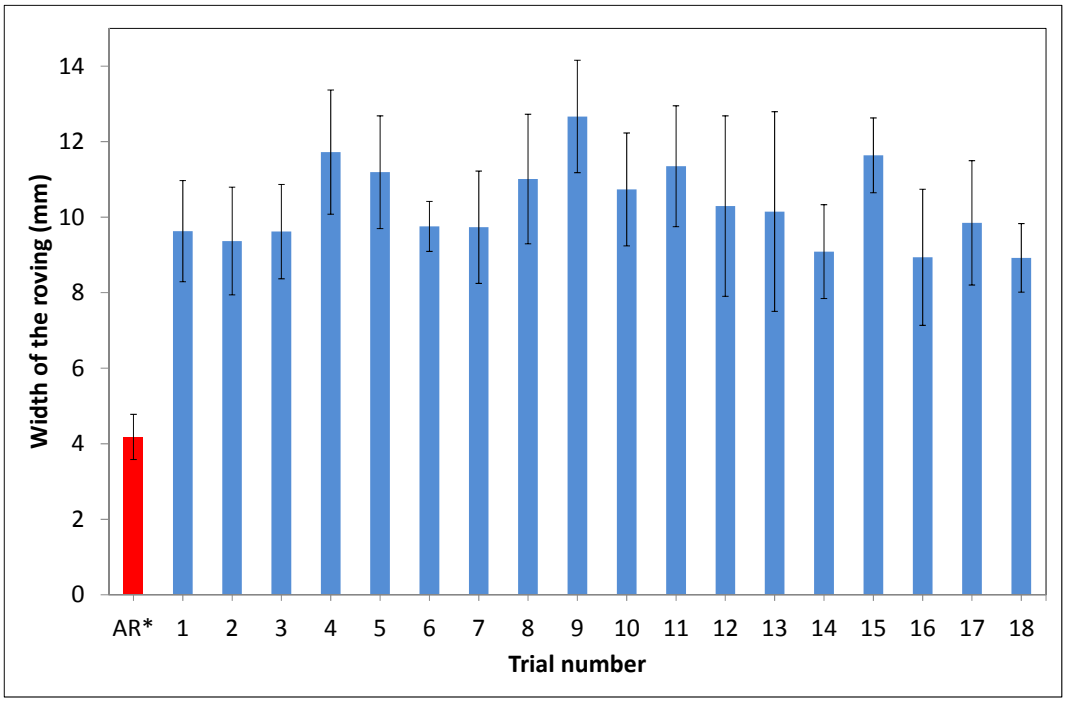


*AR = As-received roving.

**Figure 85 Summaries of the widths of the as-received and spread rovings. Each bar in the histogram represents an average of 10 individual samples.**

The S/N (signal-to-noise) ratio is the term that is used in the Taguchi method to analyse the results of the experiments. It represents the variation in the data and can be calculated as:

$$\frac{S}{N} = -10\log_{10}(MSD) \qquad \textbf{Equation 58}$$

where MSD is 'mean square deviation'. The MSD (and hence S/N) for a dataset can be expressed in different ways depending on the objective of the experiment (Ross, 1996). Since the objective of the current study was to maximise the extent of fibre spreading (the response), the S/N ratio in the Taguchi analysis was chosen to be "larger-the-better".

From the values of the fibre widths shows in Figure 85, the average width of the roving at the third roller-disk (measuring point as shown in Figure 52) for each of the levels and factors were calculated and the results are shown in Figure 86. It can be seen from Figure 86 that the optimum factors and levels that could yield the maximum fibre spreading are represented by experimental configurations A3, B3, C1 and D3. Similarly, the optimal factor and level combinations for the maximum S/N ratio is shown in Figure 87. Here, the optimum factor and level combination is the same as that seen in Figure 86.

These factors and levels represent the configuration with the three rollers (configuration 3), a pre-tension of 10 N, fibre haul-off at 1 m/min and a disk rotational rate of 100 rpm. This combination is already present in Table 11 (Trial 9). In other words, if the optimum combination was not present in Table 11, then a new set of experiment based on the optimum factors and levels would have been required.

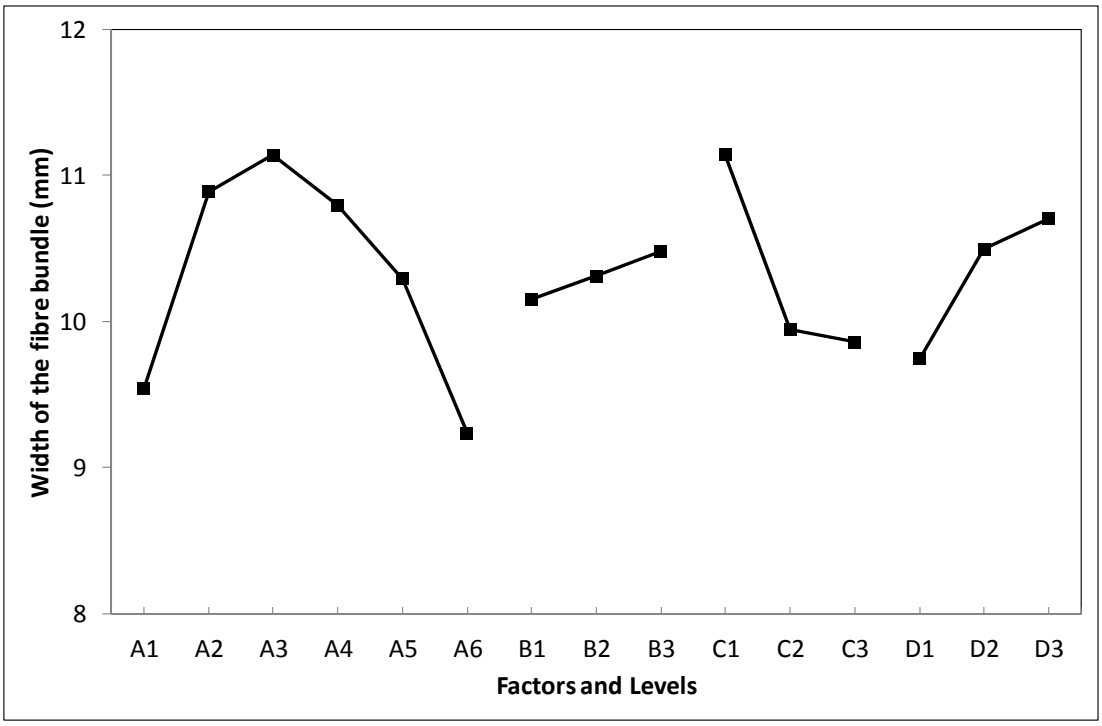


**Figure 86 Variations in the fibre spreading values as a function of factors and levels.**

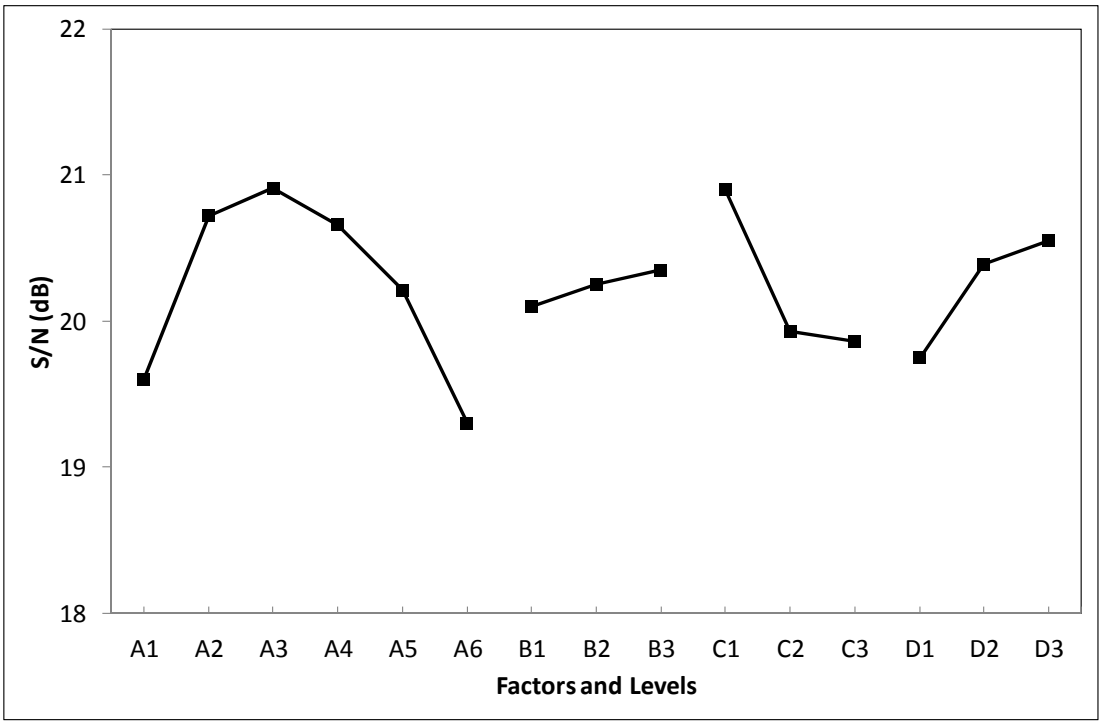


**Figure 87 Observed variations in the S/N ratio as a function of the factors and levels.**

The representative photographs of the spread rovings at the third roller-disk are shown in Figure 88.

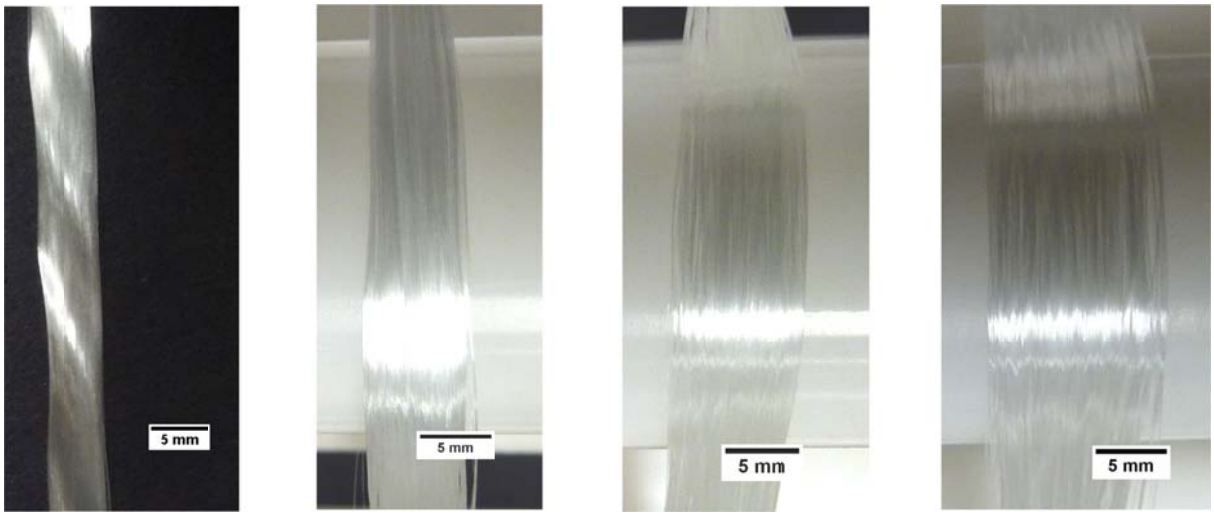


(a) (b) (c) (d)

**Figure 88 Representative photographs of the as-received and spread rovings. (a) as-received; (b) minimum observed spreading; (c) average observed spreading; and (d) maximum observed spreading.**

#### 4.2.2.2 Significance of the selected factors

Analysis of variance (ANOVA) was performed on the average values of fibre spreading and S/N ratios to estimate the significance of each of the factors that were selected for the experiments. The results are shown in Tables 22 and 23. With respect to the ANOVA results presented below, the degree of freedom (*DOF*) of a factor is equal to the number of levels of that factor minus one. The sum of the squares (*SS*) for each factor was obtained from Minitab®. The values for the mean square (*MS*) for each factor were calculated by dividing the *SS* for each factor with the *DOF* of that factor. Standard F-tests were performed to identify the significant factors (Soper, 2012). Here, the F-value was calculated by dividing the *MS* for each factor by the $MS_{error}$. $MS_{error}$ was obtained by dividing the error corresponding to the *SS* ($SS_{error}$) with that associated with the *DOF* ($DOF_{error}$). The critical value for F, expressed as $F_{critical}$, was obtained from standard F-tables (Soper, 2012).

The percentage contribution (*P%*) of each factor towards the variation was calculated using the following relationship (Ross, 1996):

$$P_X = \left[ \frac{SS_X - (DOF_X \times MS_e)}{SS_T} \right] \qquad \textbf{Equation 59}$$

Here, subscript '*X*' refers to the factor for which the percentage contribution was calculated, '$MS_e$' refers to the mean square error and '$SS_T$' refers to the total sum of squares. The pooled error was used for analysing the results. However, the effect of factor B (pre-tension) was not considered when calculating the percentage contribution of other factors because the SS for factor B in Tables 22 and 23 was not significant.

**Table 22 ANOVA table for the average fibre spreading for experiments performed with Hybon® 2026 fibres.**

| Factor | DOF | SS | MS | F-value | P (%) |
|---|---|---|---|---|---|
| A | 5 | 9.1475 | 1.8295 | 8.85[a] | 40.64 |
| B* | 2 | 0.3290 | 0.1645 | - | - |
| C | 2 | 6.0772 | 3.0386 | 14.71[a] | 28.36 |
| D | 2 | 3.0919 | 1.5459 | 7.49[a] | 13.41 |
| Error | 6 | 1.3229 | 0.2205 | - | - |
| Pooled error | 8 | 1.6518 | 0.2065 | - | 17.59 |
| Total | 17 | 19.9684 | - | - | - |

DOF=degree of freedom, SS=sum of squares, MS= mean square, P (%) = percentage contribution.

[a] at least 99% confidence, $F_{critical}$ for ($DOF_X$=5)/($DOF_T$=17) at 99% confidence is 4.33, $F_{critical}$ for ($DOF_X$=2)/($DOF_T$=17) at 99% confidence is 6.11

* SS was insignificant as compared to other factors and therefore, the factor was not considered for the pooled error.

**Table 23 ANOVA table for the S/N for the experiments performed with Hybon® 2026 fibres.**

| Factor | DOF | SS | MS | F-value | P (%) |
|---|---|---|---|---|---|
| A | 5 | 6.5885 | 1.3177 | 5.70[b] | 35.47 |
| B* | 2 | 0.4333 | 0.2167 | - | - |
| C | 2 | 5.1169 | 2.5585 | 11.07[b] | 25.86 |
| D | 2 | 1.2996 | 0.6498 | 2.85[b] | 0.94 |
| Error | 6 | 1.8773 | 0.3129 | - | - |
| Pooled error | 8 | 2.3106 | 0.2311 | - | 37.73 |
| Total | 17 | 15.3156 | | - | - |

[b] at least 90% confidence, $F_{critical}$ for ($DOF_X$=5)/($DOF_T$=17 the at 90% confidence is 2.22, $F_{critical}$ for ($DOF_X$=2)/($DOF_T$=17) the at 90% confidence is 2.64.

It can be seen from Tables 22 and 23 that the configuration of the rollers on the roller-disk assembly (factor A), fibre hall-off rate (factor C) and the disk rpm (factor D) show a significant effect on the average fibre spreading attained (at 99% confidence) and the S/N values (at 90% confidence). Pre-tension (factor B) was found to have a negligible effect for the extent of fibre spreading and the S/N values. The percentage contribution due to the error ($P_e$) is obtained by subtracting the total contribution due to the significant factors from 100% taking the difference of 100 % from the total contribution due to significant factors. In both cases, the values of $P_e$ suggest that the main factors that were chosen in these experiments were selected appropriately (Ross, 1996, Xian et al., 2006).

#### 4.2.2.3 Impact of selected parameters on fibre spreading

The configuration of the roller-disk assembly with three rollers (Figure 53) was found to yield the highest degree of fibre spreading. It can be noticed from Figure 86 and Figure 87 that the average fibre spreading and S/N ratios show a declining trend for the configuration with four, five and six rollers. The application of the force on the roving for these configurations is uniform as the configuration repeats itself after every 90°, 72° and 60° of the roller-disk rotation angle. As the number of rollers in the roller-disk is increased, tensioning the fibres becomes more uniform across the circumference of the roller-disk. Hence, less time is available for the tension-release process to take effect. In this instance, the roller-disk acts as a single roller of larger diameter rather than a collection of smaller rollers with a reduced fibre spreading efficiency. However, in the case of the 3-roller configuration, the configuration repeats itself every 120° hence, a balance of tension and tension-release acts on a unit length of the traversing roving thus improving lateral fibre spreading.

Pre-tension in the roving was found to have an insignificant effect on the average fibre spreading and S/N values. For practical reasons where the fibres are spread to aid in the impregnation process, the magnitude of the pre-tension is important. At lower levels of pre-tension, the rovings may meander and entangle. At high value of pre-tension, the fibres can be damaged. Higher values of pre-tension can also lead to the compactness of the roving which can impair impregnation. It was also found that a lower fibre haul-off speed favoured fibre spreading. This is because the residence time that is available to the roving to experience the tension-release action is increased.

Finally, it is evident from Tables 22 and 23 that a higher rotational speed of the roller-disk improves fibre spreading. This can be linked to the increase in the tension-release action per unit length of the roving per unit time. However, the contribution of this factor towards overall results is not as significant as the roller configuration and haul-off speed.

### *4.2.3 Compact fibre spreading rig*

The automatic fibre spreading rig was used to carry out some of the pultrusion experiments in the laboratory. However, due to its dimensions it was cumbersome to use under industrial conditions. Hence, the compact fibre spreading described previously in Section 3.4.3 was used. The average fibre widths at roller-3 for the three settings are summarised in Figure 89; the inserts shows the relative position of the centre-roller which defines the three settings. The average as-received width for the rovings (2400 tex, Hybon® 2026) was 4.18 ± 0.60 mm. However, it can be seen in Figure 89 that the roving width at the setting-1 is lower than the as-received value. This was due to presence of the guide plate (see Figure 90) which tended to coalesce the rovings. The spacing of the holes in the guide plate was determined by the

number of rovings (fifty two rovings in total divided into two rows of twenty six) required for the die that was used (32 mm × 2.2 mm).

It can be seen that when roller-2 is at its lowest position (setting-3 in Figure 89), the degree of spreading attained was 7.35 ± 1.05 mm. A photograph of the compact fibre spreading unit with the second roller at position-3 is shown in Figure 90.

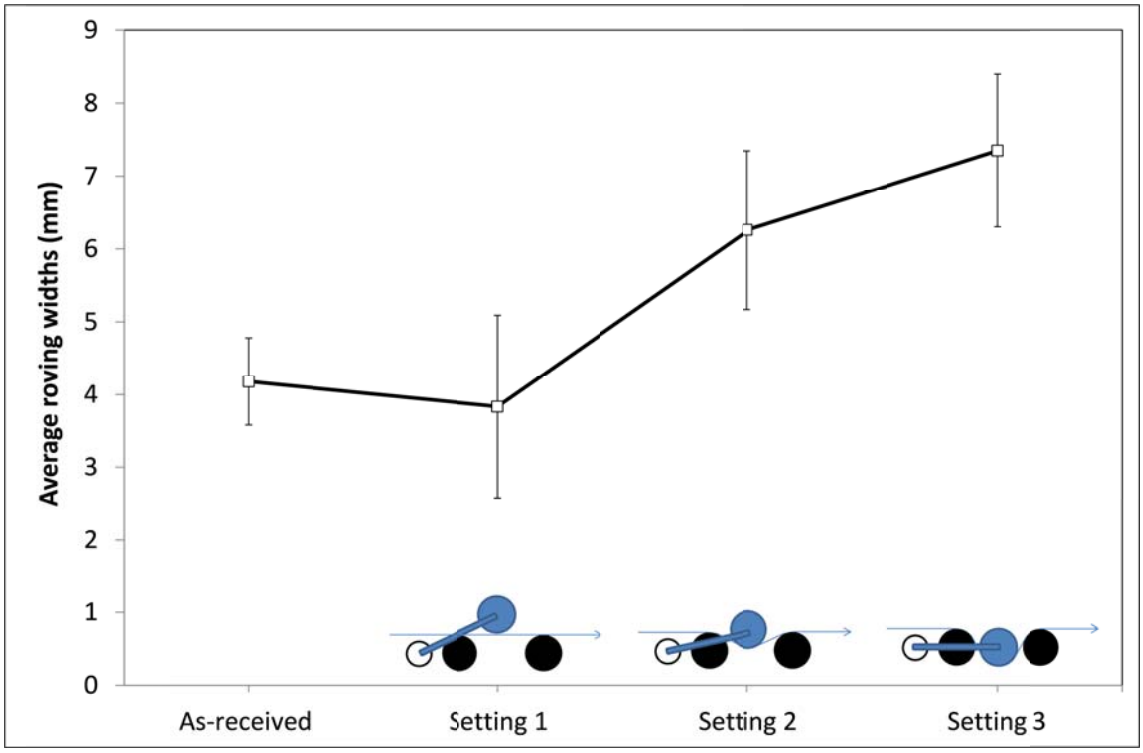


**Figure 89 Average roving widths for three settings of compact fibre spreading rig. Average width of as-received roving is also shown.**

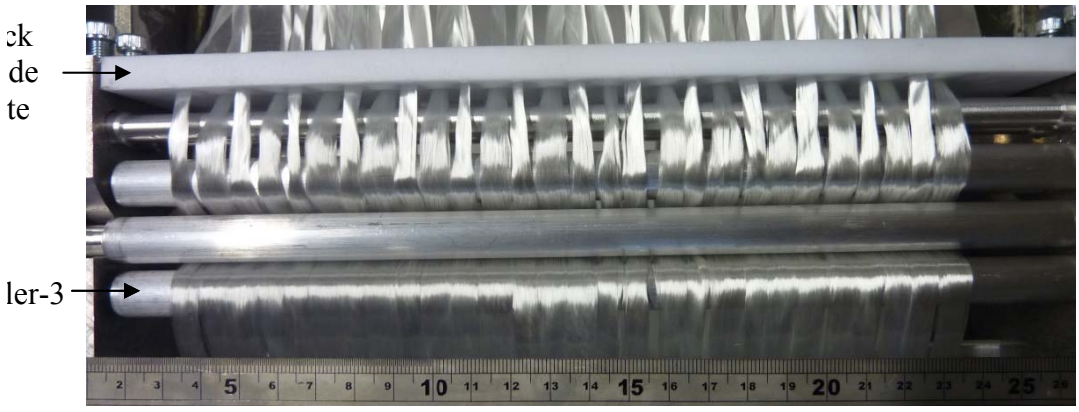


**Figure 90 Photograph of the compact fibre spreading rig at setting-3.**

The variation in the fibre widths is due to the constriction imposed by the back plate and the twists that are formed as the roving is pulled from the centre of the creels. Setting-3 was chosen for the pultrusion trials except for the experiments where automatic fibre spreading rig was used.

## 4.3 CALIBRATION OF THE RESIN DISPENSER

As mentioned previously, the resin dispensing unit was built by CTM Equipment & CTM UK Ltd as part of their deliverable for participation in an ESPRC project TS/G000387/1. The resin dispenser was designed specifically to dispense the polyurethane resin system developed by one of the project partners.

The calibration curves for the isocyanate and polyol pumps are shown in Figures 91 and 92 respectively. Here, the output from the resin dispenser was verified by comparing the set and measured volumes of isocyanate and polyol. Each point on the graphs shown in Figures 91 and 92, was obtained by setting the required flow rate in the calibration section of the resin dispenser software followed by dispensing and weighing the actual amount of the liquid dispensed from the manifold for a set time. A minimum of three repeats were performed to obtain the average value of the measured flow rates. It can be seen from Figure 91 that the coefficient of determination ($R^2$) for the isocyanate is 1; this indicated a good cross-correlation between the set and measured flow rates. With reference to Figure 92, $R^2$ for the polyol is 0.99.

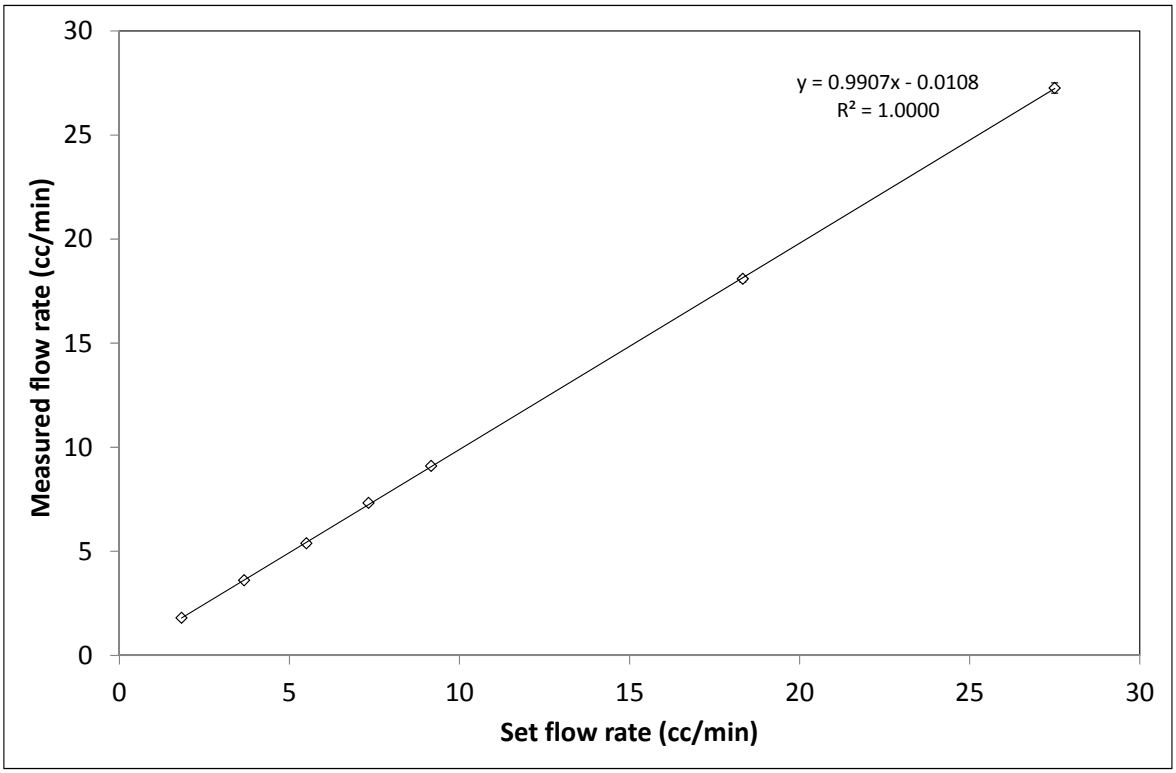


**Figure 91 Calibration curve for the isocyanate pump.**

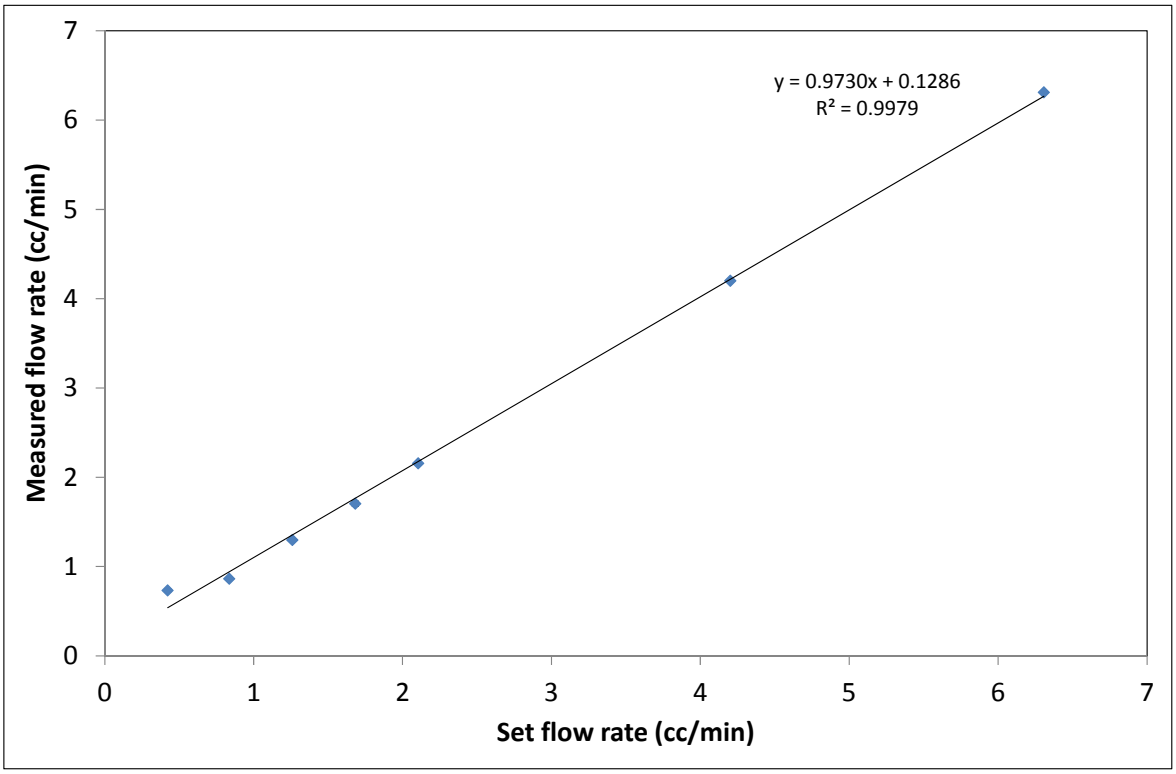


**Figure 92 Calibration curve for the polyol pump.**

The required flow rates of the isocyanate and polyol as a function of the pultrusion speed was discussed in Section 3.6.2. It was also necessary to verify experimentally the throughput rates for the isocyanate and polyol as a function of the pultrusion speed.

The procedure for this was as follows: the required flow rates for a die with a cross-section of 27 mm × 1.2 mm with 22 rovings (2400 tex, Hybon® 2026) were calculated. The individual mass of the output for the polyol and isocyanate liquid streams from the mixing head were collected and weighted. This was done for each of the set flow rates and three experiments were performed for each set flow rate. It can be seen from Figure 93 that the experimental and calculated flow rate for the polyurethane (isocyanate and polyol combined) are in good agreement. In the case of pultrusion at 0.2 m/min, the measured outputs are slightly higher than required. This is due to inability of the machine to dispense the polyol at low flow rates. However, the minimum pultrusion speed that was used for polyurethane resin system was 0.4 m/min. Hence, the discrepancy at 0.2 m/min was not a concern.

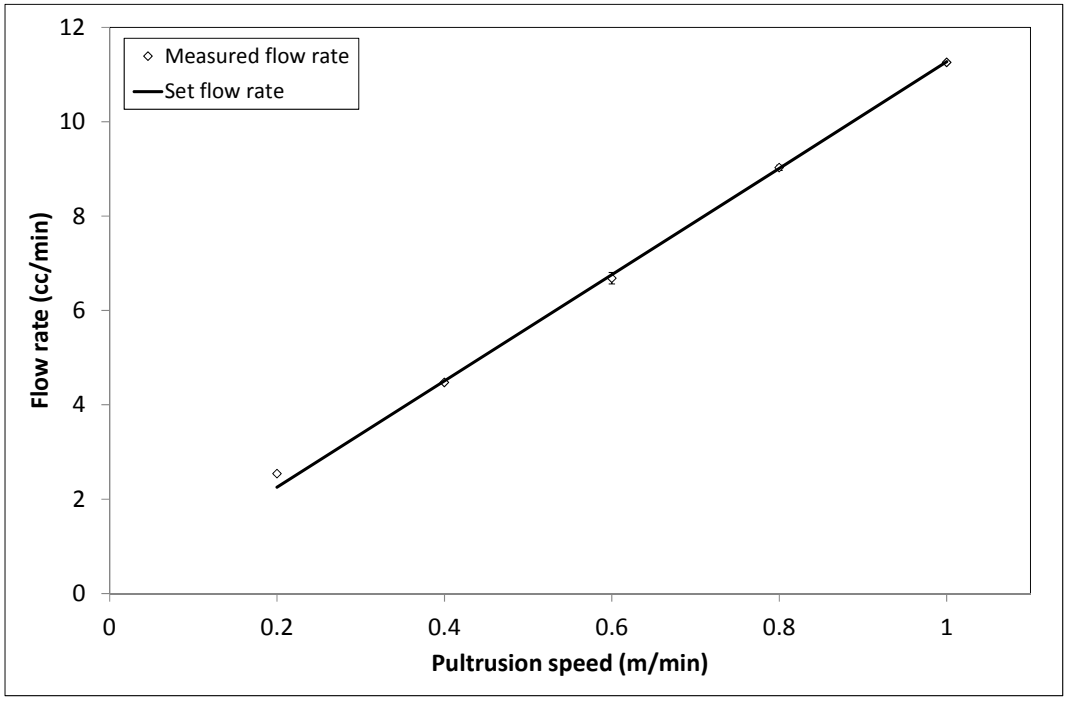


**Figure 93 Graph of the set and measured flow rates as a function of the pultrusion speed.**

## 4.4 EVALUATION OF PULTRUDED COMPOSITES

### *4.4.1 Epoxy/E-glass composites*

#### 4.4.1.1 Fibre volume fraction and density

Figure 94 shows the combined plots for the fibre volume fraction ($V_f$) and density data for the epoxy/E-glass composites produced using the: (i) resin bath; (ii) resin impregnator PUL-I; (iii) resin impregnator PUL-I with the fibre spreading rig; and (iv) the case where internal mould release (IMR) was introduced externally (not blended with the resin system). The fibre volume fraction for the resin bath samples (average of five specimens) is 65.2 %. However, the fibre volume fraction obtained with the clean pultrusion process was approximately 70%. A similar value was also obtained when the fibre spreading rig was used prior to resin impregnation.

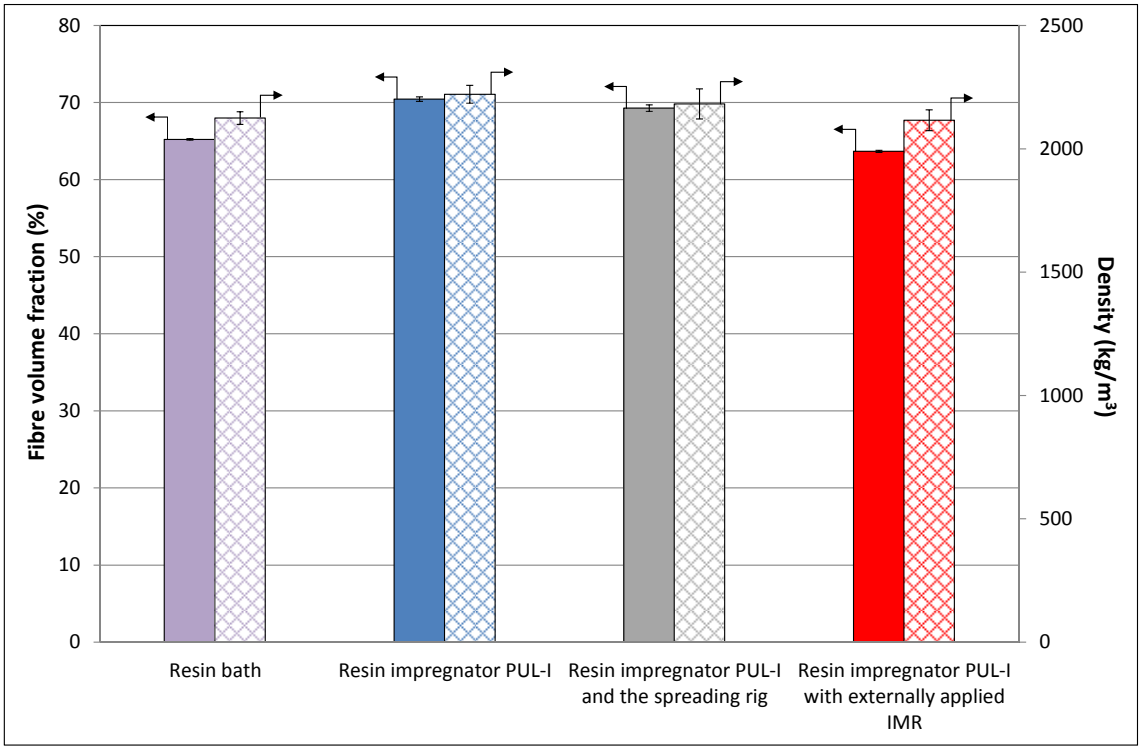


**Figure 94 Fibre volume fraction and density for the pultruded epoxy/E-glass composites produced at 0.3 m/min.**

The primary reason for the observed variations in the fibre volume fraction in the conventional and clean techniques can be related to the number of rovings that were used in each case. As discussed in Section 3.7, the die profile used in this study (32 mm × 2.2 mm) required each roving to be introduced into the die in a sequential fashion where manual hauling of the dry fibres was possible for up to twenty rovings. Further increases in the number of rovings required haul-off unit on the pultrusion machine to be used. With conventional resin bath-based pultrusion, it was only possible to introduce fifty rovings by this process whereas in the case of the clean technique using resin impregnator PUL-I, with and without the fibre spreader, fifty two rovings were accommodated without encountering any blockages at the entry point of the die. When the IMR was applied externally, the lack of "lubrication" for the rovings in the core section of the die meant that only fifty rovings could be accommodated. The density data for these samples has also been cross-plotted in Figure 94 where it is seen that the general trend is similar to that observed for the fibre volume fraction.

The theoretical maximum fibre volume fractions assuming a hexagonal or square packing of filaments within the rovings are 90.7 % and 78.5 % respectively (Hull and Clyne, 1996). For the cross-section of the die used in this study, these values correspond to 68 and 59 E-glass (2400 tex) rovings. It has been shown that the actual composites have non-regular packing and as a consequence the practical limit for commercial unidirectional composites is 70 % (Hull and Clyne, 1996). Thus it can be concluded that for resin impregnator PUL-I, the practical limit for the fibre volume fraction is attained.

#### 4.4.1.2 Void fraction

The void fractions were determined using the method specified in ASTM D 2734-03. The average void fractions for the resin bath and the clean pultrusion techniques using resin impregnator PUL-I were 1.47% and 1.04% respectively. An interesting point to note is that when the fibre spreading rig was used prior to impregnation, a noticeable reduction in the void fraction was observed. This reduction was also clearly evident in the micrographs presented in Figures 96 (A-H). Moreover, it was observed that applying the IMR externally resulted in a significant reduction in the void content. This may be attributed to the efficient wetting and impregnation of the roving when the IMR is not present in the mixed resin formulation. It is proposed that the application of the IMR externally should be considered further because it is not known at this stage if the presence of the OP wax has an influence on the interfacial bond strength.

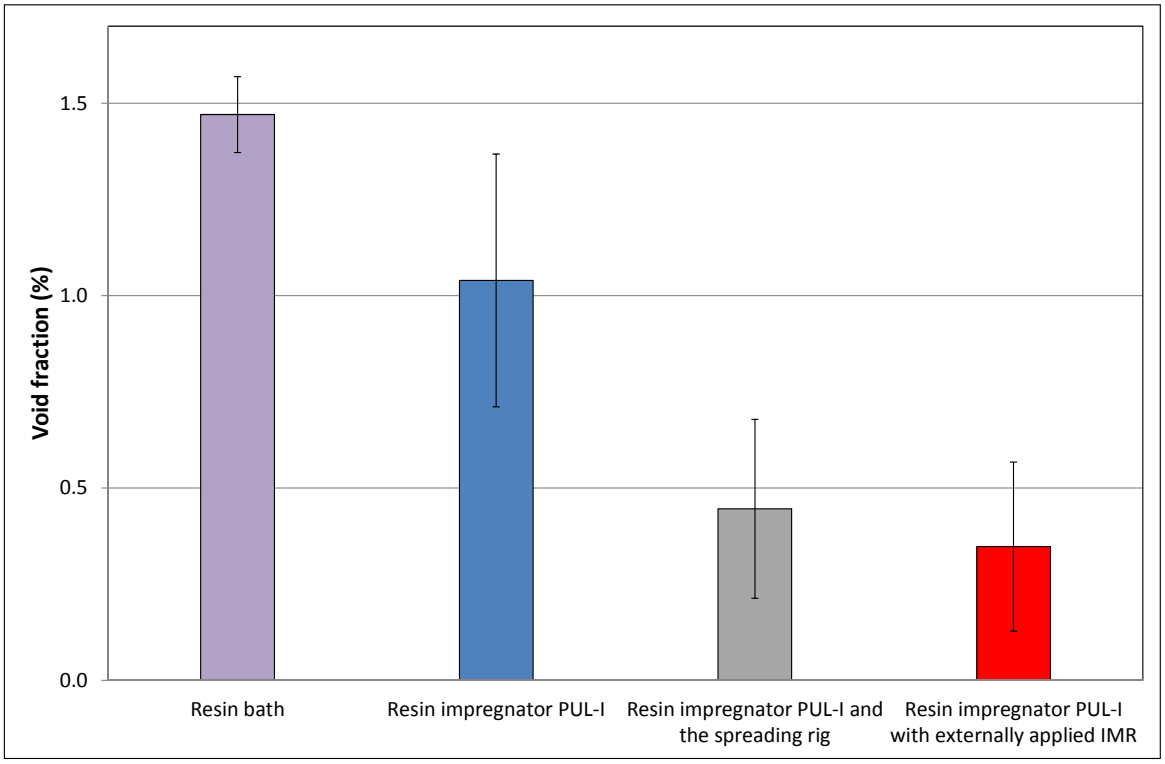


**Figure 95 Void fraction data for the pultruded epoxy/E-glass composites produced at 0.3 m/min.**

Typical micrographs for the various samples manufactured in this study are presented in Figures 96 (A-H). The micrographs on the left represent the "best" samples (as defined by the author) and those on the right, the "worst" observed visually. These paired micrographs were chosen to reflect the degree of scatter observed in the void content for the pultruded samples. A visually observed improvement in the quality in the samples is seen in the following order: externally applied IMR > resin impregnator PUL-I with the fibre spreader > resin impregnator PUL-I > resin bath. A summary of the void fraction data for the various pultruded composites obtained via image analysis and the resin burn off method is presented in the Table 24. The image analysis data confirms the trends seen in Figure 96.

**Table 24 Summary of the void fraction data for the pultruded samples obtained by image analysis and the resin-burn off methods.**

| Pultrusion method | Void fraction using the resin-burn off (ASTM D 2584–08) | Void fraction using image analysis |
|---|---|---|
| Resin bath | 1.47 ±0.10 | 1.29 ±0.56 |
| Resin impregnator PUL-I | 1.04 ± 0.33 | 0.75 ± 0.42 |
| Resin impregnator PUL-I and the spreading rig | 0.45 ± 0.23 | 0.47 ± 0.31 |
| Resin impregnator PUL-I with externally applied IMR | 0.35 ± 0.22 | 0.27 ± 0.13 |

With reference to the resin bath samples, the voiding was seen to be in clusters of 8-10 filaments, whereas with resin impregnator PUL-I, on average the voids tended to consists of areas that were equivalent to 1-3 fibre diameters. On the other hand, on inspecting the samples where the spreading rig was used and where the IMR was applied externally, the micrographs show negligible voids. One possible explanation for these observed trends with the samples produced using clean technique is that the fibre spreading breaks up the binder and this is known to aid the impregnation process, hence, the reduction in the void content.

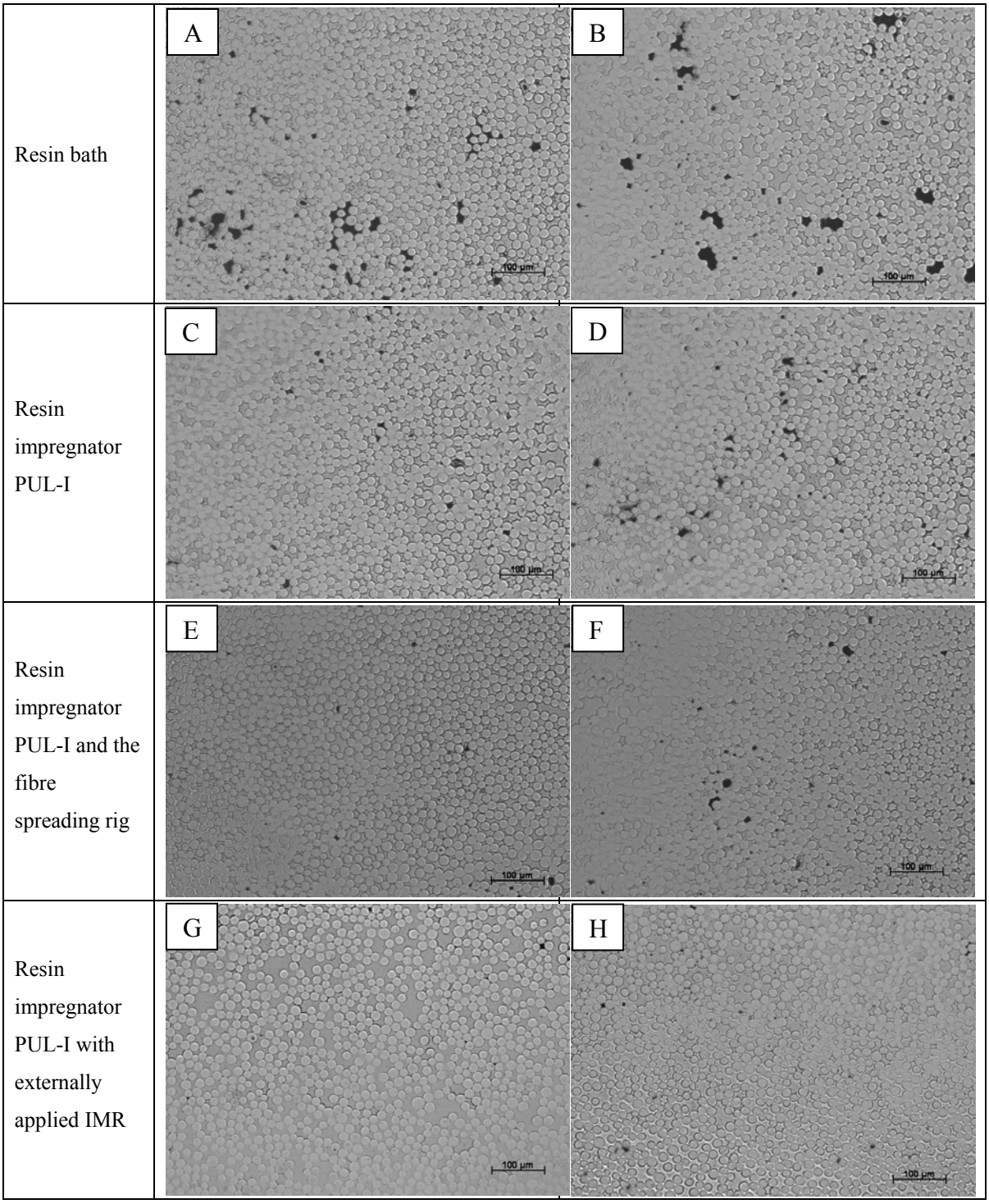


**Figure 96 Typical micrographs of the pultruded/E-glass composites: (A) resin bath (best sample); (B) resin bath (worst sample); (C) resin impregnator PUL-I (best sample); (D) resin impregnator PUL-I (worst sample); (E) resin impregnator PUL-I and the spreading rig (best sample); (F) resin impregnator PUL-I and the spreading rig (worst sample); (G) resin impregnator PUL-I with externally applied IMR (best sample); (H) resin impregnator PUL-I with externally applied IMR.**

**Table 25 Summary of selected papers to enable a comparison of the properties of the unidirectional epoxy /E-glass composites. The data in square brackets represents normalisation at 60% fibre volume fraction.**

| Reference | Resin system | Fibres | $V_f$ [%] | Flexural strength [MPa] | Flexural modulus [GPa] | ILSS [MPa] | Manufacturing Method | Other relevant information |
|---|---|---|---|---|---|---|---|---|
| Bogner et al. (2000) | Epoxy EPON® 9310 | E-glass Hybon® 2079 | 65.7 % | 592.0 [540.6] | 48.2 [44.0] | 68.9 [62.9] | Pultrusion | Flexural: ASTM 790 ILSS: ASTM D 2344 |
| Bogner et al. (2000) | Epoxy EPON® 9405 | E-glass Hybon® 2079 | 64.3 | 558.0 [520.7] | 48.2 [45.0] | 62.0 [57.8] | Pultrusion | Flexural: ASTM 790 ILSS: ASTM D 2344 |
| Bogner et al. (2000) | Epoxy EPON® 9420 | E-glass Hybon® 2079 | 64.3 | 682 [636.4] | 48.2 [45.0] | 55.1 [51.4] | Pultrusion | Flexural: ASTM 790 ILSS: ASTM D 2344 |
| Bogner et al. (2000) | Epoxy EPON® 9302 | E-glass Hybon® 2079 | 57.4 | 1019.0 [1065.2] | 41.3 [43.2] | 65.5 [68.5] | Pultrusion | Flexural: ASTM 790 ILSS: ASTM D 2344 |
| Bogner et al. (2000) | Epoxy EPON® 9500 | E-glass Hybon® 2079 | 68.7 | 1102.0 [962.4] | 48.2 [42.1] | - | Pultrusion | Flexural: ASTM 790 ILSS: ASTM D 2344 |
| Johsi (2000) | Epoxy Araldite® GY 6008 | E-glass | 60.0 | 858.0 [858.0] | 27.0 [27.0] | - | Pultrusion | Flexural: ASTM 790 |
| CMRG (2000) | Filled epoxy EPON® 9500 | E-glass | 68.0 | 1227.0 [1082.0] | - | 46.0 [40.0] | Pultrusion | Flexural: ASTM 790 ILSS: ASTM D 2344 |
| Fernando and Al-Khodairi (2003) | Epoxy Fibredux 913 | E-Glass | 62.2 | 1500.2 [1447.1] | 48.7 [47.0] | 83.0 [80.1] | Hot-press | |
| Huntsman (2007) | Epoxy Araldite® LY556 | E-glass | 60.0 | - | - | 75.0 [75.0] | Hot-press | 6.4 mm thick sample ILSS: ASTM D 2344 |
| **Current study** | | | | | | | | |
| Conventional with resin bath | Epoxy Araldite® LY556 | E-glass Hybon® 2026 | 65.2 | 944.0 [868.6] | 42.3 [38.9] | 70.5 [62.9] | Pultrusion | Flexural: ASTM 6272 ILSS: ISO 14130 |
| Clean with resin impregnator PUL-I | Epoxy Araldite® LY556 | E-glass Hybon® 2026 | 70.4 | 1157.1 [985.6] | 55.7 [47.4] | 77.4 [65.89] | Pultrusion | Flexural: ASTM 6272 ILSS: ISO 14130 |
| Clean with fibre spreading rig | Epoxy Araldite® LY556 | E-glass Hybon® 2026 | 69.3 | 1176.9 [1019.3] | 57.4 [49.71] | 75.6 [65.51] | Pultrusion | Flexural: ASTM 6272 ILSS: ISO 14130 |
| Clean where IMR applied externally | Epoxy Araldite® LY556 | E-glass Hybon® 2026 | 63.7 | 1417.3 [1335.7] | 55.9 [52.7] | 95.6 [90.1] | Pultrusion | Flexural: ASTM 6272 ILSS: ISO 14130 |

Table 25 was compiled to enable comparison of the normalised (60% $V_f$) flexural properties and inter-laminar shear strength (ILSS) of the data generated in the current work, and those reported previously in the literature for unidirectional (UD) glass fibre composites.

#### 4.4.1.3 Flexural properties

Figure 97 shows the flexural strengths (determined using ASTM D 6272-08) for the clean and conventional techniques. Here, it is clear that the data for the four-point flexural strengths are higher for the clean technique. It is appreciated that the fibre volume fractions for these samples are different and hence the data shown in Figure 97 also includes the normalised flexural strengths (normalised to 60% $v_f$) which are higher for the clean pultrusion technique. Normalisation was performed by multiplying the actual value (strength or modulus) to $60/v_f$, where $v_f$ is the actual fibre volume fraction of the sample for which normalisation is performed.

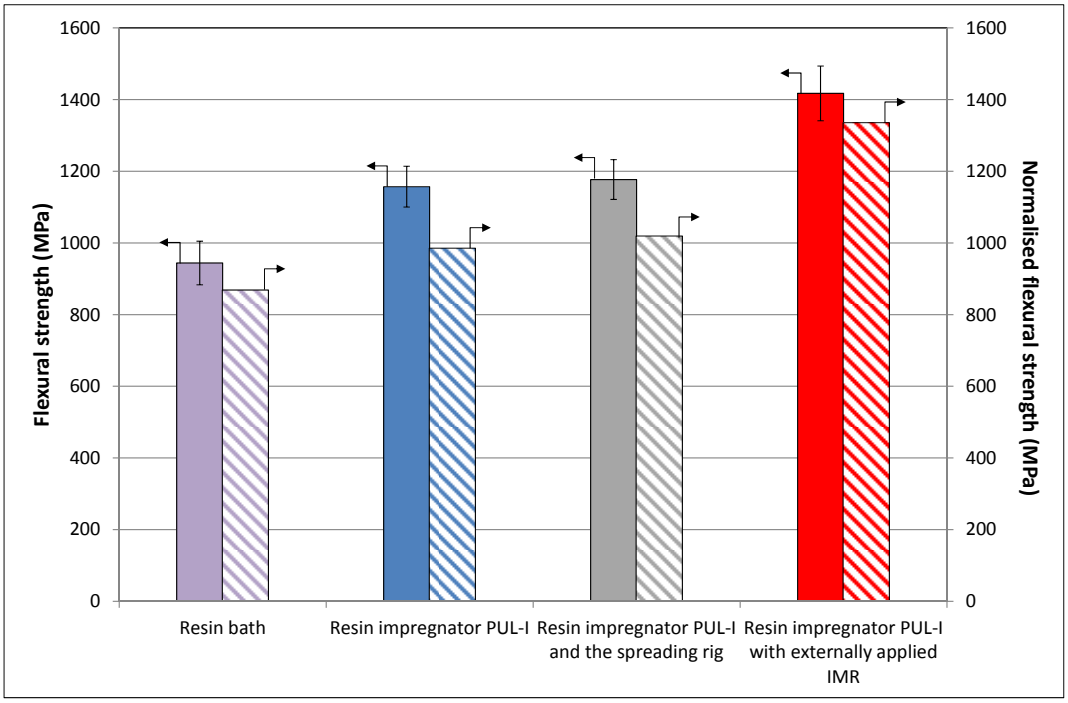


**Figure 97 Flexural strength (four-point bending) data for the pultruded epoxy/E-glass composites produced at 0.3 m/min. The corresponding normalised data at 60% fibre volume fraction are also represented.**

It is interesting to note that in the case where the IMR was applied externally, a 50% increase in the flexural strength is observed over the conventional pultrusion technique where the IMR was blended in the resin. The flexural strength can be influenced by one or more of the following: the degree of fibre alignment, the fibre volume fraction, the void content and the meandering of the reinforcing fibre as these traverse through the impregnation unit. With reference to the clean pultrusion technique, the trajectory of the E-glass rovings is better controlled when compared with the conventional process. The process of spreading the rovings improves the degree of impregnation by breaking down the binder.

The improvements in the flexural properties for the clean-pultruded composites where IMR was applied externally suggests that blending the OP wax in the resin system may have on an adverse effect on the interfacial bond strength between the matrix and the E-glass. The OP wax formulation (obtained from the data sheet) is given in Table 26.

**Table 26 Formulation for the OP Wax used in the current study.**

| Component | Weight fraction |
|---|---|
| 1-methyl-1,3-propanediyl esters | 60% – 70% |
| Calcium montanate | 30% – 40% |

With reference to Table 25, on comparing the data for the composites produced in the current study with those reported in the literature, it can be seen that the values of the flexural strengths in the current study are in the upper range of the previously reported values.

Figure 98 summarises the data for the flexural moduli that were generated in accordance with ASTM 6272–08. Here too it is readily apparent that the samples manufactured by the clean

pultrusion technique are approximately, on average, are higher by 32 % when compared to the samples produced by the conventional technique. The data obtained in this study for the moduli of the pultruded composites are either equivalent or marginally higher than those reported in the literature. Normalisation of the data was also performed as described in previous section.

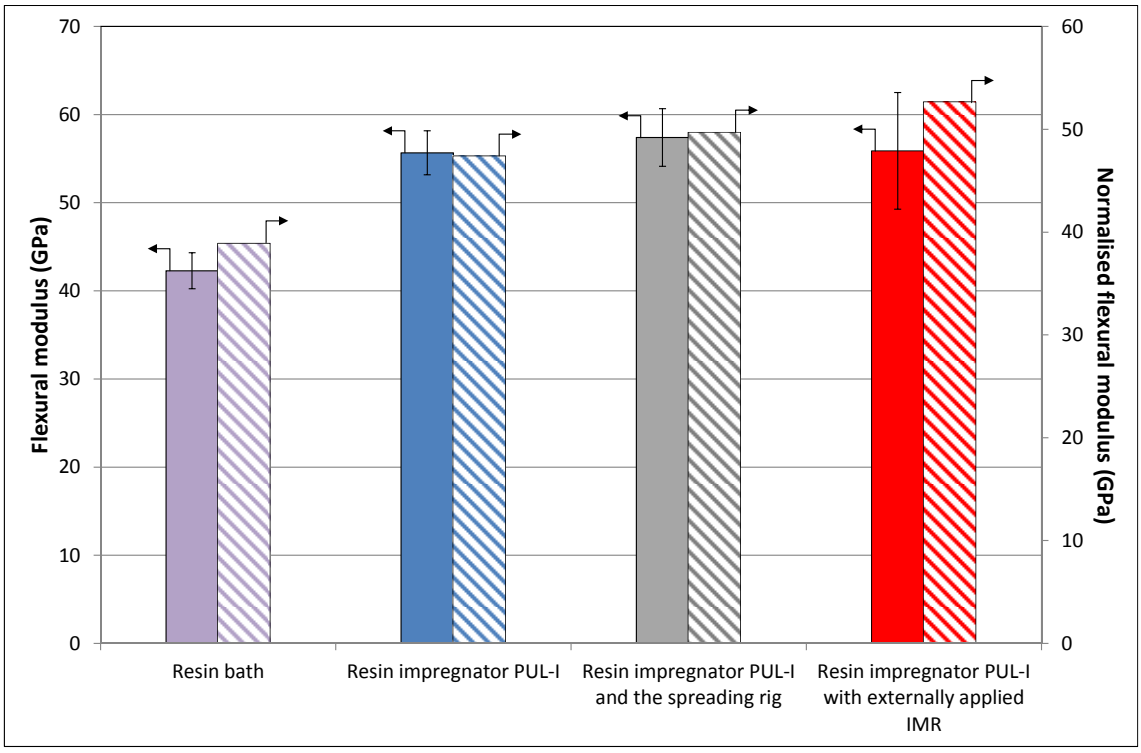


**Figure 98 Flexural moduli (four-point bending data) for the pultruded epoxy/E-glass composites produced at 0.3 m/min.**

#### 4.4.1.4 Inter-laminar shear strength

The inter-laminar shear strength (ILSS) for the pultruded composites were evaluated according to BS EN ISO 14130:1998 and the data are presented in Figure 99. It is apparent that the average ILSS values for the composites produced via clean pultrusion are nominally higher than those produced by conventional pultrusion. The values reported in the literature for the ILSS for pultruded E-glass fibre composites are summarised in Table 25. It is apparent

in Figure 99 that the samples where the IMR was applied externally yielded an average value of 95.60 MPa whereas that observed for resin impregnator PUL-I and the conventional resin bath techniques were 77.36 MPa and 70.55 MPa respectively.

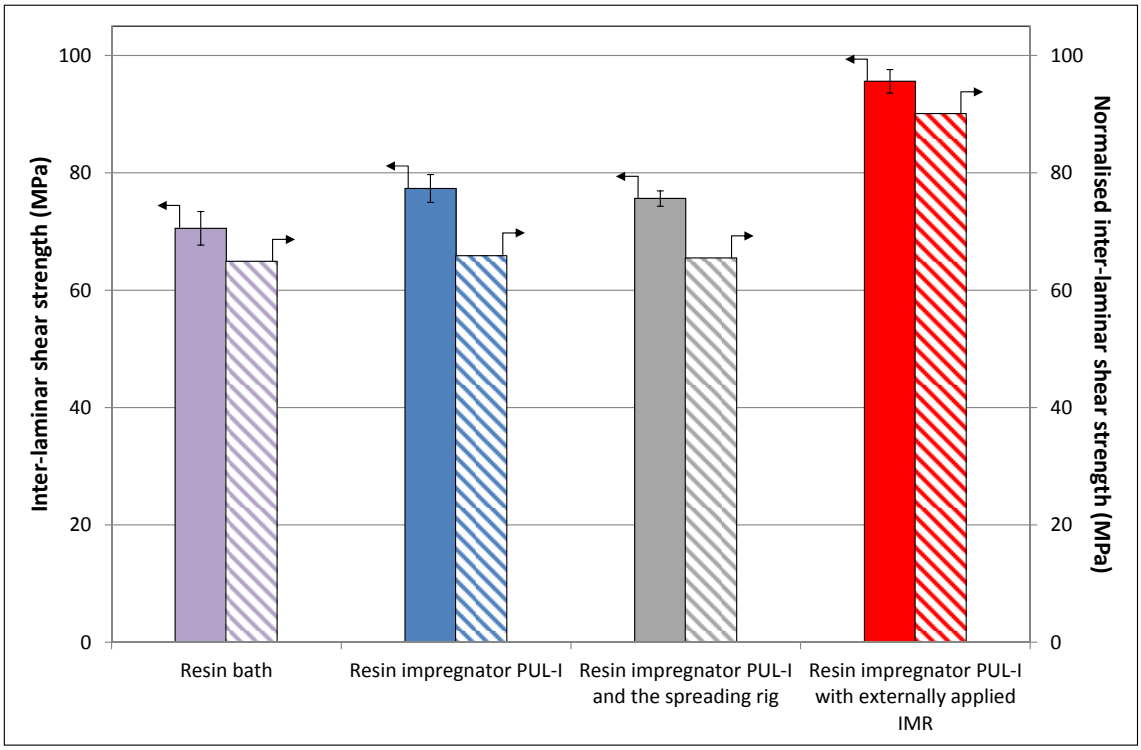


**Figure 99 Inter-laminar shear strength (ILSS) data for the pultruded epoxy/E-glass composites produced at 0.3 m/min.**

The normalised data for the ILSS is also presented in Figure 99. The normalised ILSS data for the pultruded samples produced by the clean technique is similar to those manufactured using the resin bath method. However, the normalised ILSS for the samples manufactured using the clean manufacturing technique in conjunction with the fibre spreader and when the IMR was applied externally were 2.39% and 38.81% higher respectively. On inspecting Table 25, it can be seem that the data obtained in this study for the ILSS for the epoxy/E-glass pultruded composites is either equivalent or marginally higher than those reported previously in the literature.

#### 4.4.1.5 Dynamic mechanical thermal analysis

The glass transition temperature ($T_g$) of the pultruded composites was determined from the peak of the loss tangent (*tan δ*) as described in Section 3.2.3. It is clear from Figure 100 that the $T_g$ for the clean and conventional composites where the IMR was pre-mixed in the resin are in the same range (135.8 °C - 138.8 °C). On the other hand, the $T_g$ for the composites where the IMR was applied externally is higher (149.9 ± 0.35 °C). The average $T_g$ for epoxy LY556 resin measured using DSC in this study was 143.9 ± 2.1 °C.

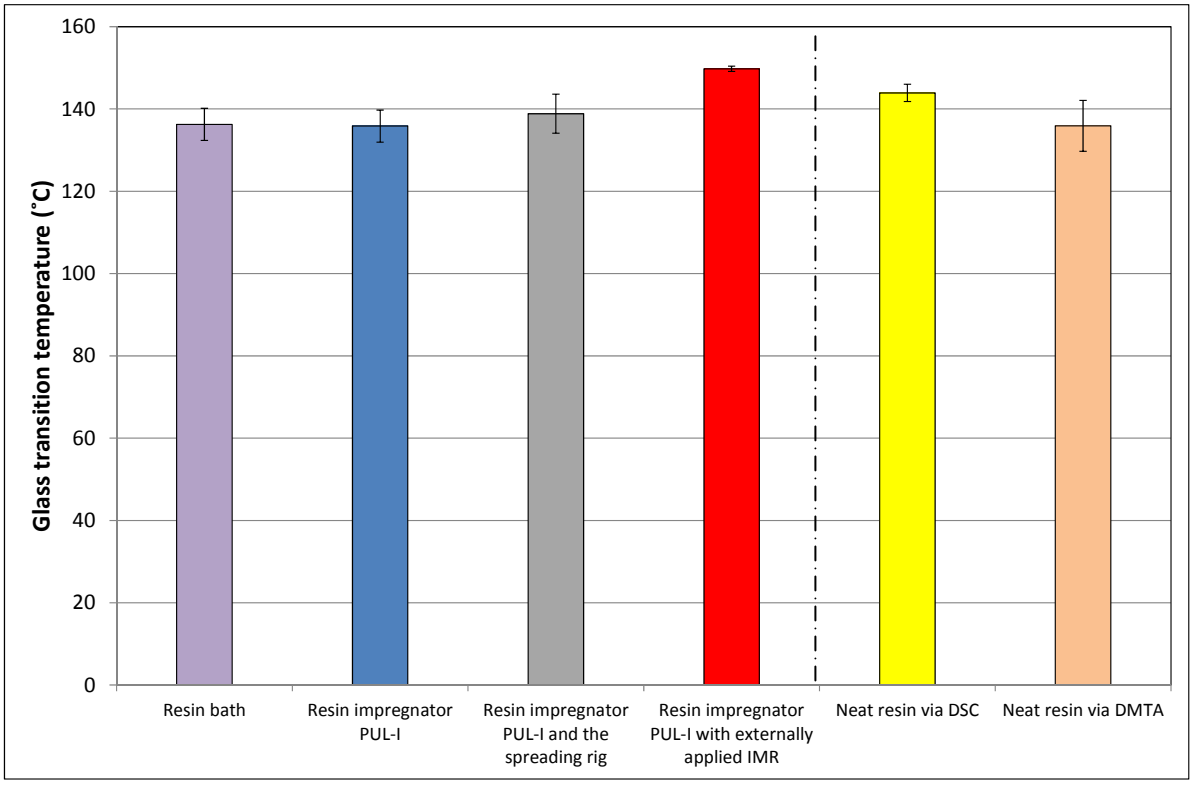


**Figure 100 Glass transition temperatures ($T_{gs}$) for the pultruded epoxy/E-glass composites produced at 0.3 m/min. The $T_g$ values for the neat resin obtained via DSC and DMTA experiments are also shown.**

The higher $T_g$ values where IMR was applied externally may be due to the absence of plasticisation effect caused by the OP Wax. Luyt and Krupa (2009) investigated the effect of adding paraffin wax on the thermo-mechanical properties of an epoxy resin system using DMTA. A decrease in the $T_g$ was observed as the wax content in the resin was increased. It

was shown that the wax particles were present in the epoxy matrix, even after heating the sample temperatures above the melting point of the wax, and cooling back to the room temperature.

The $T_g$ for the epoxy resin system (Araldite® LY556/Aradur® 917/ Hardener DY 070) from the manufacturer's data, determined by DSC, is reported to be in the range 140 °C to 155 °C. This correlates well with the data generated in this study.

The storage modulus ($E$') data for the pultruded epoxy/E-glass composites are shown in Figure 101. Here the storage moduli for the composites produced via the conventional and clean pultrusion techniques are similar. The normalised data (60% $v_f$) for the storage moduli are also cross-plotted in Figure 101.

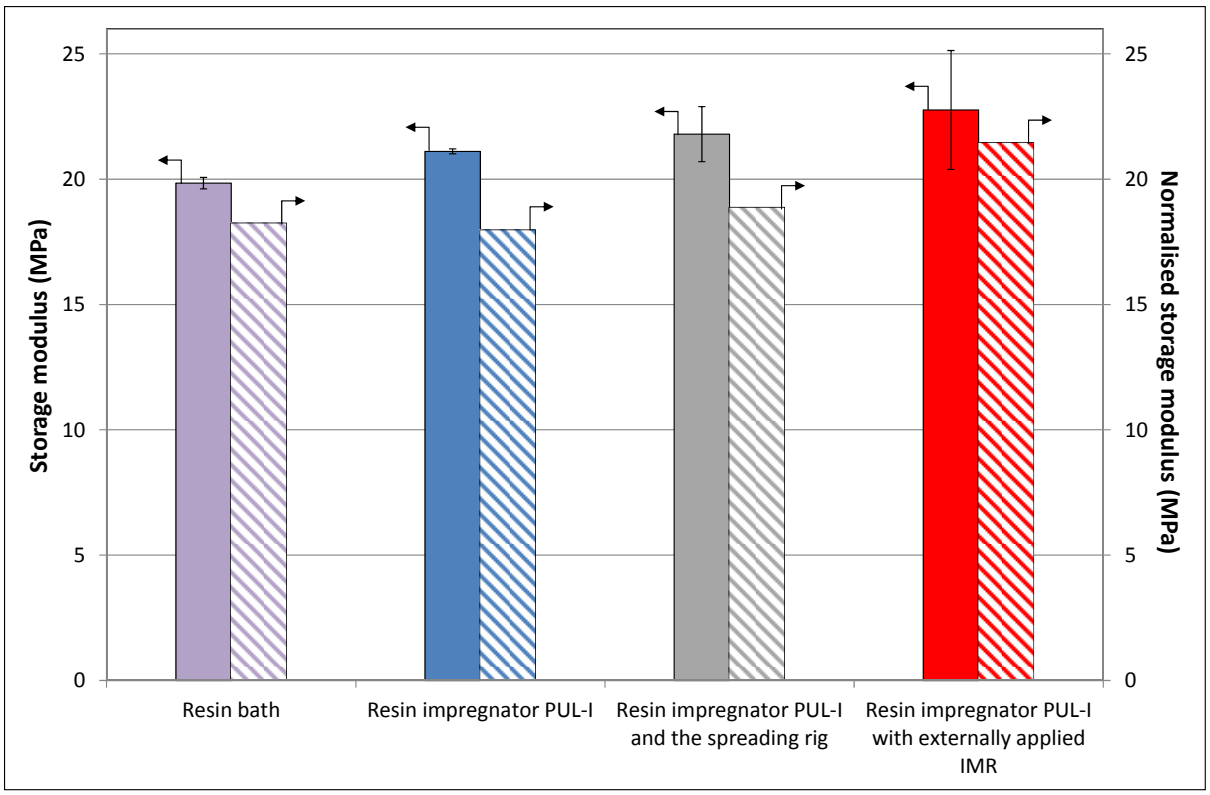


**Figure 101 Storage moduli for the pultruded epoxy/E-glass composites produced at 0.3 m/min.**

In the studies conducted by Luyt and Krupa (2009), it was shown that the storage modulus of the epoxy resin decreased as the concentration of the wax was increased. With reference to Figure 101, it is speculated that the OP wax may have a plasticisation effect on the matrix. This is reflected in the higher storage modulus when the IMR is applied externally.

#### 4.4.1.6 Comparison of properties

On comparing the properties presented in previous section it can be seen that the composites produced via clean pultrusion are exhibiting a lower void content. This is primarily related to the spreading of the rovings and breaking-up of the binder within the rovings which leads to improved impregnation as shown by the micrographs in Figure 96. The improved impregnation of the clean composites is manifested in enhanced mechanical properties. Clean pultrusion trials were also performed using resin impregnator PUL-II for the epoxy/E-glass system. The results obtained where similar to those seen for resin impregnator PUL-I. Therefore the results obtained using resin impregnator PUL-II results are summarised in Appendix-C.

Another interesting observation from previous section is that the situation where internal mould release (IMR) was applied externally the void fractions are almost zero and the mechanical properties are further improved.

### *4.4.2 Epoxy/E-glass composites manufactured at three pultrusion speeds*

The effect of the pultrusion speed on the physical and mechanical properties of the composites was also studied. The pultrusion speeds used in these experiments involving a 0.5 m long die were 0.3 m/min, 0.4 m/min and 0.5 m/min. The simulations that were carried out to attain maximum curing (see Section 4.1.1.1) indicated that the fastest pultrusion speed permissible was 0.5 m/min. With reference to the above mentioned pultrusion speeds, it is unlikely that the impregnation process would be influenced; as expected, this is reflected in the results presented in Figures 102 to 109 where the physical and mechanical properties generally do not show any significant differences between 0.3 and 0.5 m/min. This is also reflected in the micrographs presented in Figure 104 where there are no discernible differences in the visually observed quality of the samples.

The densities of the pultruded composites manufactured via the conventional and clean techniques at three pultrusion speeds are shown in Figure 102. It can be seen that for a specific pultrusion method, the densities are similar. The densities of the clean pultrusion technique are higher than that observed for the conventional method due to the differences in the number of rovings as explained in Section 4.4.1.1.

The void fractions for the composites produced using clean pultrusion technique were lower than those produced via conventional pultrusion. Within the data set of the void fractions of the composites produced via resin impregnator PUL-I, a lower value is observed at 0.4 m/min. However, it should be noted that resin burn-off method is not very accurate test at such low void fractions. Hence it can be safely assumed that there is not much variation within this data set.

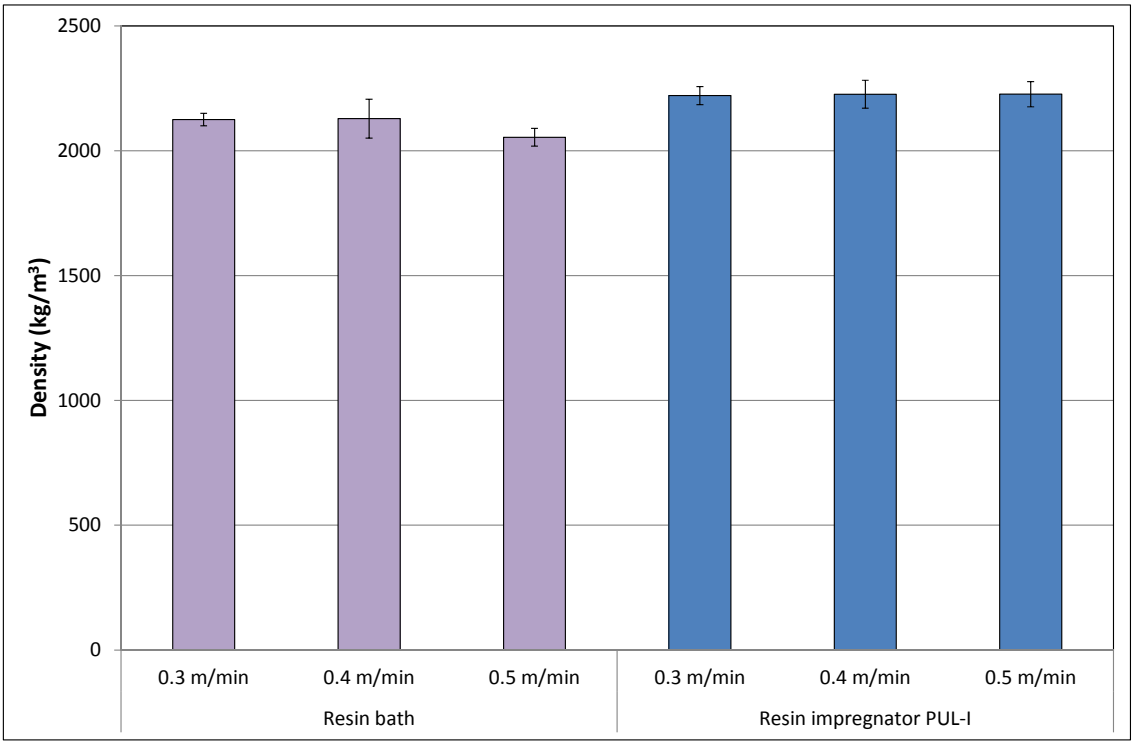


**Figure 102 Densities for the pultruded epoxy/E-glass composites produced at three pultrusion speeds using the resin bath and resin impregnator PUL-I.**

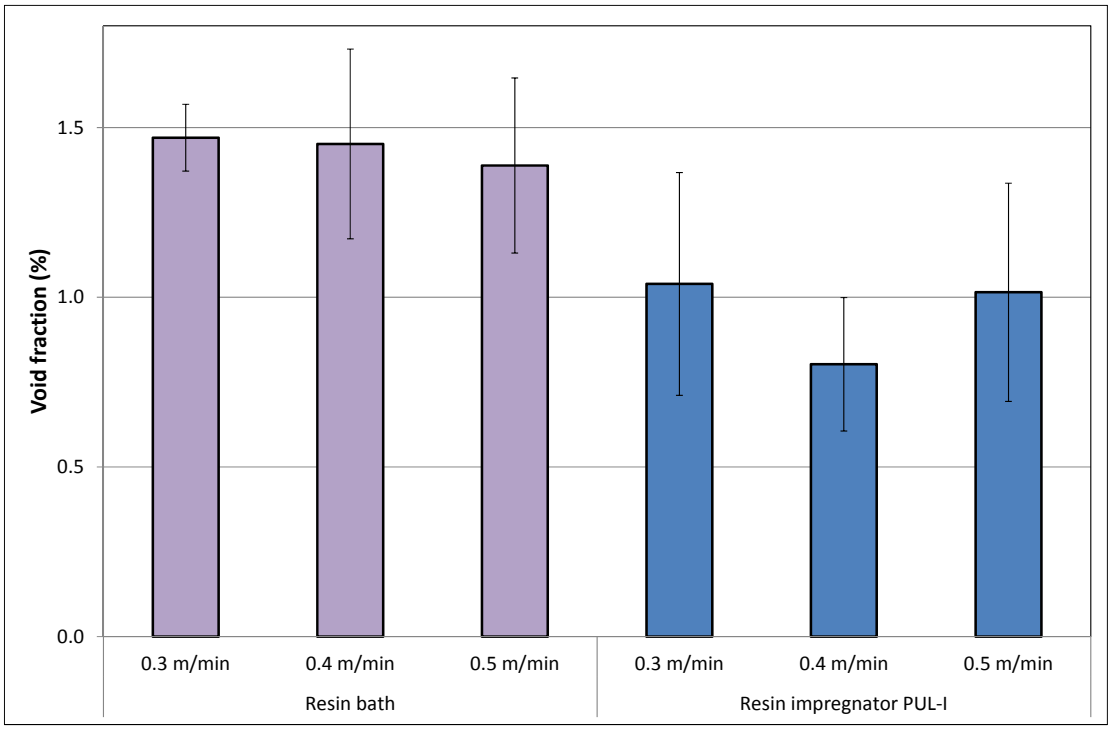


**Figure 103 Void fractions for the pultruded epoxy/E-glass composites produced at three pultrusion speeds using the resin bath and resin impregnator PUL-I.**

This trend is also evident from the micrographs shown in Figure 104. This is also manifested in the mechanical properties of the composites produced by clean pultrusion technique (flexural strength in Figure 105, flexural moduli in Figure 106, ILSS in Figure 107 and storage moduli in Figure 109) which are equal or marginally better than those manufactured via the resin bath method.

| Pultrusion speed | Conventional pultrusion using the resin bath | Clean pultrusion using resin impregnator PUL-I |
|---|---|---|
| 0.3 m/min | 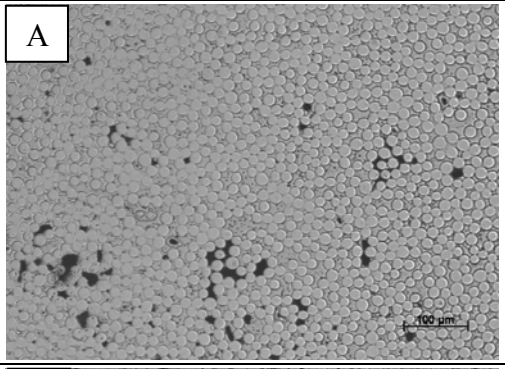  | 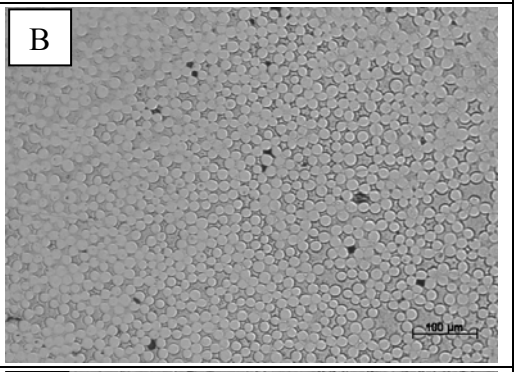  |
| 0.4 m/min | 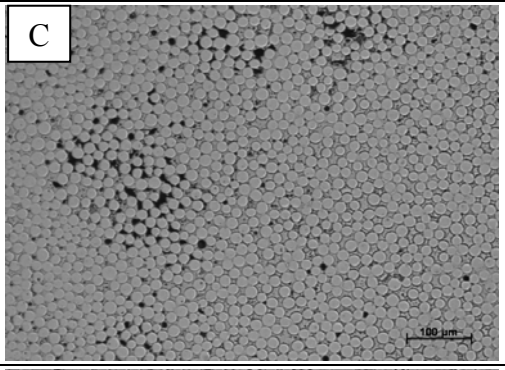  | 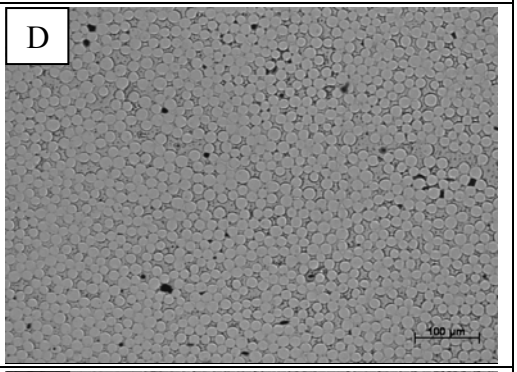  |
| 0.5 m/min | 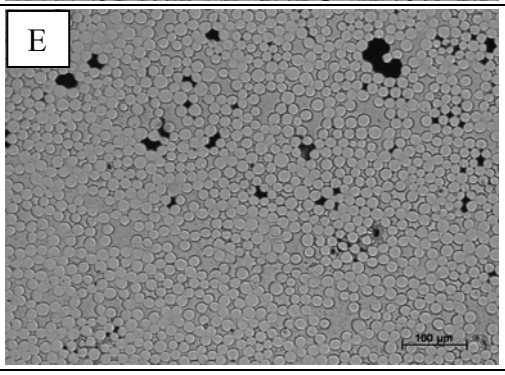  | 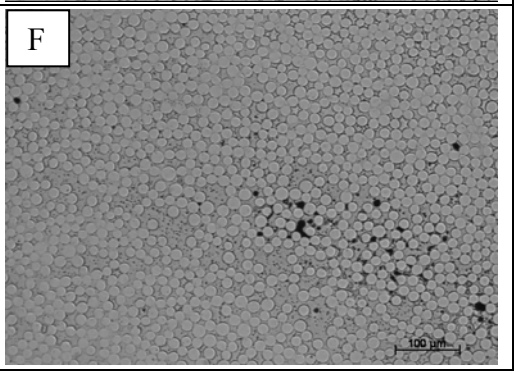  |

**Figure 104 Representative micrographs of the epoxy/E-glass composites produced at three pultrusion speeds. : (A) resin bath at 0.3 m/min; (B) resin impregnator PUL-I at 0.3 m/min; (C) resin bath at 0.4 m/min; (D) resin impregnator PUL-I at 0.4 m/min; (E) resin bath at 0.5 m/min; and (F) resin impregnator PUL-I at 0.5 m/min.**

The flexural strengths and moduli of the composites produced at three pultrusion speeds are shown in Figures 105 and 106 respectively. It can be seen that in both graphs the values for the composites produced via clean pultrusion are marginally better than those produced by conventional pultrusion. Another interesting feature to note is that the properties are showing an increasing trend with an increase in pultrusion speed. This can be related to the increase in the tension in the rovings at higher pultrusion speeds which may have resulted in improved orientation of the rovings. It should be noted that the force required to pull the rovings would also increase by increasing the pultrusion speed. Unfortunately, no mechanism was available to quantify the pulling force during the experiments reported in this work.

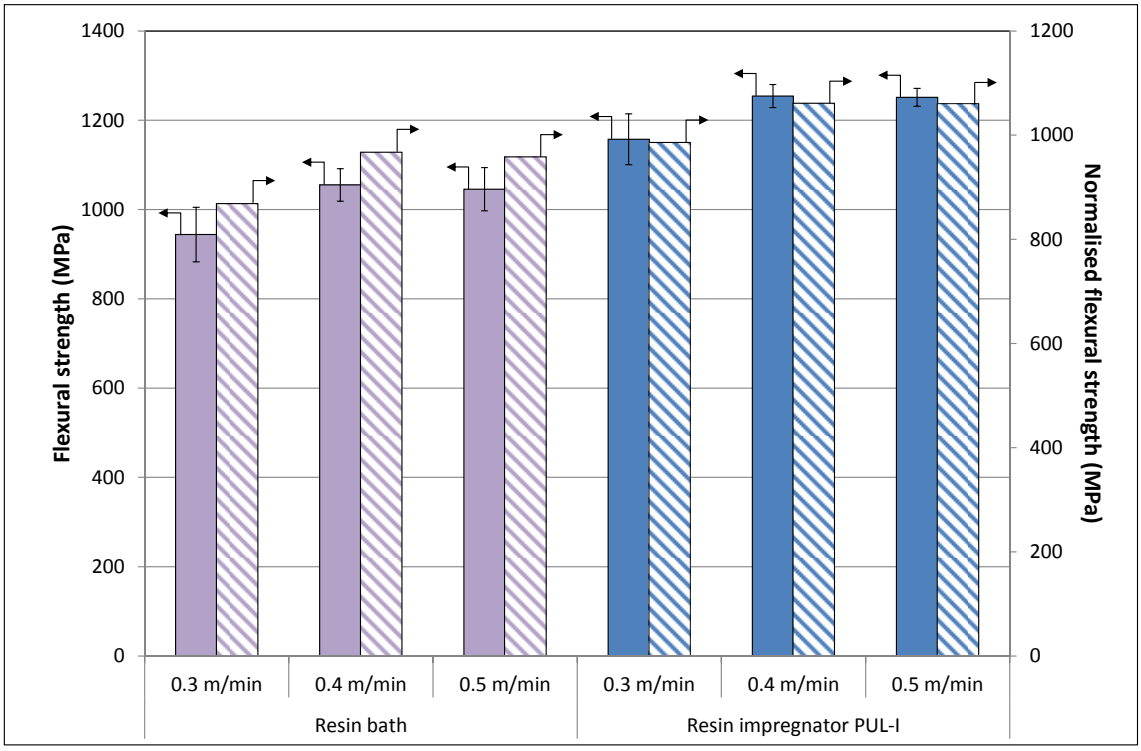


**Figure 105 Flexural strengths for the pultruded epoxy/E-glass composites produced at three pultrusion speeds.**

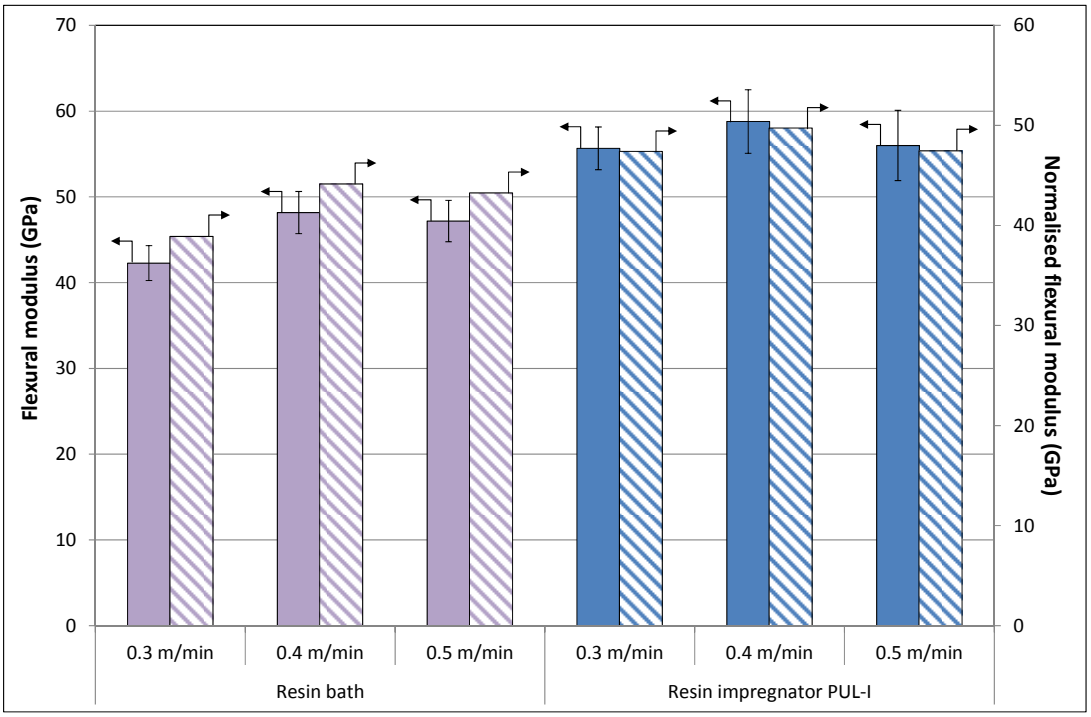


**Figure 106 Flexural moduli for the pultruded epoxy/E-glass composites produced at three pultrusion speeds.**

The normalised ILSS values are all within the same range as these are generally considered and matrix dependent property.

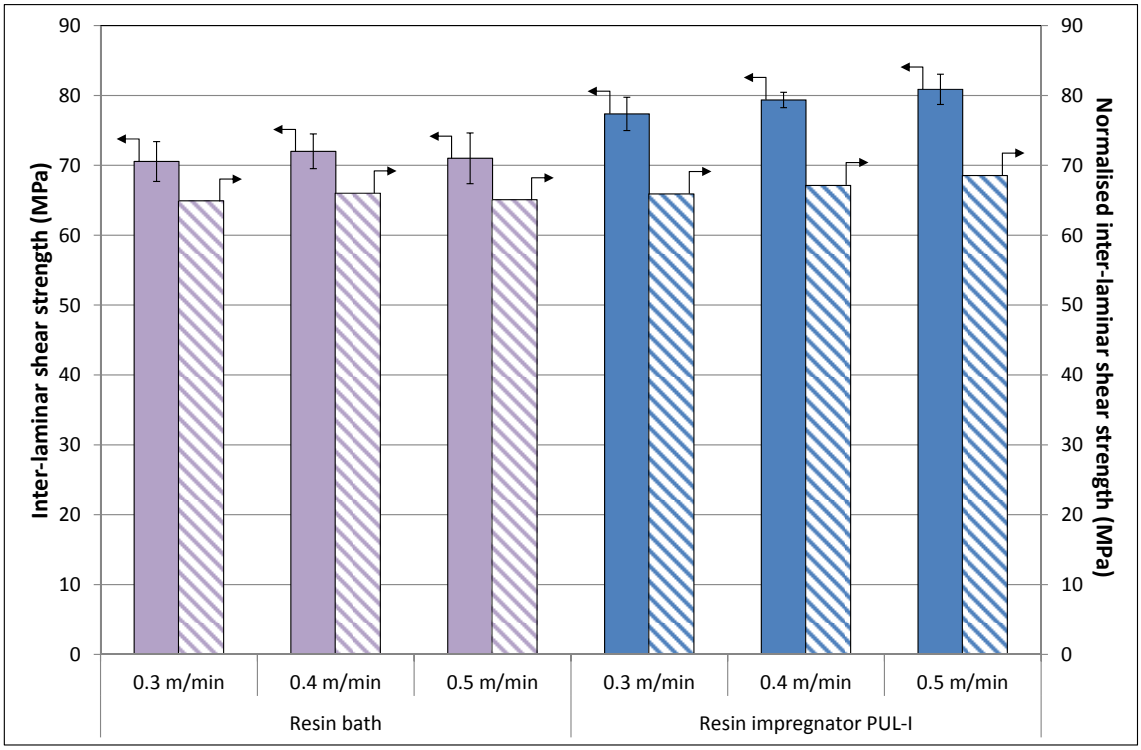


**Figure 107 ILSS for the pultruded epoxy/E-glass composites produced at three pultrusion speeds.**

The $T_{gs}$ and storage moduli are all within the same range as expected as shown in Figures 108 and 109 respectively.

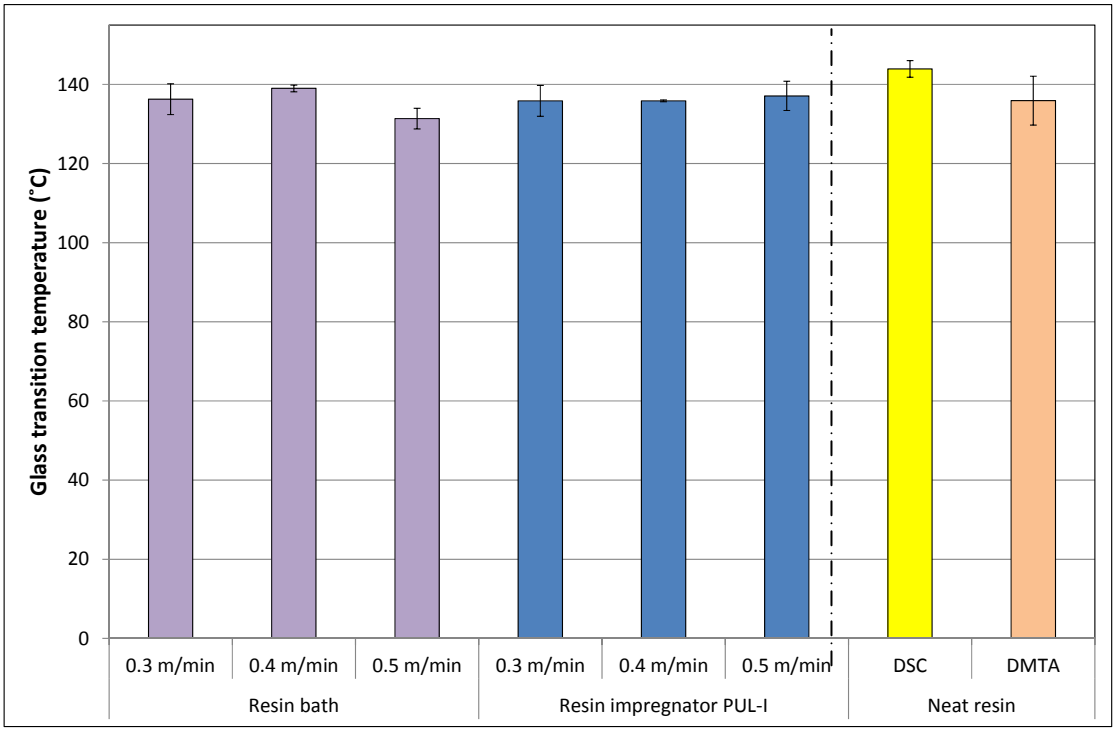


**Figure 108 Glass transition temperatures via DMTA for the pultruded epoxy/E-glass composites produced at three pultrusion speeds. The data for the neat resin is also included.**

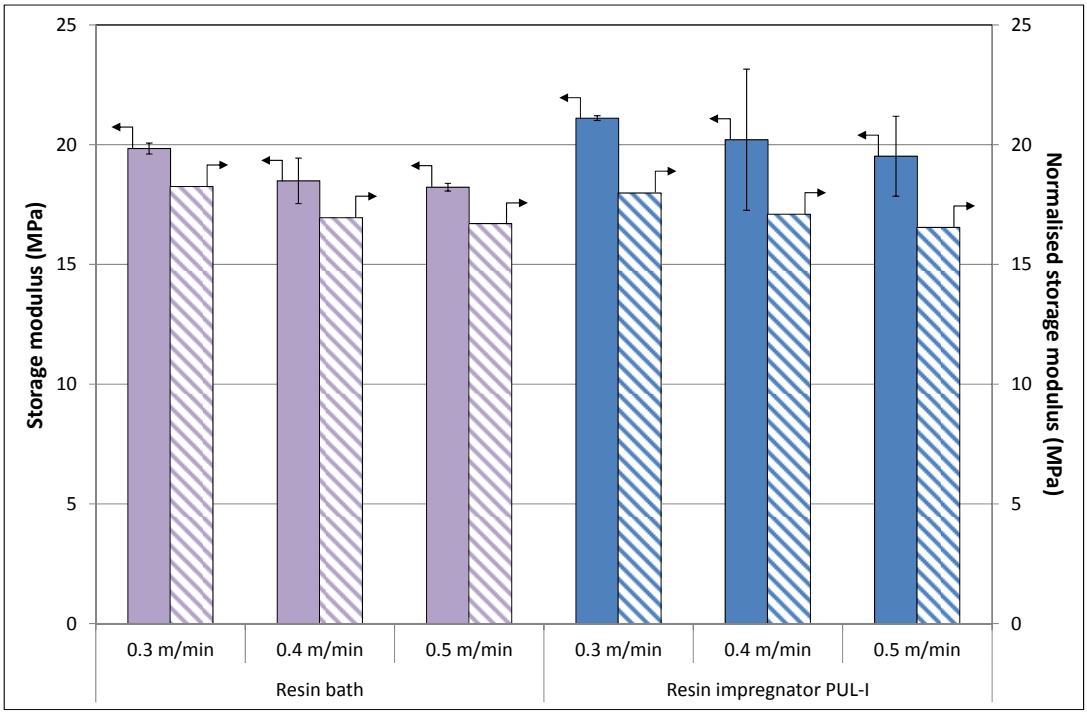


**Figure 109 Storage moduli measured via DMTA for the pultruded epoxy/E-glass composites produced at three pultrusion speeds.**

### *4.4.3 On-site pultrusion trials using vinyl ester/E-glass*

The clean pultrusion technique was also demonstrated at the premises of one of the project partners. Here filled and un-filled vinyl ester resin systems were used with 4800 tex E-glass rovings. The details of the resin system and the rovings were provided in Sections 3.1.1 and 3.1.2 respectively. The pultrusion trials were carried out using the resin bath and resin impregnator prototype PUL-I as described in Section 3.7.

#### 4.4.3.1 Fibre volume fraction and density

The fibre volume fractions and densities for the unfilled and filled vinyl ester/E-glass composites are shown in Figure 110. In case of the unfilled resin system, the fibre volume fractions and the densities for conventional and clean pultruded composites are similar. In this case, twenty eight rovings of 4800 tex E-glass were employed. On the other hand, only twenty four rovings were used in the filled system. Here too, the conventional and clean techniques show similar values for the fibre volume fractions and density.

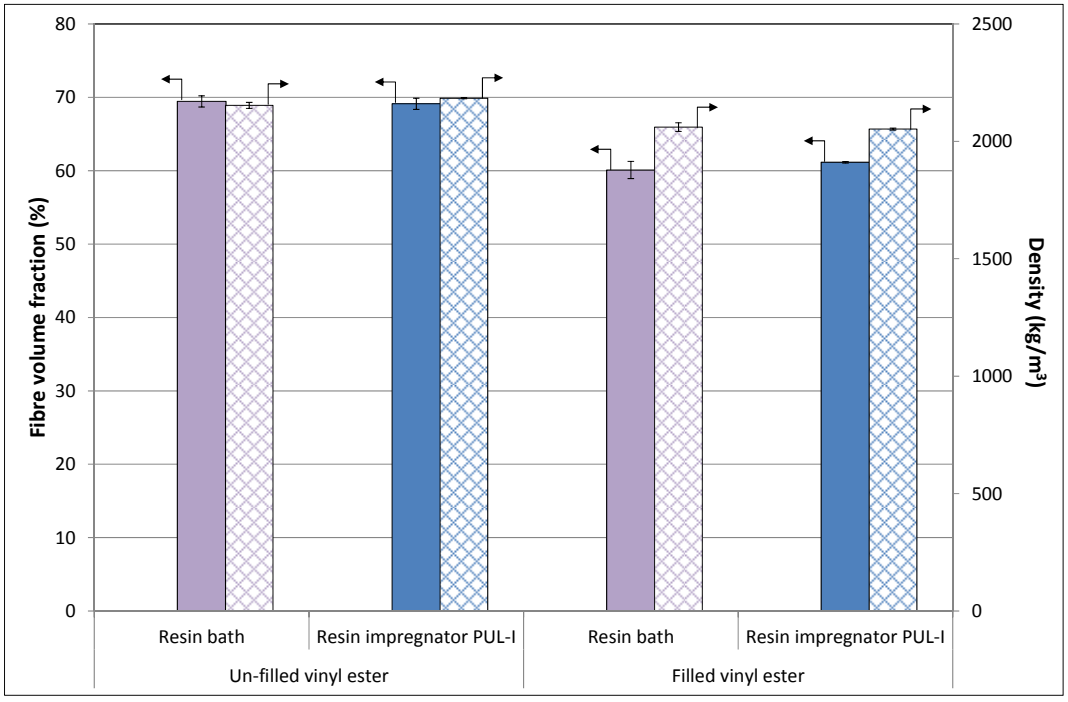


**Figure 110 Fibre volume fraction and density for the pultruded vinyl ester/E-glass composites produced on-site at 0.4 m/min.**

#### 4.4.3.2 Void fraction

The void fractions were determined using the method described in Section 3.2.6. With reference to the unfilled and filled vinyl ester systems, the void fractions for the clean composites are lower than that for composites manufactured using the resin bath. However, the void fractions for the unfilled composites are higher than the filled composites. This is also evident in the micrographs shown in Figure 112.

Vinyl ester resin systems show higher shrinkage when compared to epoxy resins. However the addition of filler in the resin reduces the shrinkage (Lampman, 2003, Cambell, 2010). It has been shown by Ashbee and Wyatt (1969) that resin-shrinkage can cause debonding between resin and fibres. The higher void fraction in the unfilled composites may be related to de-bonding caused by resin-shrinkage during cross-linking; this is seen in Figure 113.

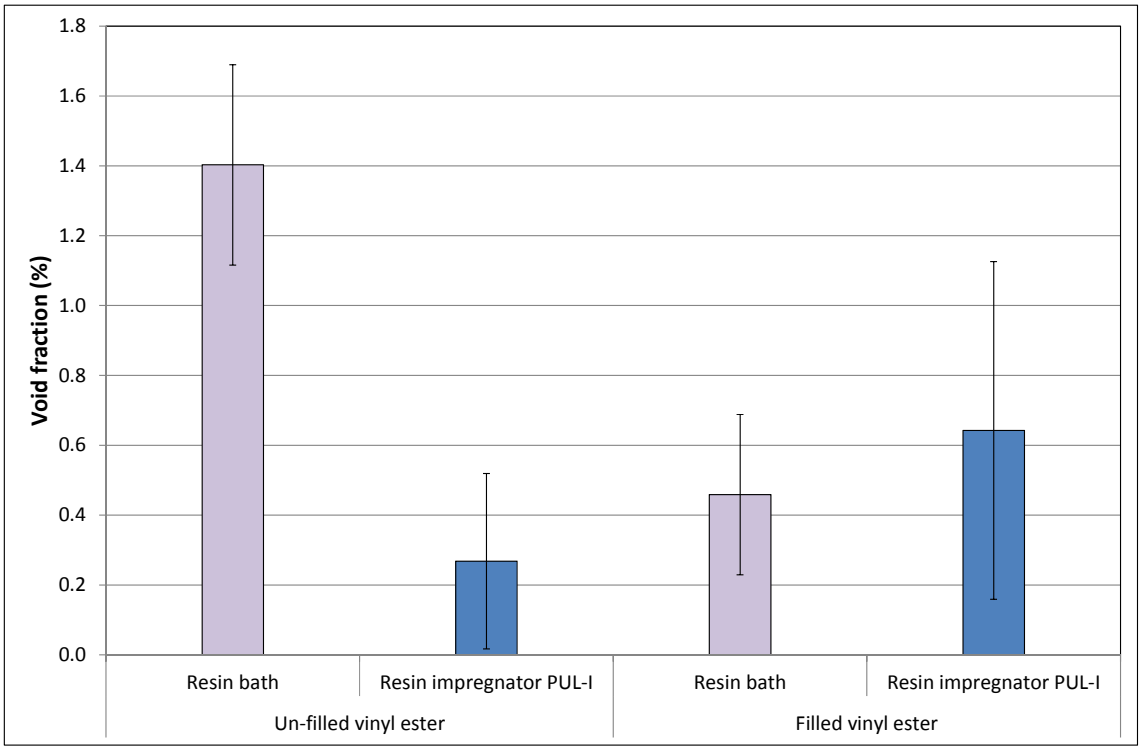


**Figure 111 Void fraction data for the pultruded unfilled and filled vinyl ester /E-glass composites produced on-site at 0.4 m/min.**

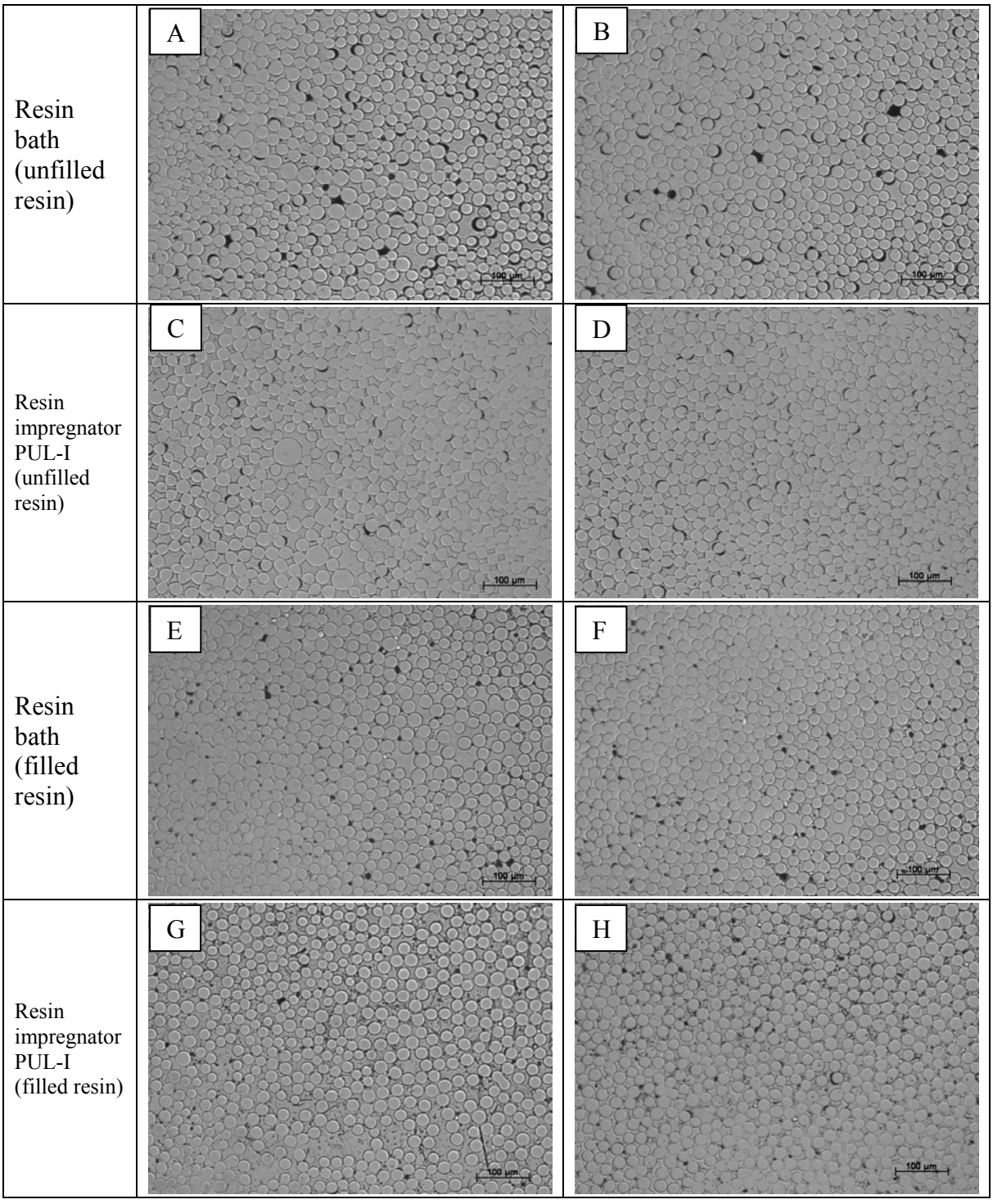


**Figure 112 Micrographs of the unfilled and filled vinyl ester/E-glass pultruded samples. (A) resin bath using unfilled resin (best sample); (B) resin bath using unfilled resin (worst sample); (C) resin impregnator PUL-I using unfilled resin (best sample); (D) resin impregnator PUL-I using unfilled resin (worst sample); (E) resin bath using filled resin (best sample); (F) resin bath using filled resin (worst sample); (G) resin impregnator PUL-I using filled resin (best sample); and (H) resin impregnator PUL-I using filled resin (worst sample).**

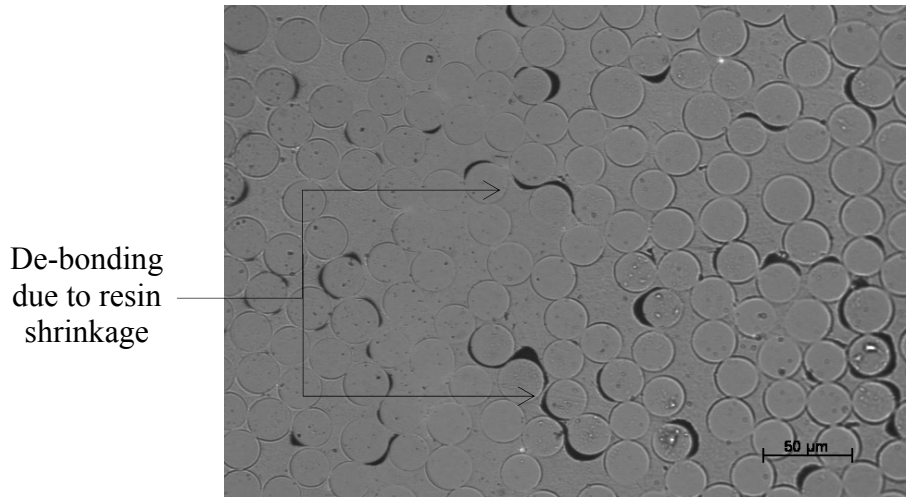


**Figure 113 Micrograph of the unfilled vinyl ester/E-glass sample showing the de-bonding of the resin from the fibres caused by the shrinkage of the resin.**

**Table 27 Comparison of the void fraction data for the pultruded vinyl ester/E-glass composites obtained by image analysis and the resin-burn off method.**

| Resin system | Pultrusion method | Void fraction using the resin-burn off (ASTM D 2584–08) | Void fraction using image analysis |
|---|---|---|---|
| Unfilled vinyl ester/E-glass | Resin bath | 1.40 ± 0.29 | 1.48 ± 0.46 |
| | Resin impregnator PUL-I | 0.27 ± 0.25 | 1.07 ± 0.29 |
| Filled vinyl ester/E-glass | Resin bath | 0.45 ± 0.53 | 0.62 ± 0.12 |
| | Resin impregnator PUL-I | 0.64 ± 0.78 | 0.62 ± 0.12 |

The effect of the higher void fraction in the unfilled composites is manifested by the lower mechanical properties (flexural and inter-laminar shear strengths) and this is discussed in the next sections.

A comparison of the normalised (60% $V_f$) flexural strength, flexural modulus and inter-laminar shear strength (ILSS) for the data generated in the current work, and those reported previously in the literature for unidirectional (UD) glass fibre composites is presented in Table 28.

**Table 28 Summary of selected papers to enable a comparison of the properties of the UD E-glass composites. The data in square brackets represents normalised fibre volume fraction at 60 %.**

| Reference | Resin system | Fibres | $V_f$ [%] | Flexural strength [MPa] | Flexural modulus [GPa] | ILSS [MPa] | Manufacturing Method | Other relevant information |
|---|---|---|---|---|---|---|---|---|
| Bogner et al. (2000) | Vinyl ester | E-glass | 35.5 | 404.0 [682.8] | 13.0 [22.0] | - | Pultrusion | Flexural: ASTM 790 |
| Bogner et al. (2000) | Vinyl ester | E-glass | 35.5 | 389.0 [657.5] | 12.3 [20.8] | - | Pultrusion | Flexural: ASTM 790 |
| Johsi (2000) | Vinyl ester Corez 153 | E-glass | 43.5 | 552.6 [762.2] | 25.4 [35.0] | - | Pultrusion | Flexural: ASTM 790 |
| Pultrex (2010) | Vinyl ester 1625 series | E-glass | - | 689.5[1] | 41.4[1] | - | Pultrusion | Flexural: ASTM 790 |
| Chu et al (2005) | Vinyl ester Dow Derakane 441– 400 | E-glass Hybon® 2100 | 62.0 | - | - | 43.0 [41.6] | Pultrusion | ILSS: ASTM D 2344 |
| **Current study** | | | | | | | | |
| Conventional with resin bath | Vinyl ester Atlac 430 | E-glass Hybon® 2026 | 69.2 | 615.0 [533.4] | 53.7 [46.5] | 48.2 [41.8] | Pultrusion | Flexural: ASTM 6272 ILSS: ISO 14130 |
| Clean with resin impregnator PUL-I | Vinyl ester Atlac 430 | E-glass Hybon® 2026 | 70.5 | 625.3 [532.5] | 51.5 [43.9] | 50.8 [43.2] | Pultrusion | Flexural: ASTM 6272 ILSS: ISO 14130 |
| Conventional with resin bath | Filled vinyl ester Atlac 430 | E-glass Hybon® 2026 | 61.9 | 785.0 [760.6] | 47.5 [46.0] | 61.7 [59.8] | Pultrusion | Flexural: ASTM 6272 ILSS: ISO 14130 |
| Clean with resin impregnator PUL-I | Filled vinyl ester Atlac 430 | E-glass Hybon® 2026 | 60.9 | 794.7 [782.8] | 46.2 [45.5] | 62.2 [61.2] | Pultrusion | Flexural: ASTM 6272 ILSS: ISO 14130 |

[1] Normalisation was not performed as the fibre volume fraction values were not reported.

#### 4.4.3.3 Flexural properties

Figure 114 and Figure 115 show the flexural strengths and flexural moduli respectively for the clean and conventional pultrusion techniques for the unfilled and filled vinyl ester/E-glass composites. It can be seen that there is no significant difference between the flexural strengths of the composites produced by the conventional and clean techniques. The flexural properties are lower for the unfilled systems which can be due to the shrinkage seen in Figure 113. On comparing the data presented in Figure 105 and Figure 114 for the epoxy/E-glass and vinyl ester/E-glass composites respectively, it is clear that the flexural properties of the epoxy/E-glass are higher than the vinyl ester/E-glass samples due to the higher strength of the neat epoxy resin.

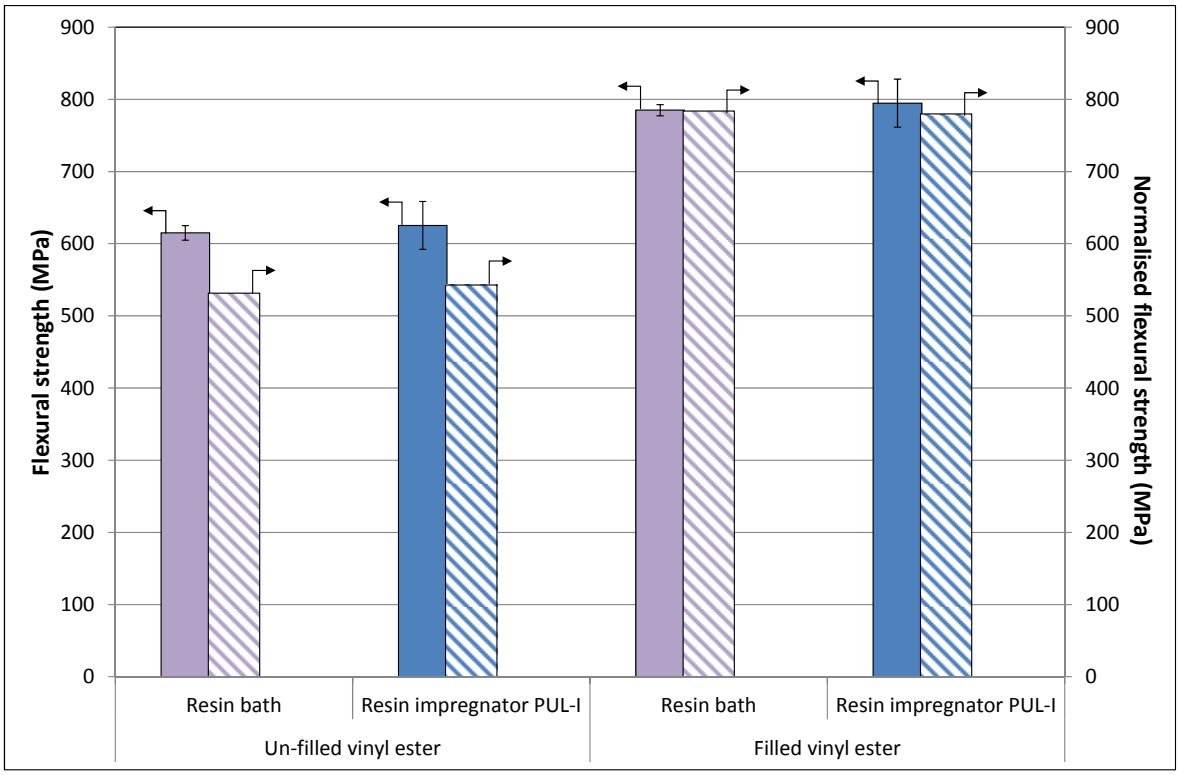


**Figure 114 Flexural strength of the vinyl ester/E-glass composites produced at 0.4 m/min.**

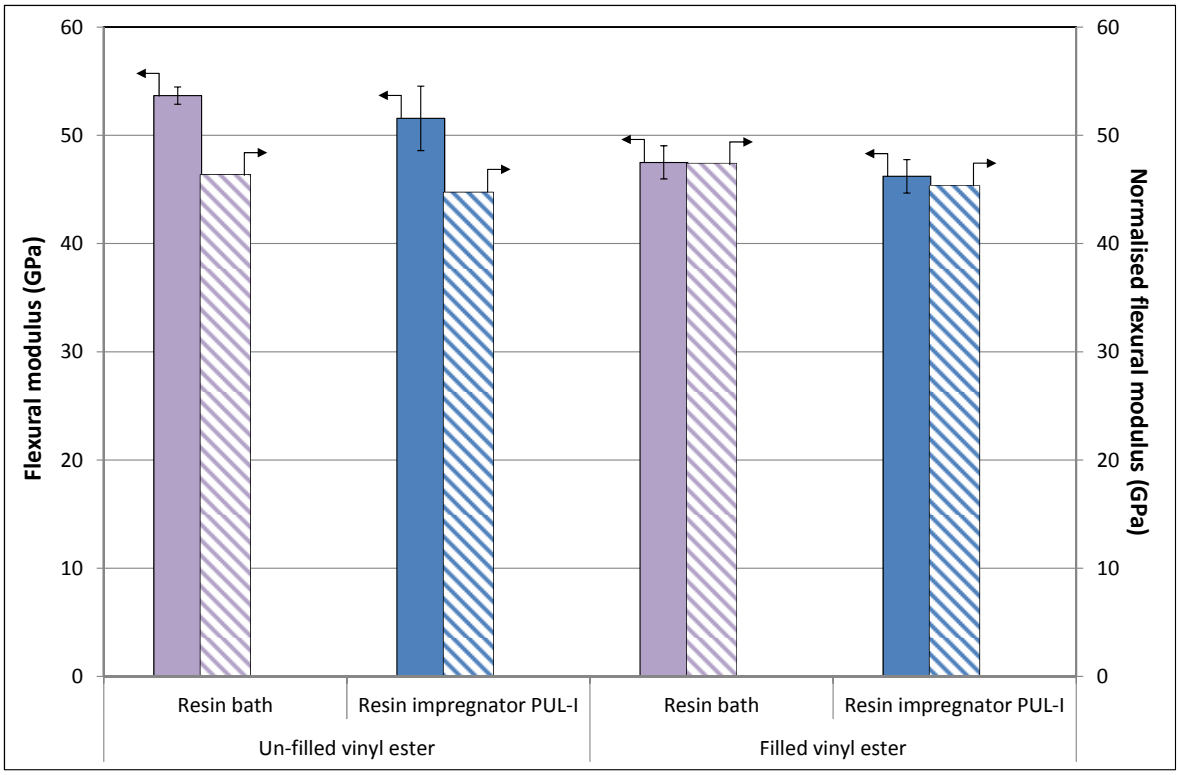


**Figure 115 Flexural moduli of the vinyl ester/E-glass composites produced at 0.4 m/min.**

On comparing the flexural strengths of the composites produced in this study with those reported in Table 28, it can be seen that the data for the filled composites are similar or higher than those reported by other researchers. On the other hand, the unfilled composites exhibit lower flexural strengths. This can be related to the presence of extensive de-bonding as explained previously.

It should be noted that for the results shown for the laboratory experiments, the composites produced via clean pultrusion showed improved properties. However, in case of the industrials experiments the strengths are similar. This is due to resin type that was used in both the cases as stated in Section 3.1.1. It can be speculated that if epoxy would have been used in industry similar results would be obtained. However, the environmental benefits for both the locations were similar regardless of the resin system.

#### 4.4.3.4 Inter-laminar shear strength

The inter-laminar shear strengths (ILSS) for the pultruded composites are presented in Figure 114. As observed with the flexural strength data, the ILSS data for the composites pultruded using the conventional and clean techniques are similar for the unfilled composites. In case of the filled composites, the ILSSs are similar for the conventional and clean techniques; however, these are higher than observed for the unfilled composites. This may be related to the void fractions shown in Figure 113. On comparing the ILSS for the epoxy/E-glass and vinyl ester/E-glass composites in Figure 107 and Figure 116 respectively, the ILSS values for the epoxy/E-glass composites are higher than vinyl ester/E-glass composites due to the higher mechanical strength of the epoxy resin system.

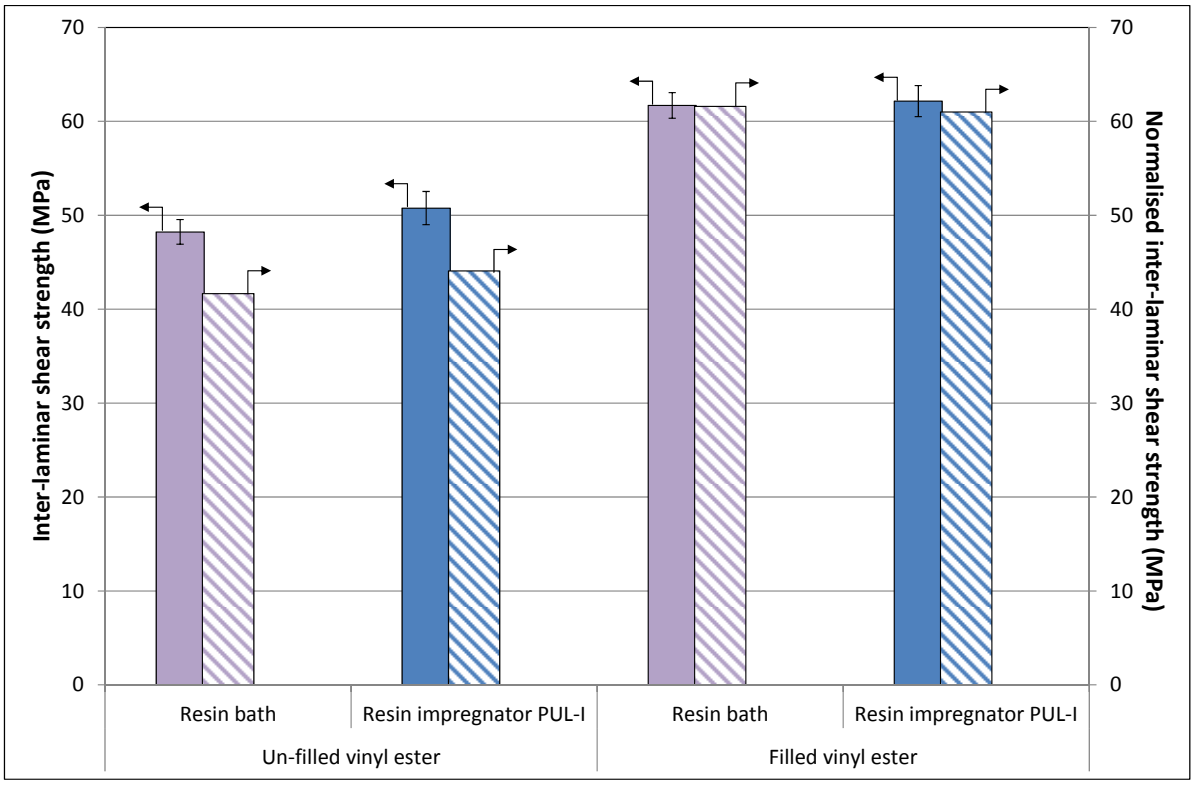


**Figure 116 ILSS for the pultruded vinyl ester/E-glass composites produced at 0.4 m/min.**

#### 4.4.3.5 Dynamic mechanical thermal analysis

The $T_g$ and storage modulus for the pultruded composites were calculated using DMTA as described in Section 3.2.3. As expected, the $T_{gs}$ are similar for the conventional and clean pultruded composites. The $T_g$ values for the filled composites are lower than that obtained for the unfilled systems.

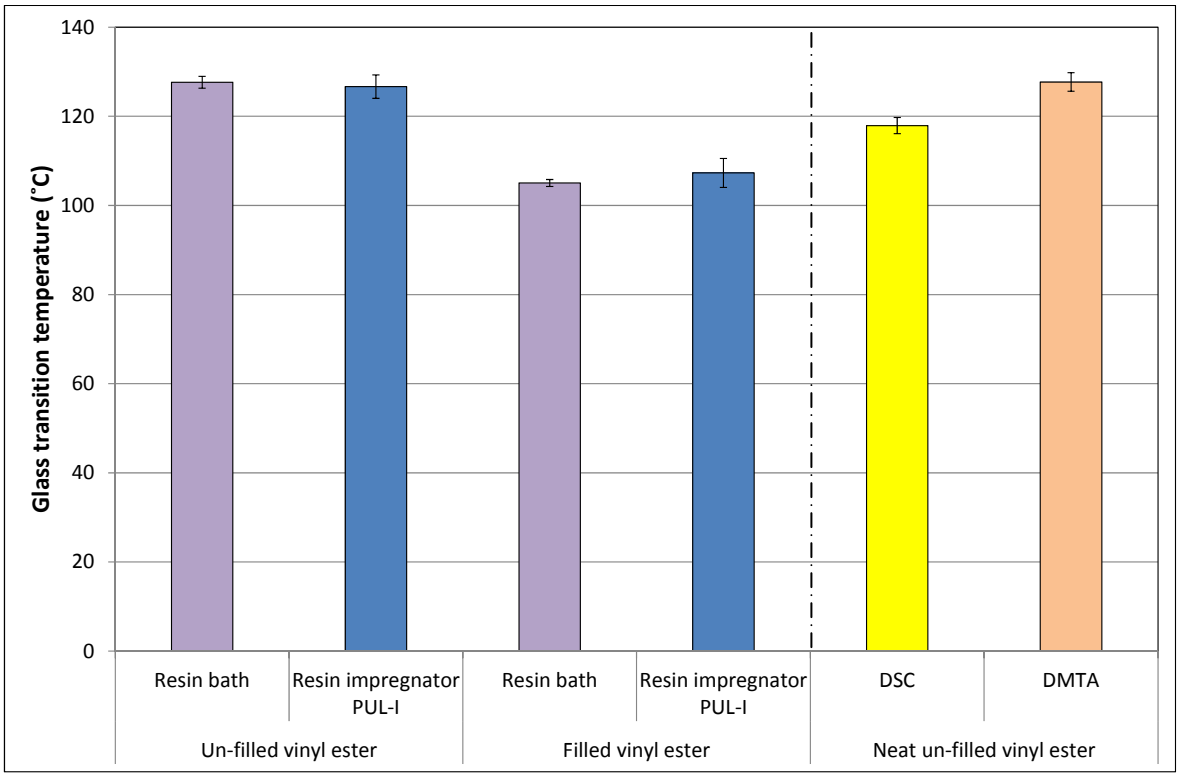


**Figure 117 Glass transition temperatures for the vinyl ester/E-glass composites pultruded at 0.4 m/min. The results for epoxy/E-glass composites are also shown for comparison.**

The addition of filler to a polymer can increase, decrease or have no effect on the $T_g$ depending upon the interaction of the filler with the polymer. Yusriah et al. (2010) performed dynamic mechanical analysis on the filled and unfilled vinyl ester/E-glass composites where calcium carbonate was used as the filler. For a similar fibre volume fraction it was shown that the $T_g$ for the filled and unfilled composites was similar. The maximum volume fraction of filler used in their studies was 5%. A vacuum bagging technique was used to prepare the

composites. On the other hand, a rise in $T_g$ with addition of filler is generally attributed to reduced molecular mobility due to presence of filler particles (Filyanov, 1978).

The lower values of $T_g$ for the filled composites in Figure 117 as compared to unfilled composites may be related the difference in the fibre volume fraction. It is speculated that at the same fibre volume fraction the $T_g$ for unfilled-composites could have been lower than the filled composites due to presence of resin-fibre de-bonding as evident from Figur e113.

The storage moduli (E') for the unfilled system are similar for conventional and clean composites however thier values are higher than filled composites, as shown in Figure 118. This can be related to the fibre volume fraction of these composites. The normalised values are similar for both unfilled and filled composites.

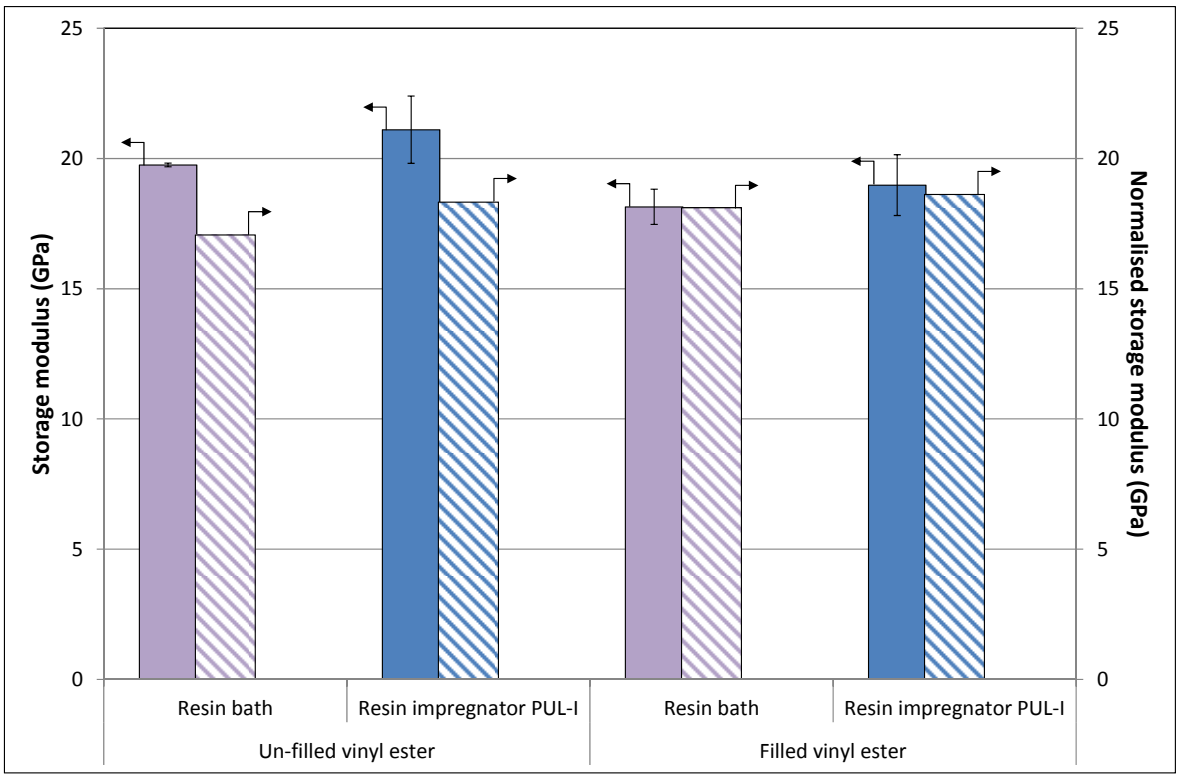


**Figure 118 Storage moduli for the vinyl ester/E-glass composites pultruded at 0.4 m/min.**

### *4.4.4 Production of pultruded polyurethane/E-glass composites*

One of the objectives of this study was to investigate the feasibility of pultruding composites using a custom-formulated PU resin system. The individual components (polyol and isocyanate) were stored in separate containers and pumped on demand from the resin dispenser (see Section 3.5). The calibration and operation of the resin dispenser was detailed in Section 4.3.

Over the course of this study, it became apparent that the surface chemistry of the E-glass fibres (from different suppliers) was having a noticeable adverse effect on the cross-linking behaviour of the PU resin. Summary of the various resin formulations, different E-glass and the pultrusion experiments that were undertaken is summarised in Table 29.

Due to the confidential reasons, the resin formulations evaluated in this study have been coded.

**Table 29 Detail of the polyurethane/E-glass pultrusion trials carried out in this study.**

| Resin system | Resin impregnation system | Fibres | Die temperature (°C) | Pultrusion speed (m/min) | Experiment Code |
|---|---|---|---|---|---|
| Polyurethane (Formulation 1) | Resin bath | Hybon® 2026 | Zone 1: 120<br>Zone 2: 140 | 0.4 | PU-1 |
| Polyurethane (Formulation 1) | PUL-I | Hybon® 2026 | Zone 1: 120<br>Zone 2: 140 | 0.4 | PU-2 |
| Polyurethane (Formulation 1) | PUL-I | TufRov® 4510 | Zone 1: 120<br>Zone 2: 140 | 0.4 | PU-3 |
| Polyurethane (Formulation 2) | PUL-I | Hybon® 2026 | Zone 1: 120<br>Zone 2: 140 | 0.4 | PU-4 |
| Polyurethane (Formulation 2) | Resin injection | JSK® 689 | 120 | 0.4 | PU-5 |
| Polyurethane (Formulation 2) | PUL-I | JSK® 689 | Zone 1: 120<br>Zone 2: 140 | 0.4 | PU-6 |


(a)


(b)


(a)

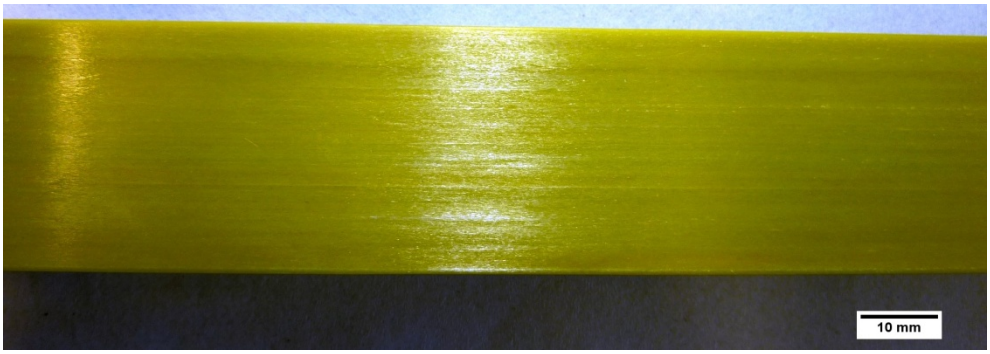


(b)

**Figure 119 Photographs of the pultruded composites: (a) polyurethane/E-glass experiment PU-1; (b) polyurethane/E-glass experiment PU-2; (c) vinyl ester/E-glass; and (d) epoxy/ E-glass. The degree of impregnation for the polyurethane resin was poor.**

It was observed that for the conventional and clean pultrusion (Experiment PU-1 and PU-2 in Table 29) the Hybon® 2026 E-glass rovings were not impregnated by the polyurethane resin. Extensive streaking of under-impregnated areas was present. This is apparent in Figure 119 (a and b). The poor wetting and impregnation is seen in the roving pack before they entered the die as shown in Figure 120.

**Figure 120 Photographs of the under-impregnated Hybon® 2026 E-glass rovings at the die entry. The resin system used here was polyurethane (formulation 1).**

It was concluded that the polyurethane (formulation 1) and Hybon® 2026 E-glass roving were not compatible. In a separate experiment, the Hybon® 2026 E-glass rovings were replaced with TufRov® 4510 E-glass rovings. TufRov® 4510 E-glass rovings showed no compatibility with the polyurethane resin (formulation 1). The same conclusion was reached with E-glass supplied by JSK Speciality Glass Fibres Ltd (JSK® 689).

Micrographs of selected composites produced using the polyurethane resins are shown in Figure 121(A-J). It can be seen that significant porosity is present. This could be due to: (i) the fibre-resin incompatibility; and (ii) initiation of some side reaction between the resin and sizing on the filaments. Due to the poor resin-fibre incompatibility problems, these composites were not evaluated.

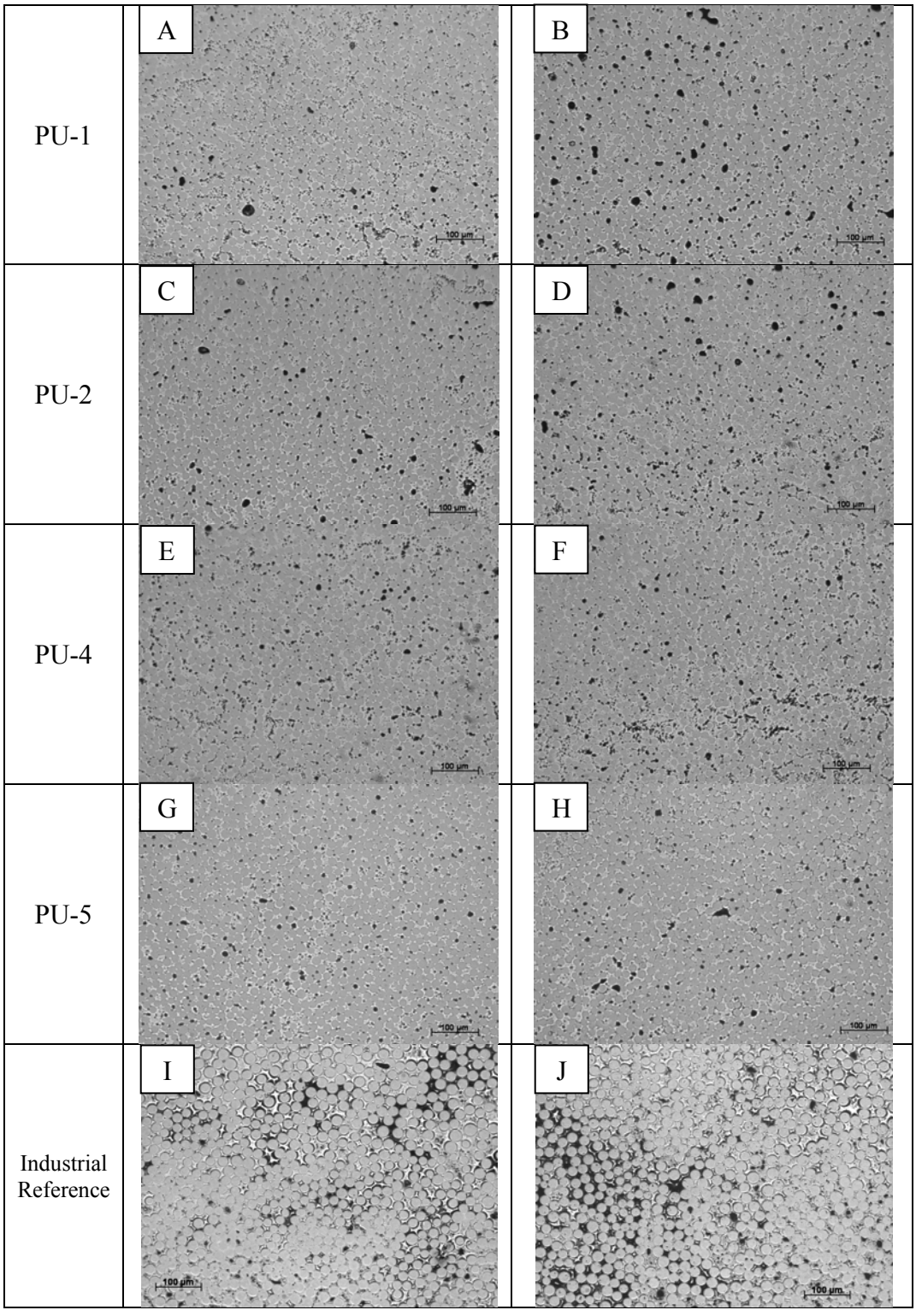


**Figure 121 Micrographs (A-J): Illustration of the porosity observed for the polyurethane/E-glass composites produced at 0.4 m/min.**

## 4.5 LIFE CYCLE ASSESSMENT

### *4.5.1 Waste reduction*

One obvious advantage of the clean pultrusion process over the conventional technique involving the resin bath was the reduction in the volume of the waste resin at the end of experiment. Furthermore, the volume of solvent that was required for cleaning the impregnation equipment was also reduced significantly. The actual volumes of the residual waste resin and solvent consumed are shown in Figure 122 where it can be seen that the clean pultrusion method resulted in more than a 90% reduction in the mass of mixed waste resin and solvent consumed. The data were collected when the pultrusion trials were undertaken using a 5 kg resin bath and resin impregnator PUL-I.

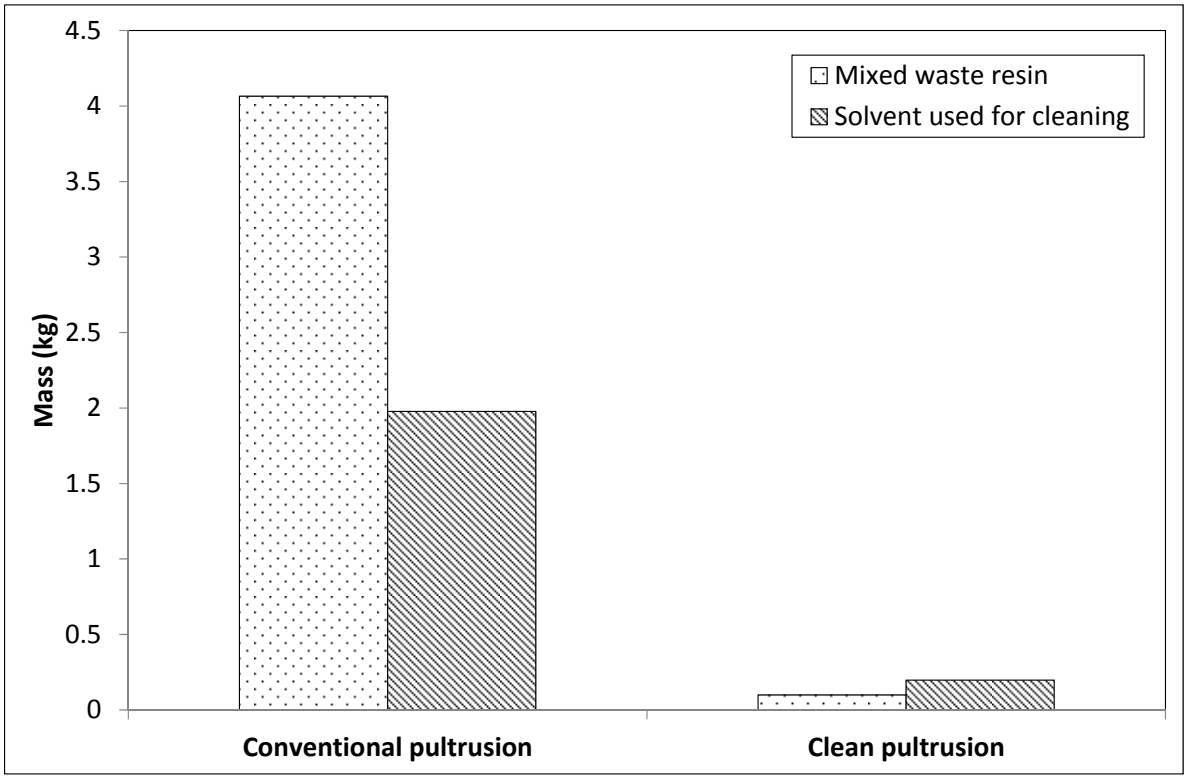


**Figure 122 Reduction in the amount of mixed waste resin and cleaning solvent for the conventional and clean techniques.**

The details of the items that required cleaning at the end of the experiment for the conventional and clean pultrusion techniques are listed in Table 30.

**Table 30 A comparison of the items that required cleaning for the clean and conventional pultrusion techniques.**

| Item | Dimensions |
|---|---|
| *Conventional pultrusion* | |
| Resin bath | 10 cm × 17 cm × 73 cm |
| Plunger | 6 cm × 15 cm × 15 cm |
| Pre-forming guide × 2 | 1 cm × 8 cm × 10 cm |
| Resin drip tray | 5 cm × 10 cm × 50 cm |
| *Clean pultrusion* | |
| Chassis of the resin impregnator | 9 cm × 31 cm × 40 cm |
| Resin injector | 2 cm × 4 cm × 31 cm |
| Rollers × 3 | 1 cm (diameter) × 28 cm (length) |

### *4.5.2 Life cycle impact assessment*

A number of life cycle impact assessment (LCIA) methods are available to evaluate the results from an LCA study (GaBi, 2013). The CML methodology, developed by the Institute of Environmental Sciences at the University of Leiden (*Centrum voor Milieukunde Leiden*) in the Netherlands, is often considered the most appropriate and the most widely-used LCIA method (Ruggles et al., 2013). In the current study, CML 2001(version Nov 2010) was used to compare the environmental impacts for the conventional and clean pultrusion processes.

A summary of the input parameters for the LCA study is summarised in Table 19. A comparison of the overall environmental impact of the conventional and clean process is shown in Figure 123. The actual values for each impact category are presented in Table 31. The LCA templates shown in Section 3.8.1 were used to calculate the environmental impacts. An explanation for each of the impact categories is provided in Appendix-E.

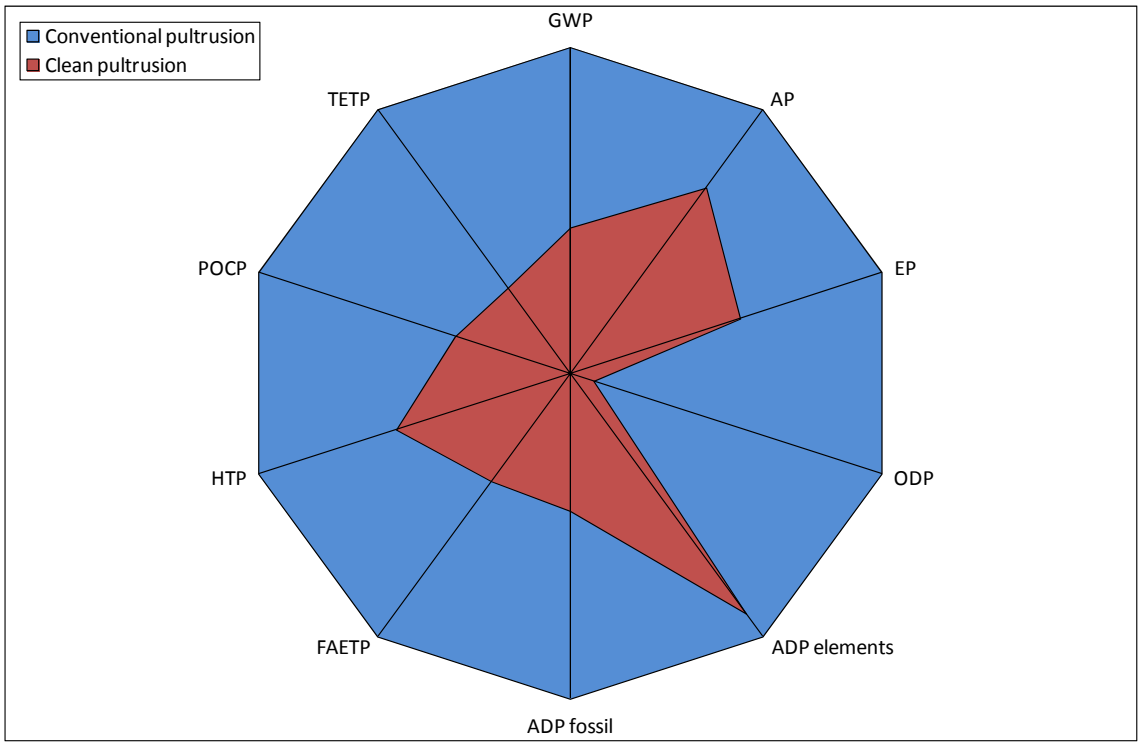


**Figure 123 Comparative values of the environmental impacts for various categories as provided by the CML 2001 LCIA method for epoxy/E-glass pultrusion.**

It is clear from Figure 123 that the overall environmental burden associated with the clean pultrusion is less than that for conventional pultrusion for all the impact categories investigated. The categories where major difference in two processes can be seen are the global warming potential (GWP) and the abiotic depletion (ADP fossil), as shown in Table 31.

**Table 31 Values of the environmental impacts for various categories as provided by the CML 2001 method for epoxy resin system.**

| Impact categories for CML 2001(Nov. 10) | Abbreviation | Conventional pultrusion | Clean pultrusion |
|---|---|---|---|
| Global warming potential (kg CO2-Equiv.) | GWP | 101.03 | 34.19 |
| Acidification potential (kg SO2-Equiv.) | AP | 0.173 | 0.112 |
| Eutrophication potential (kg Phosphate-Equiv.) | EP | 0.033 | 0.015 |
| Ozone layer depletion potential [kg R11-Equiv.) | ODP | -4.91E-07 | 5.44E-08 |
| Abiotic depletion elements (kg Sb-Equiv.) | ADP elements | 8.52E-04 | 7.62E-04 |
| Abiotic depletion fossil (kg Sb-Equiv.) | ADP fossil | 1279.75 | 393.85 |
| Freshwater aquatic ecotoxicity potential (kg DCB-Equiv.) | FAETP | 0.113 | 0.033 |
| Human toxicity potential (kg DCB-Equiv.) | HTP | 1.57 | 0.74 |
| Photochem. Ozone creation potential (kg Ethene-Equiv.) | POCP | 0.131 | 0.032000 |
| Terrestric ecotoxicity potential (kg DCB-Equiv.) | TETP | 3.31 | 0.63 |

The global warming potential (GWP) is a measure of the contribution to climate change and is expressed in terms of $CO_2$ emission to the atmosphere. The comparison of GWP generated by input materials and energy streams involved in the conventional and clean pultrusion is shown in Figure 124. An inspection of the LCA data shows that the primary source of these differences is due to the volume of the amine hardeners, epoxy resin and the solvent used for the two processes.

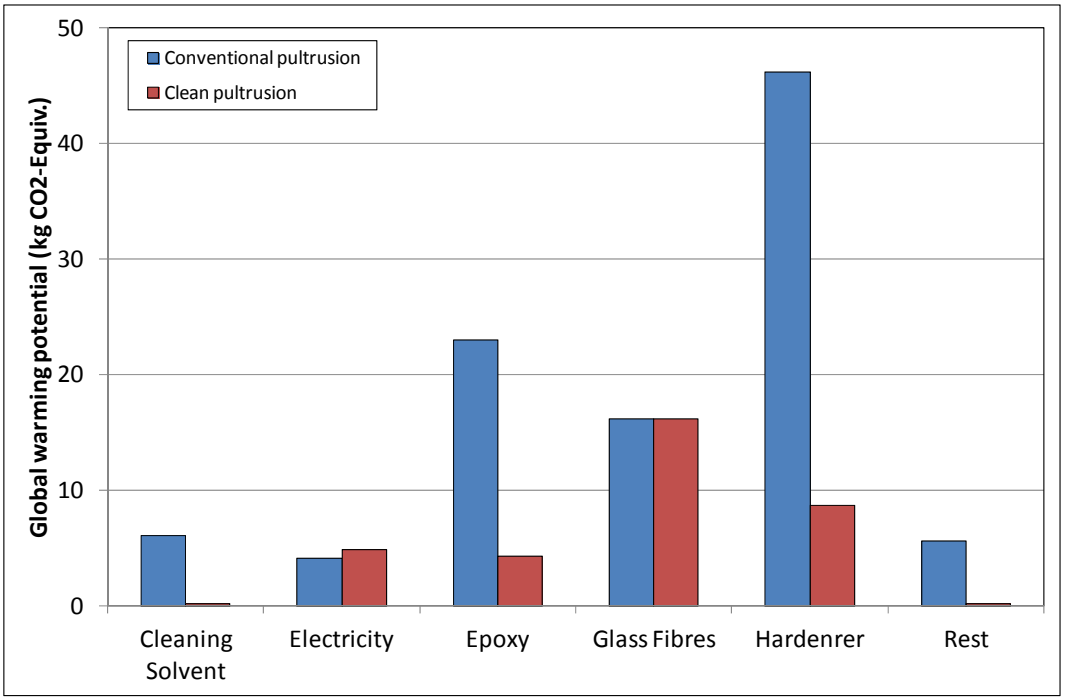


**Figure 124 Comparative values of global warming potential (kg CO2-Equiv.) corresponding to different input streams for conventional and clean pultrusion.**

Figure 125 show the comparison of conventional and clean pultrusion where only the effect of the chemicals (the amine hardeners, epoxy resin and the cleaning solvent) were considered.

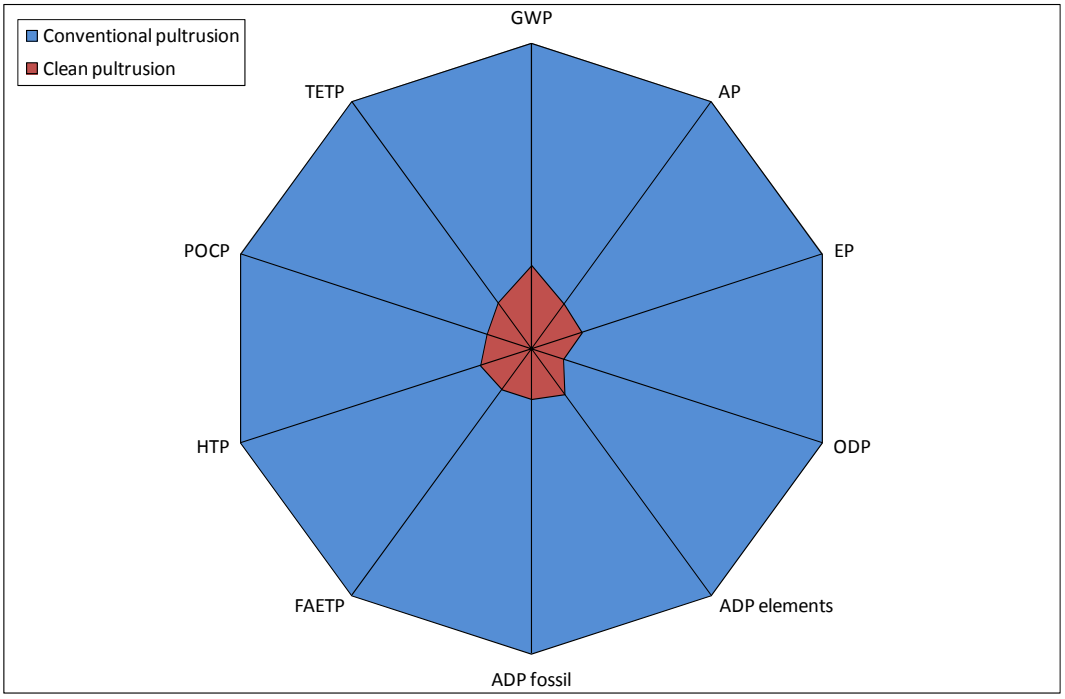


**Figure 125 Comparison of the conventional and clean pultrusion processes where only the effect of chemicals was considered.**

It can be seen from the LCA studies that the clean pultrusion has a lower environmental burden when compared to the conventional resin bath-based pultrusion. Other associated benefits include: (i) reduction in time required to clean the resin impregnation accessories; (ii) reduction in the volume of solvent required to clean the equipment at the end of each production schedule; (iii) reduction in the exposures of the workforce to the VOCs from the pultrusion line and cleaning process; (iv) the need for manual mixing of the components of the resin is avoided where the resin dispenser is used in conjunction with the clean pultrusion process.

# 5 CONCLUSIONS AND RECOMMENDATIONS FOR FUTURE-RESEARCH

## 5.1 CONCLUSIONS

The primary aim of the research reported in this thesis was to develop and evaluate an environmentally-friendly pultrusion technique for the production of fibre-reinforced composites. The newly developed technique was termed as "clean pultrusion".

Following conclusions are drawn from the research reported in the previous chapters:

*(i) Philosophy:* The strategy that was adopted in this study was to spread the filament in the E-glass rovings prior to impregnation. The approach that was taken to overcome the problems associated with the conventional resin bath was to contain the resin components in separate containers and to pump-them on-demand via precision gear pumps to a static mixer. The impregnation of the rovings by the mixed resin system (from the static mixer) was facilitated by custom-designed resin delivery system. A pressure-pot was also used to deliver the mixed resin systems.

*(ii) Mechanism for fibre spreading:* A detailed literature review was carried out to identify techniques and equipment that have been used previously to spread the filaments in a roving. A model previously proposed by Wilson (1997) was extended to estimate the degree of fibre spreading at a second rod. A series of experiments were undertaken using a modified version of the experimental setup that was previously used by Wilson. It was shown that a 4800 tex E-glass roving (Hybon® 2100) can be spread to 350-450% of its original width. A mechanism

was proposed for the spreading of the individual filaments in a roving. The finding from these experiments were reported in Irfan et al. (2011).

*(iii) Automated fibre-spreading rig:* Based upon the observed mechanism associated with fibre spreading, an automated fibre spreading rig was designed and evaluated. The Taguchi method was used to optimise the parameters affecting the degree of fibre spreading obtained via the rig. It was shown that a 2400 tex E-glass roving (Hybon® 2026) can be spread by 250% of its original width by using the optimum parameters without inducing any obvious damage to the filaments. The dimensions of the automatic fibre spreading unit were 40 cm × 50 cm × 75 cm. The finding from these experiments were reported in Irfan et al.(2013).

Although this rig was used on a pultrusion line, it was cumbersome and only 28 rovings could be accommodate; the pultrusion die used in the majority of the laboratory-based experiments required 52 rovings. Hence, a compact fibre spreading unit was designed and built. The dimensions of this compact rig were 8 cm × 10 cm × 31 cm. This compact fibre spreading rig was used successfully in the laboratory and on-site. The average degree of fibre spreading that was recorded for this rig with two rows of 28 rovings was 7.35 ± 1.05 mm. This represents 175% spreading when compared to the as-received E-glass roving.

*(iv) Design of the resin impregnators:* A literature review was undertaken to identify relevant models that have been reported previously to account for the impregnation of rovings. The models proposed by Chandler et al. (1992), Ahn et al. (1991), Gebart (1992) and Wang et al. (2012) were used to design two impregnators. The principles invoked were (a) curtain-flow followed by pin-impregnation and (b) direct resin-injection.

*(v) Modelling the resin impregnators:* The two impregnator designs (PUL-I and PUL-II) were modelled to infer the relative contributions from the various modes of impregnation as a

function of the position within the impregnators. The impregnation modes considered were pin, resin-injection, capillary and compaction. A mathematical relationship was developed to estimate the theoretical efficiency of the impregnators.

*(vi) Construction and evaluation of the impregnators:* Two impregnators were built and these were coded as PUL-I and PUL-II and they were based on resin-injection and pin-impregnation respectively. The impregnators were used to manufacture pultruded composites in the laboratory and on-site.

*(vii) Selection of pultrusion parameters*: Differential scanning calorimetry (DSC) was used to select the cure temperature of the die and pultrusion speeds. This was achieved by performing a dynamic scanning experiment and drawing a conversion-temperature curve. The temperature of the die was selected at a point on the conversion curve where greater than 85 % of cure had been attained. Once a suitable die temperature had been selected, an isothermal scanning experiment was performed and a conversion-time curve was generated. Acceptable pultrusion speeds were selected from the conversion-time curve.

*(viii) Resin dispenser:* A custom-built resin dispenser was manufactured and supplied by CTM Equipment & CTM UK Ltd (project partner). This dispenser was used with the polyurethane resin formulations. A conventional pressure-pot was used to dispense pre-mixed epoxy and vinyl ester resins to the impregnation unit.

*(ix) Pultrusion:* Pultrusion trials were performed using the conventional resin bath and the clean pultrusion techniques. Pultruded composites were manufactured using E-glass fibres and three resin systems namely epoxy, vinyl ester and polyurethane.

*(x) Properties of the pultruded composites:* The physical, mechanical and thermo-mechanical properties of the composites produced in the laboratory and on-site were evaluated. It was shown that composites produced via clean pultrusion showed marginally better properties than those produced via conventional pultrusion. For example, the void fraction reduced from 1.47 to 0.45, the flexural strength increased from 944 MPa to 1177 MPa, the ILSS increased from 70 MPa to 76 MPa, and the storage modulus increased from 20 MPa to 22 MPa.

*(xi) Life cycle assessment:* An LCA was performed on the clean and conventional pultrusion techniques. It was shown that the clean pultrusion was environmentally-friendly process when compared to conventional pultrusion in a number of ways:(a) the volume of waste resin at the end of the experiments was reduced by 95%; (b) the volume of solvent required to clean the equipment was reduced by 90%: (c) the time required to clean the equipment was reduced from 30 minutes to 10 minutes; (d) the environmental impact of the clean pultrusion was lower than that observed for the conventional resin bath pultrusion process; the prominent reduction was observed in global warming potential (66% reduction) and abiotic depletion (69% reduction).

*(xii) Site trials:* The clean pultrusion technique was deployed and demonstrated successfully on-site.

*(xiii) Benefits of the clean pultrusion technique:* The benefits of the clean pultrusion over the conventional pultrusion are: (a) reduction in the void content of the composites; (b) improvement in the properties including flexural strength, flexural modulus, ILSS and storage modulus; (c) possibility of using higher fibre volume fraction due to improved alignment of the rovings; (d) no need for mixing the resin component manually if resin dispenser is employed; (e) reduction in the volume of waste resin; (f) reduction in the volume of the

solvent required for cleaning the impregnation accessories; (g) reduction in the time required for cleaning; and (h) reduction in the environmental impact especially global warming potential and abiotic depletion potential.

## 5.2 RECOMMENDATIONS FOR FUTURE RESEARCH

(i) The reasons for the observed incompatibility between the polyurethane formulation and the E-glass fibres should be investigated.

(ii) An in-depth study should be carried out to develop techniques to apply the IMR to the external surface of the rovings just before they enter the heated-die. The effects of the IMR on the interfacial bond strength should be investigated. The pull-force should be measured for resin formulations with and without the IMR in the resin formulation.

(iii) A detailed LCA should be carried out to assess in detail the true green credentials of the clean pultrusion technique.

(iv) The clean pultrusion technique should be evaluated at other industrial sites.

(v) The feasibility of using resin systems with significantly fast cure kinetics could be investigated.

(vi) Computational fluid dynamics could be used to refine and optimise the design of the resin impregnators.

# REFERENCES


AHN, K. J., SEFERIS, J. C. & BERG, J. C. 1991. Simultaneous measurements of permeability and capillary pressure of thermosetting matrices in woven fabric reinforcements. *Polymer Composites,* 12**,** 146-152.

AKASE, D., MATSUMAE, H., HANANO, T. & SEKIDO, T. 2000. *Method and apparatus for opening reinforcing fiber bundle and method of manufacturing prepreg*. US Patent 6094791.

AMES, T., WEST, W., KENLEY, R., WYGAND, W. T. & POWERS, E. J. 2001. *Air opening jet apparatus*. US Patent 6553431 B1.

AMICO, S. C. & LEKAKOU, C. 2002. Axial impregnation of a fiber bundle. Part 1: Capillary experiments. *Polymer Composites,* 23**,** 249-263.

ASHBEE, K. H. G. & WYATT, R. C. 1969. Water damage in glass fibre/resin composites. *Proceedings of the Royal Society of London. Series A, Mathematical and Physical Sciences,* 312**,** 553-564.

ASTM STANDARDS 2011. D578/D578M, Standard specification for glass fiber strands. ASTM International, Pennsylvania, United States.

AZAPAGIC, A., EMSLEY, A. & HAMERTON, I. 2003. *Polymers: the environment and sustainable development*, John Wiley & Sons, West Sussex, England.ISBN: 978-0-471-87741-7.

BANSAL, A., PAULOTTO, C. & PRIMI, S. 2012. Effect of resin injection chamber size and shape in the pultrusion die on the quality of pultruded profile. *Conference on Civil Engineerign Infrastcructure Based on Polymer Composites.* Poland.

BATCH, G. L. & MACOSKO, C. W. 1993. Heat transfer and cure in pultrusion: Model and experimental verification. *AIChE Journal,* 39**,** 1228-1241.

BATES, J. 1988. *Improving long-fibre compounding via a novel thermoplacstic pultrusion process.* Master of Engineering, McGill University, Montréal, Canada.

BATES, P. & EKHATOR, I. 2004. Continuous consolidation of commingled glass and polypropylene roving. *Journal of Reinforced Plastics and Composites,* 23**,** 1409-1424.

BATES, P. J. & CHARRIER, J. M. 1999. Effect of process parameters on melt impregnation of glass roving. *Journal of Thermoplastic Composite Materials,* 12**,** 276-296.

BATES, P. J. & CHARRIER, J. M. 2000. Pulling tension monitoring during the melt impregnation of glass roving. *Polymer Composites,* 21**,** 104-113.

BATES, P. J., KENDALL, J., TAYLOR, D. & CUNNINGHAM, M. 2002. Pressure build-up during melt impregnation. *Composites Science and Technology,* 62**,** 379-384.

BAUCOM, R. M., SNOHA, J. J. & MARCHELLO, J. M. 1991. *Process for application of powder particles to filamentary materials*. US Patent 5057338.

BAYRAMLI, E. & POWELL, R. L. 1992. Impregnation dynamics of carbon fiber tows. *Journal of Composite Materials,* 26**,** 1427-1442.

BERDICHEVSKY, A. L. & CAI, Z. 1993. Preform permeability predictions by self-consistent method and finite element simulation. *Polymer Composites,* 14**,** 132-143.

BINETRUY, C., HILAIRE, B. & PABIOT, J. 1998. Tow impregnation model and void formation mechanisms during RTM. *Journal of Composite Materials,* 32**,** 223-245.

BINÉTRUY, C., HILAIRE, B. & PABIOT, J. 1997. The interactions between flows occurring inside and outside fabric tows during rtm. *Composites Science and Technology,* 57**,** 587-596.

BLOK, H. & ROSSUM, J. V. 1953. The foil bearing—a new departure in hydrodynamic lubrication. *Lubrication Eng,* 9**,** 316–320.

BOGNER, B. R., BREITIGAM, W. V., WOODWARD, M. & FORSDYKE, K. L. 2000. Thermoset resins for pultrusion. *Pultrusion for Engineers.* Woodhead Publishing Ltd. ISBN: 978-1855734258.

CAI, Z. & BERDICHEVSKY, A. L. 1993. An improved self-consistent method for estimating the permeability of a fiber assembly. *Polymer Composites,* 14**,** 314-323.

CAMBELL, F. C. 2010. *Structural composite materials*, ASM International. ISBN: 978-1-61503-037-8.

CAMPBELL, F. C. 2004. *Manufacturing processes for advanced composites*, Elsevier Advanced Technology, Oxford, UK.ISBN: 1-85617-415-8.

CARMAN, P. C. 1937. Fluid flow through granular beds. *Transactions, Institution of Chemical Engineers***,** 150-166.

CHANDLER, H. W., DEVLIN, B. J. & GIBSON, A. G. 1992. A model for the continuous impregnation of fiber tows in resin baths with pins. *Plastics, Rubber and Composites Processing and Applications,* 18**,** 215-220.

CHRISTENSSON, B., S, K. & C-H, A. 1999. Occupational health aspects and regulations on airborne fibrous and non-fibrous dust. *The International Conference on Composite Materials (ICCM) 12.* Berlin, Germany.

CHUNG, T.-S., FURST, H., GURION, Z., MCMAHON, P. E., ORWOLL, R. D. & PALANGIO, D. 1986. *Process for preparing tapes from thermoplastic polymers and carbon fibers*. US Patent 4588538.

COMPOSITE MATERIALS RESEARCH GROUP 2000. Composite Materials Research Group researchers team with Georgia Pacific to characterize new phenolic pultrusion resins. University of Mississippi, Mississippi, USA.

CONNOLLY, M. 2005a. Attension pultruders: is is time to explore polyurethane resin chemistry and processing? *Composite Manufacturing.* American Composite Maufacturers Association, , Arlington, Virginia, USA.

CONNOLLY, M. 2005b. Pultruding polyurethane composite profiles: practical guidelines for injection box design, component metering equipment and processing. *COMPOSITES 2005 Convention and Trade Show.* Columbus, Ohio USA.

CONNOLLY, M. 2006. Processing and characterization of pultruded polyurethane composites.Auburn Hills, Michigan 48326, USA.

CONNOLLY, M. 2008. CFD modeling of the closed injection wet-out process for pultrusion. *European Pultrusion Technology Association 9th World Pultrusion Conference.* Rome, Italy.

CORBIERE-NICOLLIER, T., GFELLER LABAN, B., LUNDQUIST, L., LETERRIER, Y., MANSON, J. A. E. & JOLLIET, O. 2001. Life cycle assessment of biofibres replacing glass fibres as reinforcement in plastics. *Resources, Conservation and Recycling,* 33**,** 267-287.

DANIELS, C. G. 1971. *Pneumatic spreading of fibres*. US Patent 3795944.

EUROPEAN COMMISION. 1999. *Council Directive 1999/13/EC of 11 March 1999 on the limitation of emissions of volatile organic compounds due to the use of organic solvents in certain activities and installations* [Online]. [Accessed].

EUROPEAN COMMISSION 2004. The Paints Directive 2004/42/EC. European Commission.

FERNANDO, G. F. & AL-KHODAIRI, F. A. A. 2003. Fatigue of hybrid fibre composites. *In:* HARRIS, B. (ed.) *Fatigue in Composites.* Woodhead Publishing Ltd.ISBN: 0-8493-1767-3.

FERNANDO, G. F., IRFAN, M. S. & SHOTTON-GALE, N. 2009. Mechanically induced fibre spreading and impregnation efficiency. University of Birmingham.

FIBREMAX COMPOSITES. 1999. Available: http://www.fibermaxcomposites.com/shop/index_files/yarntownomenclature.html [Accessed].

FILIPPONE, S. F. 1989. Using Taguchi methods to apply the axioms of design. *Robotics and Computer-Integrated Manufacturing,* 6**,** 133–142.

FILYANOV, Y. M. 1978. Effect of a filler on the glass transition temperature of an epoxy resin and its relation to the filled polymer properties. *Polymer Science U.S.S.R.,* 20**,** 2074-2078.

FOLEY, M. E. & GILLESPIE, J. W. 2005. Modeling the effect of fiber diameter and fiber bundle count on tow impregnation during liquid molding processes. *Journal of Composite Materials,* 39**,** 1045-1065.

GABI. 2013. *Life cycle impact assessment (LCIA) methods* [Online]. Available: http://database-documentation.gabi-software.com/support/gabi/gabi-5-lcia-documentation/life-cycle-impact-assessment-lcia-methods/ [Accessed].

GARKHAIL, S. K. 2002. *Composites based on natural fibres and thermoplastic matrices.* PhD, University of London, UK.

GAUCHEL, J. V., PETERS, L. & STARR, T. F. 2000. Reinforcements for pultrusion. *In:* STARR, T. F. (ed.) *Pultrision for Engineers.* Woodhead Publishing Ltd. ISBN: 978-1855734258.

GAYMANS, R. J. & WEVERS, E. 1998. Impregnation of a glass fibre roving with a polypropylene melt in a pin assisted process. *Composites Part A: Applied Science and Manufacturing,* 29**,** 663-670.

GEBART, B. R. 1992. Permeability of unidirectional reinforcements for RTM. *Journal of Composite Materials,* 26**,** 1100-1133.

GORTHALA, R., ROUX, J. A. & VAUGHAN, J. G. 1994. Resin flow, cure and heat transfer analysis for pultrusion process. *Journal of Composite Materials,* 28**,** 486-506.

GUIRMAN, J.-M., LECERF, B. & MEMPHIS, A. 2005. *Method and device for producing a textile web by spreading tows*. US Patent 6836939 B2.

HALL, J. N. 1972. *Apparatus for spreading a graphite fiber tow into a ribbon of graphite filaments*. US Patent 3704485.

HAN, C. D., LEE, D. S. & CHIN, H. B. 1986. Development of a mathematical model for the pultrusion process. *Polymer Engineering & Science,* 26**,** 393-404.

HOA, S. V. 2009. *Principles of the manufacturing of composite materials*, DEStech Publications, Inc.ISBN: 978-1-932078-26-8.

HOVEN, G. V. D. 1981. *Widening-narrowing guide for textile filament bundle*. US Patent 4301579.

HULL, D. & CLYNE, T. W. 1996. *An introduction to composite materials* Cambridge University Press. ISBN: 978-0521388559.

HUNTSMAN ADVANCED MATERIALS 2007. Araldite® LY 556 / Aradur® 917/ Accelerator DY 070. Basel, Switzerland: Huntsman Advanced Materials (Switzerland) GmbH.

IBBOTSON, S. & KARA, S. 2013. LCA case study. Part 1: cradle-to-grave environmental footprint analysis of composites and stainless steel I-beams. *The International Journal of Life Cycle Assessment,* 18**,** 208-217.

IRFAN, M. S., MACHAVARAM, V. R., MAHENDRAN, R. S., SHOTTON-GALE, N., WAIT, C. F., PAGET, M. A., HUDSON, M. & FERNANDO, G. F. 2011. Lateral spreading of a fibre bundle via mechanical means. *Journal of Composite Materials***,** 311-330.

IRFAN, M. S., MACHAVARAM, V. R., MAHENDRAN, R. S., SHOTTON-GALE, N., WAIT, C. F., PAGET, M. A., HUDSON, M. & FERNANDO, G. F. 2013. The design and optimisation of a rig to enable the lateral spreading of fibre bundles. *Journal of composite mateirals,* In-press.

IYER, S. & DRZAL, L. T. 1991a. *Method and system for spreading a tow of fibers*. US Patent 5042111.

IYER, S. & DRZAL, L. T. 1991b. *Method and system for spreading fibre tow*. European Patent 0467313 A1.

JESWANI, A. L. & ROUX, J. A. 2007. Manufacturing modeling of three-dimensional resin injection pultrusion process control parameters for polyester/glass rovings composites. *Journal of Manufacturing Science and Engineering,* 129**,** 143-156.

JESWANI, A. L. & ROUX, J. A. 2008. Modeling of processing for slot and discrete port tapered resin injection pultrusion. *Journal of Thermophysics and Heat Transfer,* 22**,** 749-757.

JESWANI, A. L. & ROUX, J. A. 2010. Impact of fiber volume fraction and resin viscosity with die-detached tapered chamber in resin injection pultrusion. *Journal of Manufacturing Science and Engineering,* 132**,** 1-11.

JESWANI, A. L., ROUX, J. A. & VAUGHAN, J. G. 2009. Multiple injection ports and part thickness impact on wet-out of high pull speed resin injection pultrusion. *Journal of Composite Materials***,** 1-19.

JOSHI, R. R. 2000. Polyurethanes in pultrusion II: Comparitive study with conventional resin systems used in the industry. *Composites.* Las Vegas, Nevada, USA.

JOSHI, R. R., VARAS, L. L. & PADSALGIKAR, A. D. 1999. Polyurethanes in pultrusion: Styrene free alternative systems. *International Composites Expo 1999.* Society of the Plastics Industry.

KAWABE, K. 2008. New fibre technology for carbon fibre tow and its application to composite materials. *Sen'i Gakkaishi,* 64**,** 262-267.

KAWABE, K. & TOMODA, S. 2006. *Method of producing a spread multi-filament bundle and an apparatus used in the same*. US Patent Application 0137156 A1.

KIM, D.-H., HAN, P.-G., JIN, G.-H. & LEE, W. I. 1997. A model for thermosetting composite pultrusion process. *Journal of Composite Materials,* 31**,** 2105-2122.

KISS, P. A., DEATON, J. M., PARSONS, M. S. & COFFEY, D. 2002. *Apparatus and method for splitting a tow of fibers*. US Patent 6385828 B1.

KOMMU, S., KHOMAMI, B. & KARDOS, J. L. 1998. Modeling of injected pultrusion processes: A numerical approach. *Polymer Composites,* 19**,** 335-346.

KRUEGER, R. G. 2001. *Apparatus and method for spreading fibrous tows into linear arrays of generally uniform density and products made thereby*. US Patent 6311377.

LACKEY, E., VAUGHAN, J. G. & ROUX, J. A. 1997. Experimental development and evaluation of a resin injection system for pultrusion. *Journal of Advanced Materials,* 29**,** 30–37.

LAMPMAN, S. 2003. *Characterization and failure analysis of plastics*, ASM international.ISBN: 0-87170-789-6.

LEPECH, M. D. 2009. Life cycle assessment methods for design and manufacturing of sustainable composites. *Composites and Polycon.* American Composites Manufacturers Association, Tampa, Florida, USA.

LI, S., DING, Z., LEE, L. J. & ENGELEN, H. 2009. Effect of die length on pulling force and composite quality in pultrusion. *COMPOSITES & POLYCON.* American Composites Manufacturers Association, Tampa, Florida, USA.

LI, S., XU, L., DING, Z., LEE, L. J. & ENGELEN, H. 2003a. Experimental and theoretical analysis of pulling force in pultrusion and resin injection pultrusion (RIP)–Part I: Experimental. *Journal of Composite Materials,* 37**,** 163-189.

LI, S., XU, L., DING, Z., LEE, L. J. & ENGELEN, H. 2003b. Experimental and theoretical analysis of pulling force in pultrusion and resin injection pultrusion (RIP) – Part II: Modeling and Simulation. *Journal of Composite Materials,* 37**,** 195-216.

LIFKE, J. L., BUSSELLE, L. D., FINLEY, D. J. & GORDON, B. W. 2000. *Method and apparatus for spreading fiber bundles*. US Patent 6049956.

LUYT, A. S. & KRUPA, I. 2009. Phase change materials formed by uv curable epoxy matrix and Fischer–Tropsch paraffin wax. *Energy Conversion and Management,* 50**,** 57-61.

MALLICK, P. K. 2008. *Fibre reinforced composites:materials, manufacturing, and design*, Taylor & Francis Group.ISBN: 978-0-8493-4205-9.

MARISSEN, R., TH. VAN DER DRIFT, L. & STERK, J. 2000. Technology for rapid impregnation of fibre bundles with a molten thermoplastic polymer. *Composites Science and Technology,* 60**,** 2029-2034.

MAZUMDAR, S. K. 2000. *Composite manufacturing: materials, product, and process engineering*, CRS Press.ISBN: 0-8493-0585-3.

MCMAHON, P. E. & CHUNG, T.-S. 1989. *Method of forming composite fiber blends and molding same*. US Patent 4799985.

MORII, T., IVENS, J. & VERPOEST, I. 1999. Interfacial effect on the mechanical properties of glass/pehmolic composites. *International Committee on Composite Materials.* Paris, France.

MURPHY, R. 2004. Life cycle assessment. *In:* BAILLIE, C. (ed.) *Green composites Polymer composites and the environment.* Woodhead Publishing Ltd, Cambridge, UK.ISBN: 978-0849325762.

NAKAGAWA, N. & OHSORA, Y. 1992. *Fiber separator for producing fiber reinforced metallic or resin body*. US Patent 5101542.

NATIONAL INSTITUTES OF HEALTH. 2013. Available: http://rsb.info.nih.gov/ij/ [Accessed].

NESTLER, J., VETTERMANN, F. & REUCHSEL, D. 2007. *Device and method for spreading a carbon fibre hank*. US Patent Application 0101564 A1.

NEWELL, J. A. & PUZIANOWSKI, A. A. 1999. Development of apneumatic spreading system for kevlar-based sic-precursor carbon fibre tows. *High Performance Polymers,* 11**,** 197-203.

NIINA, G., SASAKI, Y., TAKAHASHI, M., IWAKUNI-SHI & YAMAGUCHI-KEN. 1964. *Process for spreading or dividing textile materials*. US Patent 3358436.

PALIKHEL, D., ROUX, J. & JESWANI, A. 2012. Die-attached versus die-detached resin injection chamber for pultrusion. *Applied Composite Materials***,** 1-18.

PANDITA, S. D., IRFAN, M. S., MACHAVARAM, V. R., N. SHOTTONGALE, PAGET, M. A., MAHENDRAN, R. S., WAIT, C. F., HARRIS, D. & FERNANDO, G. F. 2012. Clean wet-filament winding – Part 1: Design concept and simulations. *Journal of Composite Materials***,** 379-390.

PANDITA, S. D., SMITH, S., S-GALE, N., PAGET, M., ALLEN, J. M. & FERNANDO, G. F. 2007. "Clean" filament winding: A new manufacturing process. *Sustainable Material Conference.* Coventry, England.

PELTONEN, P. & JÄRVELÄ, P. 1992. Methodology for determining the degree of impregnation from continuous glass fibre prepreg. *Polymer Testing,* 11**,** 215-224.

PERITT, J. M., EVERETT, R. & EDELSTEIN, A. 1993. *Electrostatic fiber spreader including a corona discharge device*. US Patent 5200620.

PETERS, S. T. 1998. *Handbook of composites*, Chapman & Hall, London.ISBN: 978-0412540202.

PITCHUMANI, R. & YAO, S.-C. 1993. Non-dimensional analysis of an idealized thermoset composites manufacture. *Journal of Composite Materials,* 27**,** 613-636.

PPG FIBRE GLASS. 2012. Available: http://www.ppg.com/glass/fiberglass/products/Pages/directrovings.aspx [Accessed].

PRYOR, J. W. 1985. *Method and apparatus for conveying filter tow*. US Patent 4537583.

PULTREX. 2012. *Pultrusion profiles and applications* [Online]. Available: http://pultrex.com/images/content/Pultruded%20Profiles%20and%20Applications%20Presentation-1.pdf [Accessed].

RABEARISON, N., JOCHUM, C. & GRANDIDIER, J. C. 2011. A cure kinetics, diffusion controlled and temperature dependent, identification of the Araldite LY556 epoxy. *Journal of Materials Science,* 46**,** 787-796.

RADAY, R. M. 2006. *Apparatus for resin-impregnation of fibers for filament winding*. US patent application 7413623.

RAHATEKAR, S. S. & ROUX, J. A. 2003. Numerical simulation of pressure variation and resin flow in injection pultrusion. *Journal of Composite Materials,* 37**,** 1067-1082.

ROH, J. U. & LEE, W. I. 2012. Effect of fibre spreading on impregnation of thermoplastic into continous fibre bundle. *SAMPE Tech.* Society of the Advancement of Materials and Process Engineering, Charleston, South Caroline, USA.

ROSS, P. J. 1996. *Taguchi techniques for quality engineering: loss function, orthogonal experiments, parameter and tolerance design*, McGraw Hill Professional.ISBN: 978-0070539587.

RUGGLES, R., PHANSEY, A. & LINDER, B. 2013. *Sustainable design guide* [Online]. Available: http://www.solidworks.com/sustainability/sustainable-design-guide/appendix-c-the-hannover-principles.htm [Accessed].

SAGER, T. B. 1990. *Method and apparatus for separating monofilaments forming a strand*. US Patent 6094791.

SHAH, D. U., SCHUBEL, P. J. & CLIFFORD, M. J. 2013. Modelling the effect of yarn twist on the tensile strength of unidirectional plant fibre yarn composites. *Journal of Composite Materials,* 47**,** 425-436.

SHAW-STEWART, D. & SUMERAK, J. E. 2000. The pultrusion process. *In:* STARR, T. (ed.) *Pultrusion for Engineers.* Woodhead Publishing Ltd. ISBN: 978-1855734258.

SONG, Y. S., YOUN, J. R. & GUTOWSKI, T. G. 2009. Life cycle energy analysis of fiber-reinforced composites. *Composites Part A: Applied Science and Manufacturing,* 40**,** 1257-1265.

SOPER, D. S. 2012. *Critical F-value calculator (Online Software)* [Online]. Available: http://www.danielsoper.com/statcalc [Accessed].

SRINIVASAGUPTA, D. & KARDOS, J. L. 2004. Ecologically and economically conscious design of the injected pultrusion process via multi-objective optimization. *Modelling and Simulation in Materials Science and Engineering,* 12**,** S205.

SRINIVASAGUPTA, D., KARDOS, J. L. & JOSEPH, B. 2003a. Rigorous dynamic model-based economic design of the injected pultrusion process with controllability considerations. *Journal of Composite Materials,* 37**,** 1851-1880.

SRINIVASAGUPTA, D., POTARAJU, S., KARDOS, J. L. & JOSEPH, B. 2003b. Steady state and dynamic analysis of a bench-scale injected pultrusion process. *Composites Part A: Applied Science and Manufacturing,* 34**,** 835-846.

STARR, T. F. 2000. *Pultrusion for engineers*, Woodhead Publishing Ltd. ISBN: 978-1855734258.

STERNBERG, E. M. 1976. *Method and apparatus for charging a bundle of filaments*. US Patent 3967118.

STRONG, A. B. 2008. *Fundamentals of composites manufacturing - materials, methods, and applications,* Dearborn, Michigan 48121, USA, Society of Manufacturing Engineers (SME).ISBN: 978-0872638549.

SUMERAK, J. E. 2000. ASM handbook volume 21. composites. *In:* MIRACLE, D. B. & DONALDSON, S. L. (eds.). ASM International Handbook Committee.ISBN: 978-0871707031.

SUMERAK, J. E. 2001. Influence of real die design features on temperature and cure predictions from pultrusion process models. *Composites 2001 Convention and Trade Show.* Tampa, Florida, USA.

TANAKA, K., OHTANI, H., MATSUMAE, H., TSUJI, S. & AKASE, D. 2004. *Production device and method for opened fiber bundle and prepreg production*. US Patent 6743392 B2.

THOMASON, J. 2012. *Glass fibre sizings: a review of the scientific literature*, Kindle Edition.ISBN: 978-0957381414.

UCHIYAMA, S., KAKU, E., KOBAYASHI, M., ZODA, T. & FUJIMOTO, S. 1972. *Method and apparatus for spreading or dividing yarn, tow or the like*. US Patent 3657871.

UCHIYAMA, S., MIYAGAWA, Y. & KOBAYASHI, M. 1973. Study on spreading multifilament yarns by electro-static method. *Journal of The Textile Machinery,* 19**,** 57-63.

VÁZQUEZ, A. & ESCOBAR, M. 2012. Pultrusion. *Wiley Encyclopedia of Composites*. 2 edition ed.: Wiley.ISBN: 978-0470128282.

VOORAKARANAM, S., JOSEPH, B. & KARDOS, J. L. 1999. Modeling and control of an injection pultrusion process. *Journal of Composite Materials,* 33**,** 1173-1204.

VOORAKARANAM, S. & JOSEPH, J. L. K. A. B. Year. Model-based control of injection pultrusion process. *In:* Proceedings of the American Control Conference, 1998 Philadelphia, Pennsylvania, USA.

WAIT, C. F. 2011. *The reuse and recycling of glass fibre waste.* M. Res, University of Birmingham, UK.

WANG, R.-G., YANG, F., HAO, L.-F., DU, G. & JIAO, W.-C. 2012. Optimizing processing parameters of pin-assisted-melt impregnation of fiber-reinforced plastics by numerical simulation. *Journal of Reinforced Plastics and Composites,* 31**,** 731-737.

WEUSTINK, T. 2008. *Development of a rapid thermoplastic impregnation device.* Ph.D., de Technische Universiteit Delft.

WILSON, S. D. R. 1997. Lateral spreading of fibre tows. *Journal of Engineering Mathematics,* 32**,** 19-26.

WOO IL LEE & SPRINGER, G. S. 1987. A model of the manufacturing process of thermoplastic matrix composites. *Journal of Composite Materials,* 21**,** 1017-1055.

XIAN, G., PU, H.-T., YI, X.-S. & PAN, Y. 2006. Parametric optmisation of pin-assisted-melt impregnation of glass fiber/polypropylene by Taguchi method. *Journal of Composite Materials,* 40**,** 2087-2097.

YAMAMOTO, K., YAMATSUTA, K. & ABE, Y. 1988. *Spreading fibre bundle*. European Patent 0292266A2.

YEN, C.-C., CHEN, C.-H. & LUE, J.-Y. 2006. In-situ pultrusion of urea-formaldehyde matrix composites. II: Effect of processing variables on mechanical properties. *Polymer Composites,* 27**,** 8-14.

YOUNG, W.-B. 1996. The effect of surface tension on tow impregnation of unidirectional fibrous preform in resin transfer molding. *Journal of Composite Materials,* 30**,** 1191-1209.

YUSRIAH, L., MARIATTI, M. & ABU BAKAR, A. 2010. Mechanical properties of particulate-filler/woven-glass-fabric-filled vinyl ester composites. *Journal of Vinyl and Additive Technology,* 16**,** 98-104.

# APPENDICES

## Appendix-A: List of publications

A list of publications during the course of this project is given below:

**Published/Presented**

1. **Irfan, M. S.**, Machavaram, V. R., Mahendran, R. S., Shotton-Gale, N., Wait, C.F, Paget, M. A., Hudson, M. and Fernando, G. F., "*Lateral spreading of a fibre roving via mechanical means*" Journal of Composite Materials, Nov 10, 2011, Volume. 46(3), Pages 311-330. DOI: 10.1177/0021998311424624.

2. **Irfan, M. S.**, Machavaram, V. R., Murray, R. C., Bogonez, F. N., Wait, C. F., Pandita, S. D., Paget, M. A., Hudson, M. and G. F. Fernando, *"The design and optimisation of a rig to enable the lateral spreading of fibre bundles"* Journal of Composite Materials, 2013, **in-press**.

3. **Irfan**, **M. S.**, Shotton-Gale, N., Wait, C. F., Pandita, S. D., Machavaram, V. R., Mahendran, R. S., Paget, M., Harris, D., Leek, C., Wootton, S., Tait, M., Fernando, G. F. '*Clean and environmentally friendly production of composites'*, International Symposium on Advanced Polymeric Materials 2012 (ISAPM 2012) under the auspices of 8th International Materials Technology Conference and Exhibition (IMTCE 2012) 7 – 12 July 2012, Kuala Lumpur, Malaysia.

4. Pandita, S. D., **Irfan**, **M. S.**, Machavaram, V. R., Shotton-Gale, N., Wait, C. F., Paget, M., Mahendran, R. S., Harris, D., Leek, C. and Fernando, G. F. "*Clean wet-filament winding – Part I: Design concept and simulations*". Journal of Composite Materials, Mar 22, 2012, Volume. 47(3), Pages 379-390. DOI: 10.1177/0021998312440474.

5. Pandita, S. D., Wang, L., Mahendran, R. S., Machavaram, V. R., **Irfan**, **M. S.**, Harris, D. and Fernando, G. F. "*Simultaneous DSC-FTIR spectroscopy: Comparison of cross-linking kinetics of an epoxy/amine resin system*". Thermochimica Acta. September 2012, Volume 543(10), Pages 9–17.

6. Wang, L., Pandita, S. D., Machavaram, V. R., Mahendran, R. S., **Irfan**, **M. S.**, Harris, D., Fernando, G. F. '*Simultaneous thermal (DSC) and spectral (FTIRS) analyses of polymers*', International Symposium on Advanced Polymeric Materials 2012 (ISAPM 2012) under the auspices of 8th International Materials Technology Conference and Exhibition (IMTCE 2012) 7 – 12 July 2012, Kuala Lumpur, Malaysia.

**Submitted**

7. Machavaram, V. R., Wang, L., Mahendran, R. S., D. Harris, Bogonez, F. N., **Irfan, M. S.**, Hellmann, S. and Fernando, G. F. *'Multiplexed Fresnel reflection sensing for monitoring cross-linking reactions'*. Journal of Applied polymer Science, **Submitted**.

8. Murray, R. C., **Irfan, M.S.**, Machavaram, V. R, White, R., Kim, H., Wait, C. F., Bogonez, F. N., Ojo, S., Papaelias, M., Curtis, P. T. and Fernando, G. F. "*Production and evaluation of intra-filament hybrids*" The 19TH International Conference on Composite Materials, USA, 2013, **Accepted**.

9. Wait, C.F., Shotton-Gale, N., Smith, C., **Irfan, M.S.**, Pandita, S.D., Wang, L., Paget, M.A., Price, R., James, J. and Fernando, G.F. '*The recovery, reprocessing and reuse of waste glass fibre fabrics: "Closed-loop recycling*" The 19TH International Conference on Composite Materials, USA, 2013, **Accepted**.

**In preparation**

10. **Irfan, M. S.**, Machavaram, V. R., Wang, L., Pandita, S. D., Bogonez, F. N., Paget, M. A., Leek, C. and Fernando, G. F. "*Clean pultrusion: Design concept, simulations and experimental*" Journal of Composite Materials, **In preparation**.

11. **Irfan, M. S.**, Machavaram, V. R., Wang, L., Pandita, S. D., Bogonez, F. N., Paget, M. A., Leek, C. and Fernando, G. F. "*Clean pultrusion: Effect of talc filler on vinyl ester/E-glass composites*" Journal of Composite Materials, **In preparation**.

# Appendix-C: Evaluation of composites produced via resin impregnator PUL-II

In this section, the physical, mechanical and thermo-mechanical properties of the epoxy/E-glass composites, produced using prototype-II, are presented. The properties for resin bath and prototype-I are also plotted (from Section 4.4.1) for comparison.

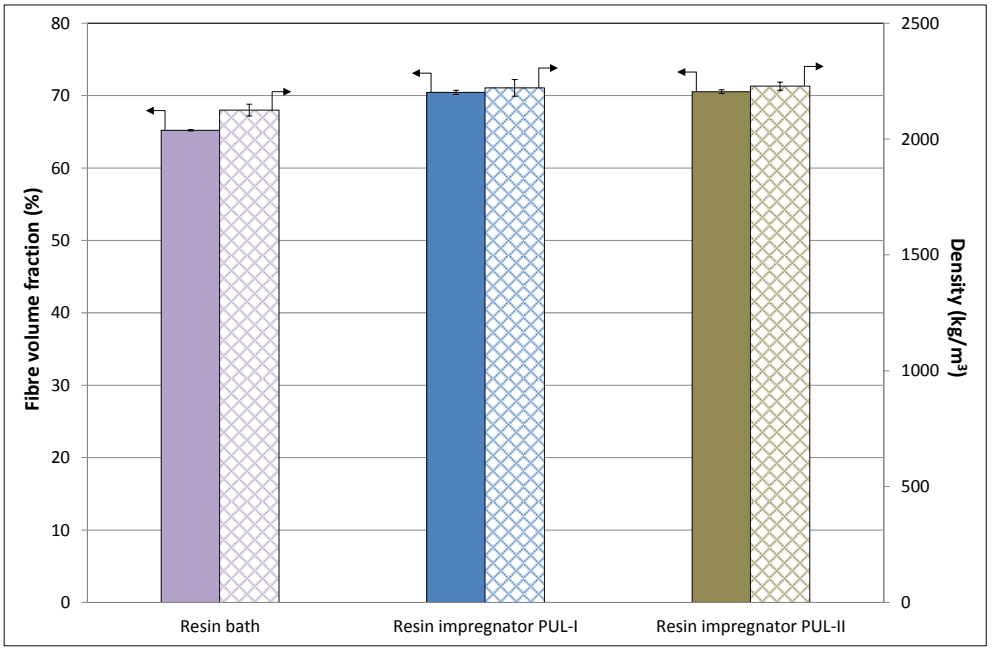


**Figure 126 Fibre volume fraction and density for the epoxy/E-glass composites produced at 0.3 m/min.**

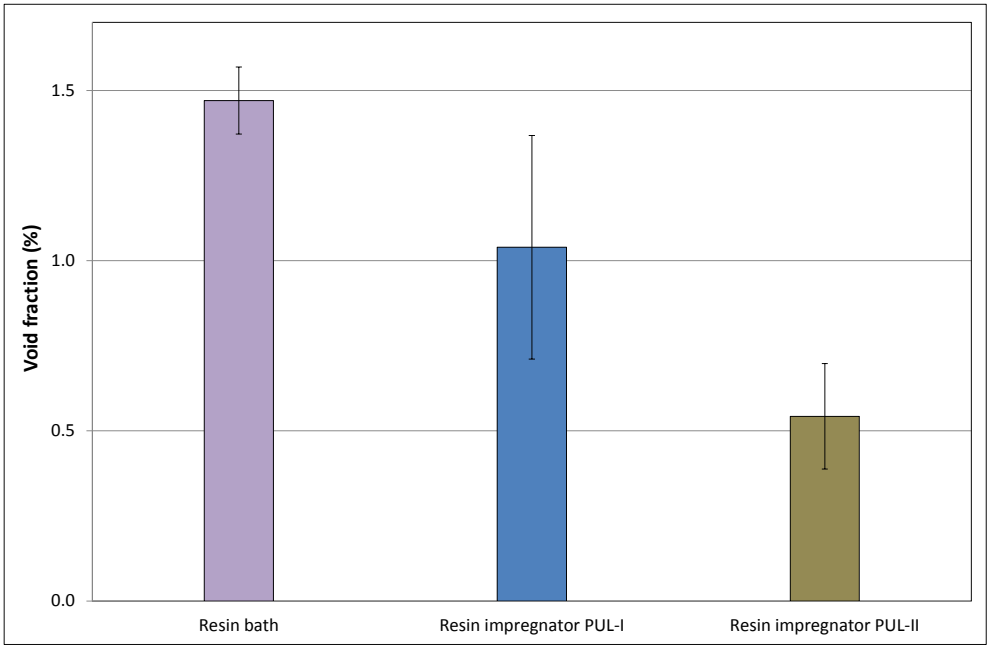


**Figure 127 Void fraction data for the epoxy/E-glass composites produced at 0.3 m/min.**

| | | |
|---|---|---|
| Resin bath | 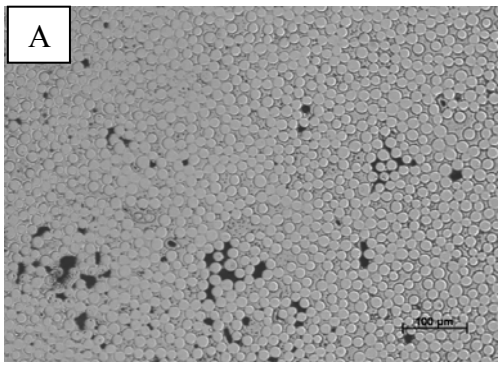 | 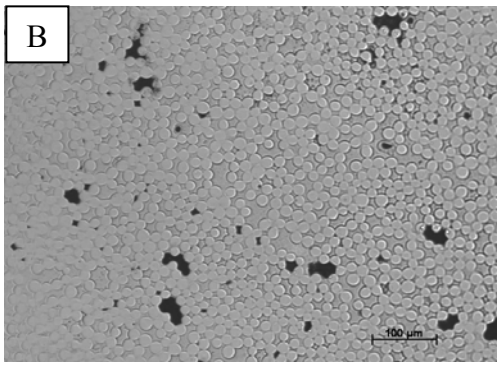 |
| Resin impregnator PUL-I | 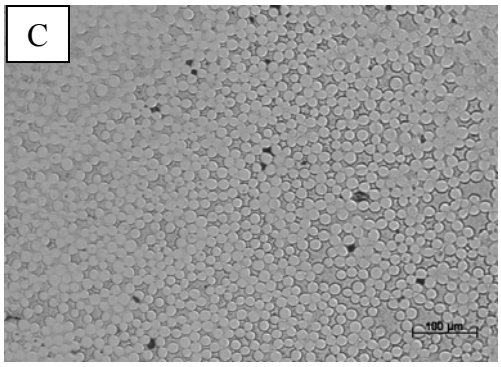 | 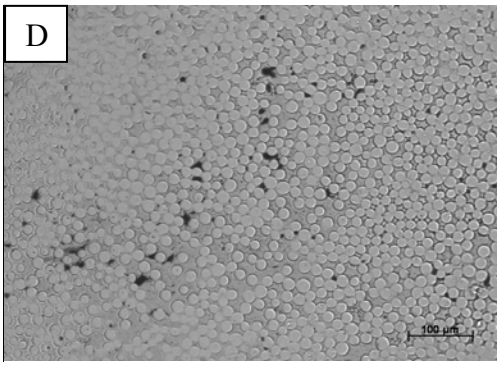 |
| Resin impregnator PUL-II | 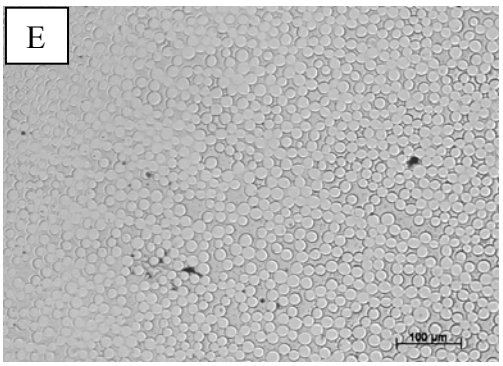 | 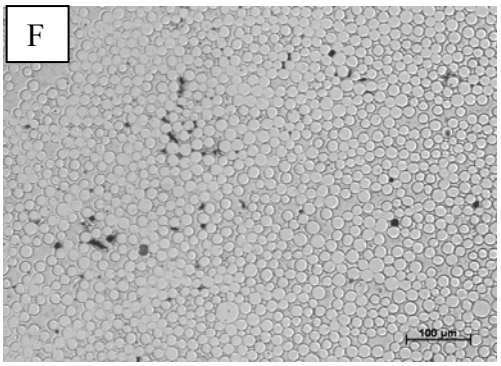 |

**Figure 128 Micrographs of the epoxy/E-glass pultruded samples**

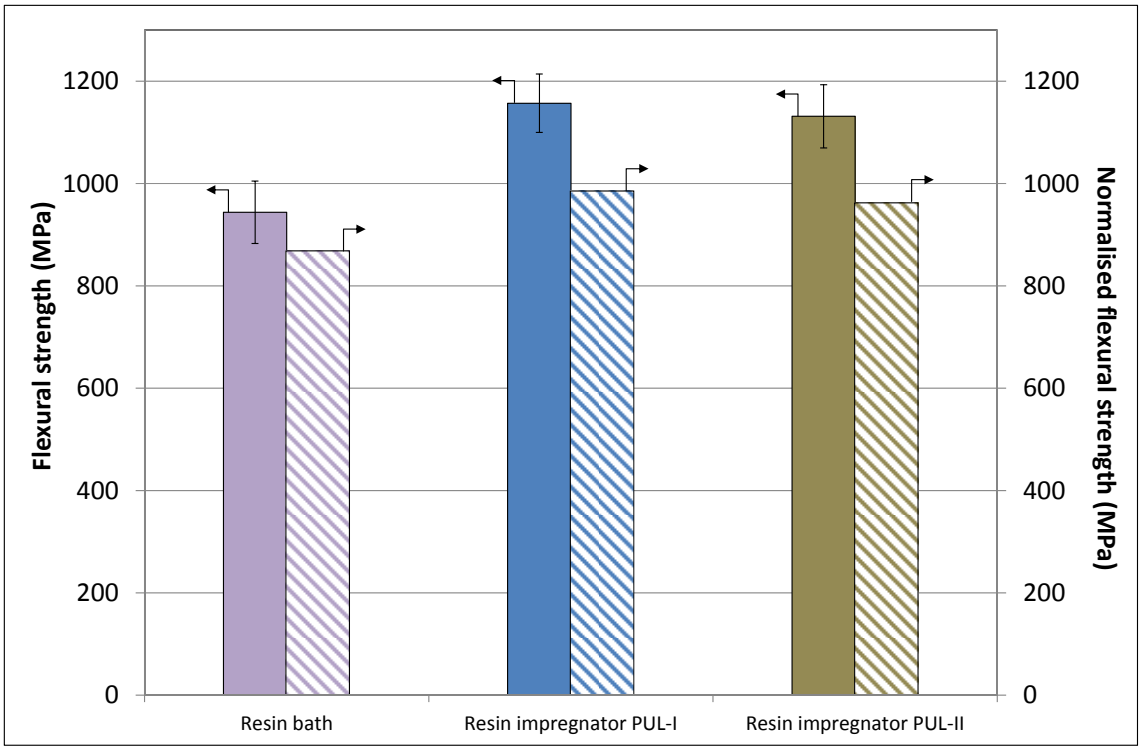


**Figure 129 Flexural strength (four-point bending) data for the epoxy/E-glass composites produced at 0.3 m/min. Normalised values are shown for 60% $V_f$.**

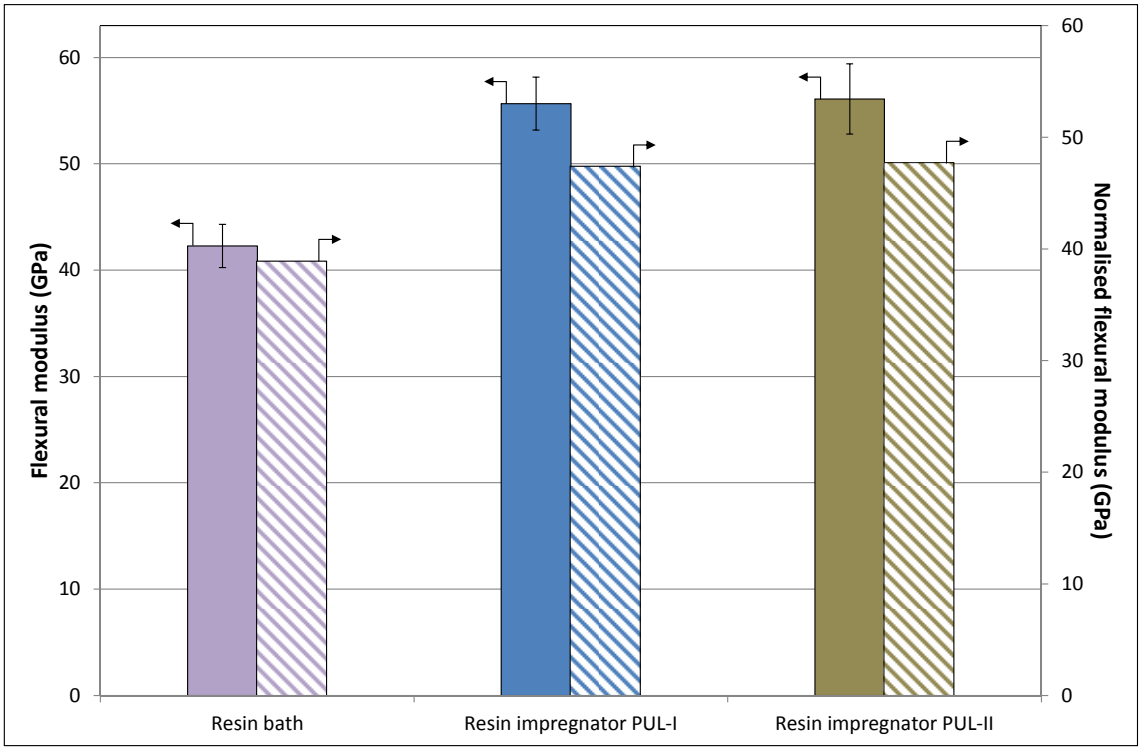


**Figure 130 Flexural moduli (four-point bending) for the epoxy/E-glass composites produced at 0.3 m/min.**

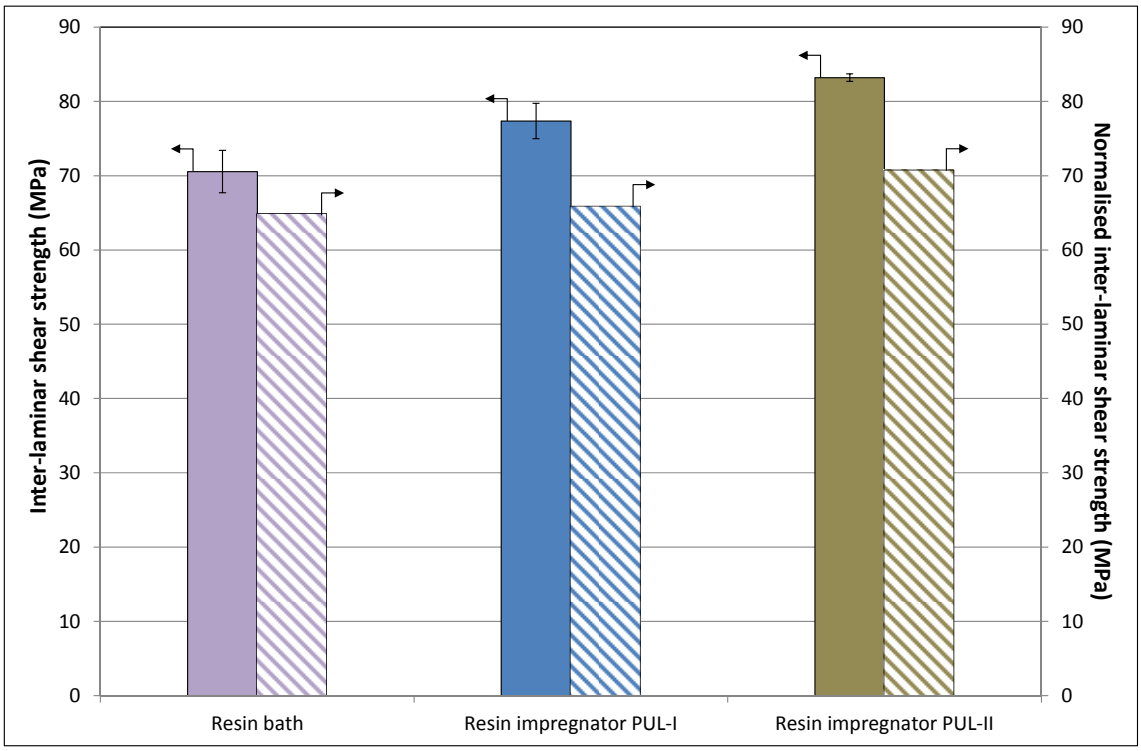


**Figure 131 Inter-laminar shear strength (ILSS) data for the epoxy/E-glass composites produced at 0.3 m/min.**

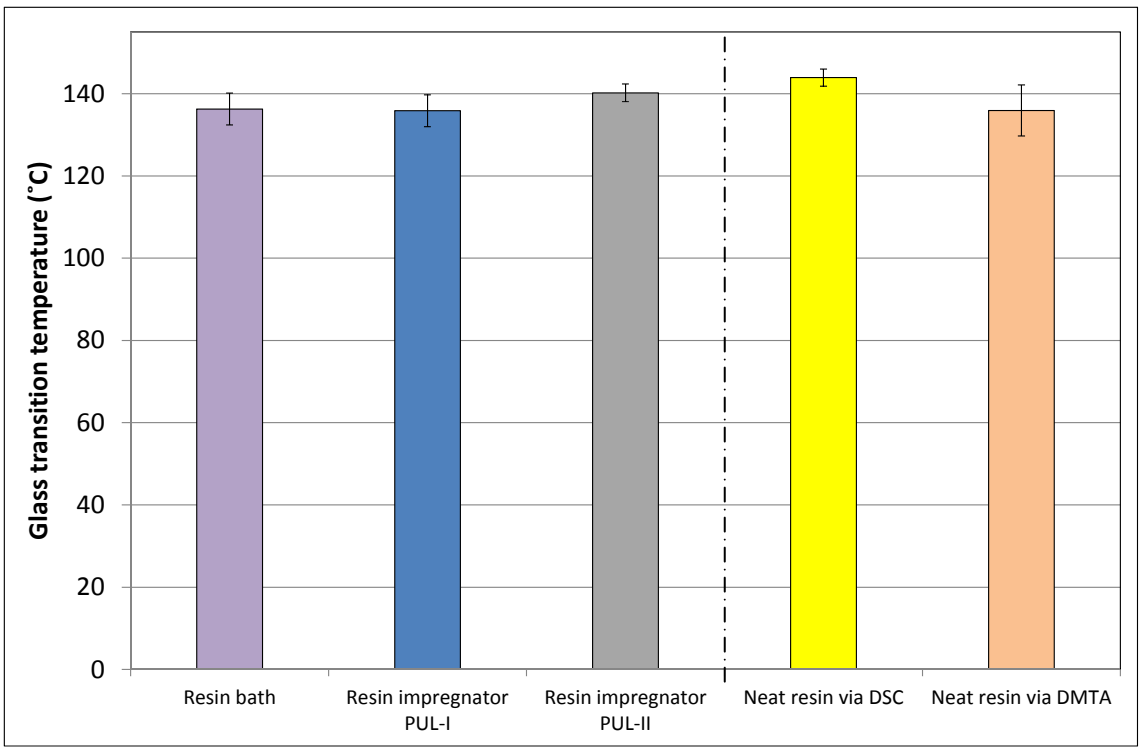


**Figure 132 Glass transition temperatures ($T_g$) for the epoxy/E-glass composites produced at 0.3 m/min.**

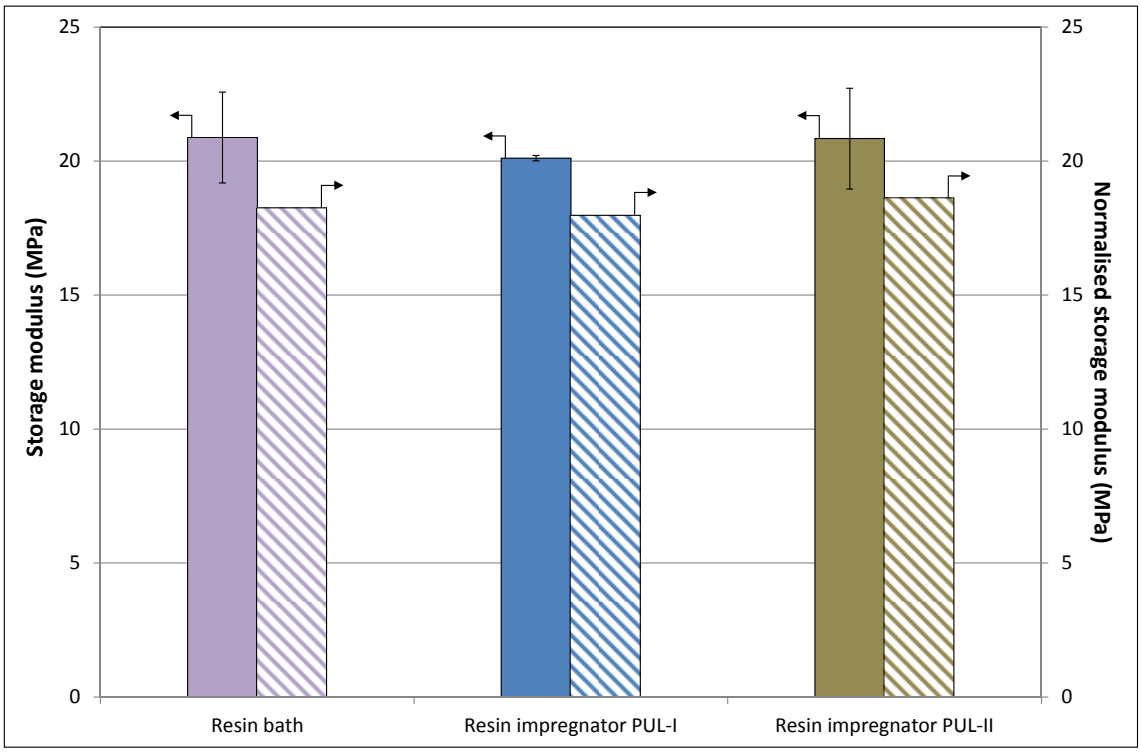


**Figure 133 Storage moduli for the epoxy/E-glass composites produced at 0.3 m/min.**

## Appendix-D: Experimental protocol for polyurethane pultrusion

**Aims:**

To pultrude with the polyurethane resin.

**Details of Experimental System:**

1. Pultrusion machine consisting of:
    a. Creel stand
    b. Resin bath/ resin impregnator prototype PUL-I or PUL-II
    c. Die
    d. Pulling station
    e. Sample cutting saw
2. Resin dispenser
3. Compressor for cleat-type tractor puller

**Procedure:**

1. Fill out the risk assessment for the pultrusion experiment.
2. Fill out the COSHH form for the polyurethane resin system.
3. Make sure that the pulmonary function tests (PFTs) tests for all the personnel involved in the experiment are valid.
4. Before starting the experiment check that the following safety arrangements are in place:
    a. LEV system is switched on and working fine.
    b. All the PPEs (goggles, lab coats, gloves) are in place.
    c. Check the expiry date for the MDI detection badges.
    d. Correct filters have been attached to the facemasks.
    e. Enough quantity of the decontaminant solution is available.
    f. Spill-kit is in place in case of any resin spills.
    g. The cloth for the MDI catchment is in place.
    h. The MDI vapour catchment-hood is at right height.
    i. Thermocouples and heating elements for the die are at correct position.
5. Set the resin-bath/ resin-impregnator.

6. Thread the rovings through the resin-bath/resin-impregnator. At least two people should be present for this activity. Die must NOT be heated during the fibre threading process.
7. In case of resin bath pultrusion, the resin components need to be mixed prior to the experiment. The resin component should be weighed as accurately as possible on a weighing balance which should be covered with a polythene sheet.
8. Mix the components. The temperature of the mixed resin system should be monitored continuously using (i) the thermocouple from the pultrusion machine, or (ii) external thermocouple. If the temperature of the mixed resin system exceeds 5-10 °C more than ambient temperature, there are ample chances of resin-exotherm.
9. Set the die temperature to desired value before staring mixing the resin.
10. Wait for the die to reach the set temperature.
11. Carefully pour the mixed resin in the resin bath.
12. Start the pultrusion process at a set speed.
13. Label the pultruded composite with a permanent marker with appropriate coding.
14. Cur the composite after they exit the puller. Make sure that a vacuum cleaner is used while cutting the composite.
15. Store the composites.
16. At the end of the pultrusion operation, keeps the machine running until dry fibres come out of the die. By doing this no threading is required for the next pultrusion operation unless the impregnation system is changed.
17. Switch off the pultrusion machine and the compressor.
18. Remove the equipment to be cleaned from the pultrusion line.
19. Clean the equipment with solvent.

## Hazards:

1. Risk of electric shock: Power connections.
2. Risk of injury due to grips of caterpillar.
3. Risk of burn due contacting with heated die.
4. Risk of inhaling the isocyanate vapours.
5. Risk of resin exotherm.

**Safety Measures:**

1. All the personnel involved in the experiment should undergo the pulmonary function tests (PFTs) test.
2. Safety protocols should be displayed at proper place in the laboratory (See Figure 1 in Section B).
3. LEV system should be switched on (See Figure 2 in Section B).
4. Isocyanate detection badges should be worn by all users (See Figure 3 in Section B).
5. Full-face masks with MDI filters should be used by all users (See Figure 4 in Section B).
6. Fire extinguishers ($CO_2$, Foam) should be available (See Figure 6 in Section B).
7. Decontaminant solution should be available.
8. Spill kit should be available with appropriate materials (See Figure 8 in Section B).
9. Refer University Health & Safety Policy (Electrical safety - UHSP/18/ES/02)
10. The machine will not operate if the safety cage for the machine is open. However inspect that the safety cage for the grippers is properly closed.
11. Use of lab coats is mandatory.

## Section B: Photographs of the safety items employed

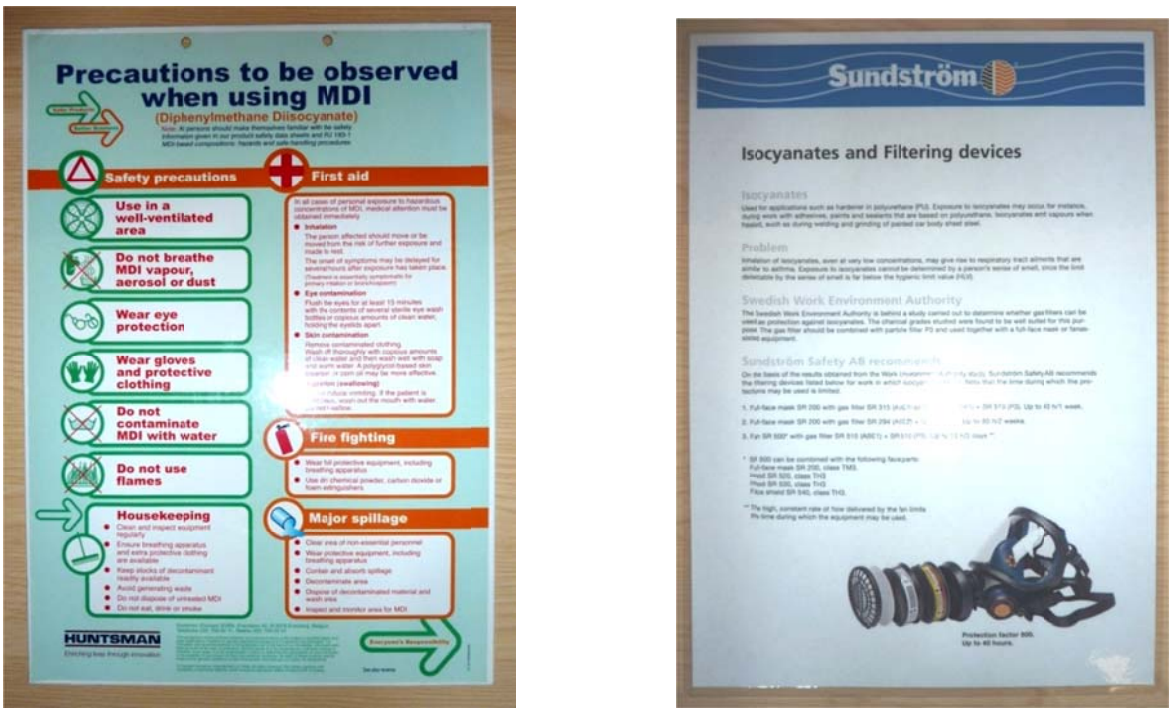


(a) (b)

**Figure 1 Brochures for (a) working with MDI, and (b) isocyanate filters.**


(a) (b)

**Figure 2 (a) Control system for LEV system, and (b) the vacuum level indicator**


**Figure 3 Photograph of the isocyanate detection badges.**


**Figure 4 Photograph of the filter system used while working with polyurethanes.**

**Figure 5 LEV system used to catch the vapours at the entry and exit of the die.**


**Figure 6 Fire extinguishers.**

**Figure 8 Photograph of the spill kit.**

## Appendix-E: LCIA impact categories

The details of the environmental impact categories used for the comparison of clean and conventional pultrusion process are provided in this section. The data provided is mainly obtained from Azapagic et al. (2003).

(i) Global warming potential (GWP) is calculated as a sum of emissions of the greenhouse gases ($CO_2$, $N_2O$, $CH_4$ and VOCs) multiplied by their respective GWP factors.

(ii) Acidification potential (AP) is based on the contributions of $SO_2$, $NO_x$ , HCl, $NH_3$, and HF to the potential acid deposition, i.e. on their potential to form $H^+$ ions.

(iii) Eutrophication potential (EP) is defined as the potential of nutrients to cause over-fertilisation of water and soil which in turn can result in increased growth of biomass.

(iv) The ozone depletion potential (ODP) category indicates the potential of emissions of chlorofluorohydrocarbons (CFCs) and chlorinated hydrocarbons (HCs) for depleting the ozone layer.

(v) Abiotic resource depletion includes depletion of nonrenewable resources, i.e. fossil fuels, metals and minerals.

(vi) Freshwater aquatic ecotoxicity potential (FAETP) and terrestric ecotoxicity potential (TETP) measure the toxicity resulted by the process in freshwater or terrestric environment.

(vii) Human toxicity potential (HTP) takes account of releases of materials toxic to humans in three distinct media: air, water and soil.

(viii) Photochemical Ozone creation potential (POCP) results from the degradation of the oxides of nitrogen (NOx) and volatile organic compounds (VOCs) in the presence of light.